REPORT NO.
UCB/EERC-91/18
DECEMBER 1991

EARTHQUAKE ENGINEERING RESEARCH CENTER

INVESTIGATION OF THE SEISMIC RESPONSE OF A LIGHTLY-DAMPED TORSIONALLY-COUPLED BUILDING

by

RUBEN L. BOROSCHEK
STEPHEN A. MAHIN

Report to the National Science Foundation

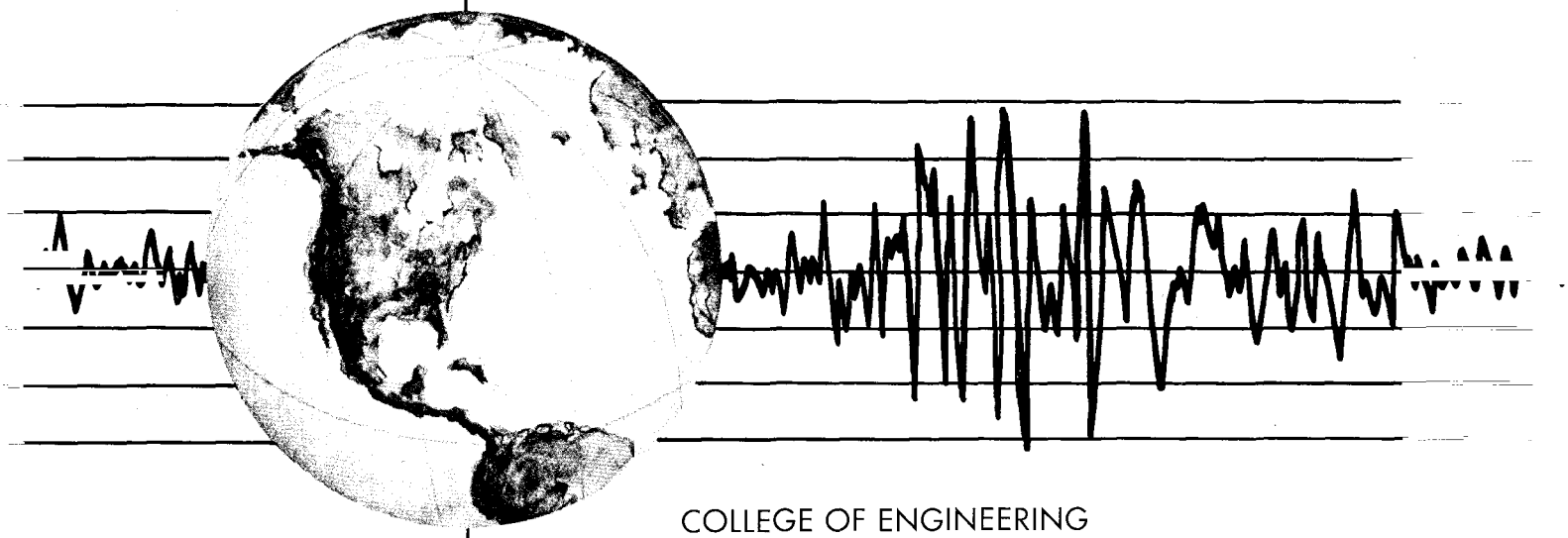

COLLEGE OF ENGINEERING

UNIVERSITY OF CALIFORNIA AT BERKELEY

For sale by the National Technical Information Service, U.S. Department of Commerce, Springfield, Virginia 22161

See back of report for up to date listing of EERC reports.

50272-101

REPORT DOCUMENTATION PAGE	1. REPORT NO. NSF/ENG-91016	2.	PB93-120335

4. Title and Subtitle

"Investigation of the Seismic Response of a Lightly-Damped Torsionally-Coupled Building"

5. Report Date: December 1991

6.

7. Author(s): Ruben L. Boroschek and Stephen A. Mahin

8. Performing Organization Rept. No.: UCB/EERC-91/18

9. Performing Organization Name and Address

Earthquake Engineering Research Center
University of California, Berkeley
1301 So. 46th Street
Richmond, Calif. 94804

10. Project/Task/Work Unit No.

11. Contract(C) or Grant(G) No.

(C) 1088089/8-9131

(G) BCS-9002718

12. Sponsoring Organization Name and Address

National Science Foundation
1800 G. Street, N.W.
Washington, D.C. 20550

California Dept. Conservation
CSMIP
801 K Street, MS 13-35
Sacramento, CA 95814-3531

13. Type of Report & Period Covered

14.

15. Supplementary Notes

16. Abstract (Limit: 200 words)

The earthquake behavior of lightly-damped, torsionally-coupled moment resisting steel space frames is investigated by analyzing the recorded three-dimensional response of a "regular" thirteen story steel frame building located in California, and by performing several elastic and inelastic computer analyses of this and similar structures. Of several earthquakes recorded in the case study building, three are considered in this report: the 1984 Morgan Hill, the 1986 Mt. Lewis and the 1989 Loma Prieta events. During these events the building responded severely, though no structural damage was observed. The recorded responses of the structure were unusual; characterized by long duration, narrow banded periodic motions, with strong amplitude modulation; by large displacements and torsional motions; by large amplification of the input ground motions; and by slow decay of the building's dynamic responses.

The investigation concludes that lightly-damped regular space frame structures like the one studied are highly susceptible to strong lateral-torsional and modal coupling because of the closeness of their predominant periods and the possible severe effects of "small" accidental eccentricities. It is shown that even small input motions can produce large responses, if the predominant periods of the structure match those of the site. These various effects together with the large flexibility often found in steel moment resisting frames can create structures that exhibit unusually severe seismic responses.

17. Document Analysis a. Descriptors

b. Identifiers/Open-Ended Terms

c. COSATI Field/Group

18. Availability Statement	19. Security Class (This Report)	21. No. of Pages
Release Unlimited	unclassified	275
	20. Security Class (This Page) unclassified	22. Price

INVESTIGATION OF THE SEISMIC RESPONSE OF A LIGHTLY-DAMPED TORSIONALLY-COUPLED BUILDING

Ruben L. Boroschek
and
Stephen A. Mahin

A Report to the National Science Foundation

Report No. UCB/EERC - 91/18
Earthquake Engineering Research Center
University of California
Berkeley, California
December 1991

ABSTRACT

The earthquake behavior of lightly-damped, torsionally-coupled moment resisting steel space frames is investigated by analyzing the recorded three-dimensional response of a "regular" thirteen story steel frame building located in San Jose, California, and by performing several elastic and inelastic computer analyses of this and similar structures. Several earthquakes have been recorded in the case study building. Of these, three earthquakes are considered in this report: the 1984 Morgan Hill, the 1986 Mt. Lewis and the 1989 Loma Prieta events. During these events the building responded severely, though no structural damage was observed. The recorded responses of the structure were unusual; characterized by long duration, narrow banded periodic motions, with strong amplitude modulation; by large displacements and torsional motions; by large amplification of the input ground motions; and by slow decay of the building's dynamic responses.

Three-dimensional linear and nonlinear numerical models of the complete structure are developed to simulate the recorded responses and to study the effects of changes in various parameters. The dynamic analyses consider unidirectional as well as bi-directional input motions with and without torsional input excitations. A "best fit" model employing standard analysis and design procedures is identified. The parameters affecting the correctness of the response are determined. The effects of such factors as inelastic behavior, amount of equivalent viscous damping, additional plan eccentricities, and input motion characteristics on the overall response of the structure are studied. Typical design code recommendations for this type of structure are also evaluated as part of this investigation.

The investigation concludes that lightly-damped regular space frame structures like the one studied are highly susceptible to strong lateral-torsional and modal coupling because of the closeness of their predominant periods and the possible severe effects of "small" accidental eccentricities. It is shown that even small input motions can produce large responses, if the predominant periods of the structure match those of the site. These various effects together with the large flexibility often found in steel moment resisting frames can create structures that exhibit unusually severe seismic responses.

ACKNOWLEDGMENTS

The authors would like to express their sincere gratitude to Professors Jack P. Moehle and Bruce A. Bolt for their valuable comments on the manuscript.

A special thanks to Jose A. Inaudi for his advice and to Susan Kern and Beverley Bolt for reviewing and correcting this manuscript.

Financial support of this work has been mainly provided by the National Science Foundation under Grant BCS-9002718 and by the California Strong Motion Instrumentation Program under contract 1088089/8-9131. The findings, observations and conclusions of this report are those of the authors alone.

TABLE OF CONTENTS

LIST OF TABLES

LIST OF FIGURES

CHAPTER 1

INTRODUCTION

1.1 General

During the past few decades extensive strong motion instrumentation programs have been undertaken around the world. One of the most densely instrumented areas is California where several hundred ground sites as well as a considerable number of structures are currently being monitored. In recent years, a series of important earthquakes has occurred in California producing a large amount of data on the response of buildings, bridges, dams and other structures. This information on the "actual" behavior of structures during earthquakes provides researchers with a unique opportunity to validate or reject analytical theories and design assumptions, to verify and improve analytical models, and to identify the basic factors governing the seismic response characteristics of various types of structures.

Some of the most significant and unusual response time histories obtained to date have been recorded in an apparently regular thirteen story government office building, located in San Jose, California (see Fig. 1.1). This building is instrumented with twenty-two unidirectional strong motion accelerographs, positioned as shown in Fig. 1.2.

Several earthquake records have already been obtained in this structure. The three most intense responses recorded to date are those obtained during the Morgan Hill earthquake of April 24, 1984 (M_l = 6.2), the Mt. Lewis earthquake of March 31, 1986 (M_l = 5.8) and the October 17, 1989 Santa Cruz Mountains-Loma Prieta earthquake (M_l = 7.1). The acceleration records are shown in Figs. 1.3 through 1.5 [20]. Peak horizontal ground accelerations recorded for these events at the base of the building (Channels A20, A21 and A22) were 4, 4 and 11 % g, respectively. The building substantially amplified these base motions so that the maximum structural accelerations during the earthquakes were 17, 32 and 36 % g, respectively. This degree of amplification is unusual, especially for the Mt. Lewis event. During each of the earthquakes, the motion of the structure caused widespread damage to contents and disruption of services. Some of this damage can be seen in Fig. 1.6.

Another unusual feature of the responses shown in Figs. 1.3 through 1.5 is that the structure continued to vibrate vigorously for more than 80 seconds. The input motion (see Channels A20, A21 and A22 in these figures) was much shorter in duration and maximum structural responses occurred generally long after the apparent end of the strong motion portion of the base

excitation. The records also exhibit a strongly modulated pattern and locally indicate that the structure experienced substantial torsion.

This behavior is apparent, for example, in the two EW direction acceleration time histories of the twelfth floor (Channels A8 and A9) obtained during the Mt. Lewis event, and shown in Figs. 1.4 and 1.7. These figures clearly show the long duration of the motions, the slow decay of the amplitudes with time and the strong modulation of the response. The response modulation can be identified in Fig. 1.7 by the large dip in amplitudes around second 25. The amplitude of the motion grows substantially after this time even though the intensity of the input motion has diminished significantly. Torsional behavior can also be observed in this figure, especially around second 25, when the records obtained at opposite corners of the building, are nearly 180° out-of-phase.

In addition, occupants of the building have indicated that even for small earthquakes the structure oscillated strongly, and for long periods of time.

This building appears to be a relatively typical example of a steel moment-resisting space frame structure. For office use, such systems generally have large open spaces, regular floor plans and lightweight exterior cladding. Because this building represents a commonly used structural system and because of its apparently unusual and severe recorded response to "service level" earthquakes, a detailed study of the building's response is warranted.

1.2 Previous Work on the Building

The response of this building has been the focus of several previous studies. Results of some of these studies will be described later in more detail.

Shakal and Huang [47] showed that the building exhibits significant torsional response. Bard [3] investigated the importance of foundation rocking on the response of the building. He found that the flexibility of the foundation did not contribute significantly to the large amplification of base motion observed in the building.

Lin and Papageorgiou [30] performed a system identification analysis of optimally synchronized records. In their investigation predominant periods and damping values were obtained as functions of selected time windows. Boroschek et al. [2, 6, 7, 8, 33] also estimated the dynamic characteristics of the structure, obtained envelopes of structural responses during the Morgan Hill and Mt. Lewis earthquakes, and suggested some causes for the behavior of this building by direct analysis and interpretation of the recorded responses. Both of these studies noted complex three-dimensional mode shapes and closely spaced natural periods.

Arnold [1] and Naaseh [37] described the behavior of the occupants of the building and the nonstructural damage observed in the building during the earthquakes mentioned.

1.3 Literature Review

Because of the possibility that the torsional response contributed to the intensity of motion observed in the building, a brief review of the literature on this topic follows. Analytical investigations are summarized and recommendations in building codes reviewed.

1.3.1 Torsional Response, Analytical Studies

Several investigations have studied torsional and lateral-torsional coupling in structures in the linear and nonlinear range. For examples, see References 10, 14, 15 17, 18, 24, 25, 26, 41, 43, 46, 50, and 55.

Linear analyses of one-story systems have indicated that coupling of lateral and torsional motions occurs when stiffness or mass eccentricities are present in a system. The structural parameters that control the response of simple linear torsionally-coupled systems under bi-directional input motion are the uncoupled translational periods, the ratios of the translational to the torsional uncoupled periods, the ratios of the stiffness eccentricities to the radius of gyration of the story, and the viscous damping coefficient.

Under unidirectional translational input, a structure with a single eccentricity (orthogonal to the direction of excitation) exhibits a torsionally-coupled response that causes, relative to a comparable uncoupled system, an increase in rotation and torque, an increase of the shear on vertical elements located away from the center of stiffness, a reduction of the displacement at the center of mass in the direction of input, and a reduction of the base shear and overturning moment. These effects are more strongly observed when the ratio of uncoupled translational to torsional period is close to unity. As observed by Newmark [40], systems tend to have identical torsional and translational uncoupled periods when they have a uniform distribution of member stiffness in plan. Closely spaced modal periods were noted for the apparently symmetric San Jose office building.

The behavior of systems with eccentricities in two orthogonal directions differs from that observed for single eccentric systems, especially when the two translational uncoupled periods are the same [25]. The behavior is quite complicated and depends not only on the properties of the system, but also on the characteristics of the input motion. Nevertheless, the following general observations have been made for eccentric models (with eccentricities in both global directions) subjected to one component of input motion [25]:

- The base shear in the direction of loading does not exceed that observed in an associated uncoupled system.
- The base shear in the direction transverse to the input motion can be large (even similar

to the shear in the direction of motion) especially for large eccentricities associated with the direction of motion.

- The torque typically increases with increase in the eccentricity transverse to the direction of loading, but could decrease if the eccentricity in the direction of loading increases.
- The effect of torsional coupling decreases with increase in the amount of viscous damping.
- Small eccentricities, in regular structures with similar uncoupled translational and torsional periods, subjected to a ground motion characterized by a hyperbolic variation of the spectral acceleration with period, produce large amplifications of the static torque (i.e., the ratio of the dynamic torque to the torque obtained by multiplying the base shear of an uncoupled system by the eccentricity present in the coupled system), when compared with a system with larger eccentricities. On the other hand the effect of small eccentricities on base shear is small for these systems.

In the inelastic range additional parameters, such as the yield characteristics of the elements and the number and distribution of elements, affect the response. These parameters determine the position of the center of strength. This center is defined in a single-story system as the point at which a lateral load should be applied so no story rotation occurs when all elements yield (i.e., the plastic centroid).

An extensive study of inelastic one-story laterally-torsionally coupled structures with one-way eccentricity and unidirectional input was recently undertaken by Goel and Chopra [14, 15]. They found that stiffness eccentricities typically increase the story rotation and reduce the displacement at the center of stiffness in comparison with the associated uncoupled system. These effects were found to be less pronounced for systems with only stiffness eccentricities (compared with systems with both stiffness and strength eccentricities). Ductility demands on elements (which typically depend on the position of the element with respect to the centers of mass and stiffness) generally increase with increasing stiffness eccentricity. This increase occurs for systems without strength eccentricities for all periods, and mainly in the constant velocity (intermediate period) portion of the input response spectrum for systems with strength eccentricities.

Special attention was given by Goel and Chopra [15] to nonlinear systems with small stiffness eccentricities. Their investigation concluded that the dynamic amplification of the static torque and the reduction of the displacement at the center of stiffness in the direction of loading caused by lateral-torsional coupling are considerably reduced in comparison with those of similar linear structures.

When bi-directional inputs are included the nonlinear problem is further complicated because torsional rotations could occur in symmetric systems (mass, stiffness and strength) if full

moment-axial load interaction is present in the resisting elements. Some examples of this effect are presented by Kobori [27], Pecknold [42] and Zeris [56]. There are only a few studies in the literature referring to nonlinear torsionally-coupled systems with bi-directional input; for example, the work by Yamazaki [55] and Prasad and Jagadish [43]. These investigators worked with simple one-story mass eccentric structures consisting of four columns having bi-directional moment interaction surfaces which do not vary with axial load. Because of the large number of parameters involved in the response and the rather small set of input motions and structural configurations evaluated, it is hard to generalize from these studies.

It is nonetheless clear that coupling of lateral and torsional responses could make an important contribution to the severity of the responses observed in the San Jose office building because of its closely-spaced modal periods and potentially small energy-dissipation capacity in the elastic range.

1.3.2 Code Recommendations for Torsionally-Coupled Structures

In contrast to the rather complex parameters and considerations employed in analytical studies of torsionally-coupled systems, building design codes generally present very simple procedures to account for these effects. For torsional design, the codes first require identification of the static stiffness eccentricity, e_{static}, or categorization of the structure as being irregular or regular in plan, or both.

To take into account different factors in the responses of torsionally-coupled buildings, the static eccentricity present in a structure is usually modified using an equation of the form [41]

$$e_{design} = \alpha e_{static} + \beta[D] \tag{1.1}$$

or

$$e_{design} = \gamma e_{static} - \beta[D] \tag{1.2}$$

in which D is a representative plan dimension of the building and α and β are constants. These equations try to include in a simple manner the dynamic amplification of the static eccentricity, input torsion, and accidental torsional eccentricities due to errors in calculation of material properties, modeling assumptions and non-uniform "live load" distributions. The modified eccentricity that produces the most severe effect on the element being designed, is used. Some codes (e.g., 1988 UBC [22]) indicate that when considering the additional eccentricity no reduction of forces should be allowed, i.e., these equations are only used to increase force levels in elements.

For example, to consider torsional effects in building structures, the 1988 and 1991 Uniform Building Codes [22, 23] and the 1988 NEHRP [11] recommendations require that the structure be

initially analyzed with an additional (accidental) mass eccentricity, taken as 5% of the building major plan dimension in the direction of loading. The structure is then characterized as being regular or irregular. A structure is considered to be torsionally irregular "when the maximum story drift, computed including accidental torsion, at one end of the structure transverse to an axis is more than 1.2 times the average of the story drifts of the two ends of the structure." If the structure is considered torsionally irregular, is under 20 meters (65 feet) in height or no more than five stories tall, and is located in the most severe seismic zone (Zone 4, Z=0.4) then an additional static analysis with an amplified (accidental) eccentricity should be used. The amplification factor ranges between 1 and 3, and depends on the ratio of the maximum in-plane displacement (including torsion) and an average floor displacement. Only increases are allowed in forces on the elements when considering this additional eccentricity. If the structure is higher than 20 meters, torsionally irregular and in seismic zone 4, then a three-dimensional dynamic analysis with the accidental eccentricity is also required. For this case and for any three-dimensional model, if a response spectrum approach is taken, a modal combination procedure that considers modal interactions shall be used.

The New Zealand building code (1984) [21] requires that "the main elements of a building that resist seismic forces shall, as nearly as is practicable, be located symmetrically about the center of mass of the building" so the ductility demands do not increase because of torsional effects. The structure is categorized as regular or irregular in terms of the geometric characteristics of the plan and in terms of the eccentricity. Regular plans are those that do not have large re-entrant corners. A moderate eccentricity is defined as one producing in the most unfavorably affected element a shear due to torsion that does not exceed three quarters of that due to lateral translational motion. For regular (geometry) structures more than four stories high with a high degree of eccentricity, the torsional effects can be considered using static or dynamic analysis of a two-dimensional mathematical model; however, a three-dimensional model is recommended. For irregular structures more than four stories high with a high degree of eccentricity, torsional effects are treated by using a dynamic analysis and a three-dimensional model. For either case (static or dynamic), an additional eccentricity of 10% of the building dimension is considered.

The 1986 Costa Rican seismic design code [21], similar to the UBC, first characterizes the structure as being regular or irregular. For this categorization, the code requires that stiffness eccentricities be evaluated at each floor (each story is treated as an independent structure). No story may have an eccentricity exceeding 5% of the largest building dimension to qualify as regular. Also, the code requires that the center of stiffness and mass for all floors be contained within a rectangle with maximum dimensions equal to 10% of the building dimension. Furthermore, for each story treated independently, the coupled translational periods should be at least 42% larger than the coupled torsional period. A static analysis can be applied, if the structure is regular

and below seven stories or not more than 30 meters in height. A dynamic analysis is required for structures over seven stories tall even if they are regular. When torsional irregularities exist, but lateral and torsional story periods are well separated, a static load procedure can be used along with a three-dimensional mathematical model. No accidental eccentricity needs to be added to the static eccentricity for these analyses. For irregular structures with close fundamental periods, a dynamic analysis is required and modal maxima should be combined by a method that considers modal interaction effects. In addition, the Costa Rican code does not permit structures that have a floor eccentricity larger than 30% of the maximum building dimension.

The 1987 Mexican seismic code [21] requires that in order to qualify a structure as regular the static stiffness eccentricity for all stories of the building should be less than 10% of the maximum planar dimension of the building. To design for torsional effects, the code sets limits on the stiffness and strength eccentricities of a given floor. It is indicated that the eccentricity of the center of strength, e_p, for a reduction factor (Q) of 3 $e_p \geq e_s - 0.2$[D] and for Q greater than 3 $e_p \leq e_s - 0.1$[D], where D is the maximum building dimension in plan. Also, lateral loads at each story should be placed at a design eccentricity given by the following equations, that is more critical for the frame or wall being designed:

$$e_{design} = 1.5e_s + 0.1[D] \tag{1.3}$$

$$e_{design} = e_s - 0.1[D] \tag{1.4}$$

There is not explicit indication in the code that forces due to this eccentricity are not to be used if they reduce the force found using the basic static eccentricity. There are two additional requirements: the static eccentricity for a given floor cannot be less than half the value of the static eccentricity for any of the floors below, and the design torque applied at a given floor cannot be smaller than half the value found for any of the upper floors.

1.4 Recorded Data

Because accelerograph records will be used to investigate the seismic behavior of the structure it is important to understand the accuracy and limitations of this data. The dynamic response of the San Jose office building was recorded using uniaxial accelerometers connected to two central recording units. The data was recorded on seven inch wide photographic film and then processed using a standard procedure defined by the California Strong Motion Instrumentation Program (CSMIP). A detailed description of this data processing technique can be found in Reference [20].

In this procedure records are typically digitized at 200 points/sec using a computer driven optical scanner. "Corrected" acceleration, velocity and displacement time histories are derived by

performing a series of data integrations and corrections. The basic corrections involve compensation for transducer errors, determination of the zero base line, making starting time adjustments, and low and high band pass filtering. The resulting data typically has 50 points/sec, a 25 Hz Nyquist frequency. An Ormsby filter is used for the filtering. The ramps on this filter are set for a group of records depending on the relative characteristics of the signal, the noise present in the records and the intrinsic "noise level" of the procedure.

The expected "noise level" for the CSMIP procedures can be seen in Figs. 1.8 and 1.9. The pseudo-velocity spectrum of the system noise, Fig. 1.8, is used to set the long period limit of the filter so that a target signal-to-noise ratio for the set of records is achieved. Typically this ratio is set to 10/1. Figure 1.9 shows the average values of peak acceleration, velocity and displacement obtained by processing several records with zero acceleration with the CSMIP procedure; they are presented as a function of the long cut-off period of the filter used. Thus, this figure is an indicator of the likely errors present in processed records. The trend shown in this figure indicates that the expected acceleration noise is independent of the filter limits and near 1.5 cm/sec/sec (0.16% g). Velocity errors tend to vary proportionally to the cut-off period ($\approx (T/10)$ cm/sec) and displacement errors vary with the period squared ($\approx (T/10)^2$ cm). Thus, when processing the accelerograph records to study the behavior of a structural system the filter cut-off ramps should be carefully set taking into account the expected predominant periods of the structure, the recording noise and the processing procedure limitations. Similarly, when using recorded response data the inherent resolution error must be recognized, especially for low-level signals.

1.5 Objectives and Scope

Because of the unusual and severe response of the San Jose office building and the opportunity to use the response records to identify the causes of this response, an investigation with the following objectives was initiated:

- To identify the basic structural and/or ground motion characteristics that caused the unusual response of the building.
- To evaluate the ability of conventional linear and nonlinear models to reproduce the response.
- To evaluate the adequacy of current design procedures to identify and control this type of response.
- To evaluate the effect that factors such as lateral-torsional coupling, modal interactions, and viscous damping have on the response of nearly regular space frame structures.

- To investigate the possible nonlinear behavior of the structure under more intense ground motions.
- To identify ways of improving the behavior of the structure.

In Chapter 2 basic formulae that demonstrate the causes and effects of torsionally-coupled response are developed for simple linear one-story systems. Also, examples are presented to describe qualitatively the effect of multi-directional input motions and viscous damping on the response of these systems.

The basic structural characteristics of the San Jose office building are described in Chapter 3 with details of the instrumentation and the site conditions.

In Chapter 4 the recorded responses of the building during the 1984 Morgan Hill, 1986 Mt. Lewis and 1989 Loma Prieta earthquakes are described. Dynamic properties of the building are obtained from analyses of the structural response records. Envelopes of derived response parameters (maximum displacements, interstory drifts, torsion, rocking, deformed shapes, base shear and overturning moments) are also presented. Similarities between the response of this building and those observations made in Chapter 2 for simple one-story structures are also discussed.

Several linear elastic computer models are developed in Chapter 5 to evaluate different aspects of the observed structural behavior. The ability of these mathematical idealizations to reproduce the recorded building response is examined. The sensitivity of the response of the model to variations in mechanical, damping and inertial properties and to different ground motion records is presented. Typical building design code recommendations for this type of structure are also examined in this chapter.

The possible effects of inelastic behavior on the response characteristics of the building are discussed in Chapter 6. A three-dimensional model of the building is analyzed to assess the effects of the severity and type of ground motion, the degree of static eccentricity present and viscous damping on the response of multi-story frame structures. Comparisons are made in this chapter between the results of the inelastic response analyses and observations made previously regarding one-story torsionally-coupled systems and systems with different amounts of viscous damping. Methods for controlling the adverse aspects of the observed response are discussed as well.

Chapter 7 presents the conclusions of this investigation and areas for future research.

Details of certain aspects of the study are contained in the Appendices. Appendix A develops simple formulae describing beating behavior resulting from constructive and destructive reinforcement of closely spaced modes. These formulae are used to simulate the response of the building.

Simple formulae to determine the ratio of uncoupled lateral and torsional periods for regular space frame structures are presented in Appendix B.

Appendix C presents the results of an investigation carried out to help clarify the effect of viscous damping on the dynamic response of inelastic one degree-of-freedom systems. The effect of damping on maximum ductility demand, cumulative ductility demand, and the amplitude and apparent duration of the response envelope are examined considering single degree-of-freedom systems.

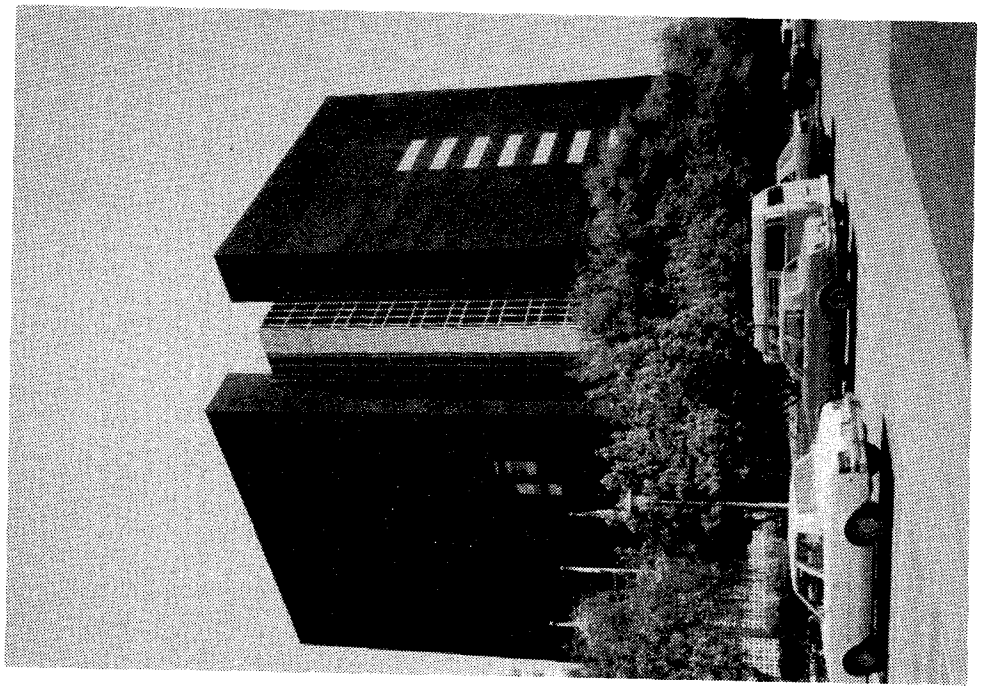

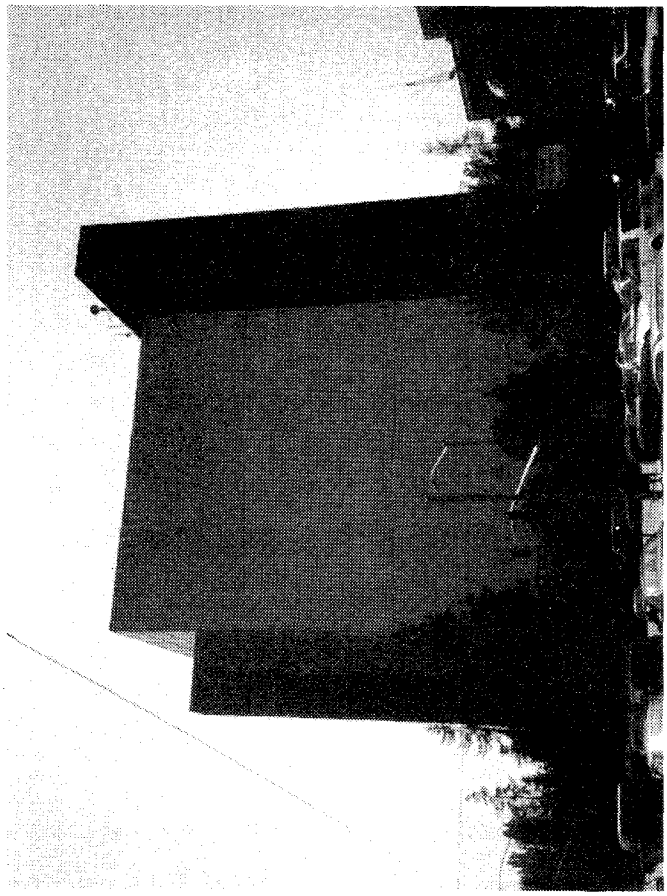

Figure 1.1: Thirteen story government office building.

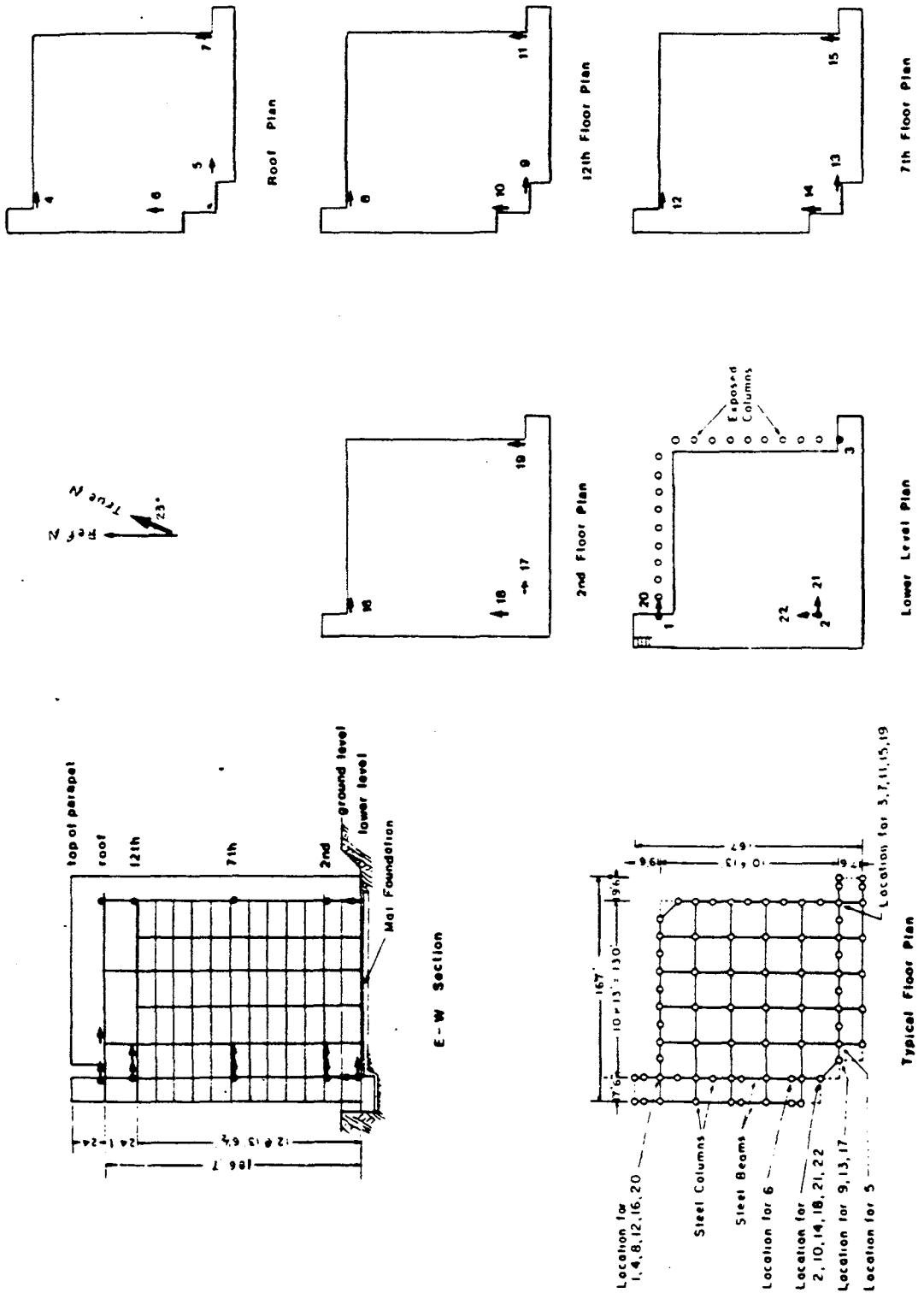

Figure 1.2: Building plans and sensor layout [20].

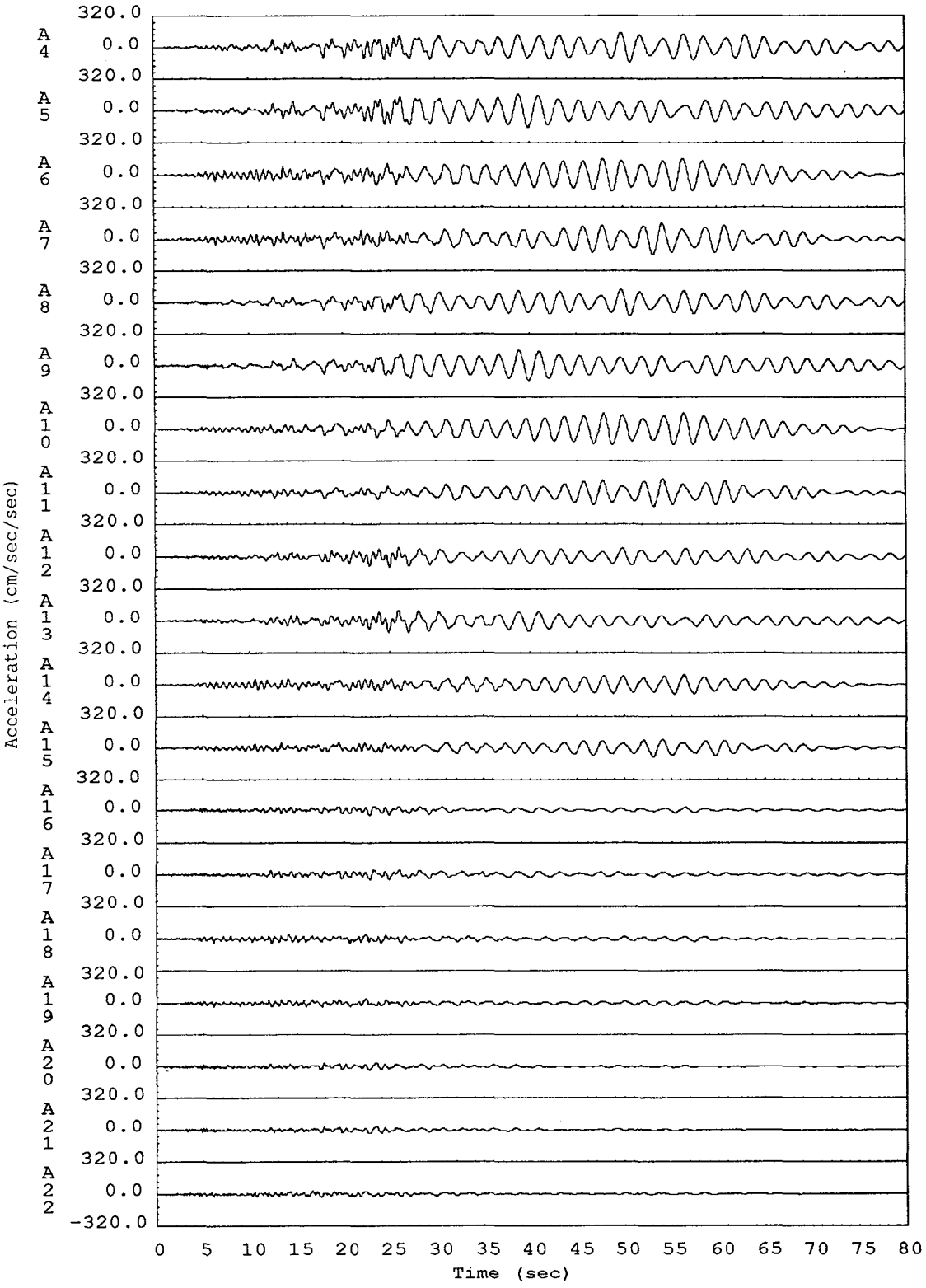

Figure 1.3: Building horizontal acceleration records. Morgan Hill earthquake.

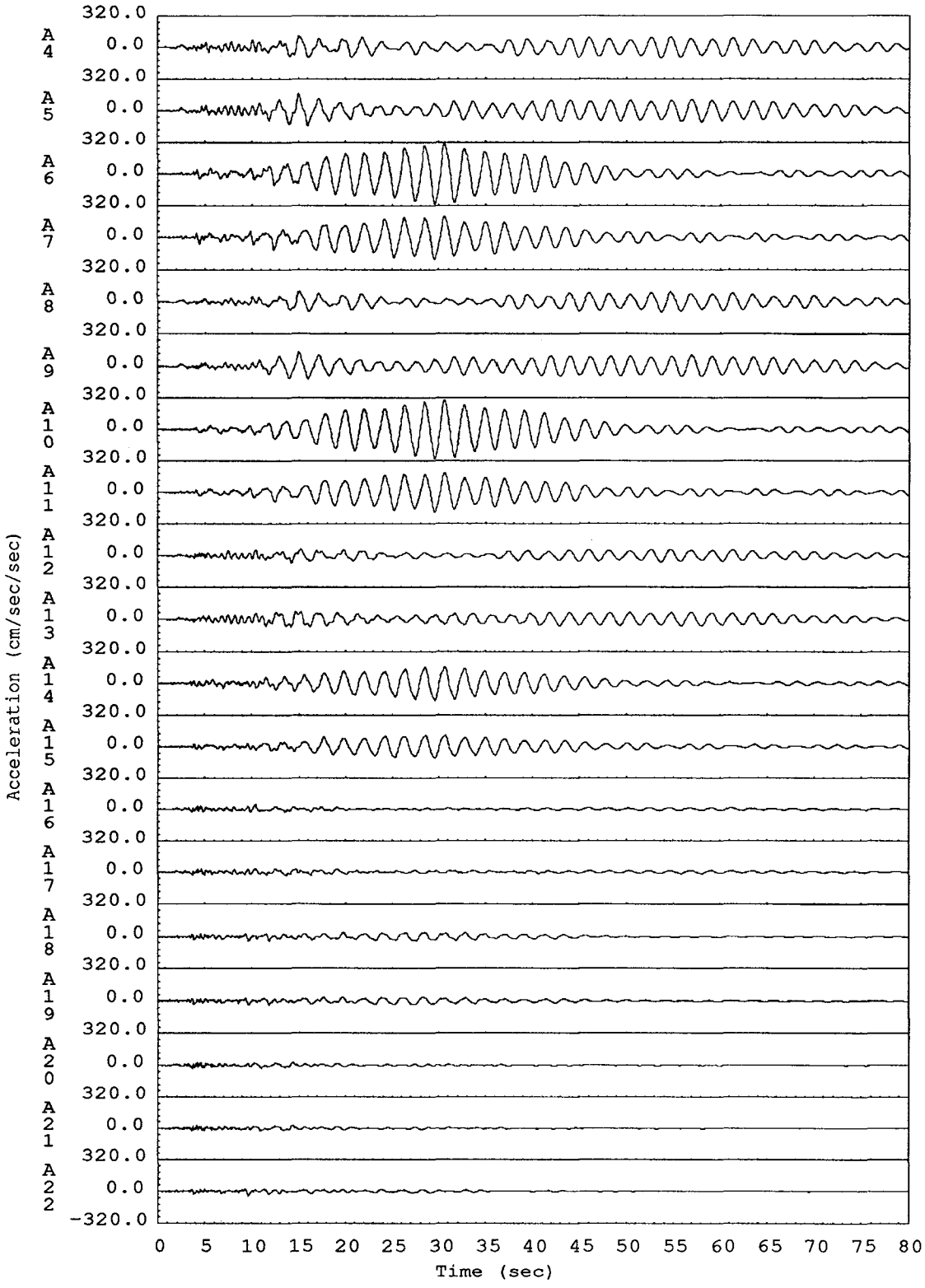

Figure 1.4: Building horizontal acceleration records. Mt. Lewis earthquake.

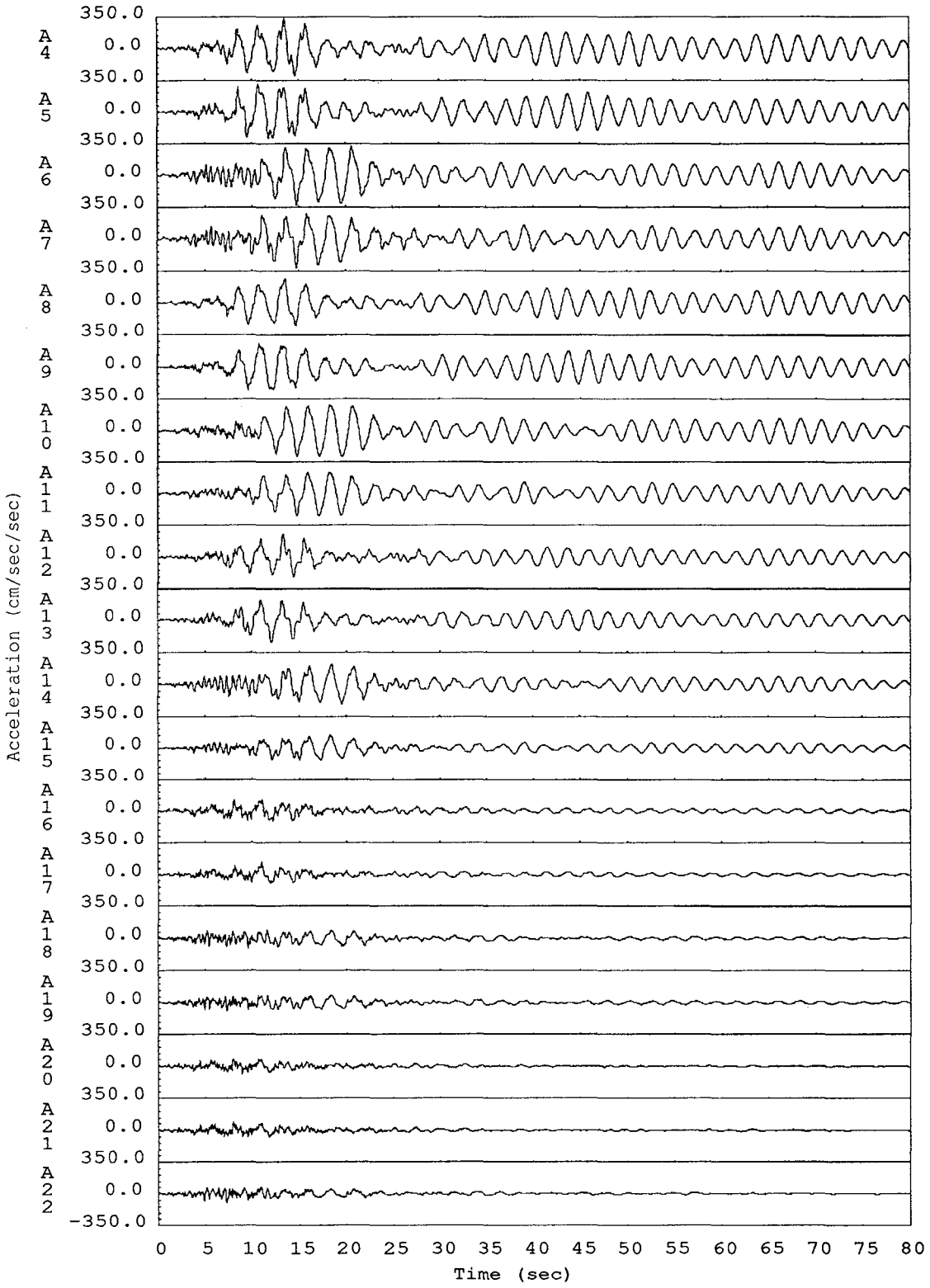

Figure 1.5: Building horizontal acceleration records. Loma Prieta earthquake.

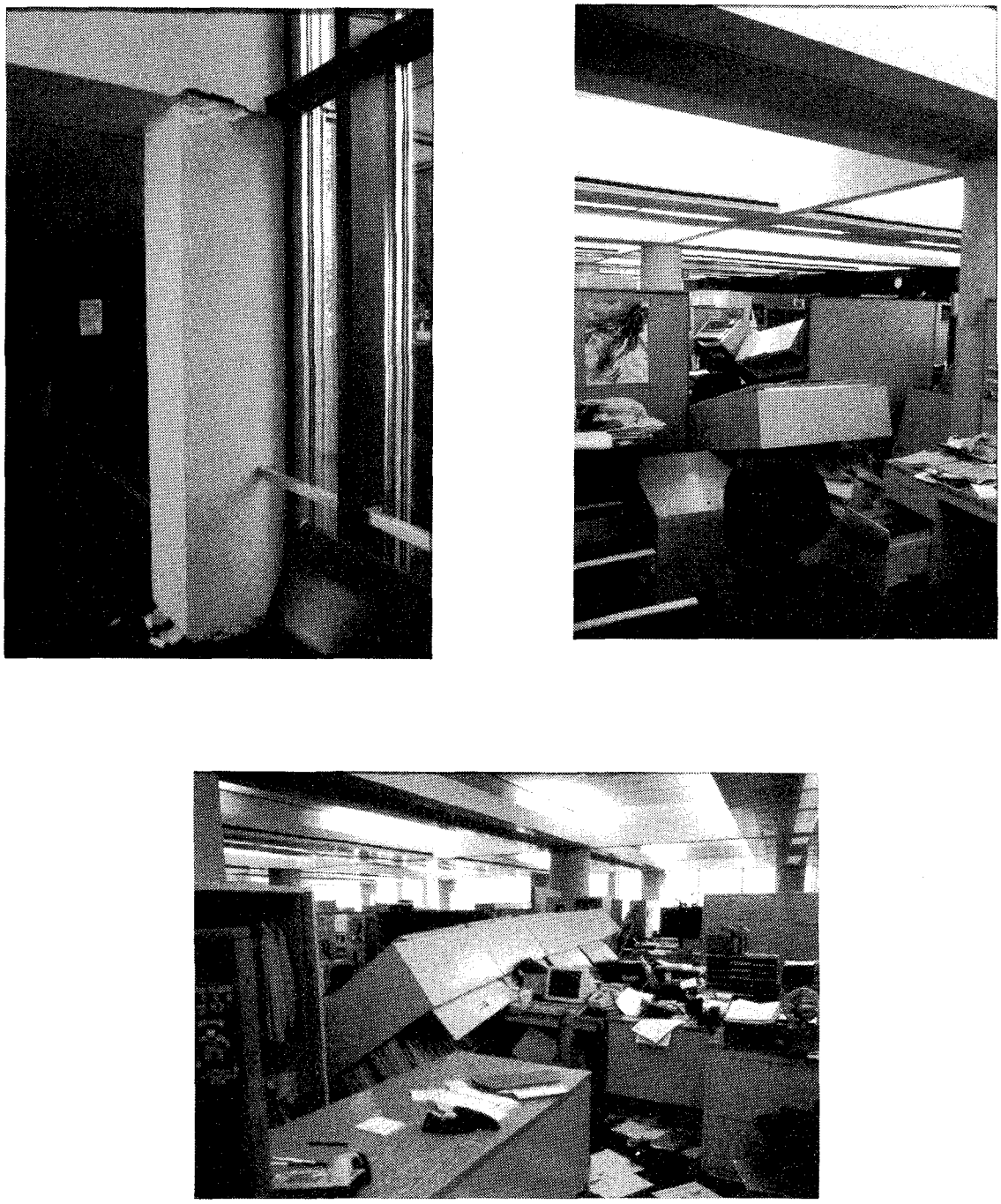

Figure 1.6: Non-structural damage observed during the Santa Cruz Mountains-Loma Prieta event.

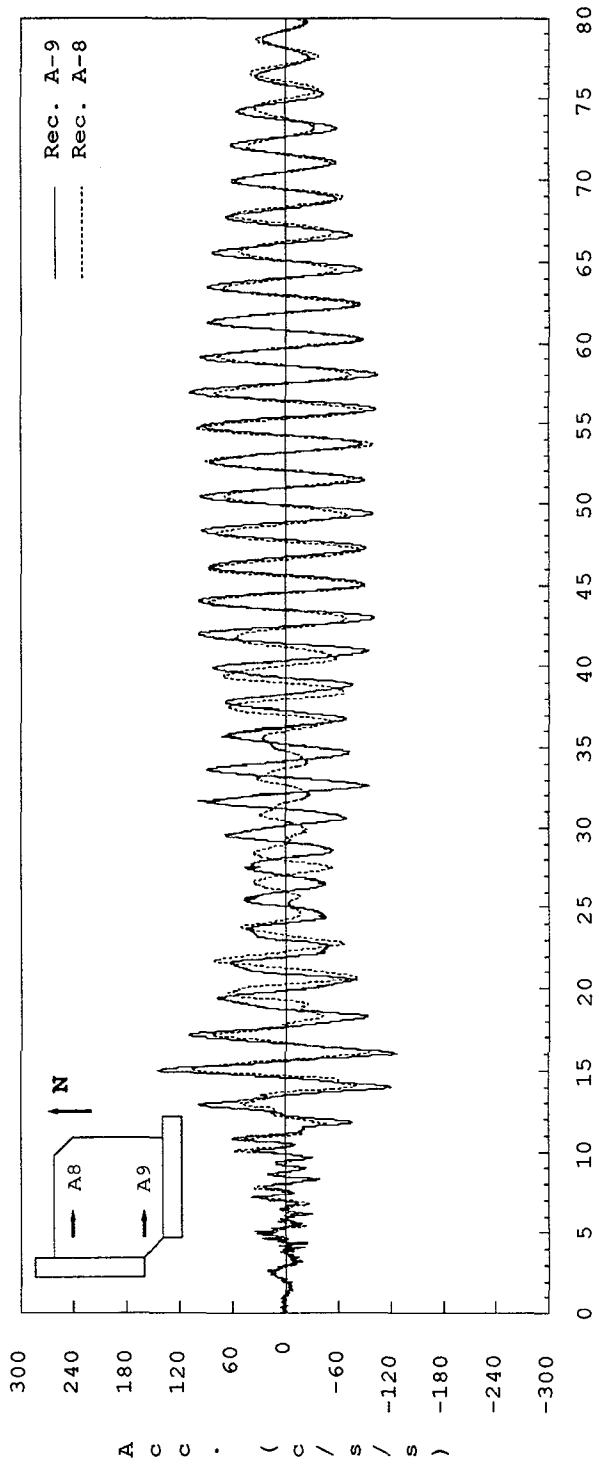

Figure 1.7: Twelfth floor acceleration records. EW direction. Mt. Lewis Event.

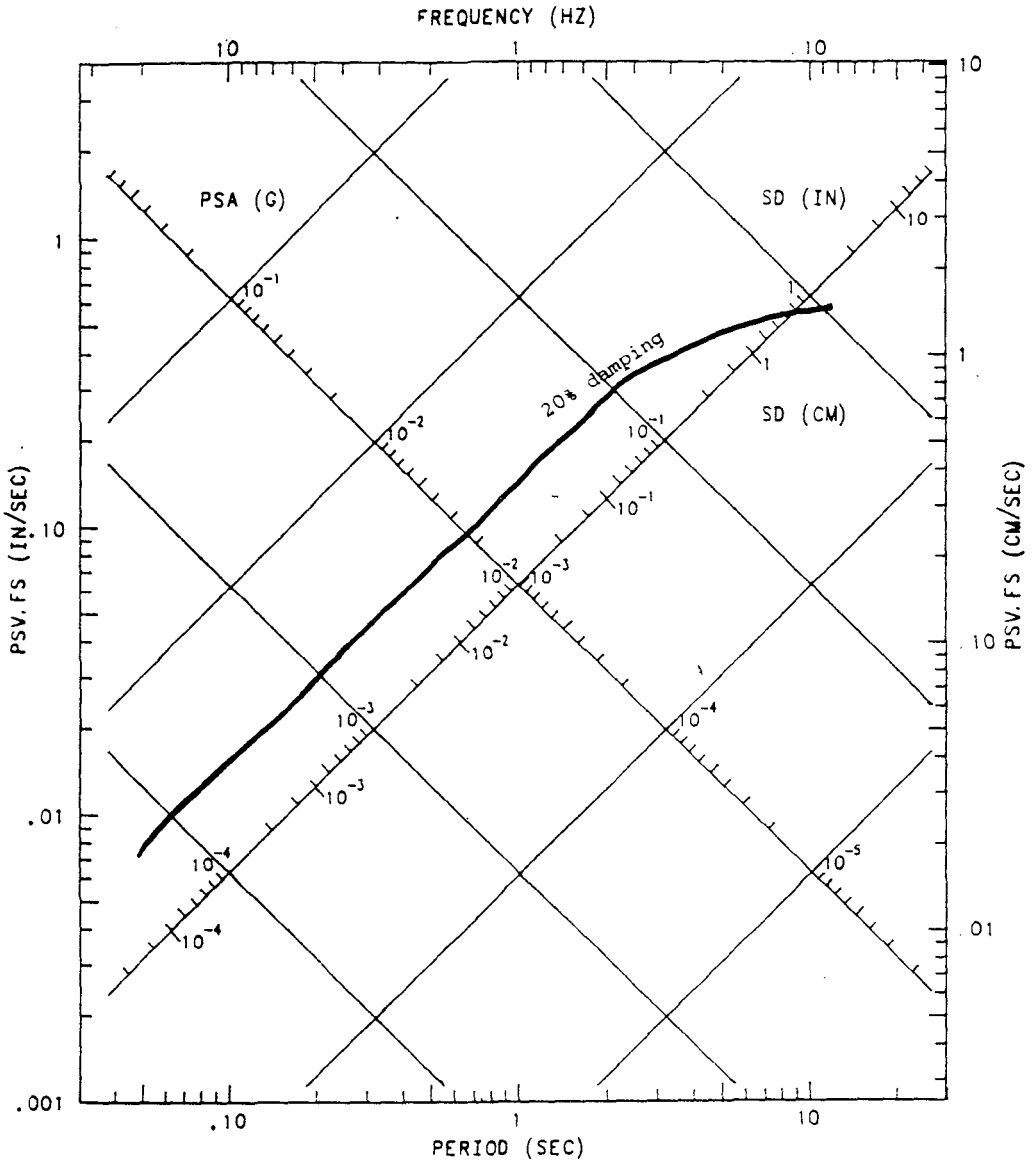

Figure 1.8: CSMIP noise spectrum [20].

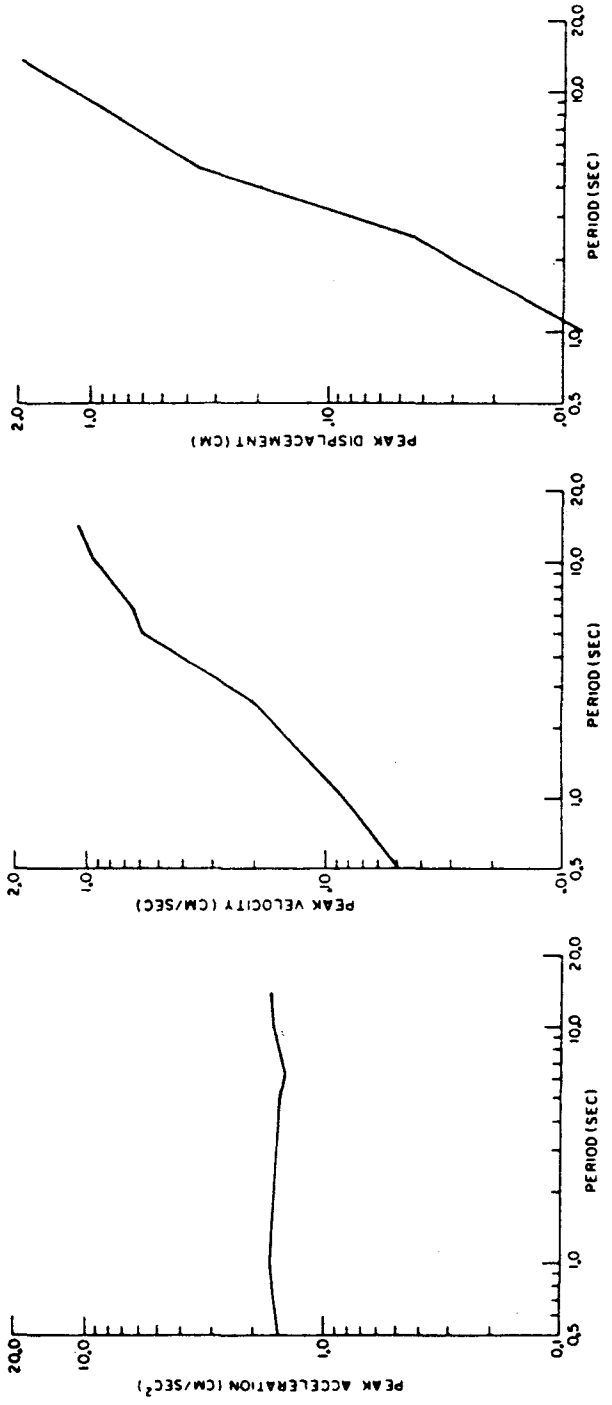

Figure 1.9: Processing noise present in a typical acceleration (left), velocity (middle) and displacement (right) record, for different filter cut-off periods [20].

CHAPTER 2

TORSIONALLY-COUPLED RESPONSE OF ONE-STORY SYSTEMS

2.1 General

The coupled lateral-torsional responses of one-story systems have been studied extensively for several years [10, 14, 15, 17, 18, 24, 25, 26, 41, 43, 46, 50, 55]. Some general conclusions from these investigations were reviewed in Section 1.3. In this chapter an attempt is made to describe in more detail the basic dynamic and behavioral characteristics of one-story systems with small eccentricities. The results obtained are compared in subsequent chapters with observations developed from analyses of the case study structure.

A simplified analytical approach is used in this chapter to study the effects of small eccentricities on the dynamic and response characteristics of simple elastic systems. The general equation of motion for a one-story structure, with three degrees of freedom, is formulated. Closed form solutions for the natural periods and mode shapes are then obtained for a system with identical translational stiffness in orthogonal directions. The causes and effects of modal interaction and beating in laterally-torsionally coupled systems are then investigated for a general eccentric system. Numerical sensitivity studies are also perform to identify the effect of damping and the direction of input motion on the response of these systems. Nonlinear effects are not presented in this chapter, but are reviewed later in Chapter 6.

2.2 The Eigenvalue Problem for a Simple Eccentric System

The period and mode shape characteristics of a linear one-story system with three degrees of freedom (Fig. 2.1) can be obtained by formulating an eigenvalue problem about its center of mass in terms of the global stiffness at the center of stiffness and the distance between these centers, as follows:

$$\left[\begin{bmatrix} K_x & -K_x e_y & 0 \\ -K_x e_y & (K_\theta + K_x e_y^2 + K_y e_x^2) & K_y e_x \\ 0 & K_y e_x & K_y \end{bmatrix} - m w_n^2 \begin{bmatrix} 1 & 0 & 0 \\ 0 & r^2 & 0 \\ 0 & 0 & 1 \end{bmatrix}\right] \begin{bmatrix} v_{xn} \\ v_{\theta n} \\ v_{yn} \end{bmatrix} = \begin{bmatrix} 0 \\ 0 \\ 0 \end{bmatrix} \qquad (2.1)$$

where

K_x is the story translational stiffness in the X direction at the center of stiffness,

K_y is the story translational stiffness in the Y direction at the center of stiffness,

K_θ is the story torsional stiffness at the center of stiffness,

r is the story radius of gyration,

e_x is the distance from the center of mass to the center of stiffness in the global X direction,

e_y is the distance from the center of mass to the center of stiffness in the global Y direction,

w_n is the natural frequency for mode "n" and $n = 1, 2, 3$,

v_{xn}, $v_{\theta n}$, and v_{yn} are the translational and rotational components of mode n, and

m is the story mass.

The general eigenvalue problem presented here cannot be solved in closed form because of the cubic form of its characteristic equation. Nevertheless, this equation can be solved for the special case of identical translational stiffnesses in the X and Y directions. In this case $K_x = K_y = K$. The solution of this special problem, provides, as shown below, good insight into the more general problem. If Equation 2.1 is divided by K and the matrices are transformed to evaluate $rv_{\theta n}$ instead of $v_{\theta n}$, then the following equation is obtained:

$$\begin{bmatrix} 1-\Omega_n & -\frac{e_y}{r} & 0 \\ -\frac{e_y}{r} & \left(\left(\frac{e_o}{r}\right)^2 + \left(\frac{e_y}{r}\right)^2 + \left(\frac{e_x}{r}\right)^2 - \Omega_n\right) & \frac{e_x}{r} \\ 0 & \frac{e_x}{r} & 1-\Omega_n \end{bmatrix} \begin{bmatrix} v_{xn} \\ rv_{\theta n} \\ v_{yn} \end{bmatrix} = \begin{bmatrix} 0 \\ 0 \\ 0 \end{bmatrix} \tag{2.2}$$

where

$w^2 = \frac{K}{m}$ is the square of the uncoupled translational natural frequency of the system,

$\Omega_n = \left(\frac{w_n}{w}\right)^2$ is the square of the ratio of coupled to uncoupled frequency, and

$e_o^2 = \frac{K_\theta}{K}$ is the ratio of torsional to translational stiffness at the center of stiffness. Note that $(e_o/r)^2$ for a mass eccentric system is equal to the ratio of translational to torsional uncoupled period.

The eigenvalue solution for this system can be expressed as

$$\Omega_1 = \frac{1}{2}\left\{\left(1+\left(\frac{e_o}{r}\right)^2+\left(\frac{e}{r}\right)^2\right) - \left[\left(1+\left(\frac{e_o}{r}\right)^2+\left(\frac{e}{r}\right)^2\right)^2 - 4\left(\frac{e_o}{r}\right)^2\right]^{\frac{1}{2}}\right\}$$

$$\Omega_2 = 1 \tag{2.3}$$

$$\Omega_3 = \frac{1}{2}\left\{\left(1+\left(\frac{e_o}{r}\right)^2+\left(\frac{e}{r}\right)^2\right) + \left[\left(1+\left(\frac{e_o}{r}\right)^2+\left(\frac{e}{r}\right)^2\right)^2 - 4\left(\frac{e_o}{r}\right)^2\right]^{\frac{1}{2}}\right\}$$

where

$$e^2 = e_x^2 + e_y^2$$

After some numerical manipulation it can be shown that

$$(1 - \Omega_1)(1 - \Omega_3) = -\left(\frac{e}{r}\right)^2 \tag{2.4}$$

Figures 2.2 and 2.3 present the variation of the eigenvalues with respect to the parameters $(e_o/r)^2$ and $(e/r)^2$. These figures show that these functions are smooth and that an increase in the global static eccentricity (e) produces a separation of the natural periods of the coupled system. Additionally, for torsionally flexible systems (i.e., $(e_o/r)^2 < 1$) and small global eccentricities Ω_1 has values smaller than unity and the values of Ω_3 are close to one. The opposite is found for torsionally stiff systems. This implies that for e_o/r close to one and small static eccentricities, the three coupled natural periods of the system could be extremely close.

The mode shapes that correspond to this special eigenvalue problem have the following form, if $e_x \neq 0$ and $e_y \neq 0$:

$$\Phi = \begin{bmatrix} \frac{e_y/r}{1-\Omega_1} & \frac{e_x}{e} & \frac{e_y/r}{1-\Omega_3} \\ 1 & 0 & 1 \\ \frac{-e_x/r}{1-\Omega_1} & \frac{e_y}{e} & \frac{-e_x/r}{1-\Omega_3} \end{bmatrix} \tag{2.5}$$

The mode shape that corresponds to Ω_2 is purely translational; the predominant direction of the mode is skewed relative to the reference axes, in accordance with the static eccentricity.

For the case of systems with small eccentricities $((e/r)^2 \ll 1)$, and similar lateral and torsional uncoupled natural periods $((e_o/r)^2 \approx 1)$, Equations 2.3 and 2.5 can be approximated by

$$\Omega_1 \approx 1 - \frac{e}{r}; \quad \Omega_2 = 1 \text{ and } \Omega_3 \approx 1 + \frac{e}{r} \tag{2.6}$$

and

$$\Phi = \begin{bmatrix} \frac{e_y}{e\sqrt{2}} & \frac{e_x}{e} & -\frac{e_y}{e\sqrt{2}} \\ \frac{1}{\sqrt{2}} & 0 & \frac{1}{\sqrt{2}} \\ -\frac{e_x}{e\sqrt{2}} & \frac{e_y}{e} & \frac{e_x}{e\sqrt{2}} \end{bmatrix} = [\Phi_1 \quad \Phi_2 \quad \Phi_3] \tag{2.7}$$

where the mode shapes are normalized so that $\Phi_i^t \Phi_i = 1$.

Similar torsional and translational uncoupled periods are typically observed in systems that have uniform distribution of stiffness in plan [40], like regular space frame structures (see Appendix B for more information) and base isolated structures [26].

Finally, the coupled natural frequencies of such systems can be estimated from Equation 2.6 making use of the assumption of small eccentricities, i.e.,

$$w_1 \approx w\left(1-\frac{1}{2}\frac{e}{r}\right);\quad w_2 = w;\ \text{and}\ w_3 \approx w\left(1+\frac{1}{2}\frac{e}{r}\right) \tag{2.8}$$

Similar equations were obtained by Kelly [26] for structures with small eccentricities, starting from more restrictive model assumptions.

These equations for predominant periods and mode shapes will be used subsequently to study the effect of modal interaction on the response of structures with small eccentricities.

2.3 Equations of Motion and Beating Behavior for Coupled Lateral-Torsional Systems with Multi-Directional Inputs

The equation of motion for a one-story, three degree-of-freedom system can be expressed in matrix form as

$$[M][\ddot{V}] + [C][\dot{V}] + [K][V] = -[M][R][\ddot{V}_g(t)]$$

where

$$[M] = m\begin{bmatrix} 1 & 0 & 0 \\ 0 & 1 & 0 \\ 0 & 0 & 1 \end{bmatrix} = m\,[I_3]$$

$[\ddot{V}_g(t)] = \begin{bmatrix} \ddot{V}_{gx}(t) \\ r\ddot{V}_{g\theta}(t) \\ \ddot{V}_{gy}(t) \end{bmatrix}$ is the matrix of effective ground accelerations, and

$[R]$ is the influence coefficient matrix, taken as $[I_3]$ for the following studies.

Using a modal solution, the elastic response of the system is

$$[V] = [\Phi]\,[Y]$$

where the components of $[Y]$ are given by

$$Y_n(t) = \int_0^t \frac{P_n(t)}{w_{dn}} e^{-\xi_n w_n (t-\tau)} \sin(w_{dn}(t-\tau))d\,\tau\ ;$$

where

$$P_n(t) = -\frac{[\Phi_n]^T[M][R][\ddot{V}_g(t)]}{[\Phi_n]^T[M][\Phi_n]}$$

ξ_n is the viscous damping ratio associated with mode n, and

$w_{dn} = w_n\sqrt{1-{\xi_n}^2}$ is the damped frequency associated with mode n.

For a single acceleration impulse

$$Y_n(t) = \frac{1}{w_{dn}} \left(\int P_n(t)\, dt \right) e^{-\xi_n w_n t} \sin(w_{dn} t) \tag{2.9}$$

To study some of the effects of modal superposition, the case of a one-story system with small eccentricities (Equations 2.7 and 2.8) and similar damping ratios for all modes subjected to an acceleration impulse will be considered. In this case $e^{-\xi_1 w_1 t} \approx e^{-\xi_2 w_2 t} \approx e^{-\xi_3 w_3 t} \approx e^{-\xi w t}$. Then, the motion of the system has the following form for the global X or Y direction:

$$V_{x \text{ or } y} = e^{-\xi w t}(A \ \sin(w_{d1} t) + B \ \sin(w_{d2} t) + C \ \sin(w_{d3} t)) \tag{2.10}$$

where

A, B and C are constants.

The responses in the X and Y directions are a combination of three trigonometric series with closely space periods. As shown in Appendix A, the sum of these trigonometric series results in a strong modulation of the response, because of the constructive and destructive interference of each term in the series. The resulting "beating" phenomenon is often observed in the response of lightly damped mechanical systems with closely spaced coupled modes.

For small amounts of damping, w_{dn} can be approximated by w_n. Using formulae developed in Appendix A, and assuming that the trigonometric functions have similar characteristic amplitudes, the beating periods of the response can be approximated by

$$T_{B1} = T_{B2} = \frac{8\pi r}{we} \quad \text{and} \quad T_{B3} = \frac{4\pi r}{we} \tag{2.11}$$

and the apparent periods of oscillation are given by

$$T_{N1} = \frac{2\pi}{w\,(1 - (e/4r))}; \quad T_{N2} = \frac{2\pi}{w} \quad \text{and} \quad T_{N3} = \frac{2\pi}{w\,(1 + (e/4r))} \tag{2.12}$$

Assuming no torsional input motion, noting that

$$P_1(t) = -P_3(t)$$

and taking

$$\frac{P_1(t)}{w_1} \approx -\frac{P_3(t)}{w_3}$$

an estimate can be obtained for the rotational component:

$$rV_\theta = \sqrt{2}\frac{e^{-\xi w t}}{w_1} \left(\int P_1(t)\, dt \right) [\cos(wt) \sin(w\frac{e}{2r} t)] \tag{2.13}$$

for which the beating period is

$$T_B = \frac{4\pi r}{we} \tag{2.14}$$

and the apparent period of oscillation is

$$T_N = \frac{2\pi}{w} \tag{2.15}$$

It can be seen from Equations 2.11 to 2.15, that the response in each degree of freedom is characterized by a relatively rapid oscillation and a slowly varying amplitude envelope, typical of beating behavior.

2.4 Response of Coupled Systems: Examples

Some examples of the modal superposition effects on torsionally-coupled systems, subjected to simple acceleration impulses or more complex acceleration histories, are presented in Figs. 2.4 to 2.13. Five structural models are presented in these figures. The parameters of the models as related to the eigenvalue problem presented in Equation 2.2, are as follows:

- Model A: $(\frac{e_o}{r})^2 = 1.0$ and $\frac{e_x}{r} = \frac{e_y}{r} = 0.0$, m = 1 and no damping.
- Model B: $(\frac{e_o}{r})^2 + (\frac{e}{r})^2 = 1.0$ and $-\frac{e_x}{r} = \frac{e_y}{r} = 0.05$, m = 1 and no damping.
- Model C: $(\frac{e_o}{r})^2 + (\frac{e}{r})^2 = 1.1$ and $-\frac{e_x}{r} = \frac{e_y}{r} = 0.05$, m = 1 and no damping.
- Model D: $(\frac{e_o}{r})^2 = 1.062$ and $\frac{e_x}{r} = \frac{e_y}{r} = 0.0$, m = 0.125 and 1 and 5% modal damping.
- Model E: $(\frac{e_o}{r})^2 + (\frac{e}{r})^2 = 1.072$ and $\frac{e_x}{r} = -\frac{e_y}{r} = 0.072$, m = 0.125 and 1 and 5% modal damping.

The models were subjected to a triangular acceleration pulse of relative amplitude one and one time step duration, in the X direction, and alternately, -1, 0 or 0.85 in the Y direction. In addition, Models D and E were also subjected to the two base acceleration records obtained at CSMIP Station 57357 (the case study building) during the 1986 Mt. Lewis earthquake. Further descriptions of these records can be found in the following chapters and in Appendix C.

Responses of the models to these input motions are shown in Figs. 2.4 through 2.13. Figures 2.4, 2.10 and 2.12 present the response of the uncoupled Models A and D for a bidirectional pulse and the ground acceleration histories. Figures 2.5 through 2.13 present the response of the coupled models for different input combinations. The displacement histories shown were obtained at the "center of mass" of the system.

Some important results are observed from these figures.

- Small eccentricities between the center of mass and stiffness result in coupled lateral and torsional responses, and large modifications of the response envelope (amplitude and apparent duration) relative to the associated uncoupled system.

- The response of coupled systems is sensitive to small changes in the uncoupled periods. For example, compare the responses of Model B (Fig. 2.5) and Model C (Figs. 2.6).

- The coupled models subjected to a unidirectional pulse (X=1 and Y=0), Figs. 2.5 and 2.6, exhibited a modulated response envelope in the direction orthogonal to the input motion (Y direction). The envelope in this direction starts from zero and reaches a first maximum after several cycles of the apparent natural period of the signals. The number of cycles that the structure has to undergo to reach this first maximum can be estimated in the following manner. The beating and the apparent natural period present on the response of the system can be estimated from the following equations (developed in Appendix A) for the interaction of two trigonometric signals with natural periods T_1 and T_2 ($T_1 > T_2$).

  The period of the envelope modulation (beating)

$$T_B = \frac{2T_1T_2}{T_1 - T_2} \tag{2.16}$$

  and the apparent natural period

$$T_N = \frac{2T_1T_2}{T_1 + T_2} \tag{2.17}$$

  The number of cycles to reach the first maximum in the response can then be estimated as

$$\frac{1}{4}\frac{T_B}{T_N} = \frac{T_1 + T_2}{4(T_1 - T_2)} \tag{2.18}$$

  and the time needed to reach this point is $T_B/4$. It can be observed that the time of occurrence of the maximum increases rapidly as modal periods approach one another.

  It must be recognized that damping could have a strong effect on the overall elastic response of such systems by diminishing the amplitude of the oscillations in each mode before the maximum superimposed response of the undamped system is reached. As an example, Figure 2.9 shows the decay envelope for a single oscillating signal for different percentages of critical damping. For free oscillations of systems with little (1% of critical) or no damping the attenuation of the response is not sufficient to invalidate the trends suggested by the equations presented above. However, for moderate amounts of damping (5% of critical), the beating and modal reinforcement are not as noticeable.

- The response characteristics of coupled systems, subjected to multi-dimensional input, depend strongly on the relation between the direction defined by the vector between the centers

of mass and stiffness and the "predominant direction" of the input motion. Figures 2.6 through 2.8 present the response of Model C to a combination of impulses in both directions (X=1, Y=-1, 0 and 0.85). It can be observed from these figures that the torsional response increases or decreases depending on the combination of impulses used. The envelopes of the translational components of motion are also greatly modified, but the responses are never larger than those obtained for the associated uncoupled system.

- The response of the coupled model to an earthquake record is more complex. Figures 2.10 through 2.13 show that the effect of coupling tends to increase considerably the response of the lightly damped system (Model E, 1% of critical) after the maximum has been attained in the associated uncoupled model. This effect is caused by modes of the structure constructively reinforcing each other. The system with higher damping (Model E, 5% of critical) is not affected by this constructive modal reinforcement as expected from the observations made above for the systems subjected to impulse loads.

2.5 Conclusions

In this chapter the closed form solution for the predominant periods and mode shapes of a coupled, linear, three degree-of-freedom system were derived in terms of the basic dynamic properties of an associated uncoupled system and the eccentricity between the centers of mass and stiffness present in the system. The form of this solution and the responses of the coupled systems studied indicate the following:

- The natural periods of a coupled system are smooth functions of the eccentricity between the centers of mass and stiffness and the ratio of the uncoupled translational and torsional periods of the associated uncoupled system.
- Systems with small eccentricities and similar uncoupled periods have closely spaced natural periods.
- Systems with coupled modes, closely spaced predominant periods and low damping can increase considerably the severity (effective duration and amplitude) of the response because of modes constructively reinforcing one another.
- Damping has a strong effect in modifying the duration and the amplitude of the response of the coupled system, especially in the free decay portion of the response.
- The orientation of the eccentricity with respect to the "predominant direction" of the multi-directional input has a strong effect on the response of coupled systems.

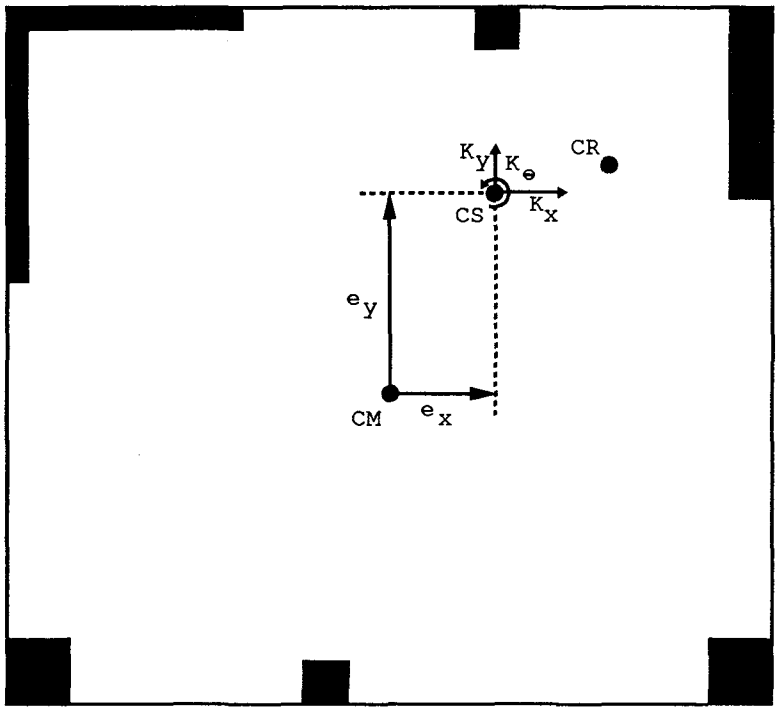

Figure 2.1: One story plan definitions.

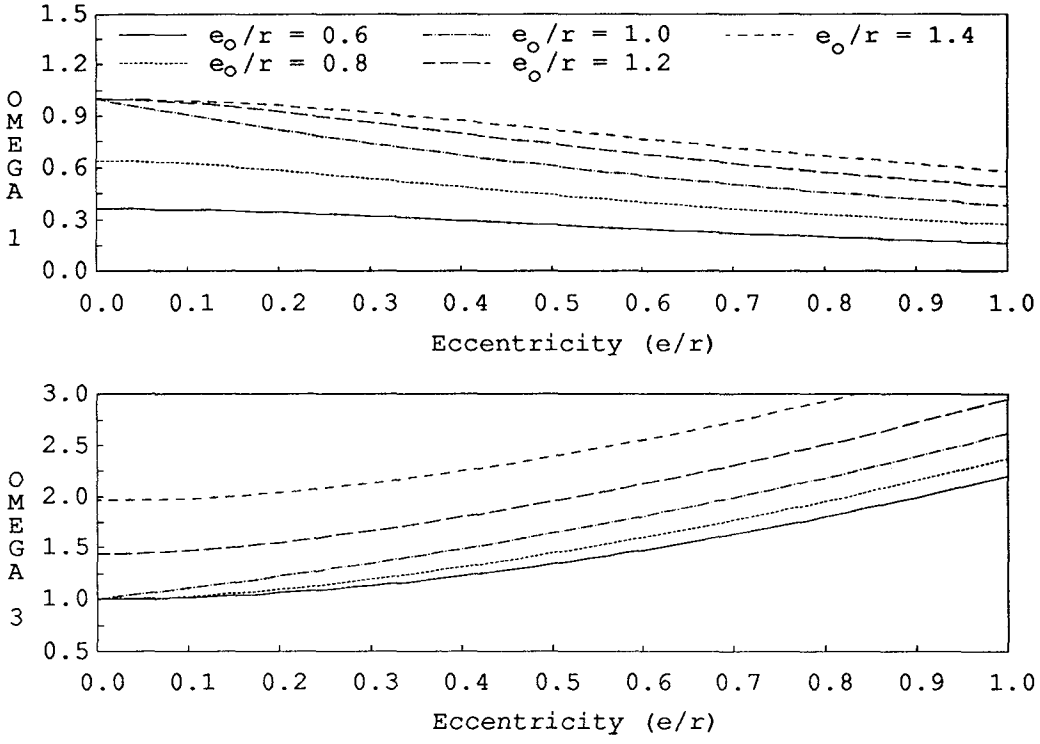

Figure 2.2: Ratio of coupled to uncoupled frequencies as a function of $(e_o/r)^2$ and $(e/r)^2$.

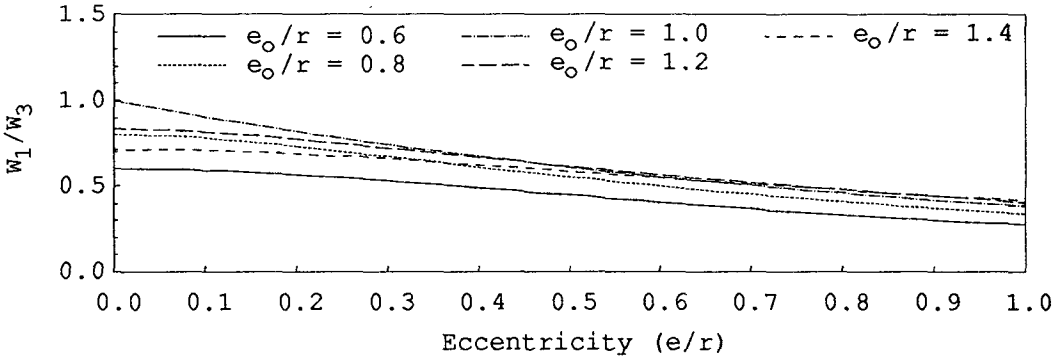

Figure 2.3: Ratio of coupled frequencies as a function of $(e_o/r)^2$ and $(e/r)^2$.

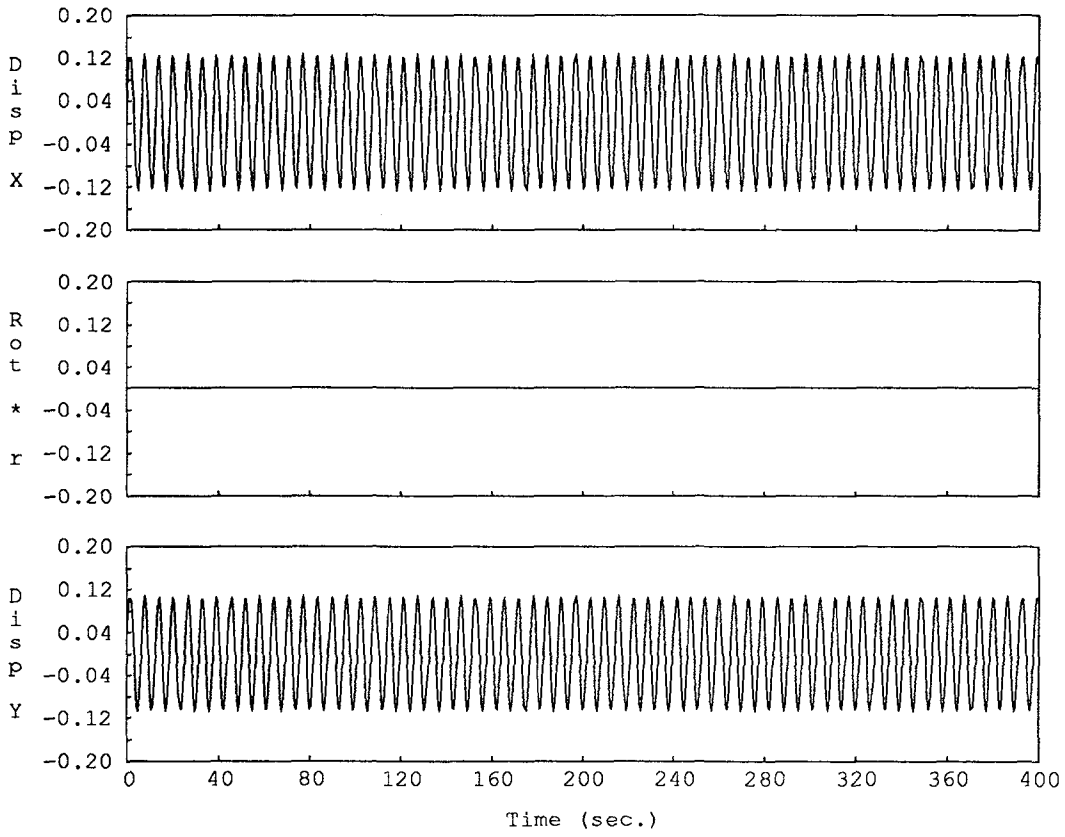

Figure 2.4: Model A. Bidirectional acceleration impulse input, X=1.00 Y=0.85.

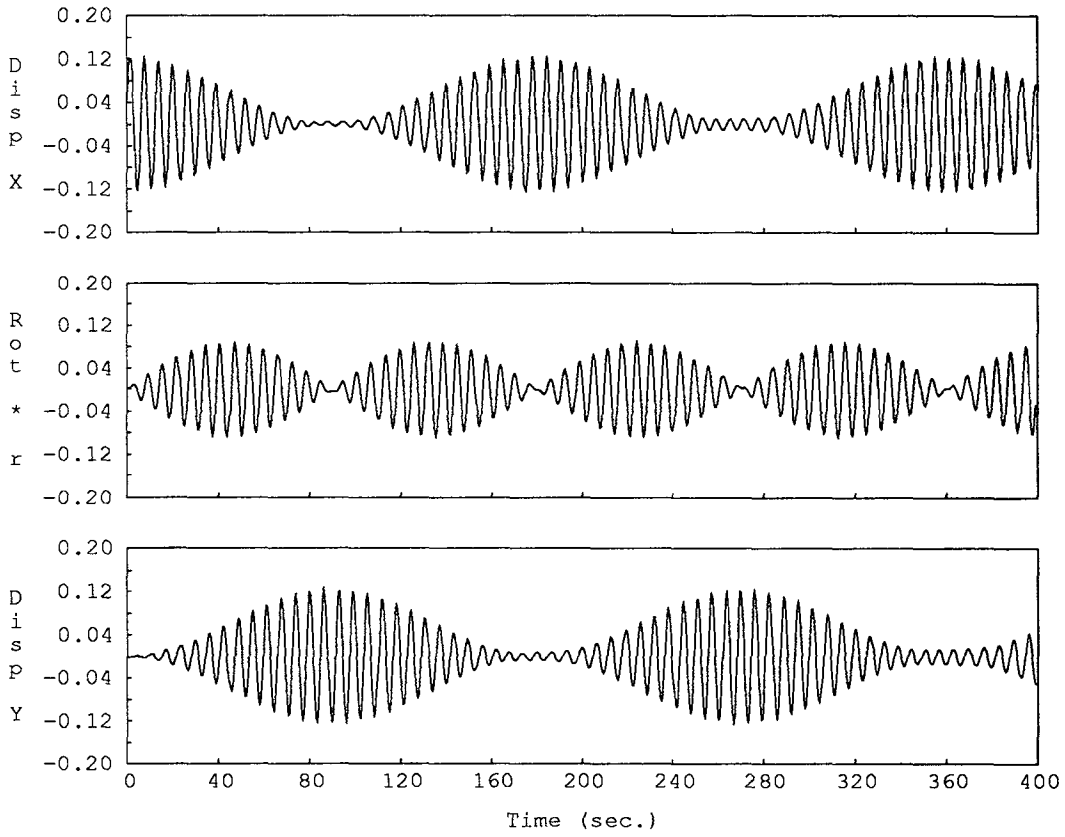

Figure 2.5: Model B. Unidirectional acceleration impulse input, X=1.00 Y=0.00.

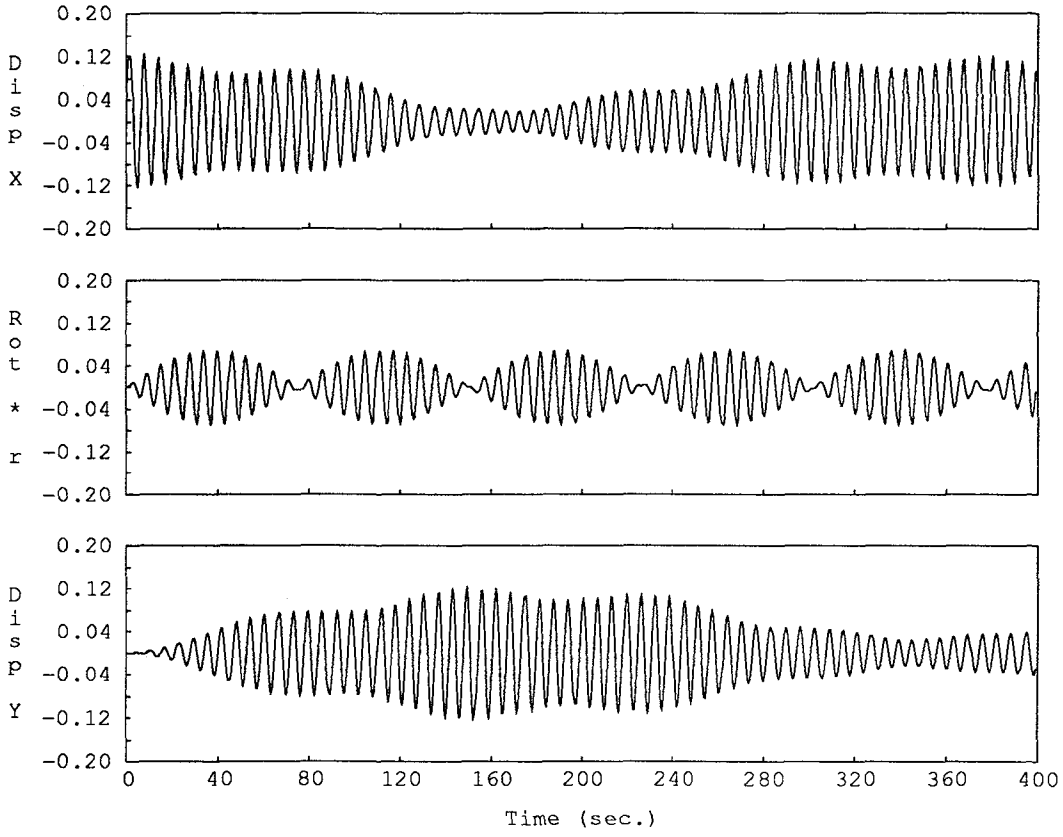

Figure 2.6: Model C. Unidirectional acceleration impulse input, X=1.00 Y=0.00.

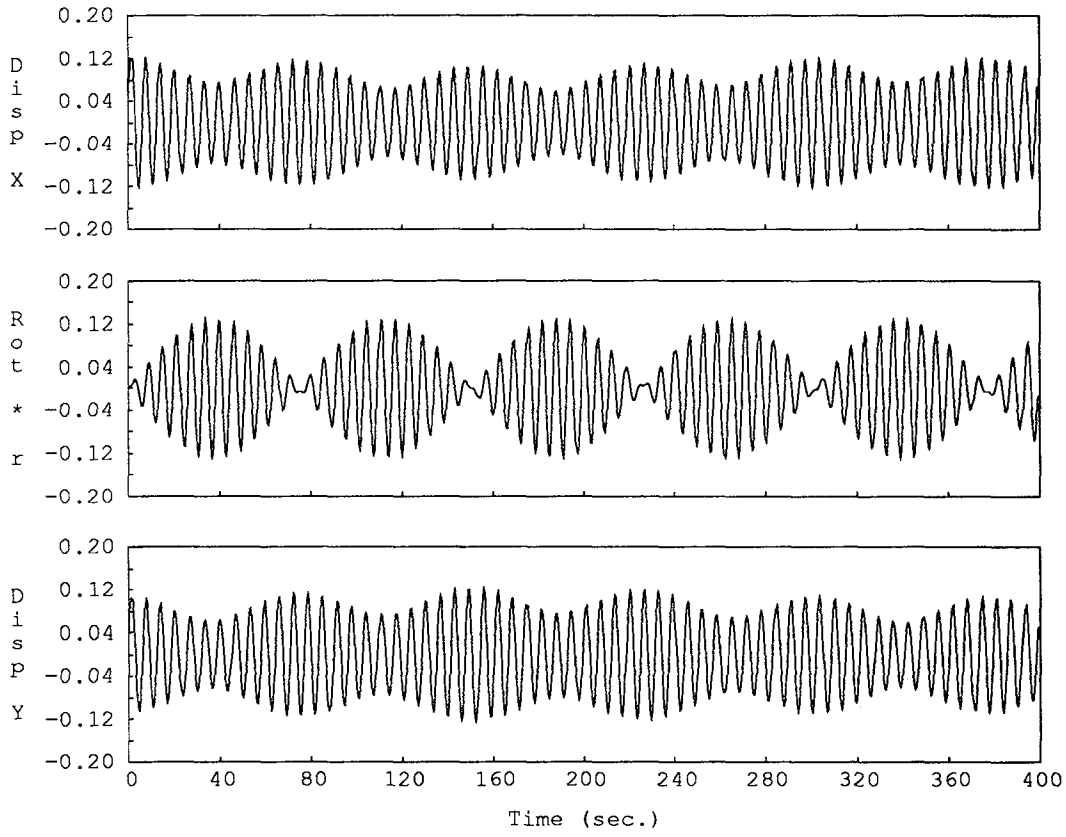

Figure 2.7: Model C. Bidirectional acceleration impulse input, X=1.00 Y=0.85.

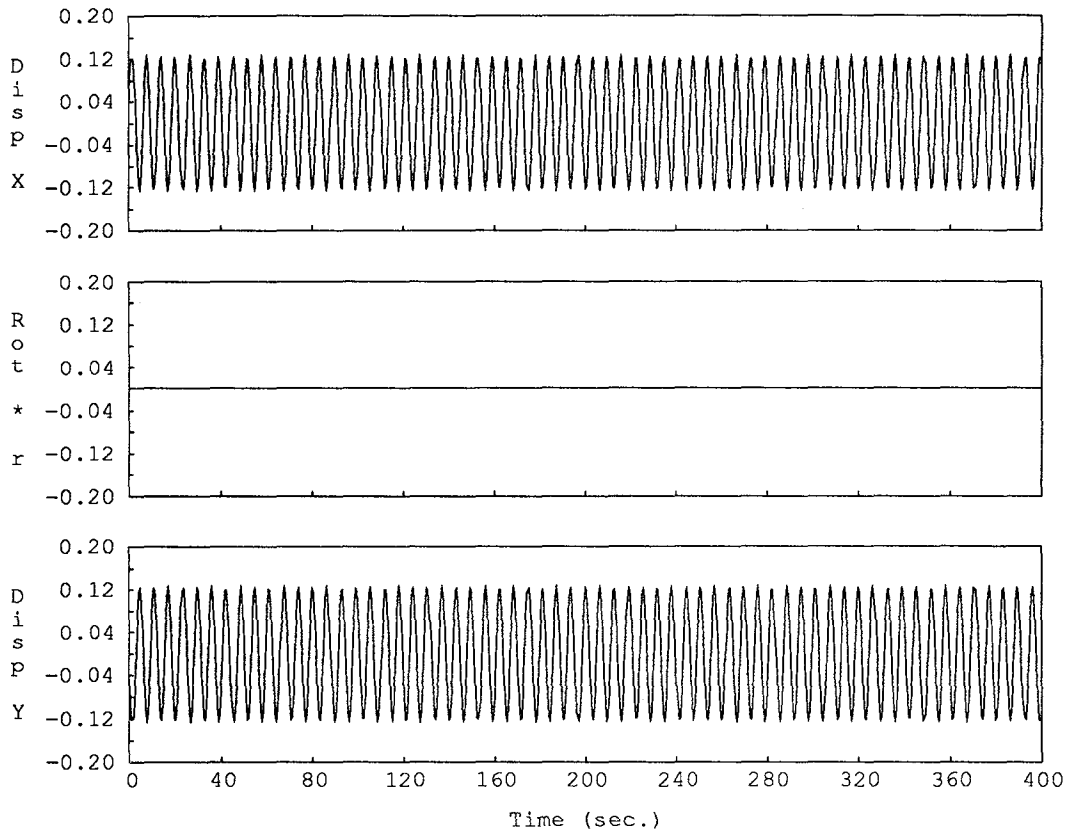

Figure 2.8: Model C. Bidirectional acceleration impulse input, X=1.00 Y=-1.00.

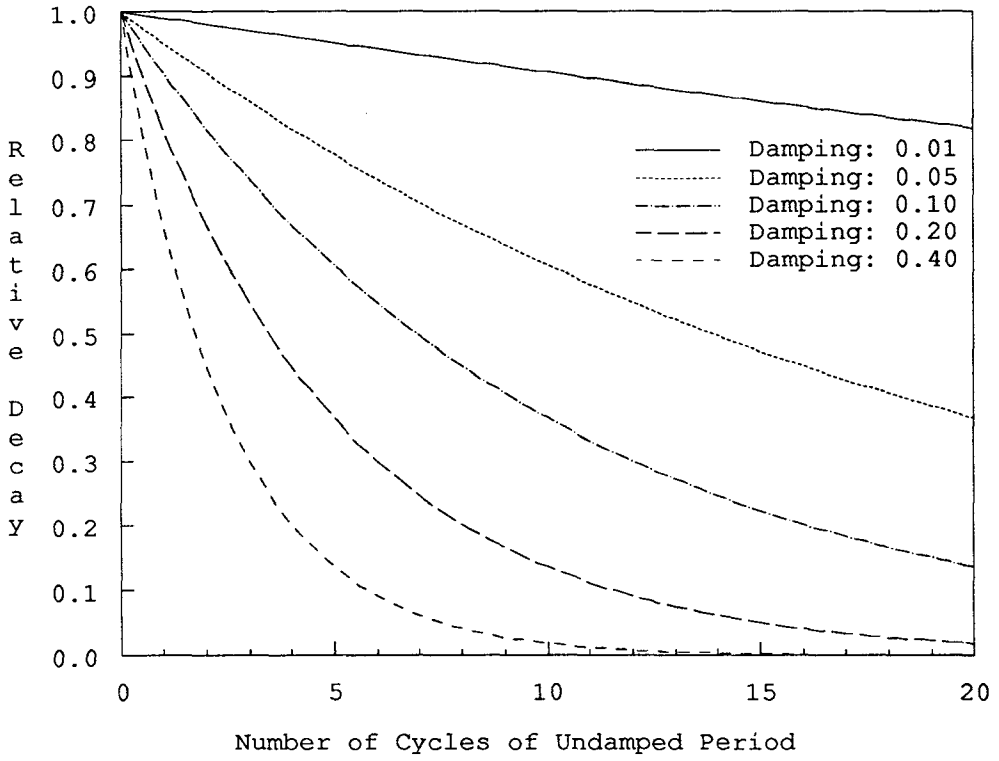

Figure 2.9: Decay of response envelopes for different values of damping.

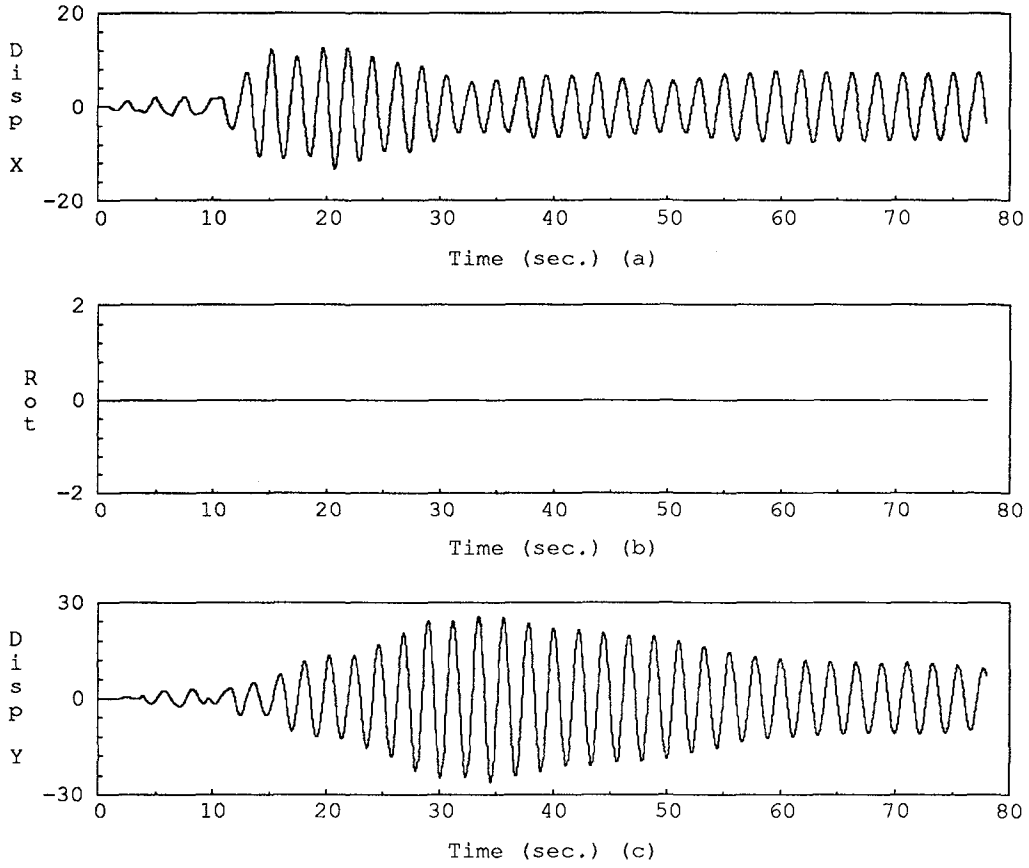

Figure 2.10: Model D. Viscous damping 1% of critical. Bidirectional input. From 1986 Mt. Lewis earthquake at CSMIP station 57357.

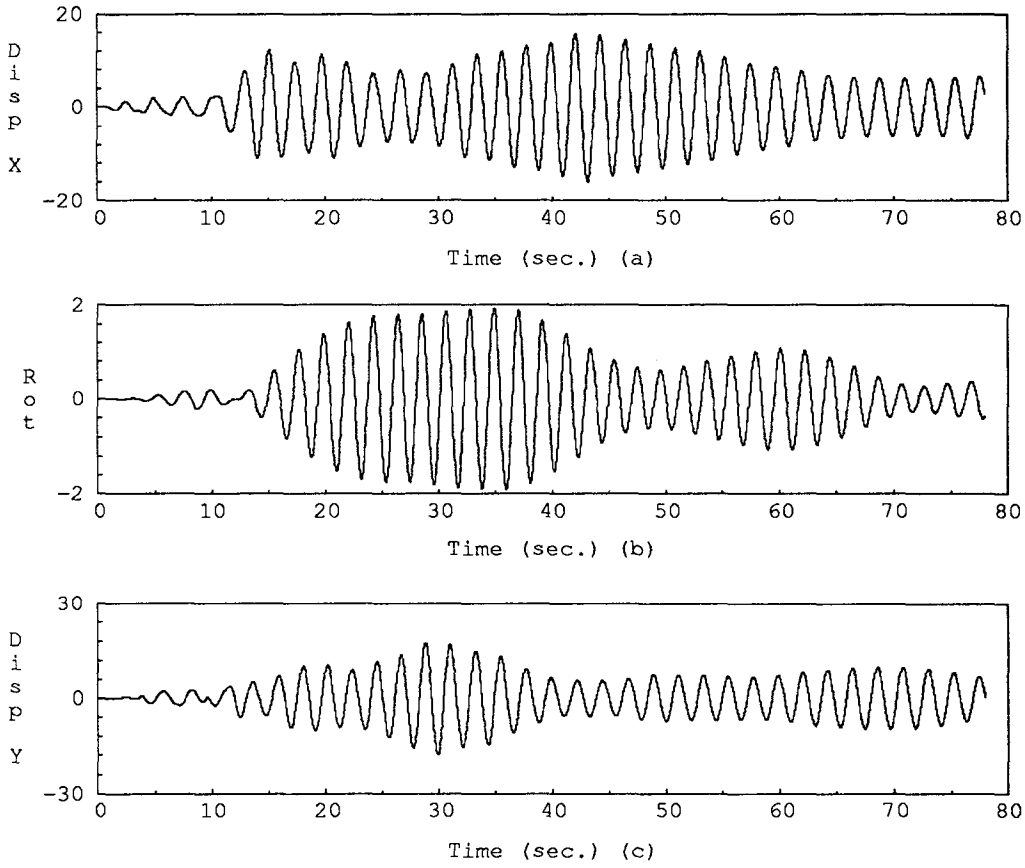

Figure 2.11: Model E. Viscous damping 1% of critical. Bidirectional input. 1986 Mt. Lewis earthquake at CSMIP station 57357.

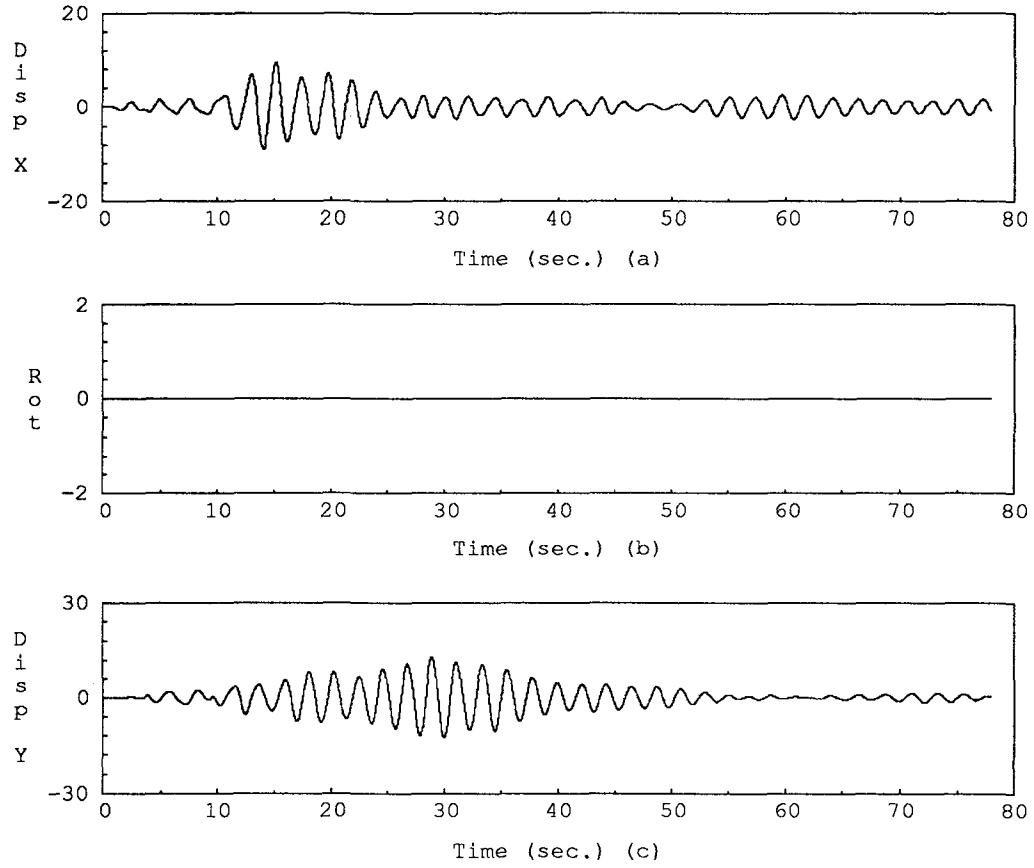

Figure 2.12: Model D. Viscous damping 5% of critical. Bidirectional input. From 1986 Mt. Lewis earthquake at CSMIP station 57357.

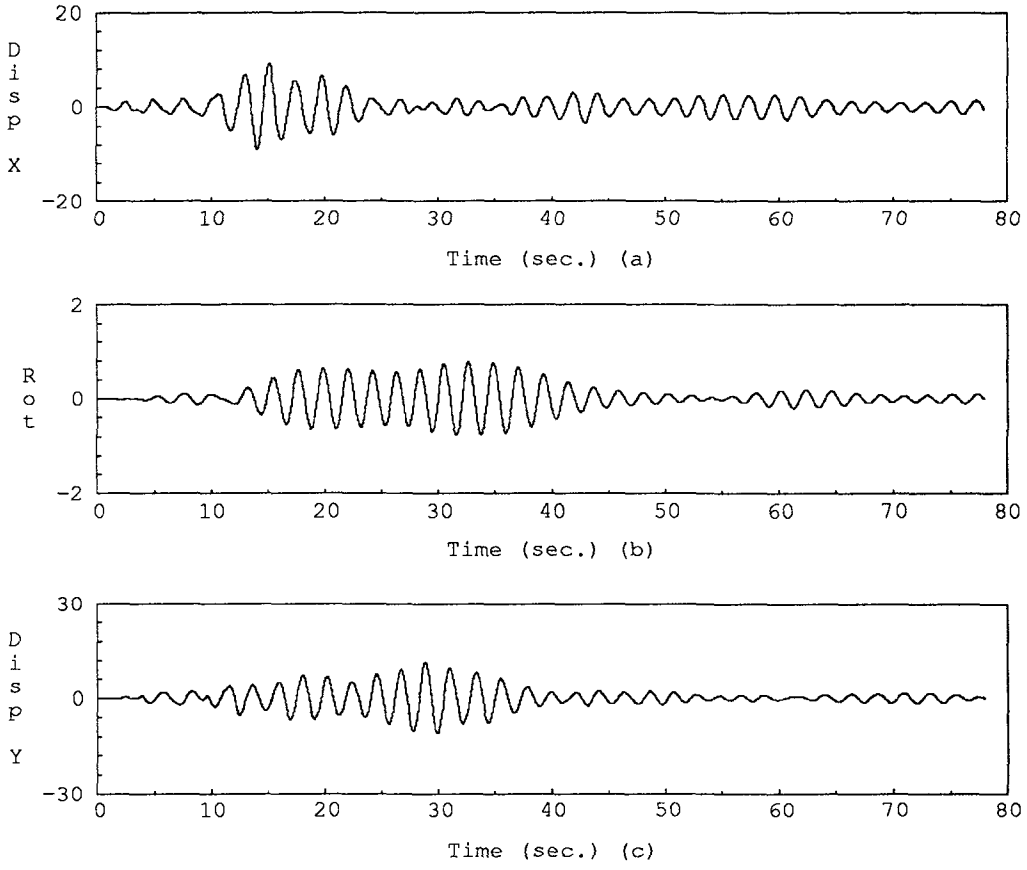

Figure 2.13: Model E. Viscous damping 5% of critical. Bidirectional input. From 1986 Mt. Lewis earthquake at CSMIP station 57357.

CHAPTER 3

CASE STUDY BUILDING AND SITE DESCRIPTION

3.1 Building Location and Structural Characteristics

The building studied (shown in Fig. 1.1) is located at 70 West Hedding Street, San Jose, California (Coordinates : 37.353 N, 121.903 W). It is a thirteen-story steel building designed in 1972 and constructed between 1975 and 1976. It has a nearly rectangular base and floor plan with external dimensions 52.7 x 50.9 meters (173 x 167 feet) at the base and 50.9 x 50.9 meters (167 x 167 feet) at a typical floor. Story heights are 4.1 meters (13 feet 6 1/2 inches), Fig. 1.2.

The vertical load carrying system consists of an 8.9 cm (3 1/2 inches) thick light-weight concrete slab on a metal deck supported on steel beams, girders and columns. The lateral force-resisting system consists of four interior moment frames in each orthogonal direction and a perimeter moment-resisting frame with tapered girders. The perimeter frame is aligned along lines B, M, 2 and 12 in Fig. 3.1. Structural steel for the main members is ASTM A572 Grade 50; for other members it is ASTM A36.

Interior floor girders are typically 53 cm (21 inch) deep wide-flange sections and most perimeter frame girders are built-up members, Fig. 3.2. The elevation of the tops of the interior girders oriented in the EW direction and of all of the perimeter girders is 91 cm (3 feet) below the nominal floor level. The floor deck system is oriented in the EW direction. Because of this floor framing system, only the NS oriented girders are in contact with the floor deck. An additional set of NS oriented beams at floor level is provided between column lines. These beams are supported on a short stub-column resting at the midspan on the EW oriented girders, as shown in Fig. 3.3. Full composite action, between girders and floor slab is not expected because shear connectors are not provided. Typical connections between deck and floor girders are specified as 1.9 cm (3/4 inch) plug welds in each trough.

Columns are typically 35 cm (14 inch) wide-flange sections with full height, 1.9 cm (3/4 inch) thick cover plates provided to form a box column. Heavy built-up box columns are provided at the corners of the perimeter frame. Typical frame connections on the perimeter and interior frames are moment resisting. Joint plate stiffeners and cover plates are provided (2.9 cm (1 1/8 inch) thick), Fig. 3.4.

An additional external bent is supplied along each of the West and South sides of the building to accommodate elevators, stairs and enclosed offices. Lighter steel framing elements are

found in this area. Some connections for the EW oriented beams in this area are only shear resisting.

A mat foundation is provided to support the structure. A typical interior and perimeter frame footing detail is shown in Fig. 3.5. Base plate dimensions are generally 91 x 91 x 10 cm (3 x 3 x 1/3 feet). Welds are specified between column and base plate. No plate stiffeners are indicated on the plans.

The exterior of the building is covered on the West and South sides with corrugated weathering steel siding attached by clips. The East and North sides are covered with glass curtain walls. The building interior is generally open except on frame lines A, B, 12 and 13, (Fig. 3.1), where partitions are provided. Typical partitions consist of gypsum wall boards or perforated metal sheathing.

Using building plans and site inspection the dead weight of the building was estimated as 4788 N/m^2 (100 psf). Considerable additional weight is present in the structure because of the existence of large amounts of stored material.

The structural and architectural drawings for the building are available from the California Division of Mines and Geology, Strong Motion Instrumentation Program.

3.2 Site Soil Characteristics

The building is situated in the Santa Clara Valley. The valley is characterized by deep alluvial deposits [9, 45, 53, 54]. A detailed evaluation of the near-surface soil characteristics was obtained from three soil studies carried out by Woodward-Clyde-Sherard Associates [53, 54] and Earth Sciences Associates [9]. The latter study classified the first 15 meters (50 feet) of soil as stiff to very stiff brown clay with an average undrained shear strength of 96 kPascal (2000 psf). Layers of sand and gravel were found beneath the clay.

Depth to bedrock in the area is not known exactly. Nonetheless, well boring logs obtained near the structure indicate that the depth is at least 244 meters (800 feet) [45]. Other reports suggest that bedrock could be located as deep as 460 meters (1500 feet) [9].

Microtremor studies by Gibbs and Borcherdt [13] provide additional information on site characteristics. It can be concluded from their work that predominant periods around 2 seconds could be expected at sites close to the building. Also, transfer functions presented in their investigation at nearby sites show higher spectral amplitudes in the NS direction than in the EW direction, for periods over one second. This signal directionality could be related to the underlying geologic structure of the valley (approximately aligned in the NS direction [54]), but it could also be related to the direction of the incoming waves considered in their studies.

Further evidence of this characteristic directionality and of the site periods can be found

on response spectrum plots derived from strong motion records at SMIP stations No. 57355 and 57356 during the 1984 Morgan Hill, 1986 Mt. Lewis and 1989 Santa Cruz Mountains earthquakes, Fig. 3.6. These records were obtained at the base of two, ten-story structures located close ($\approx$ 2 km) to the case study building. Although the ground motion records were modified by the building motion [7] it appears that above 1 second the period content in the records was not severely affected, since the values of the fundamental periods of the building for SMIP station No. 57355 are 0.6 second in the EW direction and 0.95 second in the NS direction and, for SMIP station No. 57356, 0.5 and 0.7 second, for the EW and NS directions, respectively, [7]. Also, the close agreement between recording stations for periods above 1 second can be noticed from these spectra. A more detailed study is required to assess more definitively the dynamic characteristics of the site.

3.3 Sensor Layout

Twenty-two analog accelerometers are installed in the case study structure [SMIP Station No. 57357]. These accelerometers are connected to two separate central recording units. The nominal time difference between the recording systems is 0.1 second [20]. The accelerometers are distributed, as shown in Fig. 1.2, with

- three vertical accelerometers at the base located at the NW, SW and SE corners,
- three horizontal accelerometers at the base, with two in the EW direction and one in the NS direction, and
- four horizontal accelerometers at the second, seventh and twelfth floors and at roof level, with two in the EW direction and two in the NS direction.

This sensor layout permits the evaluation of such response features as drift, torsional motion, modal characteristics, roof amplification, in-plane floor slab deformation and foundation rocking.

A free-field instrument had been installed, but the owner requested that it be removed shortly before the Morgan Hill event. It was re-installed following the Loma Prieta earthquake.

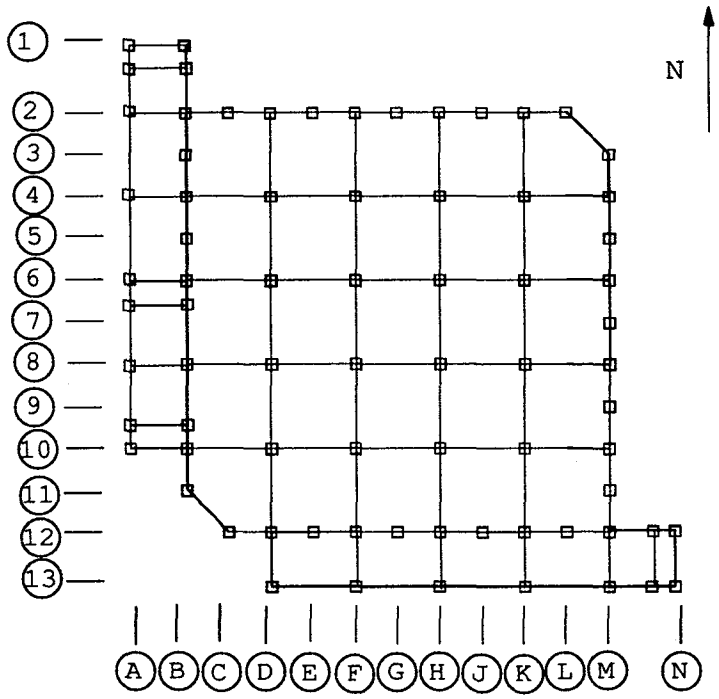

Figure 3.1: Building plan and framing.

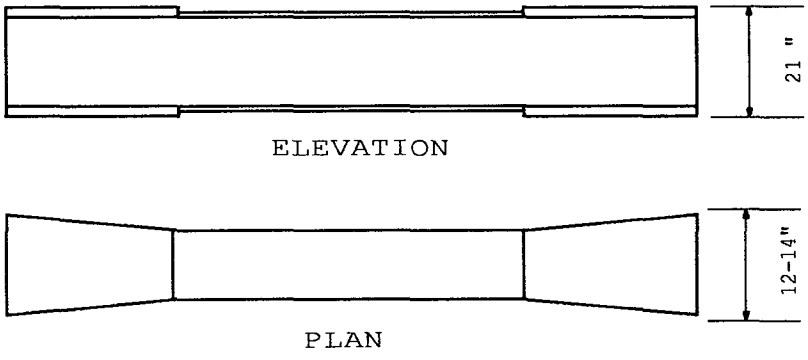

Figure 3.2: Typical perimeter frame tapered girder.

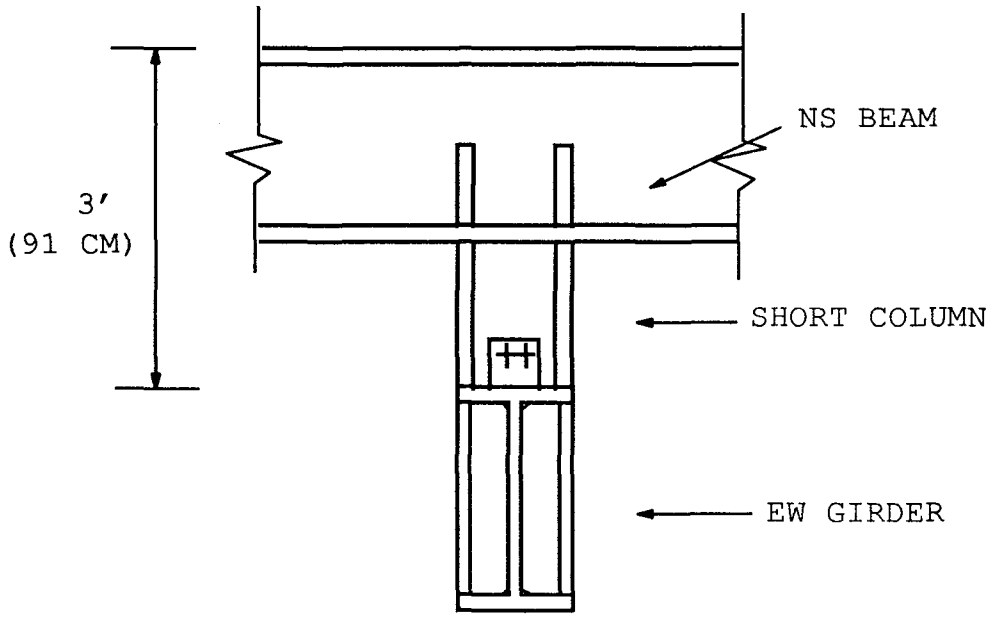

Figure 3.3: Connection detail at mid-length of NS and EW oriented beams.

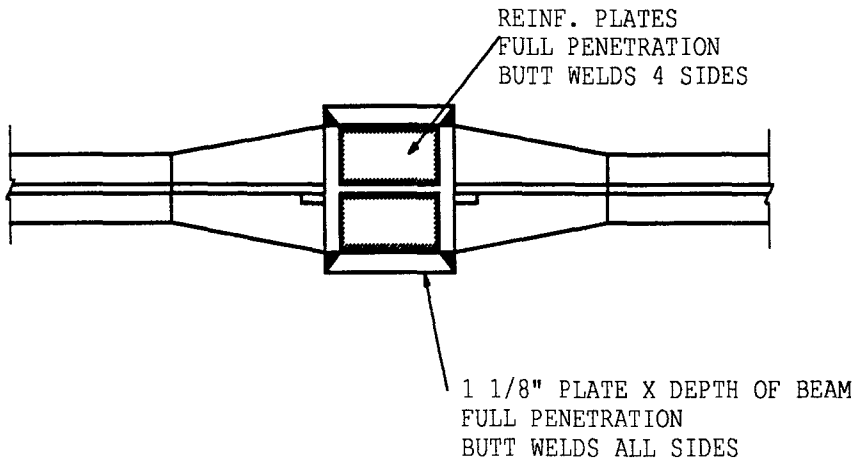

(a)

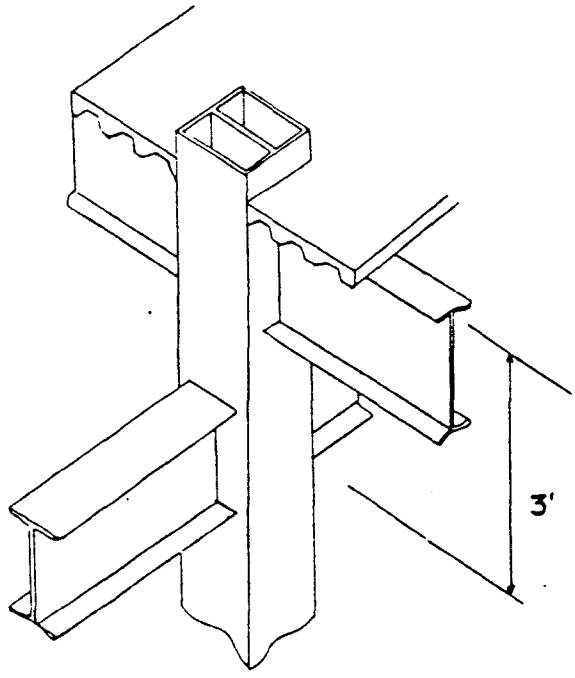

(b)

Figure 3.4: (a) Joint detail on perimeter frame. (b) Typical interior frame joint.

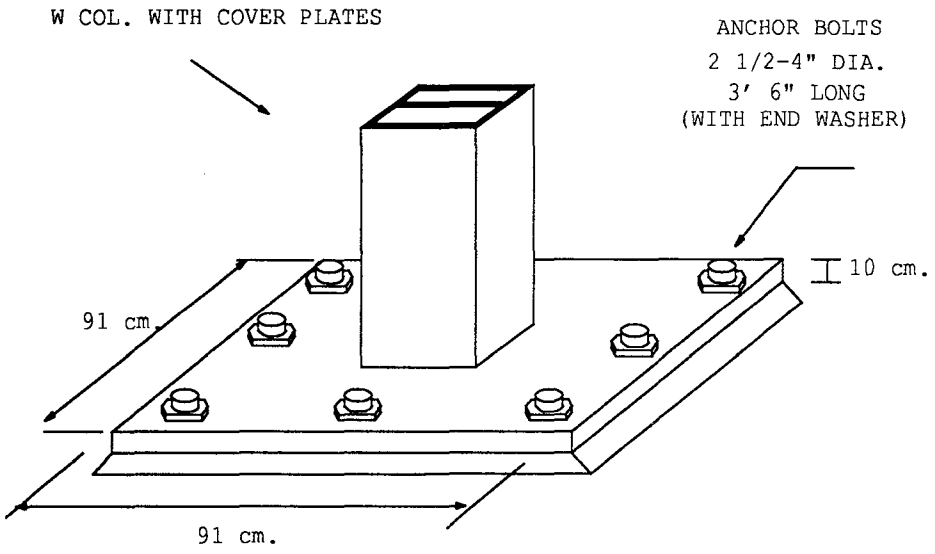

Figure 3.5: Typical base plate detail.

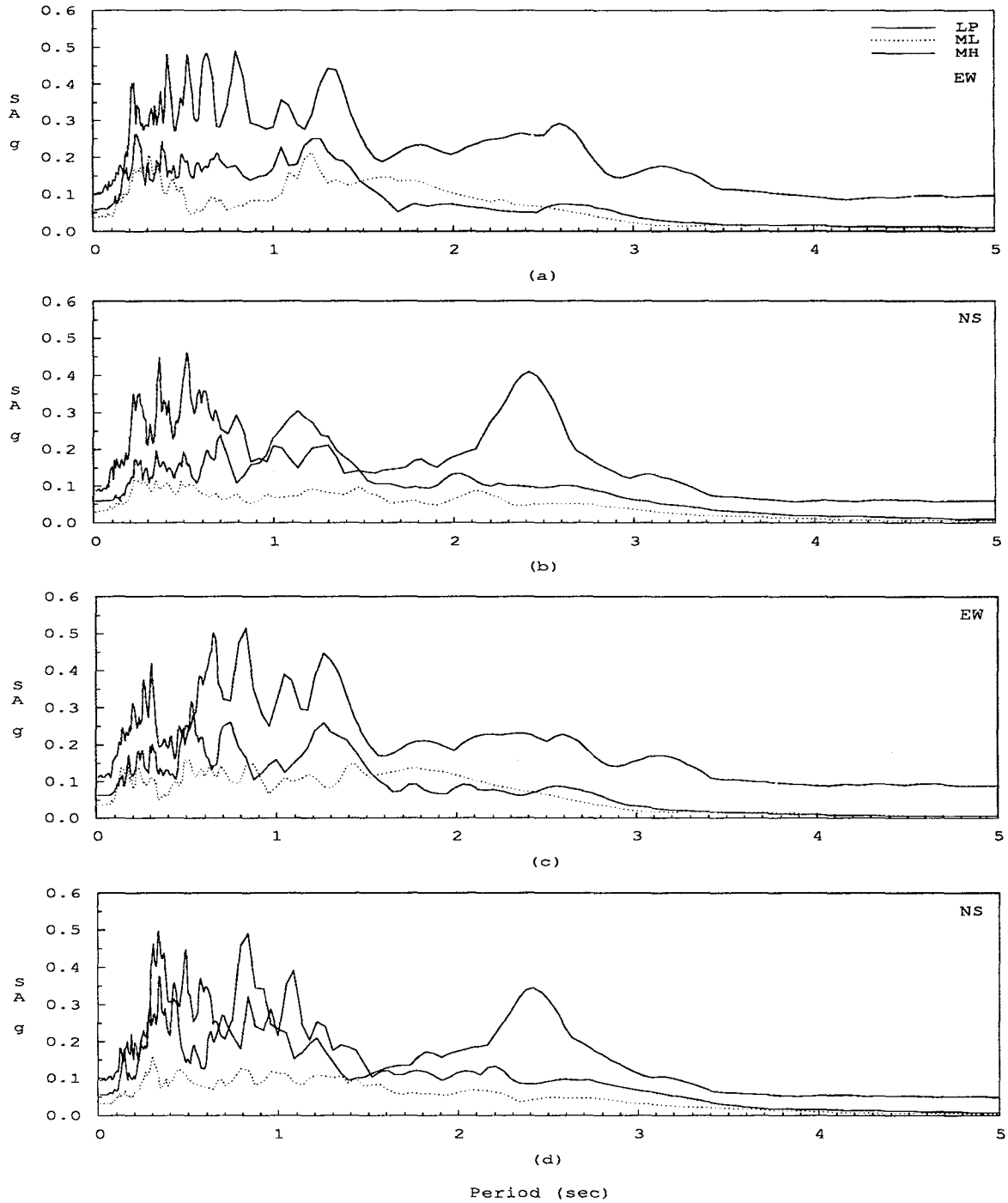

Figure 3.6: Acceleration response spectra, 2% damping. (a) SMIP station 57355 EW base records. (b) SMIP station 57355 NS base records. (c) SMIP station 57356 EW base records. (d) SMIP station 57356 NS base records.

CHAPTER 4

DYNAMIC CHARACTERISTICS AND RECORDED RESPONSE

4.1 General

The building studied has been subjected to several earthquakes. Its recorded responses during the Morgan Hill (1984), Mt. Lewis (1986) and Loma Prieta (1989) earthquakes, are described below. These events caused major disruption to the contents and occupants of the building, but only minor damage to non-structural elements.

The basic response values presented in this chapter were obtained using CSMIP acceleration records and derived velocity and displacement histories. No analytical models of the structure were used for this part of the investigation. A series of specialized programs for vector manipulation, frequency domain analysis (Fourier amplitude spectra, transfer functions, moving window Fourier amplitude spectra and power spectral densities) and animation were developed and used to reduce the large amounts of data available for the building [5].

4.2 Earthquake Records

Three different sets of earthquake records were considered to evaluate the behavior and dynamic characteristics of the building. The first earthquake, designated Morgan Hill, occurred at 13:15 local time (21:15:19 GMT) on April 24, 1984. The epicenter of this magnitude 6.2 (M_l) event was South-East of the building, at 37.31 N and 121.68 W; a focal depth of 8.4 km (5.3 miles) was reported [20]. The second earthquake, designated Mt. Lewis, occurred at 3:56 local time (11:55:40 GMT) on March 31, 1986. This earthquake was somewhat smaller, $M_l = 5.8$; it was located more to the North (37.466N, 121.69W), and had a shallower focus, 6.5 km (4.1 miles). The third earthquake, designated Loma Prieta, occurred at 17:04 local time (00:04:02 GMT) on October 17, 1989. The epicenter of this magnitude 7.1 (M_l) earthquake was South-West of the building, at 37.037N and 121.883W; with a focal depth of 18 km (11 miles) [48]. The distances from the epicenter to the building were 21, 23 and 35 km (13, 14 and 22 miles) for the Mt. Lewis, Morgan Hill and Loma Prieta earthquakes, respectively.

4.3 Record Processing and Description

The records from the earthquakes studied were processed by CSMIP using standard procedures [20]. An Ormsby filter, with low and high-band pass ramps of 0.20-0.30 and 23-25 Hz, respectively, was used for the Morgan Hill and Mt. Lewis earthquakes. For the Loma Prieta earthquake the filter ramps were 0.12-0.24 and 23.0-25.0 Hz, respectively. These filter ramps generated records with an expected signal-to-noise ratio higher than 10 to 1. According to SMIP [20], the use of a low ramp near 0.25 Hz gives a reliability of about 1.5 cm/sec/sec (0.0015 g) and 0.1 cm (0.04 inch) for absolute accelerations and displacements, respectively, Fig. 1.9.

In this study, records from the horizontal sensors are denoted by a symbol indicating their recording orientation, followed by the floor level and the side of the building where the instrument was installed. Thus, EW/r/S refers to the East-West direction roof record obtained on the South side of the building. The records from the vertical sensors at the foundation level are specially identified using the letters "VER" and the corner where the sensor is located. Thus, VER/NW is the vertical record obtained in the North-West building corner. Table 4.1 list the different positions of the sensors.

Analysis of the records indicated the presence of a time shift between signals. As an example of this time shift, the absolute acceleration at the EW/7/N station was calculated using the other three recordings obtained at the floor level and the assumption of an in-plane rigid diaphragm. Channel EW/7/N was stored on a different recorder than the other sensors on the floor. The calculated and recorded motions are presented in Fig 4.1. The systematic time shift observed in this figure can be associated with the presence of two recording units and/or the difference in setting the beginning of each record trace at the time of processing. The presence of this time shift will have an effect on the identification of higher modes from transfer functions and in-plane diaphragm deformations. Correction of this time shift was not accomplished in this investigation. No other appreciable recording or processing errors were observed from the records studied.

4.4 Dynamic Characteristics

4.4.1 General

The strong building response during the earthquakes considered allowed identification of several modal parameters and the investigation of other important dynamic response characteristics of the structure.

4.4.2 Natural Periods and Mode Shapes

Several analyses in the time and frequency domain were performed on the response records to estimate the natural periods of the structure. Some results are presented in Table 4.2 and in Figs. 4.2, 4.3, 4.4.

Because of apparently small mass and stiffness eccentricities present in the structure, the building exhibited coupled lateral-torsional responses and beating during the excitations studied. The periods that correspond to the three-dimensional modes participating in the response can be identified from the Fourier amplitude spectra computed for the roof records during the Morgan Hill earthquake, Fig. 4.2. Similar results are found from the other earthquakes. Figures 4.2(b) and 4.3 show the Fourier amplitude spectra for the EW roof and twelfth floor records. Here, the two peaks between 2.2 and 2.0 seconds denote the first two three-dimensional modes. The predominant direction of these modes can be obtained directly from Figs. 4.2(c) and (d). The figures indicate that the shorter period (2.0 sec) corresponds to the NS direction and the longer one (2.2 sec) to the EW direction. The predominantly torsional period is observed in these figures with its peak near 1.7 seconds. It is important to note from these figures that the amplitude of this "torsional" peak is much larger for motions recorded at the NW and SE corners than for the SW corner, indicating that the eccentricities present cause the structure to have higher torsional deformation in these areas. Fourth and fifth predominant periods are observed between 0.6 and 0.7 second. The period estimates are summarized in Table 4.2.

The closeness of the natural periods obtained for this building is typically associated with structures with similar structural systems in orthogonal directions and a uniform distribution of the stiffness in plan (see Appendix B). For example, for "regular" one-story shear frames (as defined in Appendix B), the square of the ratio of the uncoupled translational and torsional predominant period $\left((T_{ux} \,/\, T_{u\theta})^2\right)$ is given by

$$\left(\frac{T_{ux}}{T_{u\theta}}\right)^2 = \frac{[(d_x/d_y)^2(k_y/k_x)({N_x}^2-1)+({N_y}^2-1)]}{(N_x-1)^2(d_x/d_y)^2+(N_y-1)^2} \tag{4.1}$$

where

$N_{x\ or\ y}$ is the number of column lines in the x or y direction. This value must be greater than one.

$d_{x\ or\ y}$ is the spacing between two consecutive columns in the x or y direction;

$k_{x\ or\ y}$ is the effective stiffness of a column in the x or y direction; and

$T_{u\theta\ or\ ux}$ is the uncoupled natural torsional or translational period.

For the special case of a building with identical element stiffness and number of elements in the X and Y directions, this formula is simplified since

$N_x = N_y = N$, $k_x = k_y$ and N > 1.

Then,

$$\left(\frac{T_{ux}}{T_{u\theta}}\right)^2 = \frac{(N+1)}{(N-1)} \tag{4.2}$$

This ratio quickly approaches unity, as the number of columns increases, Fig. B.2. Equation 4.2 for 6 column lines gives a ratio of 1.4, and for 10 column lines it gives a ratio of 1.2. These values could give an indication of the uncoupled period of the structure. Because the eccentricities present in the building are not known, the "uncoupled periods of the structure" cannot be found, but they are expected to be relatively close to the coupled period of the structure. The ratio of coupled periods for the building is 1.3 (2.2/1.7).

Because of the three-dimensional nature of the motion and the closeness of the natural modes, a clear identification of the different mode shapes cannot be obtained with the simple non-parametric techniques used here. Nevertheless, from drift plots presented later (c.f. Section 4.5.3), a shear deformed shape, typically associated with frame structures, is apparent. Some irregularities in the displaced shape occur at the roof level. These are apparently related to a change in vertical structural elements that occurs at the twelfth floor, and the effect of the higher modes.

A comparison of the Fourier spectra, moving window Fourier amplitude spectra and response spectra for the different earthquakes, presented in Fig. 4.4, shows no significant change in building response periods during the earthquakes. This indicates that no appreciable yielding occurred in the structure during these events.

As indicated above, because of the difference in the time base for each record, it was expected that higher modes would be difficult to identify using transfer function techniques. Nonetheless, it was found from the Fourier amplitude spectra, that most of the response was controlled by the first five three-dimensional modes, which were clearly identified.

4.4.3 Damping

Because of the closeness of the natural modes, damping could not be accurately estimated from the records. On the basis of the long duration response and the slow decay of the response envelope, it is believed that damping is about 2-4% for the predominant modes; see Table 4.2. Lin and Papageorgiou [30] applied system identification techniques based on a modal minimization method to a three-dimensional model of the structure. They found that the damping for the first mode varied during the Morgan Hill earthquake from 0.2% to 12.1%. For the second mode the damping value varied from 1.0% to 3.7%. These values should be interpreted with caution, because of the difficulty of determining damping in highly-coupled systems [4].

4.5 Building Response

4.5.1 General

In general, the structural response to the events studied was characterized by a long duration, narrow-banded, periodic motion with strong amplitude modulation, by large lateral and torsional motions, and by large amplification of the input signals. The responses were more than 80 seconds in duration. The set of acceleration records used in this study is presented in Chapter 1, Figs. 1.3 to 1.5. A summary of the peak response values, as obtained from the records, is presented in Table 4.3.

4.5.2 Acceleration

The maximum horizontal ground acceleration at the building site was 0.04 g for the Morgan Hill and Mt. Lewis earthquakes and 0.11 g for the Loma Prieta earthquake, Figs. 4.5, 4.6, 4.7. Maximum vertical accelerations were half the horizontal values at the ground for the Morgan Hill and Mt. Lewis events and 10% larger than the ground horizontal values for the Loma Prieta earthquake.

Figure 4.8 presents the response spectra for the horizontal components of motion at the base of the building, for the earthquakes studied. These spectra show well defined peaks near 2 and 1 second. These peaks are believed to be associated mainly with the input signal and to a lesser degree with modification of the base motions due to feedback from the structural response. Predominant peaks for the Morgan Hill and Mt. Lewis earthquakes were at 2.1 and 1.0 seconds. For the more intense Loma Prieta event the peaks were slightly shifted, with predominant periods near 2.4 and 1.2 seconds. As obtained in other structures in the area, predominant periods were more strongly present in the NS direction than in the EW direction, indicating a strong directionality of the input motion (Fig. 3.6).

The calculation fo the strong motion duration of the building base records was based on the criterion that the slope of the cumulative root mean squared acceleration (CRMSA) [35] remains positive.

The cumulative root mean squared acceleration (CRMSA) is defined as follows:

$$\text{CRMSA} = \sqrt{\frac{\sum_{j=1}^{N} (a(t_j))^2}{N-1}} \tag{4.3}$$

where

$a(t_j)$ is the acceleration at time step (t_j), and

N is the maximum number of points considered in the analysis.

This criterion establishes that when the slope of the CRMSA is negative, the strong motion duration has ended or the "periods of high energy pulses" on the site have ceased. To obtain the time of the beginning of the strong motion duration, the slope of the CRMSA is calculated for the acceleration histories reversed. And to obtain the time of the end of the strong motion duration, the slope of the CRMSA is calculated for acceleration histories as recorded. Maximum durations of 56, 32 and 35 seconds were obtained for the Morgan Hill, Mt. Lewis and Loma Prieta earthquakes, respectively. These long durations, relatively large for the magnitude of the earthquakes that produced them, had an important impact on the overall behavior of the structure, especially for the Morgan Hill event.

The maximum structural acceleration obtained during these events was 0.34 g for the Loma Prieta earthquake. A study of the records indicates that the time of occurrence of the maximum recorded acceleration above the ground was considerably later than that corresponding to the base, especially during the Morgan Hill and Mt. Lewis earthquakes. This indicates that the structure during these events resonates with the input signal (Fig. 4.9) thereby amplifying its response. The longer predominant input period observed in the Loma Prieta input records seems to have prevented the formation of the strong resonance observed during the previous two events.

The foundation of the structure was observed to rock during the events studied. This effect can be seen in Fourier amplitude spectrum plots of the vertical acceleration records in Figs. 4.10, 4.11 and 4.12. These figures show, for the Mt. Lewis and Loma Prieta earthquakes, a rocking motion with a period similar to that found for the predominant structural period, near 2.2 seconds. The maximum difference of the vertical acceleration histories across the base of the building was found for the Loma Prieta earthquake. It was obtained between the VER/NW and VER/SW sensors and had a magnitude of 0.06 g. Despite the high value of this difference, relative to the peaks value of the records, the maximum difference is part of a high frequency signal so the actual effect on the lateral response of the structure is expected to be small. For example, analyses were performed to estimate the effect of foundation rocking on the relative horizontal acceleration of the structure. The difference between the vertical SW and NW corner records was scaled properly to simulate a horizontal motion at the location of sensor NS/7/W assuming the structure to be a rigid body. Then, the Fourier amplitude spectra of the actual record and the predicted rigid body motion caused by the rocking were compared, around the predominant period. In this way, it was found that for all the events studied, the rigid rocking motion of the structure had an effect of less than 1% on the first mode relative acceleration. Also, using moving window techniques, it was found, as expected, that the rocking occurred mainly at times of strong response of the structure, see Fig. 4.12.

It is interesting to note that the "maximum acceleration amplification ratio" (defined as

the ratio of the peak acceleration at a location to the corresponding acceleration at the ground) was 4.9, 7.1 and 3.8 for the Morgan Hill, Mt. Lewis and Loma Prieta events, respectively. It appears that the difference between these values, for example, for the Mt. Lewis and Loma Prieta events, is not necessarily due to higher energy dissipation in the structure associated with structural and non-structural damage. Rather, differences in the input frequency content, Fig. 4.8, and the duration of the input are believed to be responsible.

4.5.3 Displacements

Analyses of derived displacement histories indicate that the building suffered large lateral drift and torsional rotations during the events studied. Some of the records of displacement and relative drift studied are presented in Figs. 4.16 to 4.25.

Story relative displacements were obtained by subtracting the story absolute displacement and the corresponding displacement at the ground. Displacements for stories without recording instruments were estimated by linearly interpolating the displacements obtained on floors with recording stations. A more sophisticated interpolation scheme, for example one that takes into account typical modal shapes, was not considered because mode shapes are complicated by the three-dimensional nature of the structural response. In view of the many assumptions needed, this increased complexity was not believed to be necessary.

The expected error in the displacement records obtained from the CSMIP procedures is 0.1 cm (0.04 inch) for the filter long-period cut-off ramp used (3.3 to 4.1 seconds). For relative displacements, an upper bound for the error will be about twice this amount. Because displacements recorded on the structure are considerably larger than these values (see below) it is not likely that these errors would affect the interpretation of the response.

The maximum roof displacement relative to the ground, 38.2 cm (15.0 inches), was obtained at the SW building corner (instrument location), during the Loma Prieta event. Average story drift ratios (IDX) were found by subtracting displacements at two adjacent instrumented levels and dividing the result by the difference in floor elevation. The drift indices were greatest between the second and seventh floors. These were about 0.40%, 0.72% and 0.85% for the Morgan Hill, Mt. Lewis and Loma Prieta events, respectively. The maximum displacements occurred for all the earthquakes at the SW corner of the building. Associating this behavior with simple one-story structures would indicate that the "center of mass" of the structure is to the West and South of the "center of stiffness".

Significant torsion occurred in the building during the earthquakes (see Figs. 4.14, 4.15, 4.17, 4.18, and 4.21). For example, torsion can be observed in Fig. 4.17 between seconds 25 and 35 for the Mt. Lewis earthquake and in Fig. 4.21 between seconds 15 and 25 for the Loma Prieta

event.

The maximum torsional deformations were observed for the Loma Prieta earthquake. In this event the maximum relative displacement obtained between two recording stations on opposite sides of a floor (which is a measure of torsional deformation) was 12.32 cm (4.85 inches).

Figure 4.22 presents the deflected shape of the building at different times during the Mt. Lewis earthquake. The pairs of lines in this figure represent the motion of the SW and SE corners in the NS direction and the motion of the SW and NW corners in the EW direction. A shear type deflected shape is apparent for the motion in the NS direction. Figure 4.23 shows the motion of the twelfth floor slab during the same period. Large torsional deformations can be seen in the EW direction during the strong response in the NS direction. At other times the motion in the EW direction exhibits shear type deformations or nearly pure torsional responses. The behavior during the three earthquakes studied was similar, for example see Fig. 4.24.

Figure 4.25 presents the total and relative particle motion of the twelfth floors, at the SW corner. These plots show a strong bi-directional response. Comparisons of total and relative displacement plots indicate that structure deformations were far larger than those associated with movement of the ground. These figures show that the predominant axis of motion were not similar for the earthquakes. The principal axes of motion for the Morgan Hill earthquake were approximately at 45 and 110 degrees of azimuth with respect to the reference North. For the Mt. Lewis event the azimuths of these axes were approximately 90 and 165 degrees; and for the Loma Prieta event the azimuths were approximately 45 and 165 degrees. Animation of the drift plot indicates that, during the free vibration, the building's motion slowly changed from one predominant axis to the other. This effect was apparently caused by the constructive and destructive reinforcement of the three-dimensional modes of the structure during the different portions of the response.

Several of the observations made in Chapter 2 for a simple torsionally-coupled system with low damping can be seen in the response records of the building.

The motion of the building shows the three-dimensional interaction of more than three modes with close natural frequencies. This phenomenon is clearly shown for the Mt. Lewis and Loma Prieta events where the beating modulation of the records is strong, Figs. 4.13 to 4.21. For example, Fig. 4.16 shows the interaction between the EW and NS directions, presenting a large dip in the envelope for the EW direction at second 25. The long duration amplitude modulation in this figure has a beating period of nearly 100 seconds. The long duration of the response observed during this earthquake in the EW direction, Fig. 4.17, as will be demonstrated in Chapter 5, was caused by the interaction of the three-dimensional modes of the lightly damped structure and not by the input motion. The shorter beating observed in the derived torsional records and displacement records has a period of 16 seconds.

These beating periods are directly related to the first three modes of the structure. It can be shown, by use of the formulae presented in Appendix A, that this beating modulation and the apparent periods found from the records (2.2 seconds for translational records and 1.85 for derived torsional records) were produced by three time series with periods close to 2.2, 2.1 and 1.7 seconds. These indeed correspond to the first three natural periods found from the frequency domain analysis of the response records. The apparently longer beating period observed for the Morgan Hill earthquake with a period of 140 seconds appears to be strongly influenced by the input characteristics and by the sensitivity of the beating period (see Fig. A.2) to small changes in the periods of the individual signals (small structural nonlinearities).

4.5.4 In-Plane Diaphragm Flexibility

The in-plane flexibility of the floor diaphragms was investigated by comparing the maximum torsional motions computed from EW and NS displacement records, Fig. 4.15. The difference between maximum values of the computed torsional motion was calculated to be equivalent to a shear strain of 0.0005. However, the imprecise location of some of the instruments, the presence of noise and the different time bases used for some of the recordings at the same level, could contribute to this value as well.

4.5.5 Base Shear and Force-Displacement

Story shears and overturning moments were estimated as functions of time from acceleration records and story masses (associated with dead weight). Total accelerations at the floor "center of mass" were estimated for the instrumented floors. Then, the "center of mass" values were linearly interpolated, at every time step, to the rest of the floors. Inertial forces were calculated by multiplying the mass and acceleration at every level.

The maximum base shear calculated from this procedure was obtained for the Loma Prieta earthquake. It was calculated as 22685 and 21350 kN (5100 and 4800 kips) for the EW and NS directions, respectively. These values correspond to base shear coefficients (V/W) of 0.18 and 0.17 for the EW and NS directions, respectively. The maximum calculated overturning moment was also obtained for the Loma Prieta event. This had a value close to 760,000 kN-m (560,000 kip-feet) for both directions.

Figure 4.26 was generated by plotting the calculated base shear versus the seventh floor relative displacement. It is believed that the complex hysteresis loop shapes in these figures are not those typically associated with structural yielding, but rather the combined effect of higher modes, as found by Lin and Mahin [31] and others, and the simplicity of the method used. The overall slope of these curves is nearly constant for all the earthquakes with a value between 980 and

1015 kN/cm (560 and 580 kip/inch) for the EW direction and between 1050 and 1120 kN/cm (600 and 640 kip/inch) for the NS direction. If the twelfth floor relative drift is considered, the slopes during the Morgan Hill and Mt. Lewis earthquakes are close to 630 and 700 kN/cm (360 and 400 kip/inch) for the EW and NS directions, respectively.

As a measure of the distribution of the earthquake forces on the structure, the approximate position of the centroid of the shear force (a) needed to produce the computed overturning moment was calculated as

$$a = \frac{M}{Vh} \tag{4.4}$$

where

M is the overturning moment,
V is the base shear, and
h is the total height of the structure.

Figure 4.27 presents the curves that result from plotting the base overturning moment against the base shear, for the earthquakes studied. The slopes observed from these plots corresponds to the position of the base shear required to produce the corresponding overturning moment (ah). These slopes are similar for all the earthquakes and for both directions. The value a was found to be close to 0.67 indicating that the distribution of load at the maximum response was approximately triangular.

4.6 Conclusions

It can be concluded from the analysis of the response records that the building is a rather flexible structural system with relatively low damping. The predominant period was found to be near 2.2 seconds and modal damping is believed to be below 3% of critical. Because of the similar structural characteristics of the frame in both directions and the relatively uniform distribution of stiffness in plan, the predominant periods of the system are quite close. The closeness of the periods together with the small eccentricities present in the structure produce the strongly coupled lateral-torsional behavior observed in the records. Because of the spatial characteristics of the frame, the coupling affects motions in both directions as well as the rotation. The eccentricity that produced the torsionally coupled response is likely associated with the irregular distribution of the mass and stiffness (a greater number of structural and nonstructural elements on the west and south sides of the building).

The structure responded strongly to these relatively minor earthquakes. It is believed that the intensity of the structural response was caused by the relatively low energy-dissipating

capacities of the building (in the linear range), the three-dimensional modes of the building constructively reinforcing one another during portions of the motion, the long input duration, the possible resonance effect on the building caused by the close match of the dynamic characteristics of the site and the structure, and the relatively large flexibility of the structure.

The following maximum response values were found from the analysis of the building response records during the 1984 Morgan Hill, 1986 Mt. Lewis and 1989 Loma Prieta events:

- Acceleration : 0.34 g
- Relative Displacement (between recording stations) : 38.17 cm
- Interstory drift ratios (between recording stations) : 0.85%,
- Base shear coefficient : 0.18
- Torsional rotations (between recording stations) : 12.32 cm

Taking into account that no appreciable change in period or behavior was observed for the different records, any yielding that might have occurred in the structure did not substantially affect the dynamic characteristics and response of the structure.

Table 4.1: **Record Description**

POSITION	RECORD
VER/NW	1
VER/SW	2
VER/SE	3
EW/r/N	4
EW/r/S	5
NS/r/W	6
NS/r/E	7
EW/12/N	8
EW/12/S	9
NS/12/W	10
NS/12/E	11
EW/7/N	12
EW/7/S	13
NS/7/W	14
NS/7/E	15
EW/2/N	16
EW/2/S	17
NS/2/W	18
NS/2/E	19
EW/0/N	20
EW/0/S	21
NS/0/W	22

Table 4.2: **Natural Periods and Damping**

PREDOMINANT DIRECTION	MODE	PERIOD (sec)	DAMPING[i] (%)
EW	First	2.15-2.20	2-3
NS	Second	2.05-2.10	2-4
Torsion	Third	1.70	-
EW	Fourth	0.65-0.75	-
NS	Fifth	0.60-0.70	-

(i) Values based on the appearance of response wave forms.

Table 4.3: **Summary of Response**

RESPONSE VALUES	M. HILL 1984	MT LEWIS 1986	L. PRIETA 1989
Horizontal Base Peak Rec. Acceleration (g)	0.04	0.04	0.10
Vertical Base Peak Rec. Acceleration (g)	0.02	0.02	0.11
Maximum Structural Acceleration (g)	0.17	0.32	0.34
Maximum Structural Amplification[i]	4.87	7.05	3.84
Maximum Structural Drift (cm)[ii]	18.64	33.19	38.17
Maximum Floor Torsional Displacement (cm)[iii]	7.28	12.22	12.32
Maximum Interstory Drift Index[ii]	0.41	0.72	0.85
Input Duration EW (sec.)	55	27	28
Input Duration NS (sec.)	56	32	35
Maximum Base Shear EW (kN) (V)	10450	8010	22685
Maximum Base Shear NS (kN) (V)	10675	18235	21350
Maximum Base Shear Coefficient EW (V/W)	0.08	0.06	0.18
Maximum Base Shear Coefficient NS (V/W)	0.09	0.15	0.17
Maximum Base Overturning Moment EW (kN-m)	403870	322745	782510
Maximum Base Overturning Moment NS (kN-m)	405770	708845	753750
Base Shear-Displacement Slope EW (kN/cm)[iv]	980	1010	1015
Base Shear-Displacement Slope NS (kN/cm)[iv]	1050	1075	1120

(*i*) Defined as the ratio of the peak acceleration at a location to the corresponding acceleration at the ground.

(*ii*) At recording position.

(*iii*) Maximum difference between recordings at same building side.

(*iv*) At Seventh floor.

Table 4.4: **Estimated Story Weights**

LEVEL	WEIGHT (kN)
13	9450
12	14175
11	9000
10	9225
9	9225
8	9225
7	9225
6	9450
5	9450
4	9450
3	9675
2	9675
1	9675

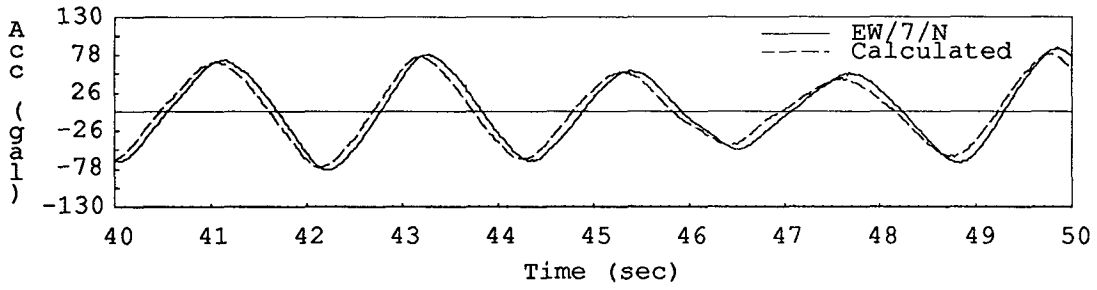

Figure 4.1: Time shift. Morgan Hill earthquake.

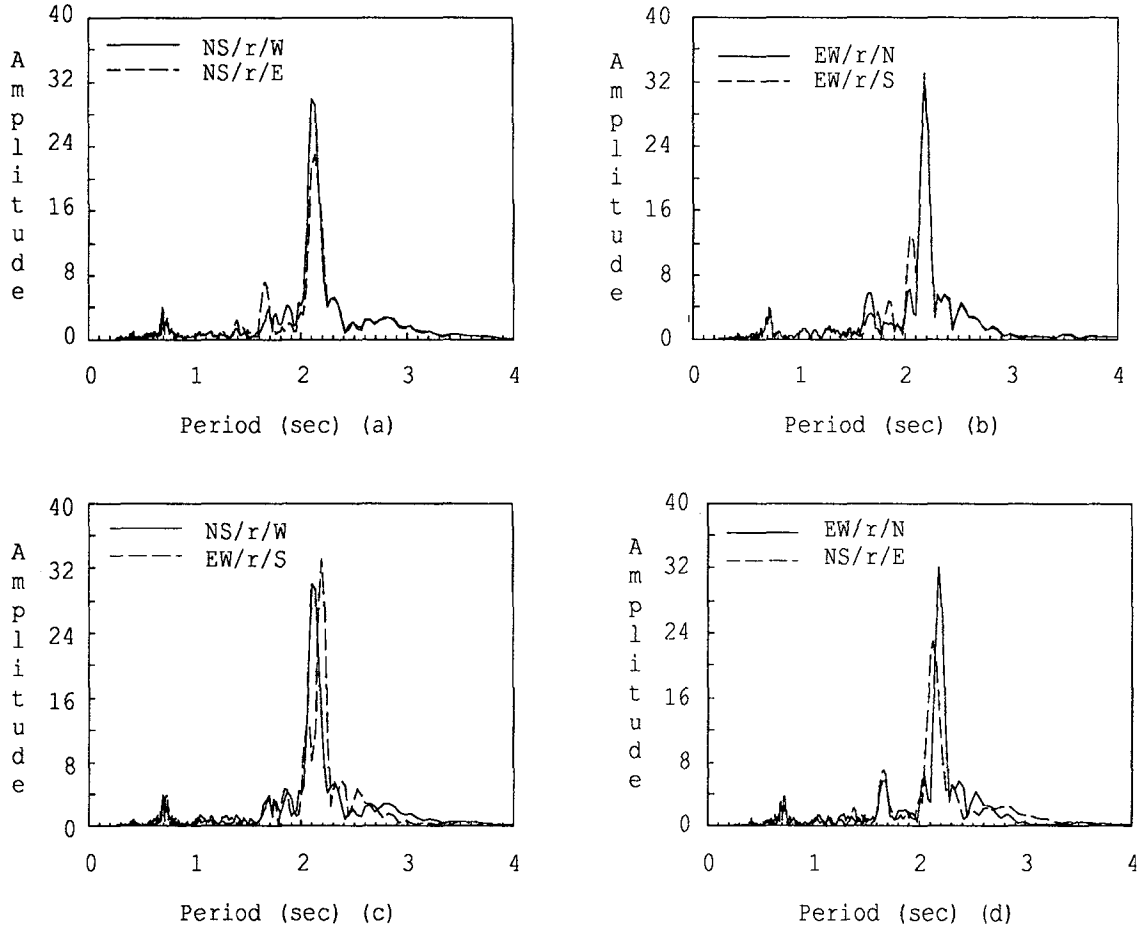

Figure 4.2: Roof Fourier amplitude spectra. Morgan Hill earthquake.

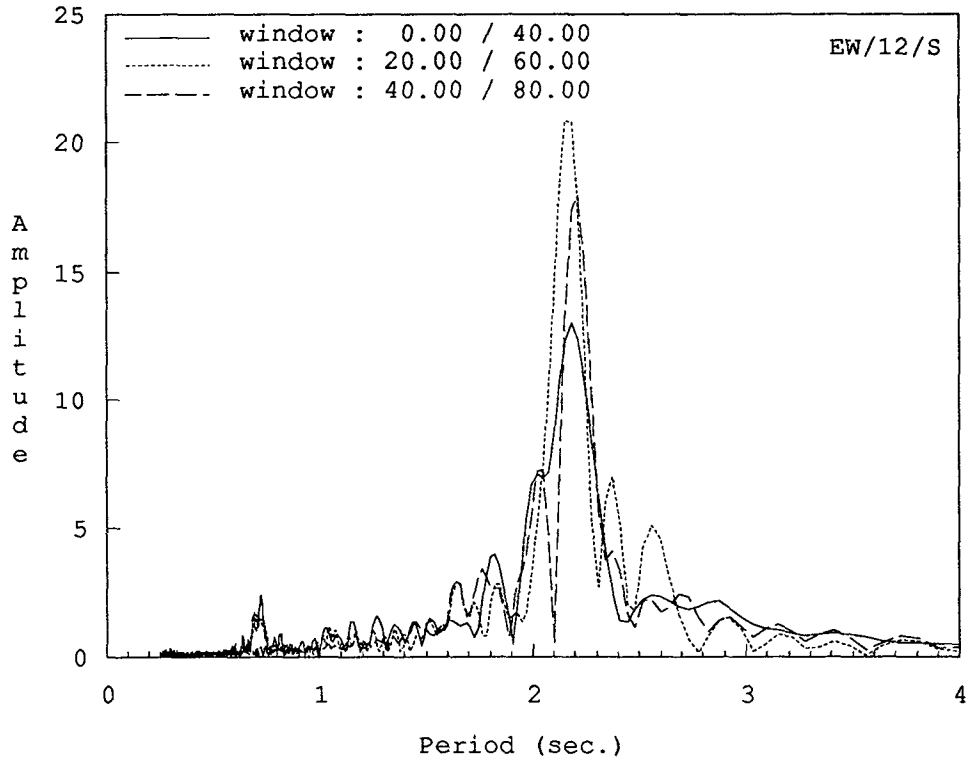

Figure 4.3: Moving window Fourier amplitude spectra. Morgan Hill earthquake.

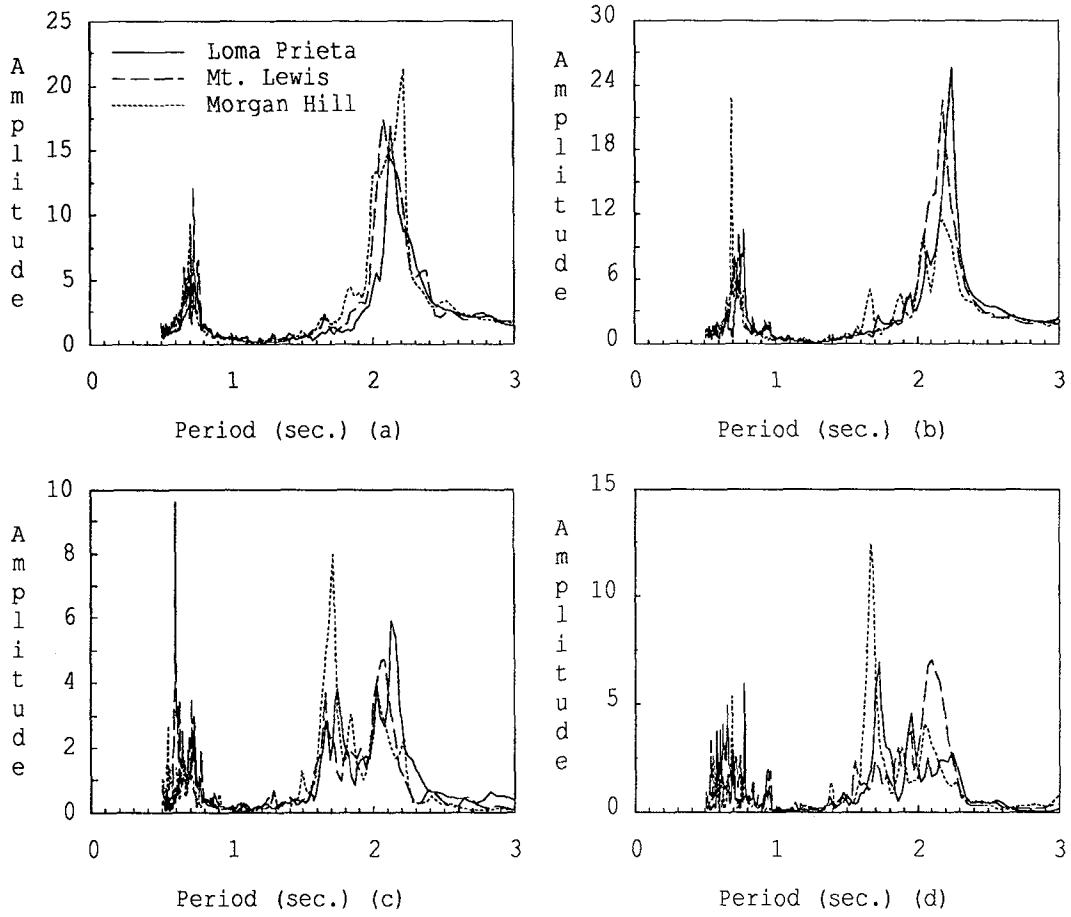

Figure 4.4: Seventh floor transfer function. (a) NS direction [NS/7/W+NS/7/E]. (b) EW direction [EW/7/N+EW/7/S]. (c) NS direction [NS/7/W-NS/7/E]. (d) EW direction [EW/7/N-EW/7/S].

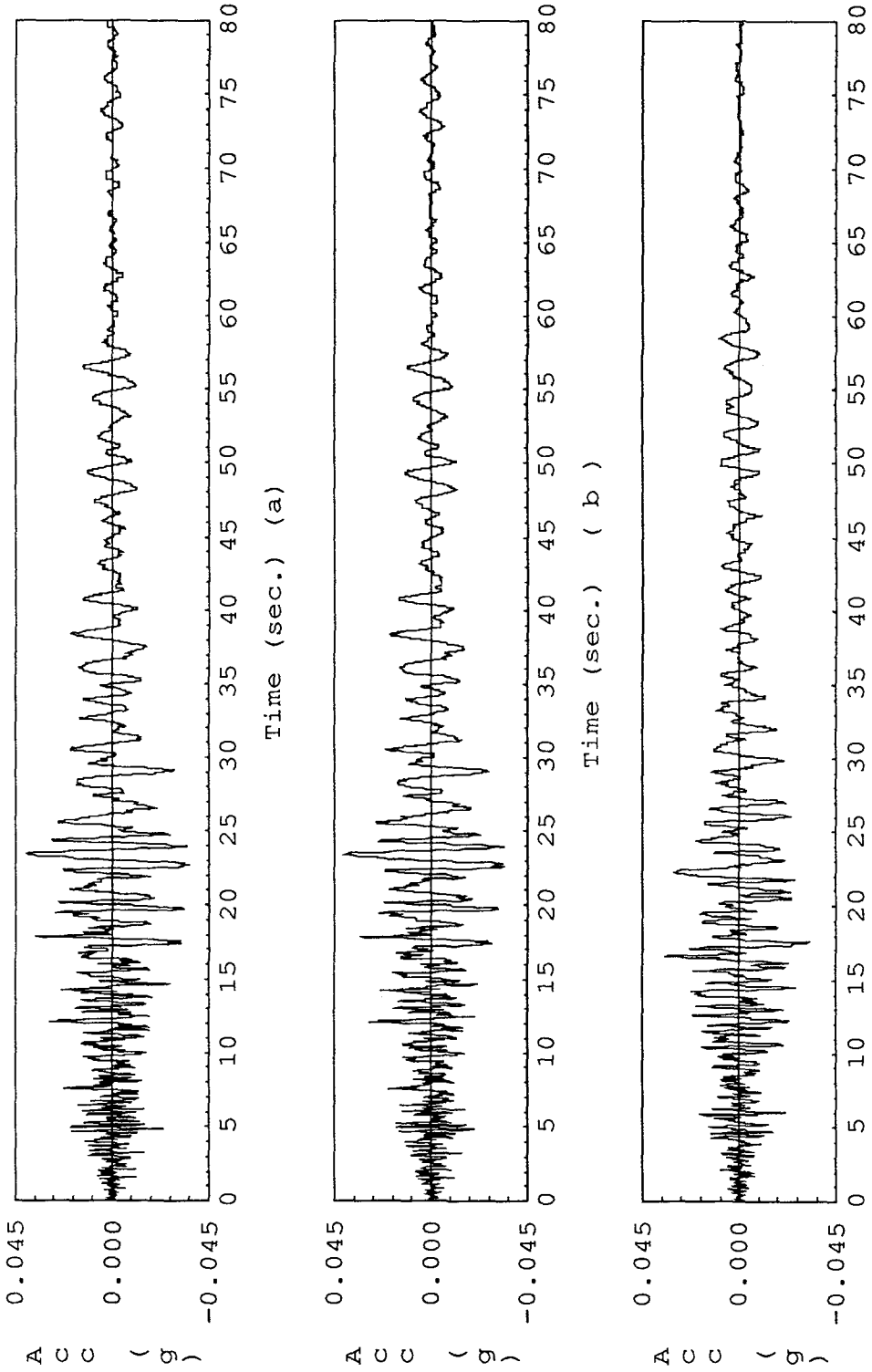

Figure 4.5: Ground acceleration records. Morgan Hill earthquake. (a) EW/0/N. (b) EW/0/S. (c) NS/0/W.

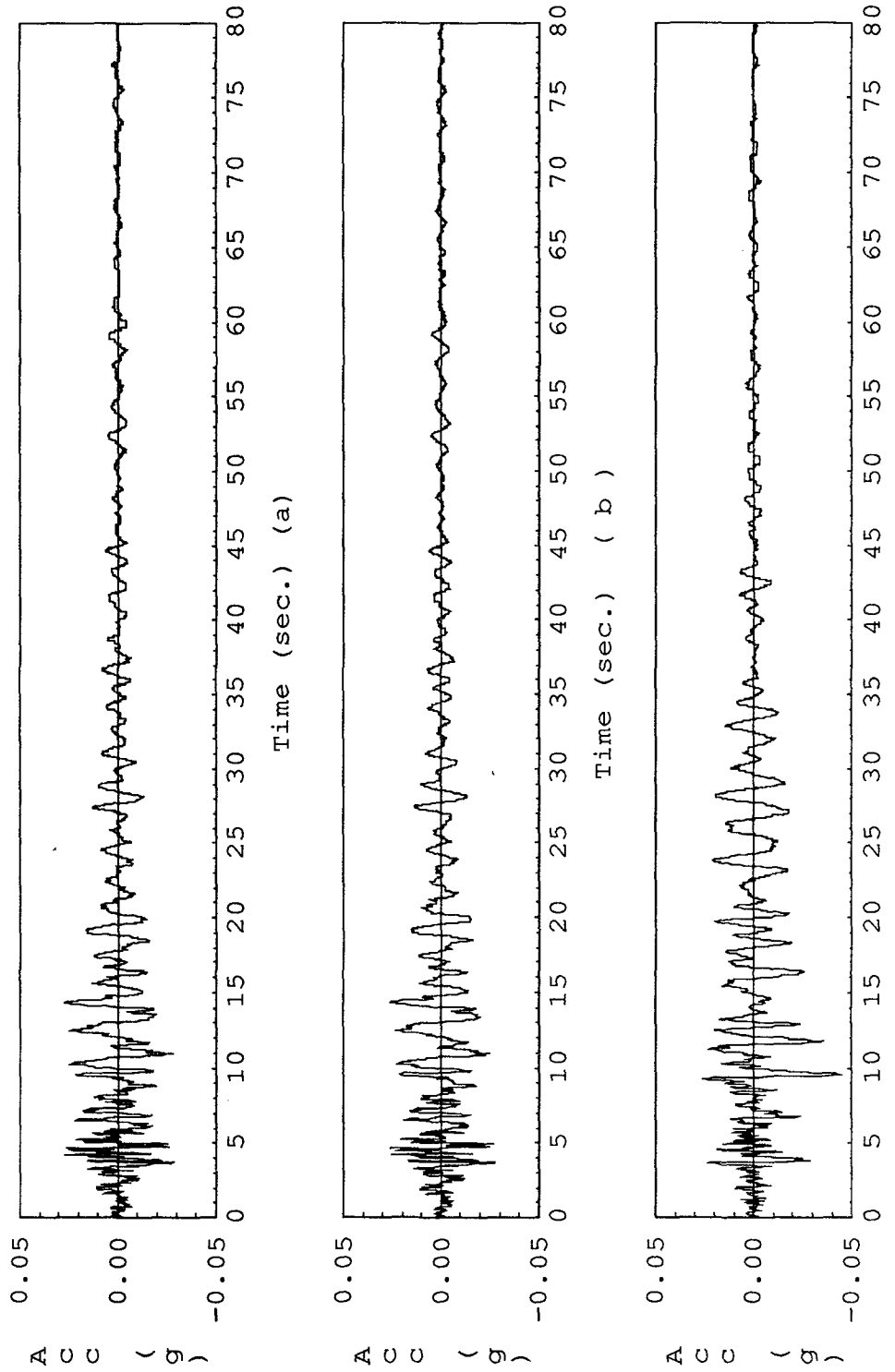

Figure 4.6: Ground acceleration records. Mt. Lewis earthquake. (a) EW/0/N. (b) EW/0/S. (c) NS/0/W.

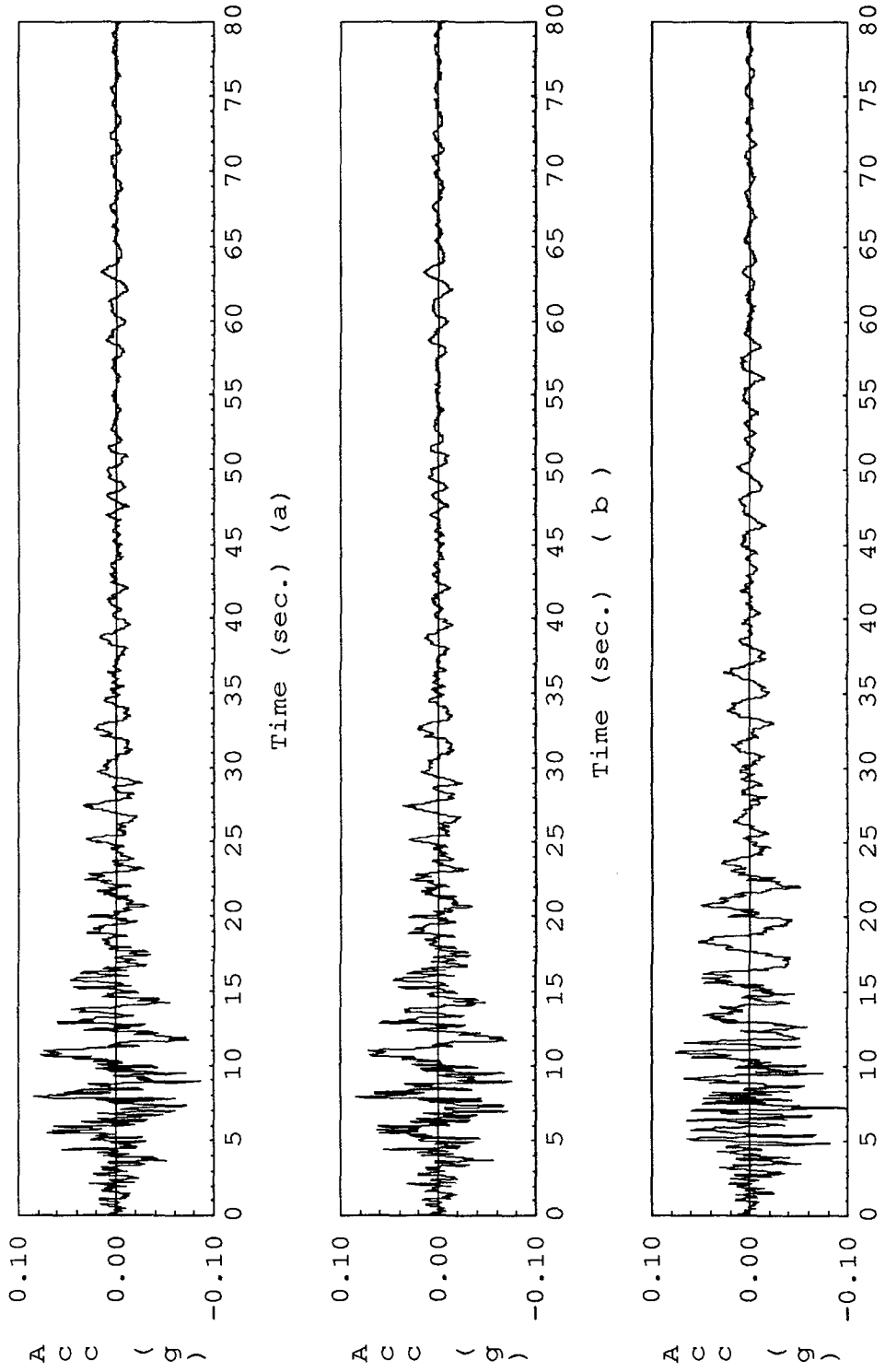

Figure 4.7: Ground acceleration records. Loma Prieta earthquake. (a) EW/0/N. (b) EW/0/S. (c) NS/0/W.

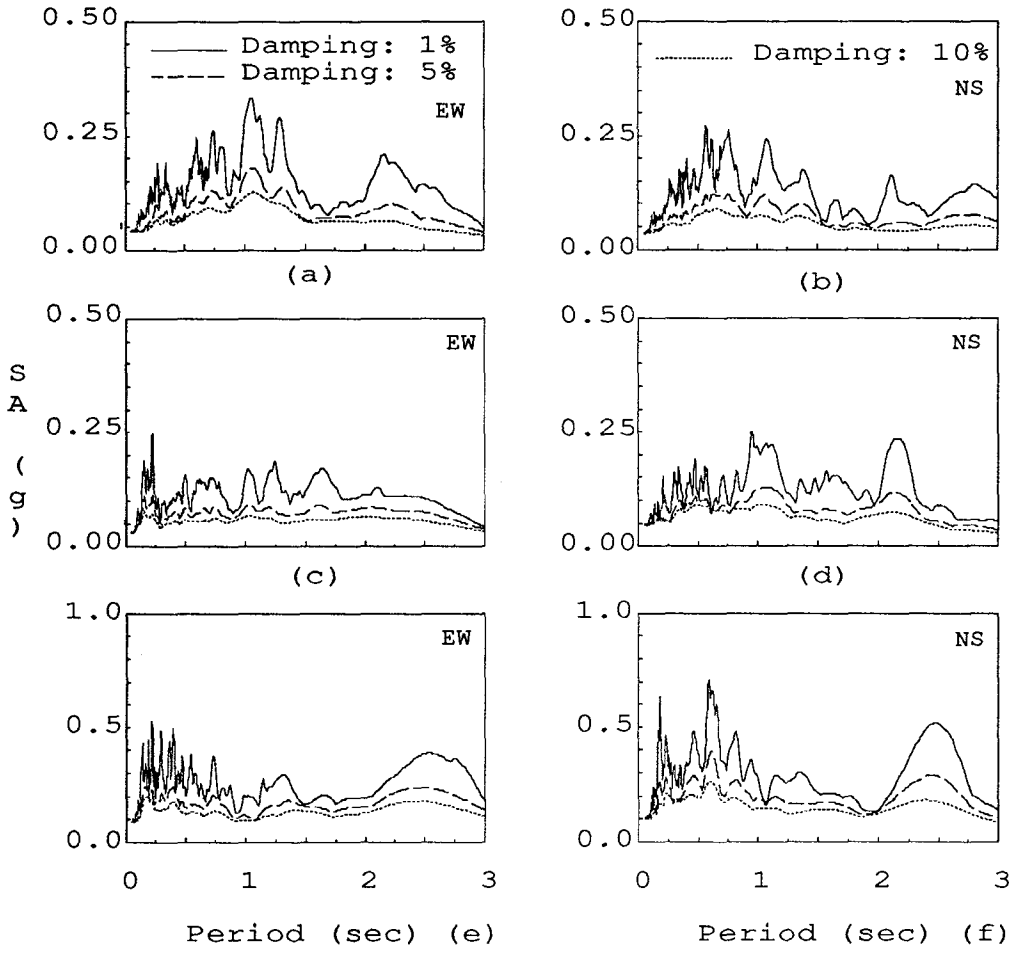

Figure 4.8: Acceleration response spectra of building base records. (a) EW direction, Morgan Hill earthquake. (b) NS direction, Morgan Hill earthquake. (c) EW direction, Mt. Lewis earthquake. (d) NS direction, Mt. Lewis earthquake. (e) EW direction, Loma Prieta earthquake. (f) NS direction, Loma Prieta earthquake.

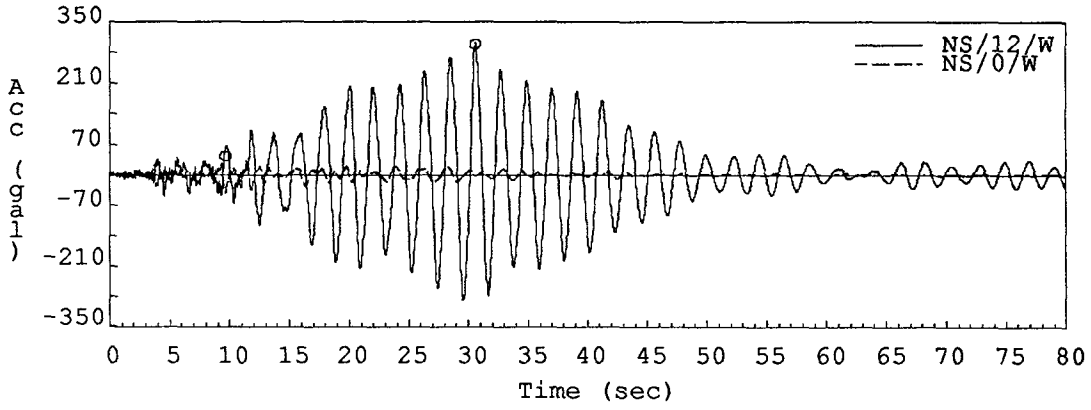

Figure 4.9: NS twelfth and ground level acceleration record. Mt. Lewis earthquake. Circle indicates occurrence of peak record acceleration.

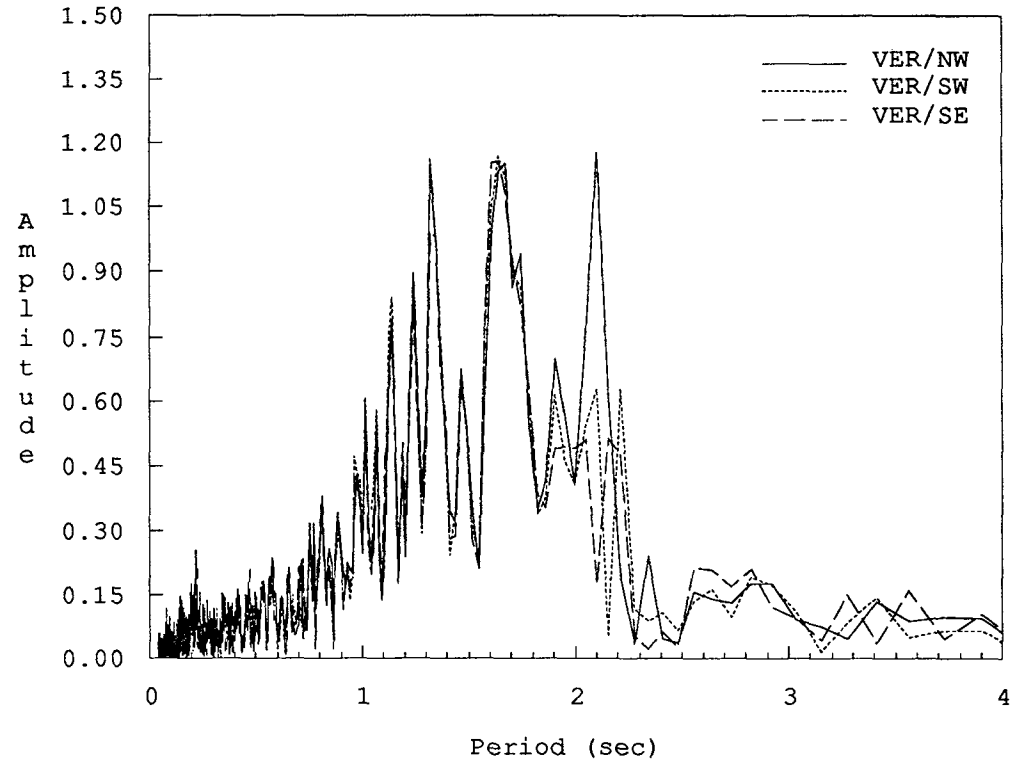

Figure 4.10: Fourier amplitude spectra. Mt. Lewis earthquake.

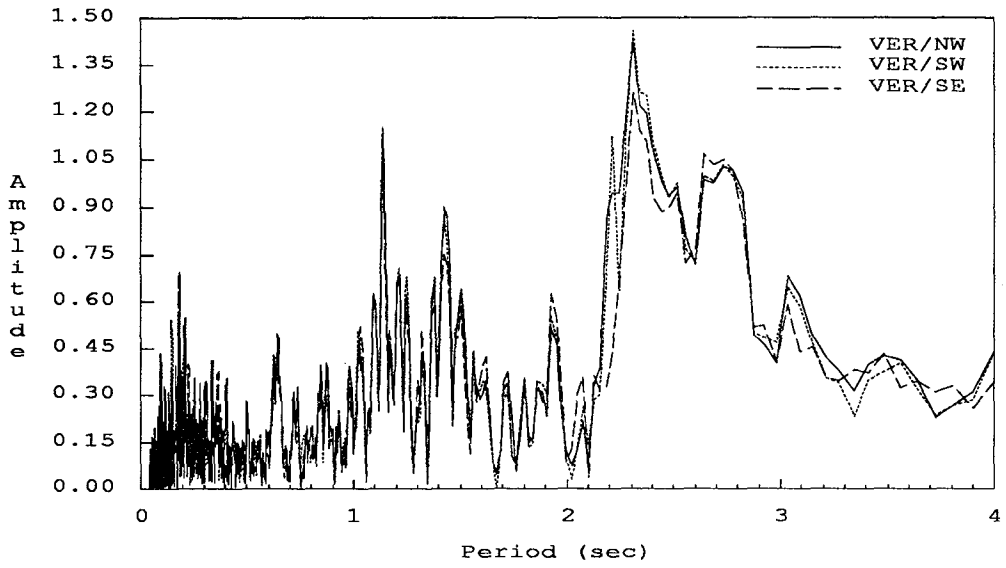

Figure 4.11: Fourier amplitude spectra. Loma Prieta earthquake.

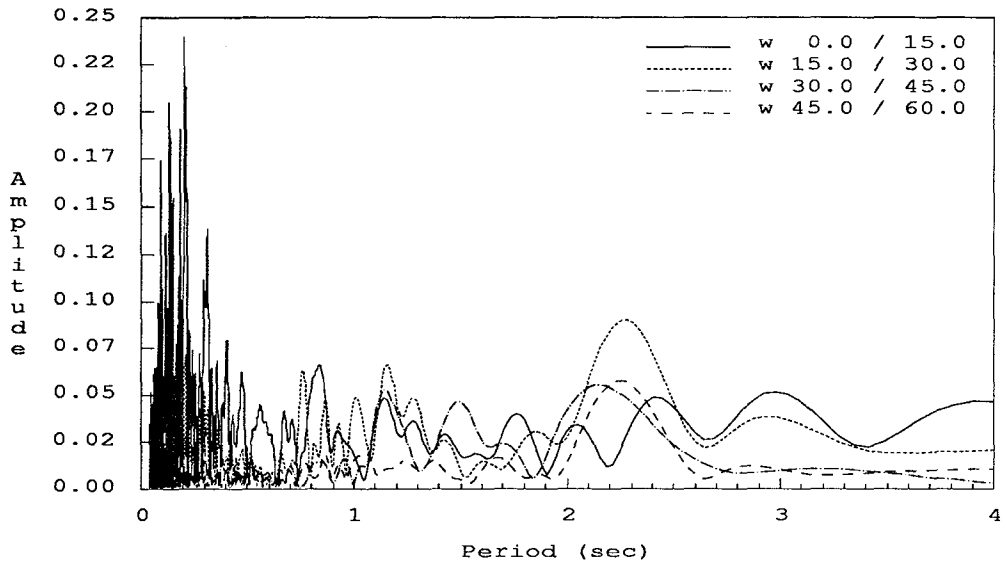

Figure 4.12: Calculated rigid body motion at seventh floor based on vertical rocking motion measured at the base. Moving window Fourier amplitude spectra. Loma Prieta earthquake.

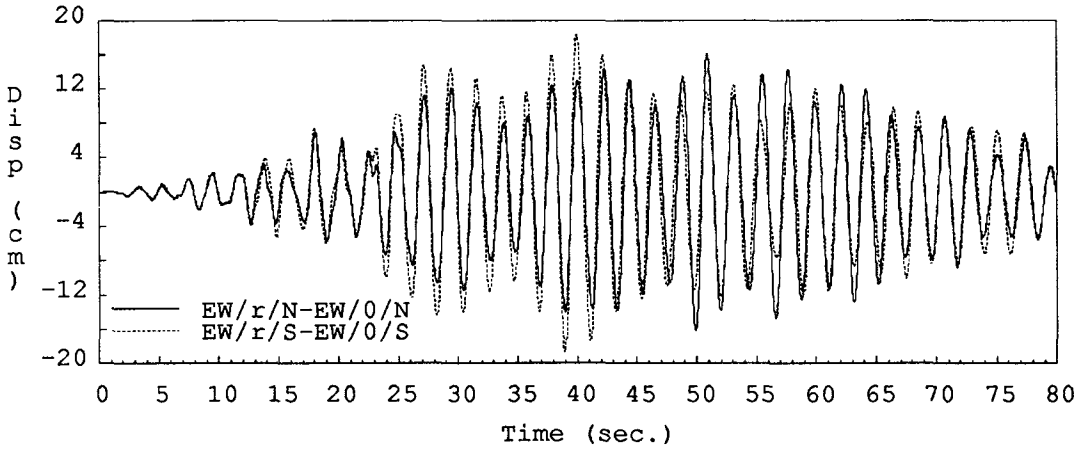

Figure 4.13: Roof relative displacements. Morgan Hill earthquake.

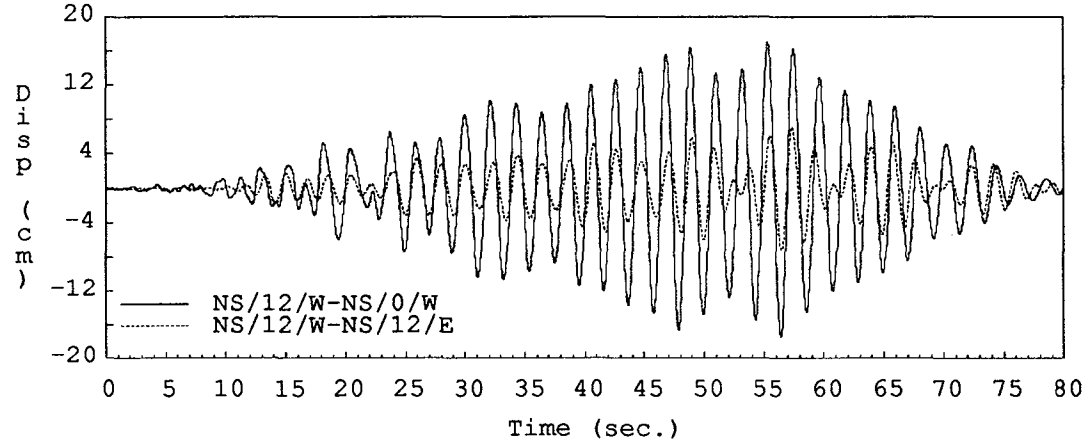

Figure 4.14: Twelfth floor relative displacements and torsion. Morgan Hill earthquake.

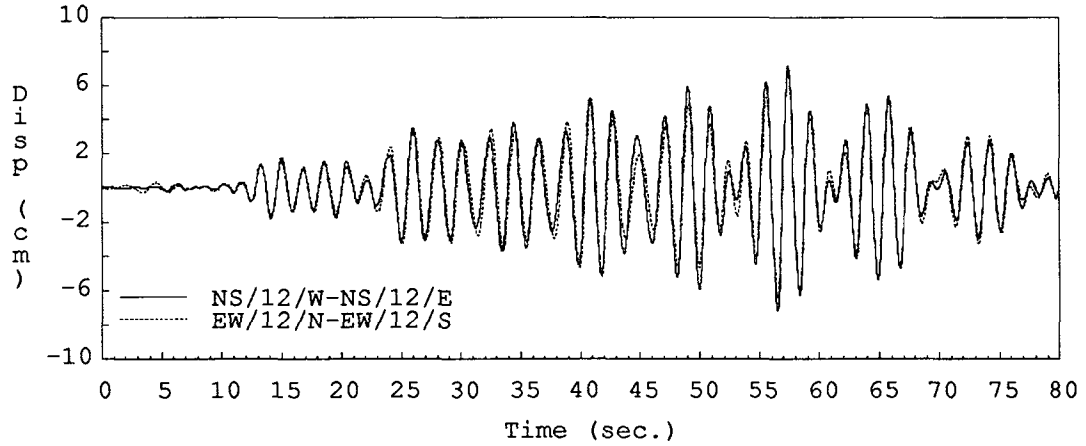

Figure 4.15: Twelfth floor torsion. Morgan Hill earthquake.

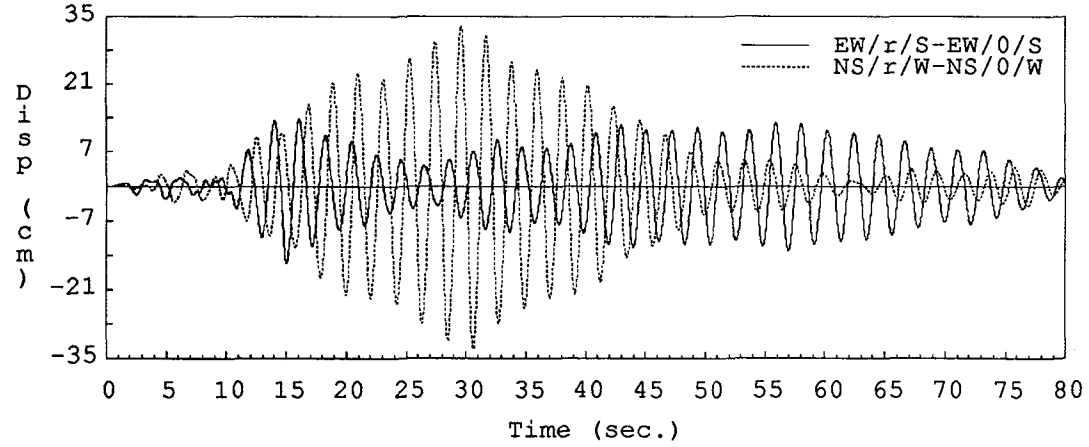

Figure 4.16: Roof corner relative displacements. Mt. Lewis earthquake.

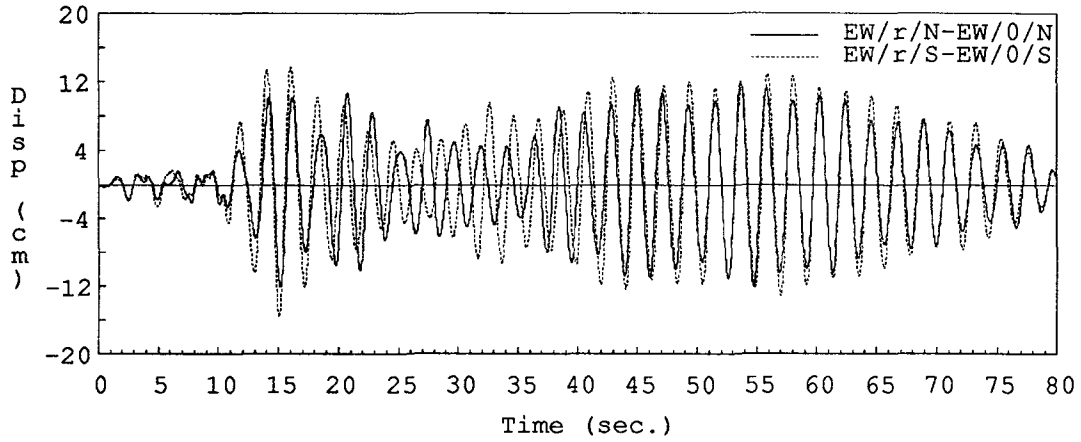

Figure 4.17: Roof relative displacements, EW direction. Mt. Lewis earthquake.

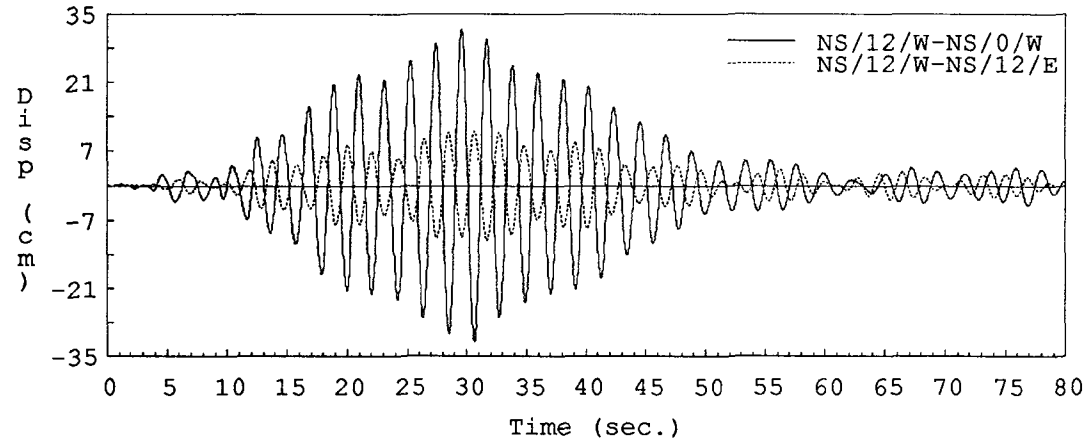

Figure 4.18: Twelfth floor relative displacements and torsion. Mt. Lewis earthquake.

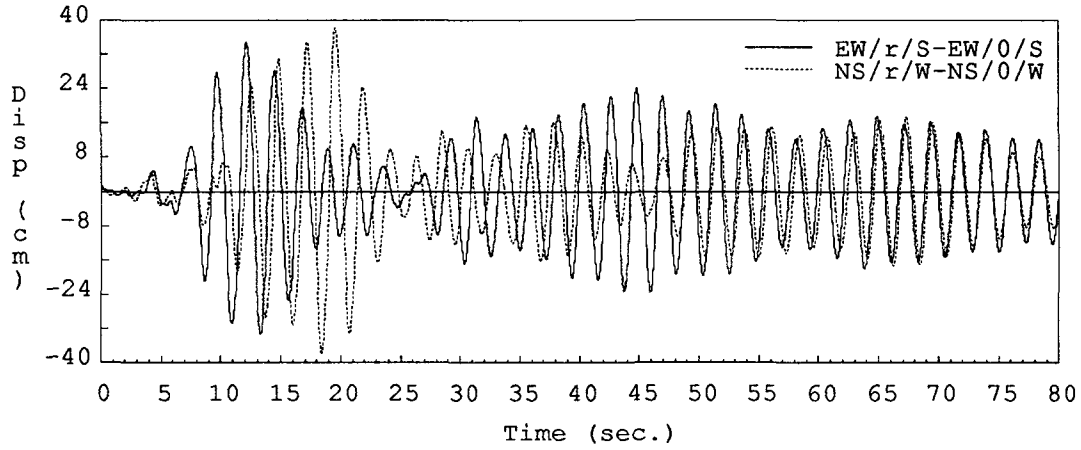

Figure 4.19: Roof corner relative displacements. Loma Prieta earthquake.

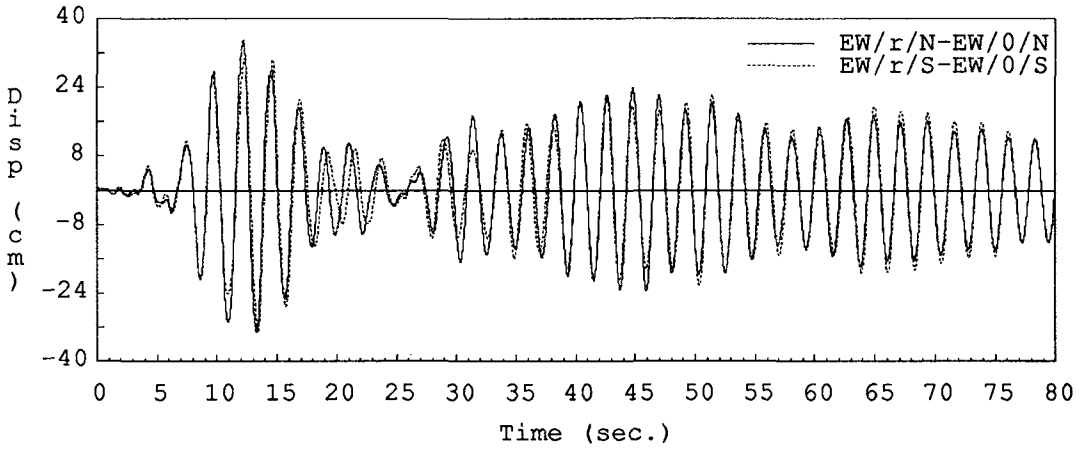

Figure 4.20: Roof relative displacements, EW direction. Loma Prieta earthquake.

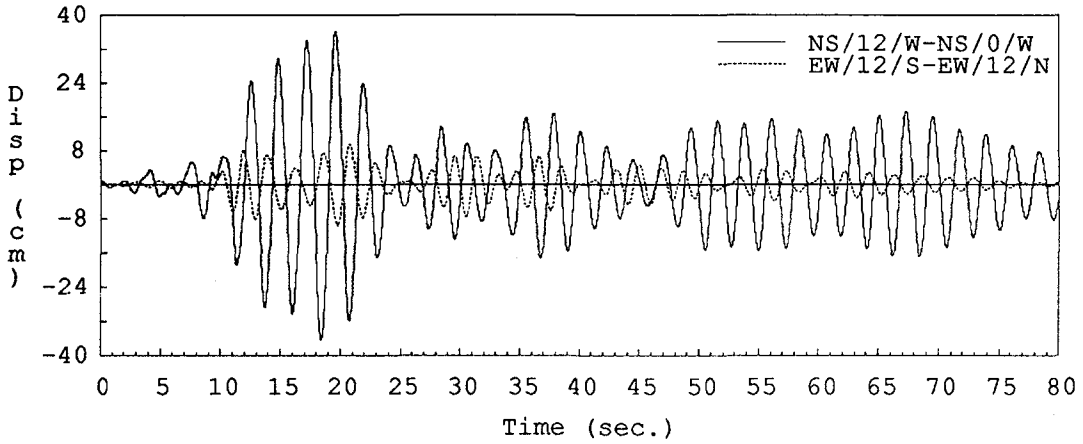

Figure 4.21: Twelfth floor relative displacements and torsion. Loma Prieta earthquake.

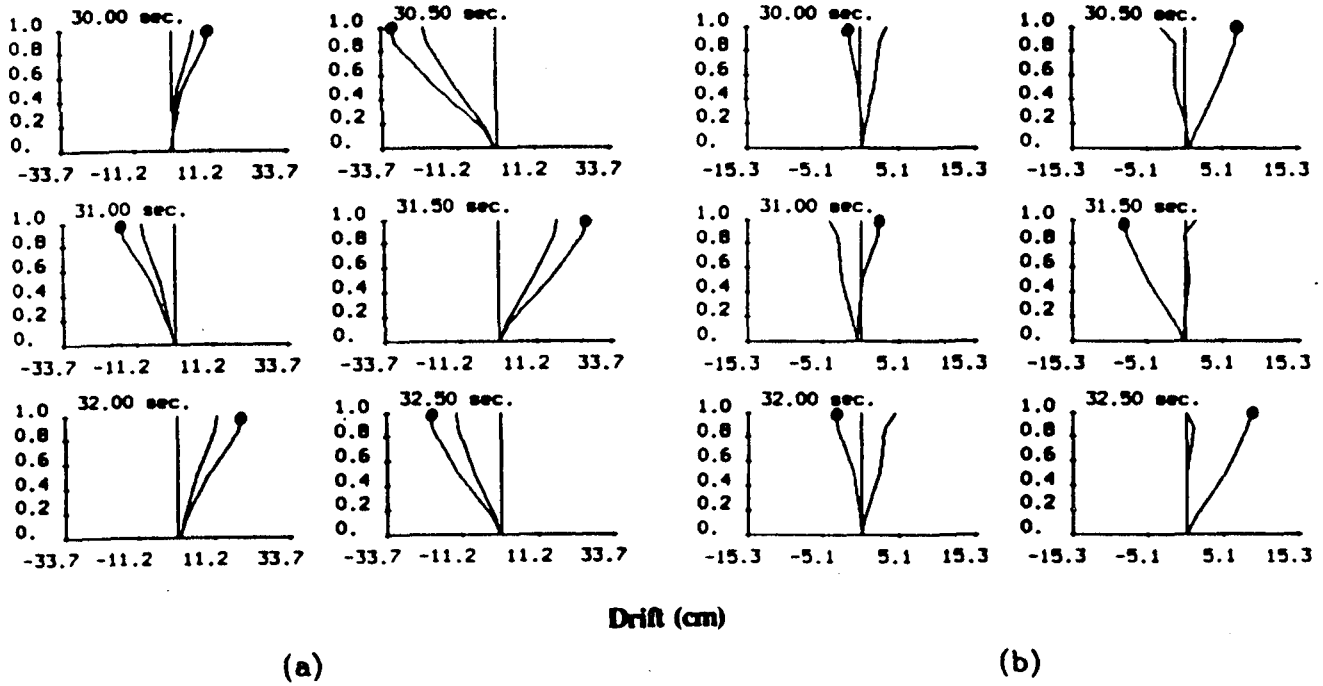

Figure 4.22: Relative deflected shapes at different time intervals. Mt. Lewis earthquake. (a) Motion of SW and SE corners, NS direction. (b) Motion of SW and NW corners, EW direction. [• South-West corner].

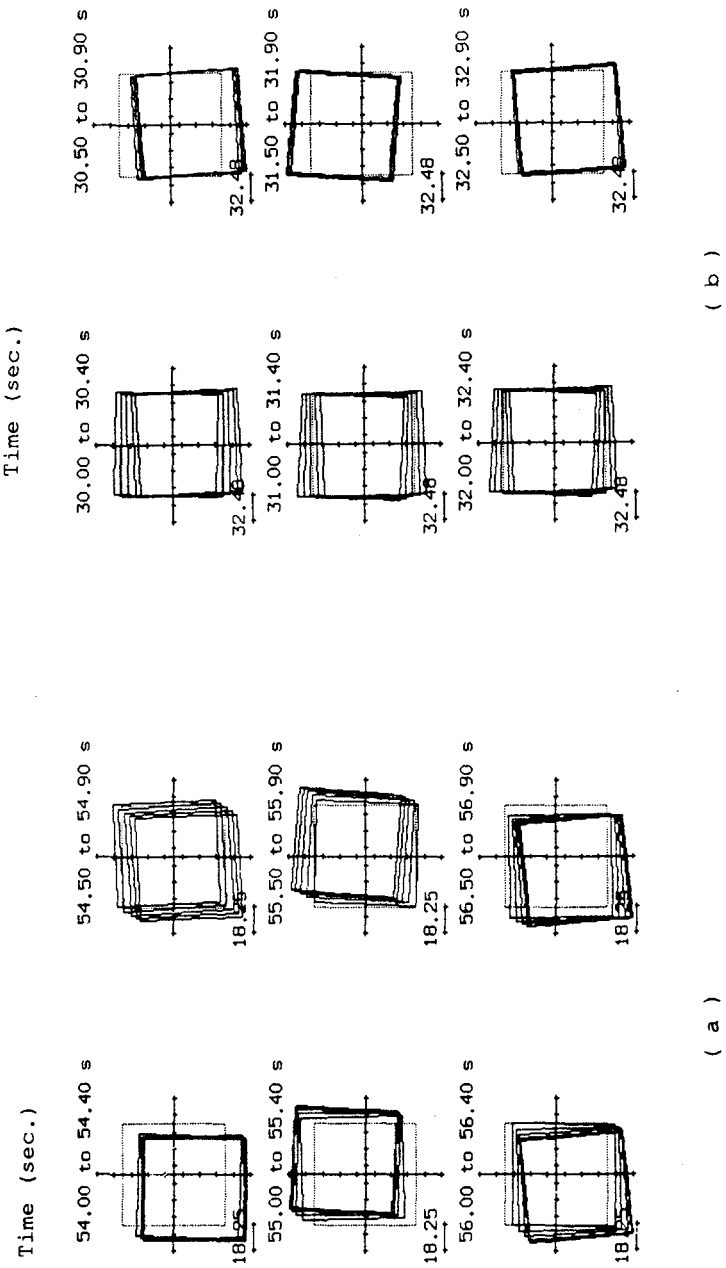

Figure 4.23: Twelfth floor slab motion. (a) Morgan Hill earthquake (b) Mt. Lewis earthquake.

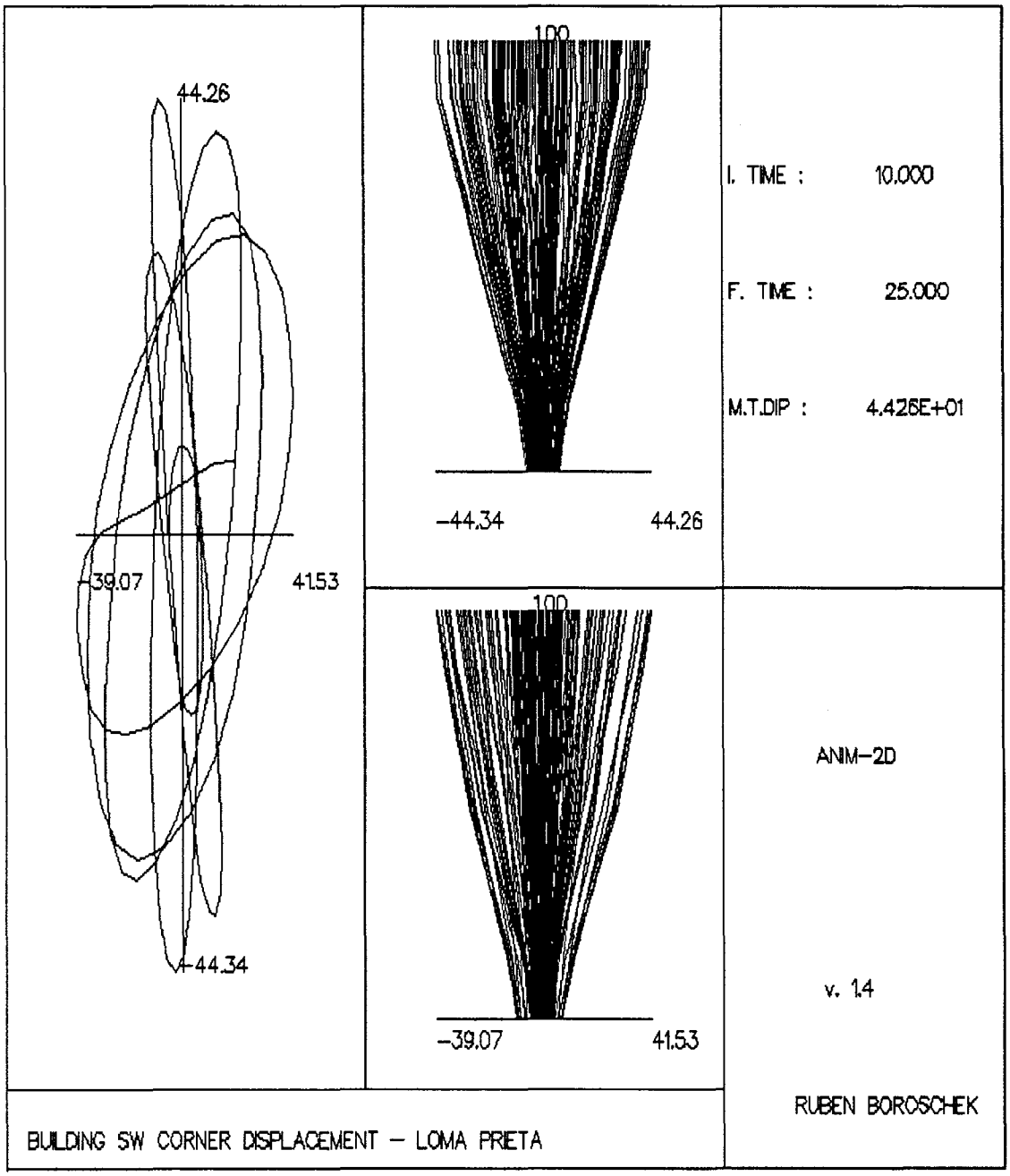

Figure 4.24: Building twelfth floor SW corner locus and building deflected shapes during time of strong response (seconds: 10-25). Loma Prieta earthquake. NS direction vertical axis and upper deflected shape. EW direction horizontal axis and lower deflected shape.

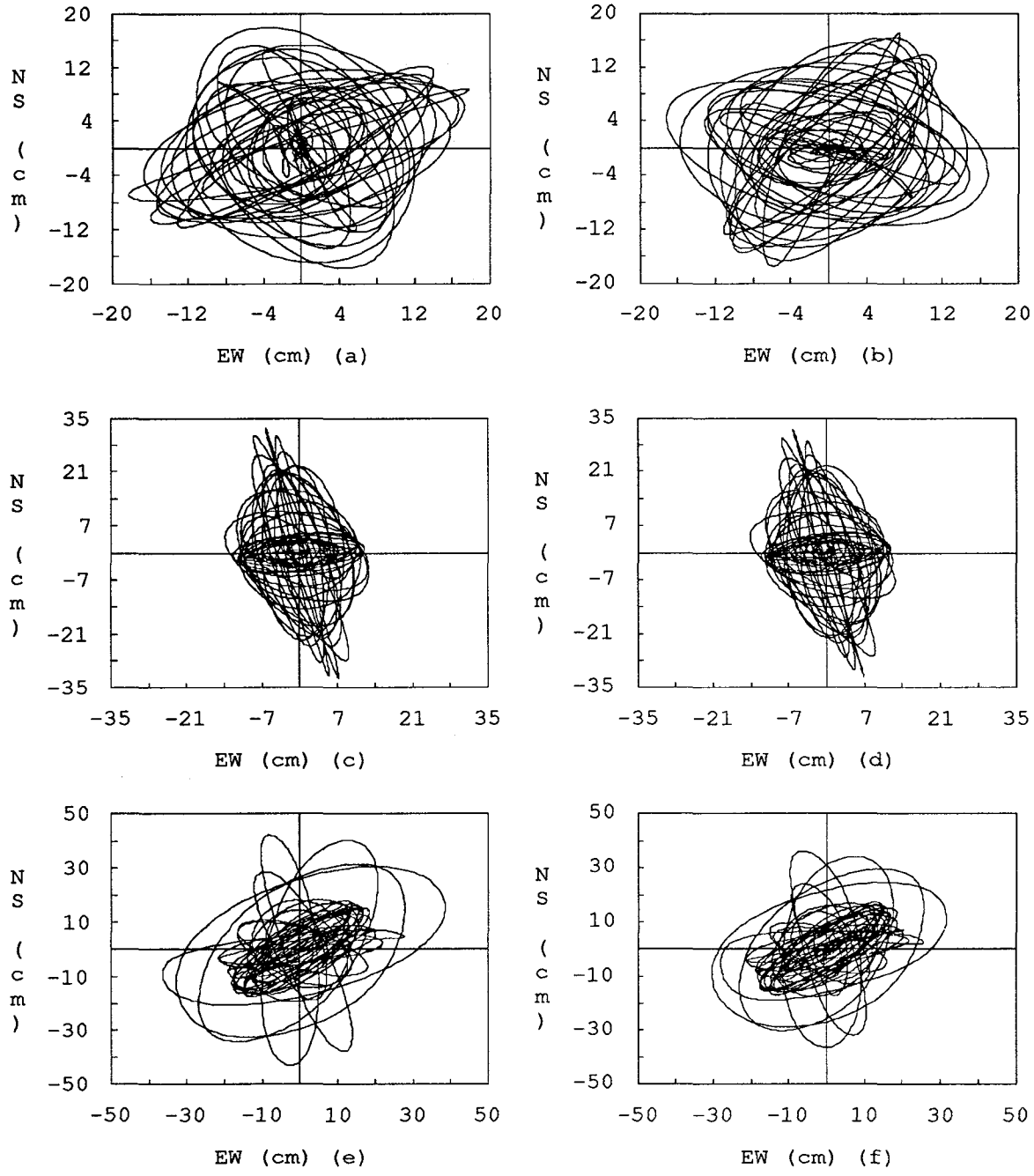

Figure 4.25: Twelfth floor SW corner motion. (a) Total displacement. Morgan Hill earthquake. (b) Relative displacement. Morgan Hill earthquake. (c) Total displacement. Mt. Lewis earthquake. (d) Relative displacement. Mt. Lewis earthquake. (e) Total displacement. Loma Prieta earthquake. (f) Relative displacement. Loma Prieta earthquake.

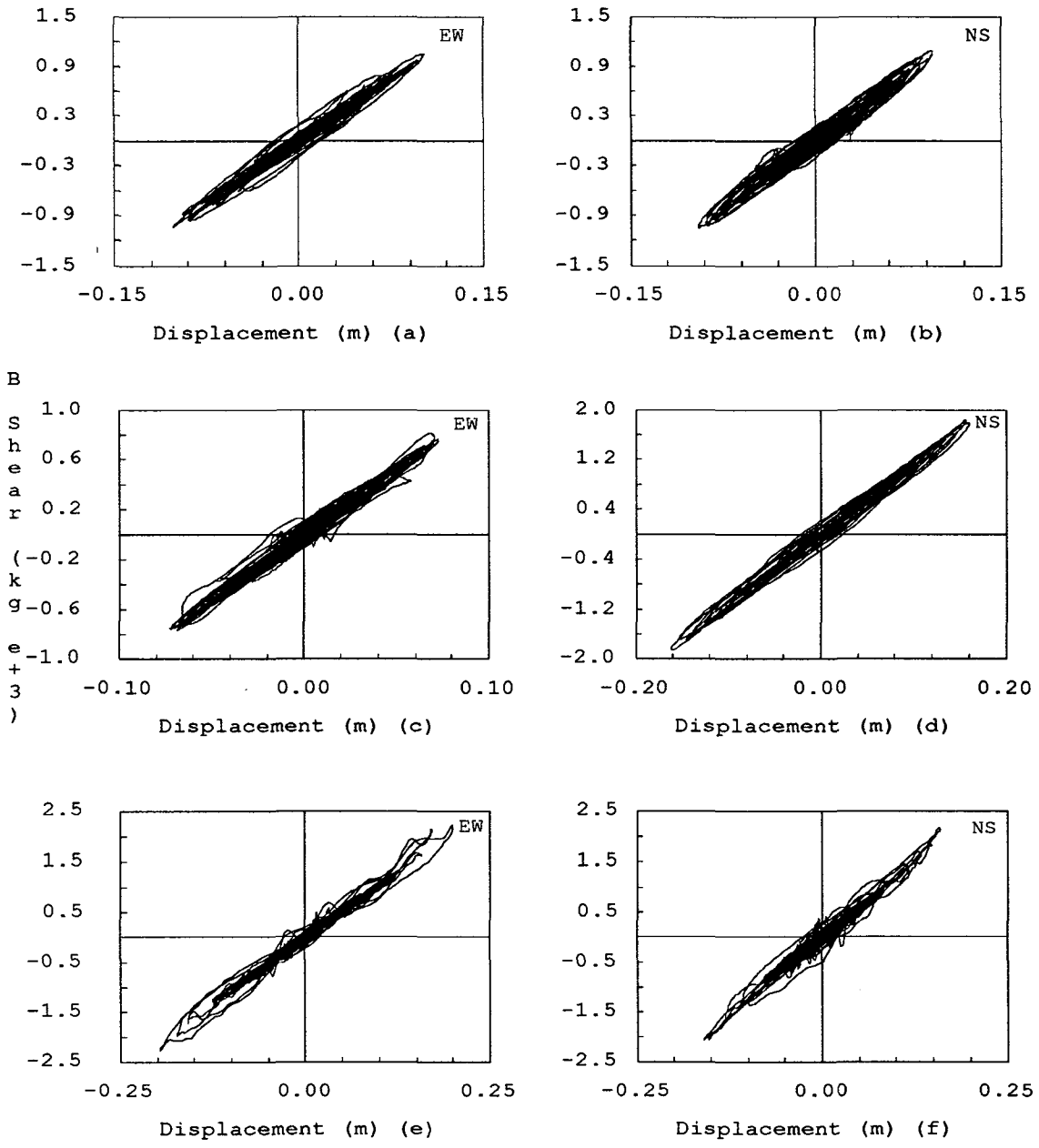

Figure 4.26: Base shear-seventh floor drifts. (a) EW direction. Morgan Hill earthquake. (b) NS direction. Morgan Hill earthquake. (c) EW direction. Mt. Lewis earthquake. (d) NS direction. Mt. Lewis earthquake. (e) EW direction. Loma Prieta earthquake. (f) NS direction. Loma Prieta earthquake.

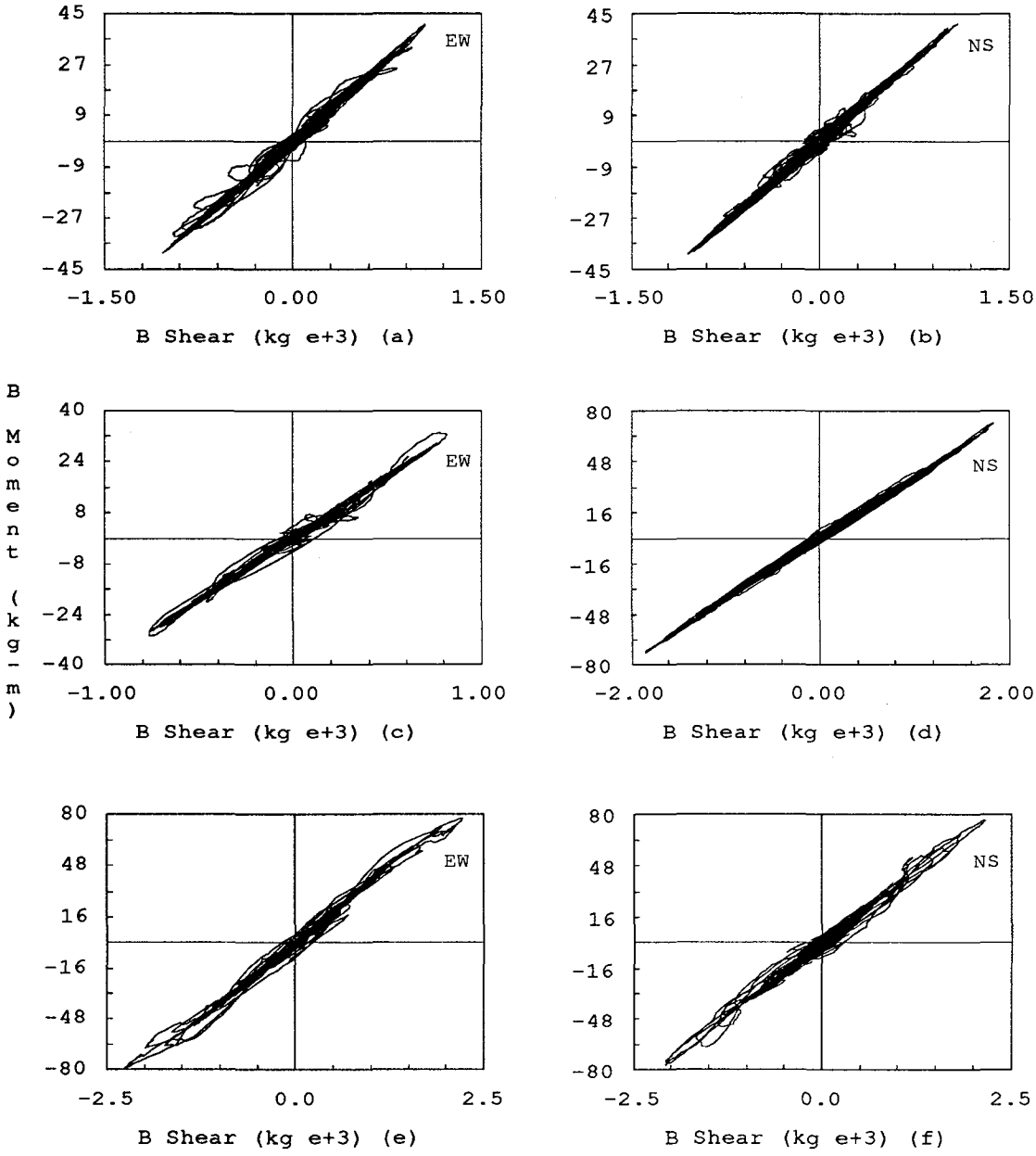

Figure 4.27: Base shear-overturning moment. (a) EW direction. Morgan Hill earthquake. (b) NS direction. Morgan Hill earthquake. (c) EW direction. Mt. Lewis earthquake. (d) NS direction. Mt. Lewis earthquake. (e) EW direction. Loma Prieta earthquake. (f) NS direction. Loma Prieta earthquake.

CHAPTER 5

ANALYTICAL MODELS AND RESPONSE: LINEAR CASE

5.1 General

Several analytical computer models were developed to study different aspects of the structural behavior described in the previous chapter and to confirm the ability of mathematical idealizations to reproduce the observed building response. Then the sensitivity of these models to different design parameters and load conditions was investigated.

Since the building response appeared to be essentially linear elastic, a modified version of the linear analysis structural program ETABS [34] was selected for the analyses reported in this section. This program models a building as a three-dimensional grid of columns, panels, braces and beams. Each floor diaphragm is assumed rigid in its own plane, giving the structure up to two lateral and one rotational dynamic degrees of freedom per floor. Static gravity loads, lateral loads, and ground input acceleration histories can be specified in the analysis. Rigid beam-column joints of finite size may be incorporated in the model. Options are also available in the program to consider P-Δ effects, and UBC and ATC equivalent static lateral loads. The original program allowed only one component of input to be considered. Because of the three-dimensional nature of the building response, the program was modified for this investigation to include two horizontal orthogonal input ground motions, a torsional base input, and base rocking accelerations. In addition, a modal response output option was added. Because of the large size of the structure, a graphic interface, based on the Graphic Kernel System (GKS), was developed. This interface allows the user to corroborate visually the geometry of the structure and element property assignment.

5.2 Model Description and Procedure

Different models were developed to identify the parameters affecting the building response. Once a model matching the recorded response was found, a series of sensitivity studies were performed to identify the contributions of various design variables to the behavior of the building.

Two of the models were developed using information available only from the building plans (Models 1 and 2). They were intended to represent analytical models that might be typically used for design.

The model of the structure was then modified until the recorded behavior was reproduced more closely. Parameters considered in these analyses were the amount of viscous damping, the

mass distribution, the partial composite action of floor beams with the deck, the participation of non-structural elements and the beam-column joint flexibility. Models 3 and 4 are the result of this process. Of these four models, Model 3 provided the best correlation with the recorded results.

Sensitivity analyses were then performed on Model 3 to estimate the effect of several basic analytic assumptions on the response. The parameters studied were stiffness of main floor beams (Model 5), P-Δ effects (Model 6), the position of the center of mass (Model 7) and the amount of inertial mass (Model 8).

In addition, the standard design model (Model 2) was modified to evaluate the ability of the static lateral force procedures considered in the 1988 UBC [22] and ATC 3-06 [38] to identify the base response characteristics of the structure. To comply with these documents, the center of mass of the model was moved in-plane to provide a 5% in-plane additional torsional eccentricity. The resulting model was designated Model 9.

The models are described below. Results of the analyses are presented in subsequent sections.

5.2.1 Model 1 : Bare Frame - Rigid Joints

For this model, the basic geometry and element characteristics were obtained from the building plans. The complete structure was modeled as a single frame. The floor diaphragms were considered rigid so there were three dynamic degrees of freedom per story. Thirteen stories were defined.

Story weights were estimated from structural and architectural drawings. Nevertheless, some uncertainties remained regarding the mass, especially at the mechanical level. The average value used for the story dead weight was 4800 N/m^2 (100 psf). No masses corresponding to live loads were considered in the dynamic analyses. The location of the center of mass was based on the first moment of area of the floor plan (2.24 meters from the geometric center of the square made by the perimeter frame, in the direction of the SW building corner). Assuming that the elements between frame lines A and B, and 12 and 13 do not provide any stiffness to the structure and that the remaining stiffness is uniformly distributed in plan, the selected position of the center of mass will correspond to an equivalent story mass eccentricity of 3.5% of the maximum building plan dimension.

The basic geometry was defined using frame element centerlines. The model considered the beam-column connections as being rigid. The finite size of the joints was taken into account by providing rigid zones at the element ends: 18 cm (7 inches) wide at the end of each beam and 53 cm (21 inches) tall at the top of each column. Twenty one different column properties and seventeen different beam properties were used in the analysis. Taking into account the foundation detailing

and service level loads, column bases were assumed fixed. The different elevations of the beams at the floor level (described in Section 3.1 and Fig. 3.4) were disregarded in this simplified model. Floor elevation was taken as the elevation of the top of the concrete slab. Non-structural elements were not considered in the analyses.

The dynamic analysis was performed using the first nine modes of the analytical model; this allowed the participation in the response of more than 90% of the structural mass for each principal direction.

Viscous damping was assumed to be 3% of critical for all modes. This value is consistent with welded steel buildings in which the element stress level is below the yield point.

5.2.2 Model 2 : Bare Frame - Flexible Joints

Model 2 is similar to Model 1; however, the possible flexibility of the beam-column joints was approximated by eliminating the rigid zones used in Model 1. Past experiences have shown that modeling steel frames with center-to-center dimensions and no element rigid zones helps to balance the error caused by neglecting the shear distortion that develops in the panel zones [28, 29, 52]. More complex modeling of the beam-column connection flexibility was not considered necessary at this stage of the investigation. This model was viewed as being a reasonable design oriented model.

5.2.3 Model 3 : Adjusted Model - "Normal" Damping

This model was developed to find a better correlation with the recorded values. Thus, knowledge of the behavior of the building and its dynamic characteristics were used to modify the parameters of Model 2 to obtain a better match with the response. The changes performed are described below.

Four additional beam properties were defined to incorporate the effects of possible composite action of the floor deck and girders, and to model more closely the framing near the elevators. The floor system consists of a structural deck, with no special provision to develop full composite action between floor and steel beams. Nevertheless, the moment of inertia of the NS oriented beams was increased by 10%, as an approximation of the possible participation by the deck in the response and in order to reduce the predominant NS period value to that found from the study of the seismic records.

A study of the building after the Morgan Hill and Mt. Lewis earthquakes, determined that little damage occurred to the exterior and interior steel siding or to the interior gypboard partitions. Nevertheless, connection details found on the architectural plans and during building inspections indicate that there are areas where interaction was possible. This was confirmed by investigations of the building behavior and damage during the 1989 Loma Prieta earthquake which

showed that some partitions did interact with the framing (resulting in partition cracking). The exterior steel siding is attached to the frame system using light clips. As a result the cladding system is rather flexible and believed to introduce little stiffness to the system. The interior steel sheathing could contribute to the stiffness, but its effect could only be roughly estimated. Using shear values obtained for typical metal decks, an equivalent story stiffness of 770 kN/m (4 kips/inch) per floor was selected to model this effect. Interior gypboard partitions could also contribute to the stiffness of the structure. Because of the method of attachment, the gypboard partition stiffness could change considerably with the level of shaking. Using the work presented by Freeman [12], a shear modulus of 20700 kPa (3 kips/inch/inch) was selected: this gave an equivalent story stiffness in each direction of 3190 kN/m (18 kips/inch). To include the effect of the partitions on the structural stiffness, two shear panels per story were included in the model. These were located on the West and South sides of the building (lines A and 13).

To obtain a better match for the torsional response, the story rotational mass moment of inertia was also increased by 10%. This is reasonable, considering the presence of enclosed office space in the exterior bent on the South and West sides and the tendency of the occupants to store considerable material around the perimeter "aisles" of the building.

Viscous damping for the second predominant mode was changed to 2% of critical for this model; other modes remained at 3% of critical.

5.2.4 Model 4 : Adjusted Model - "Low" Damping

Model 4 is similar to Model 3, but damping is changed for all modes to 1% of critical. This model tried to obtain a better match of some model response values when subjected to the Mt. Lewis and Loma Prieta events and to estimate the sensitivity of the system to damping.

5.2.5 Model 5 : Reduced Beam Stiffness

Model 5 is similar to Model 3, but the moment of inertia of the interior frame beams, in both directions, are reduced by 10%. This model estimated the sensitivity of the system to this design parameter.

5.2.6 Model 6 : P-Δ Effects

Model 6 is similar to Model 3, but includes the P-Δ effect. P-Δ effects are considered in the ETABS program by way of a geometric stiffness matrix that reduces the lateral structural stiffness of the system. The vertical load, considered in the analysis, is based on the assigned mass of the story times a scale factor. In the analysis this factor was considered to be 1.4 times

the gravity value to include, conservatively, dead and live load effects. This model was used to estimate the sensitivity of the system to geometric effects.

5.2.7 Model 7 : Position of the Center of Mass

Model 7 is similar to Model 3, but the center of mass is displaced 5% (2.25 meters (7.4 feet)) of the largest planar dimension of the building towards the West side of the building. This model was used to estimate the sensitivity of the system to accidental eccentricities.

5.2.8 Model 8 : Inertial Mass

Model 8 is similar to Model 3, but translational (both directions) and rotational masses at each level are reduced by 10%. This model was used to estimate the sensitivity of the system to uncertainties in estimating the reactive mass.

5.2.9 Model 9 : Code Static Lateral Forces

Model 9 is similar to Model 2, but the center of mass is displaced 5% of the building's largest planar dimension towards the West side. This model was used to perform a code type static analysis on a typical design model with the required "accidental" eccentricity.

5.3 Loading Cases

The models presented above were subjected to various loading conditions:

The Morgan Hill, Mt. Lewis and Loma Prieta earthquakes were used to match the model's response against the recorded motions and to evaluate the building behavior under different earthquake loadings. For each model different combinations of horizontal and derived torsional base accelerations were imposed. The derived torsional motion was obtained from the difference of the EW horizontal input ground motions. In the EW direction the horizontal input was the average of the existing EW base records. Input rocking accelerations were not considered in these analyses because of the expected small effect that the rocking deformations had on the observed response of the structure and the absence of unperturbed vertical acceleration records.

The NS component of the 1940 El Centro and the N90W component of the SCT record obtained during the 1985 Mexico earthquake were used to evaluate the sensitivity of the structure to other ground motions. For these analyses, the originally recorded maximum accelerations of 0.34 g for El Centro and 0.17 g for the SCT record were used. The input ground motions were applied in these cases only in the NS direction.

Static design lateral loads were established using ATC 3-06 and 1988 UBC. These were applied to Model 9

5.4 Results of the Analyses

The particular combinations of model and load conditions are identified below first by the model used (1 to 9), second by the earthquake record considered (Morgan Hill (MH), Mt. Lewis (ML), Loma Prieta (LP), Transverse SCT 1985 (SCT) and El Centro (CENT)), and third by the input type (i.e., bi-directional with torsion (BT), bi-directional without torsion (B), torsional (T), unidirectional, North-South only, (NS)). For example, CASE 3-MH-B corresponds to an analysis where Model 3 was subjected to bi-directional input, without torsion, corresponding to the Morgan Hill earthquake.

Table 5.1 presents the predominant periods and effective mass factors (EMF) of the analytical models considered. The EMF is defined as the fraction of the total mass participating in each of the global translational or rotational directions for a given mode [34]. Mathematically, the factor is as follows:

$$EMF_{iv} = \frac{([\Phi_i]^T [M] [R_v])^2}{M_T} \tag{5.1}$$

where,

EMF_{iv} is the fraction of the total translational or rotational mass of mode i that is participating in the global v direction,

M is the diagonal mass matrix,

Φ_i is the vibrational mode shape for the i^{th} mode,

R_v is the earthquake influence coefficient vector for the direction v, and

M_T is the total translational mass or rotational mass moment of inertia of the building.

This factor was used to determine the number of modes required in the analysis. The sum of the EMF was at least 90% for all the cases studied.

Because the EMF shows the ratio of the mass participating in each global degree-of-freedom for each mode, its relative magnitude can be used to indicate the degree of lateral-torsional coupling present in each model. This is also true because the version of the program used sets the modes of the uncoupled system, with identical predominant periods, to uncoupled shapes in the global degrees of freedom.

Tables 5.2, 5.3 and 5.4 present the maximum building response values at the center of mass derived from the strong motion records (designated RECORDED in the Tables) and the ones obtained from the different analytical models. Parameters considered include the maximum

twelfth floor relative displacements and rotation at its center of mass, the center of mass maximum interstory drift and the story of its occurrence, and the maximum base shear. (The program employed estimates the base shear from the sum of inertial forces at all levels, not by the sum of shear in the elements connected at the base.) Figure 5.1 presents the modal shapes obtained for Models 1 and 3. Figures 5.2 to 5.20 present the twelfth floor SW corner relative displacements and derived torsional histories (SW corner minus NW corner relative displacement records) obtained from the different models and input records.

5.5 Model Validation

In this section, results of analyses of the first four models are presented to identify the "best fit" model. Two key limitations affect the results presented below. First, the input ground motion records obtained from the events studied were probably modified by the response of the building. If so, they do not represent the actual motion to which the whole soil-structure system was subjected and the model being fitted will not correspond to the actual building structure. Nevertheless it is assumed, that these effects are small. Second, the response of the system is likely to be sensitive to small modeling changes (i.e., small period shifts) because of the rapid variation of spectral acceleration with period at the low levels of viscous damping considered.

5.5.1 Model 1 : Bare Frame - Rigid Joints

This model includes the basic frame geometry, beam-column elements and the rigid joint assumption. Model 1 represents a typical design model. The first three predominant periods obtained from the analysis were 1.93, 1.87 and 1.40 seconds (about 90% of the recorded ones). However, the computed response values, CASE 1-MH-BT, Fig. 5.2, were about half those observed during the Morgan Hill earthquake. The EMF values for this model, listed in Table 5.1, showed a high degree of lateral-torsional coupling. The roughly 10% difference between model and structure periods changed the ordinate on the pseudoacceleration response spectrum (3% damping) from 0.12 g to 0.09 g. The ability of this model to simulate the dynamic response was unsatisfactory.

5.5.2 Model 2 : Bare Frame - Flexible Joints

The periods and displacements were improved by including the flexibility of the panel zones on Model 1, Fig. 5.3, 5.4 and 5.5. Results from CASES 2-MH-BT, 2-ML-BT, 2-LP-BT show that the maximum twelfth floor displacements differ from the recorded ones by a maximum of 18% in the NS direction and only 9% in the EW direction. Drift coefficients differed by a maximum of 16% from those estimated from the records. The maximum base shear coefficients had a maximum

error of 13% in the EW direction for the Morgan Hill earthquake and 12% in the NS direction for the Mt. Lewis earthquake. This simple model, representative of another possible design approach, gave good results and permitted the identification of the basic response characteristics of the structure. The EMF values were similar to those found for Model 1.

5.5.3 Model 3 : Adjusted Model - "Normal Damping"

This model further adjusted the mass, the contributions of the architectural details to the lateral stiffness of the structure, the deck contribution to beam stiffness and the amount of viscous damping. The results obtained with this model were virtually identical to those observed from the records, see Figs. 5.6, 5.9 and 5.10.

From CASES 3-MH-BT, 3-ML-BT and 3-LP-BT the maximum difference of 12% in displacement response values was found for the NS direction during the Loma Prieta event. The drift coefficients were closer to the average coefficients estimated from the records with a maximum difference of 13%. The base shear had a maximum difference of 13% for the Morgan Hill earthquake.

Model 3 was developed from Model 2 by making minor changes in some parameters. A systematic analysis of interim models showed that increasing the moment of inertia for the NS oriented floor beams to include the effect of partial composite action had the strongest effect. This resulted in a greater separation of the predominant periods of the building and a reduction of the modal coupling. Evidence of this was the change in the EMF ratio for the first mode translational components (EMF_{1y}/EMF_{1x}) from 0.44 to 0.11. The large effect that changing beam moments of inertia had on modal coupling shows the strong sensitivity of the model to this parameter and points out the difficulties in reproducing coupled behavior in the analysis of space frame structures.

Including non-structural elements in the model, did not have an important effect on the response envelopes. Nevertheless, it helped to get a better visual match between recorded and computed response histories.

The increased rotational mass moment of inertia changed the predominantly torsional period of the system by 5% and increased the torsional EMF of the predominant translational modes. If this last change had not been made in Model 3, the maximum displacement in both directions would have changed by less than 1%. Nevertheless, the maximum rotation would have been reduced by 13%.

Element stresses were obtained from the model subjected to the Morgan Hill and Mt. Lewis earthquakes. They show that for the main elements of the perimeter and interior frames, the stresses, including gravity and earthquake loads, were below the yield capacity. Maximum beam stresses were around 70% of yield and typical column stresses were around 85% of yield. It should

be recalled that the peak ground accelerations in these cases were only 4% g. A more detailed distribution of capacity demands for these and the Loma Prieta earthquake is given in the next chapter.

5.5.4 Model 4 : Adjusted Model - "Low Damping"

Model 4 was constructed to obtain a better match than Model 3 of some displacement histories at the twelfth floor for the Mt. Lewis and Loma Prieta earthquakes, and to evaluate the effect of damping on the response. Modal damping was reduced to 1% of critical for all the modes considered in the analysis. As observed from the results, shown in Figs. 5.11 to 5.14 and Tables 5.3 and 5.4, the reduction of the damping caused the response values to be overestimated. The maximum difference between recorded and computed relative displacements was about 16% for the Mt. Lewis event and 26% for the Loma Prieta event. Interstory drifts were overestimated by as much as 28%. The maximum difference in computed and derived base shear, obtained for the NS direction during the Mt. Lewis event, was 33%. The better amplitude match for Model 4, observed in the EW direction during the Mt. Lewis earthquake, was caused mainly by the reduction of the damping in the predominant EW mode. The actual building response can be assumed to be bounded by Models 3 and 4.

An element stress check was performed for Model 4 for the Mt. Lewis bi-directional input. For this case some beams and columns just reached their theoretical yield capacity. Because this model overestimated the base shear, the stress values found are not necessarily those that occurred in the structure.

This model also gave some insight into the apparent causes of the severity and duration of the response. Figure 5.13 shows the response of Model 4 to the first 40 seconds of the Mt. Lewis earthquake (Fig. 5.12 shows response to the complete input record). In part (a) of Fig. 5.13, the response of the analytical model with 1% viscous damping is compared with the recorded motion. Parts (b) and (c) show the first and second mode contributions to the displacement in the EW direction. Here it can be seen that the first and second modes individually have lightly attenuated responses after about 30 seconds of motion. However, the two modes go in and out of phase; this results in constructive and destructive interference that produces a large dip in the combined response at second 30 and an increase in response up to second 60. This analysis confirms that the severe response observed at the end of the records was not associated with the input motions.

An analysis was also performed considering 5% viscous damping. Here (Fig. 5.13d), the responses of the individual modes attenuate so quickly that virtually no beating under free vibration can occur and little significant motion occurs after 35 seconds.

5.6 Sensitivity Studies

The models developed were also used to assess the sensitivity of the response of the building to certain design parameters. A complete parametric study was not performed because of the large dimensions of the structure and associated computer costs.

5.6.1 Earthquake Components

The models were subjected to different combinations of input motions. Comparisons of the results for the CASES 3-MH-BT and 3-MH-B, 4-ML-BT and 4-ML-B, and 4-LP-BT and 4-LP-B, in Tables 5.2, 5.3 and 5.4 indicate that input torsion had only a small effect on the overall building response. The maximum difference was found for the twelfth floor torsional rotation with a 12% increase. Nonetheless, including this component had less than a 2% effect on the twelfth floor SW corner displacements. For other response values the effect was below 2%. In one case, the Mt. Lewis event, including the torsional input actually reduced torsional rotations in the structure by 5%.

Model 3 was also subjected to a case with only the NS component of the Morgan Hill earthquake, CASE 3-MH-NS, Fig. 5.8. Maximum displacements, drift coefficients and base shear in the NS direction were reduced by 20% when one, rather than two, horizontal components of excitation were considered.

5.6.2 Reduced Beam Stiffness

To evaluate the sensitivity of the response to uncertainties in the calculation of the moments of inertia of the interior frame beams (both directions), Model 5 was subjected to the Morgan Hill earthquake, CASE 5-MH-BT, Fig. 5.15. The 10% reduction in the beam moment of inertia from that of Model 3 produced a 2% increase in the predominant periods and had minor effects on the EMF. The maximum difference in displacements and base shear between CASE 5-MH-BT and CASE 3-MH-BT was 6%. As mentioned above (Section 5.5.3) the model is very sensitive to the variation of the beam moment of inertia in only one direction because of the separation of natural periods and uncoupling that could occurs in the model.

5.6.3 P-Δ Effects

Because of the flexibility of the building and the relatively large lateral displacements developed, geometric nonlinearities (P-Δ effects) could be important. To evaluate the sensitivity of the response to this effect, Model 6 was subjected to the Morgan Hill earthquake, CASE 6-MH-BT, Fig. 5.16. For this case the changes in response values were less than 7% and the increases in the

predominant periods were less than 3%, when compared with CASE 3-MH-BT. Thus, P-Δ effects appear not to have a significant influence on the observed linear response of this building.

5.6.4 Position of the Center of Mass

To study the effect of the uncertainty in the position of the center of mass on the building response a 5% eccentricity was added to Model 3, CASE 7-MH-NS, Fig. 5.17. The following effects were found in comparison with CASE 3-MH-NS: the twelfth floor maximum displacement was reduced by 3% in the NS direction and 36% in the EW direction; and the maximum rotation was increased by 144%. Also the SW corner NS maximum displacement increased by 18%. The base shear in the NS direction decreased by 6%, and by 36% in the EW direction. The base torsional moment was increased by 160%. (These values imply an increase in the ratio of the maximum base torsional moment to maximum base shear of 181%.) This is consistent with observations made on the basis of analyses of simpler structures, see for example References [25, 17]. It appears that the response of the building was very sensitive to small changes in the location of the center of mass.

5.6.5 Inertial Mass

To evaluate the sensitivity of the response to uncertainties in the calculation of the mass of the structure, Model 8 was subjected to the Morgan Hill earthquake, CASE 8-MH-BT, Fig. 5.18. The 10% reduction in translational (both directions) and rotational mass produced a 5% decrease in the predominant periods and, as expected, did not change the EMF. Nevertheless, maximum displacement and base shear decreased by 43% in the NS direction when compared with that of CASE 3-MH-BT. This effect, as noted before, was likely associated with the rapid variation in spectral acceleration at the low damping values considered. The effect of changing only the rotational mass is considerably lower as noted in Section 5.5.3.

5.7 Model Uniqueness

The models developed are not unique. It is expected that other models with different assumptions and parameter combinations could also predict the observed response. Nevertheless, the importance of the models presented is that they were all developed using a set of assumptions consistent with those typically employed in seismic design and analysis of structures.

Although the response characteristics (amplitude envelope, beating phenomenon, displacements, interstory drifts and base shear) predicted by the analytical models (Model 2, 3 and 4) were close enough to the observed behavior to identify the factors controlling the structural response, some features observed in the records were not completely reproduced. For example, maximum tor-

sional rotations were underestimated by nearly 30% in some of the models. Although more detailed analyses and system identification studies could be undertaken to determine precisely the most suitable model for the structure, the overall response characteristics were adequately established using procedures commonly employed in design practice.

5.8 Response to Static Lateral Forces

Model 9 was used to evaluate the response parameters generated by applying the 1988 UBC and ATC 3-06 equivalent static lateral force methods. This model was similar to Model 2 (the model based only on information from building plans) with an additional 5% eccentricity as required by the design recommendation considered. For simplicity of presentation equivalent static lateral loads were applied only in the NS direction. Consequently, two positions for the center of mass were investigated, one to the West and one to the East of the computed center of mass. Maximum diaphragm torsional rotations were obtained for the case where the eccentricity was applied to the West of the original center of mass. Only these results are presented below.

Using criteria established by the 1988 UBC (Section 2312 (d) 5 and Tables No. 23-M and 23-N) the building was determined to be a "regular structure." "Torsion irregularities," as stated by the UBC, exist when "the maximum story drift computed, including accidental torsion, at one end of the structure transverse to an axis [of load application] is more than 1.2 times the average of the story drifts of the two ends of the structure" [22]. For Model 9 this ratio was computed to be 1.11, so the building does not need to be designed considering torsional irregularities. Because the structure is considered regular in plan and in elevation and its height is less than 73 meters (240 ft.), the equivalent static load procedure described by the UBC could be used for this structure.

Design code base shear demands are a function of structural period. The 1988 UBC presents two methods (A and B) to estimate the natural period of the building. Method A, with the formula for steel moment-resisting frames, $T = 0.035\ (h)^{3/4}$, gave a value of 1.77 seconds (80% of the observed value). Method B allows the use of a period "calculated using the structural properties and deformation characteristics of the resisting elements in a properly substantiated analysis" [22]. For Model 9 a value of 2.2 seconds was computed. This period value complied with the requirement that the base shear coefficient (C), obtained by this method, would not be less than 80% of the coefficient obtained with the period calculated by Method A. ATC 3-06 has similar recommendations for estimating natural periods. Nonetheless, a constraint on the value of the calculated period, and not on the value of the seismic coefficient (C or C_s), is prescribed. According to ATC 3-06, the period estimated from structural properties of the building should not exceed 1.2 times the value obtained by the formula shown above. Thus, the period used for the

ATC 3-06 analysis was limited to 2.12 seconds. The selection of these periods implies approximately 15% reduction in base shear in comparison with the base shear given by the standard formula recommended by these regulations for steel moment-resisting frames (i.e., T = 0.035 $(h)^{3/4}$).

The site soil coefficient was selected for the analysis assuming that soil properties were not known in sufficient detail (i.e., S=1.5 for the 1988 UBC and S=1.2 for ATC 3-06). Other parameters for the evaluation of the design base shear were taken as follows:

- The importance factor (I) was taken as 1.0 in both cases;
- The structural system factor (R_w or R) was assumed to be 12 for the 1988 UBC and 8 for ATC 3-06.
- The seismic zone factor (Z, or A_v and A_a) was taken as 0.4 in both cases.

Results for the static load application are shown in Table 5.6. Code-based shears were substantially smaller than those derived from the earthquake records even though the peak ground accelerations were quite small. The non-factored, 1988 UBC working stress level base shear was 43, 25, and 21% of the demand for the Morgan Hill, Mt. Lewis and Loma Prieta events, respectively. For ATC 3-06 these values were 75, 44 and 36%, respectively. The differences between the two documents are in part due to the fact that the UBC forces are computed at working stress levels whereas ATC uses ultimate strength procedures. The structural analyses also show that the building members would not generally be overstressed when subjected to 1988 UBC lateral forces. The maximum model story drift ratio obtained from the applied UBC static loadings was 72% of the limit established by that Code ($0.03/R_w$, with R_w=12). For the ATC static loading the maximum story drift ratio was 81% of the limit established by that recommendation (i.e., $0.0015/C_d$, with $C_d = 5.5$).

Thus, it appears that the design recommendations studied would have shown that the building was generally satisfactory and the unusually severe response exhibited by the structure would not have been identified using equivalent static design procedures alone.

5.9 Response to Other Ground Motions

The likely effect of more intense input ground motions on the response of the structure is briefly presented in this section.

5.9.1 Response to the NS component of the 1940 El Centro Record

Model 3 was used to estimate the response of the building to the NS component of the 1940 El Centro earthquake, see record spectrum in Appendix C. This record is commonly used in

seismic analysis of structures. The peak ground acceleration used in this analysis was 0.34 g. The input ground motion was applied to the model in only the NS direction. Results are presented in Table 5.5 and Fig. 5.19.

Relatively large displacements, torsional rotations, and story drifts were observed. Although the response was severe, it did not exhibit the large amplification observed for the previous events. The peak ground acceleration of the El Centro record was 8.5 times the recorded Morgan Hill and Mt. Lewis values, but the base shear was only 2.3 times the value obtained for the Morgan Hill event and 1.4 times that for the Mt. Lewis event. The main reason for this behavior is that the predominant period of the El Centro record is near 0.3 second. Consequently for 3% damping its spectral acceleration at 2.2 seconds is 0.21 g, only 1.5 times the value obtained for the Mt. Lewis event. Thus, the frequency characteristics of the input ground motion have a large effect on the response. It is clear that the ground motions used for design analyses must be selected with care, especially where the predominant period of the ground motion may be similar to one of the fundamental periods of the structure.

5.9.2 Response to the Transverse Component of the Mexico City 1985 Record

Model 3 was also subjected to the N90W (transverse) component of the SCT record obtained during the 1985 Mexico earthquake, see record spectrum in Appendix C. This ground motion was recorded on soft soil and has a predominant period similar to that of the building. The input motion was applied to the model in the NS direction. The peak base acceleration was 0.17 g, 4.3 times greater than the Morgan Hill and Mt. Lewis events and 1.7 times greater than the Loma Prieta earthquake. However, its response spectrum has predominant periods near 2 seconds resulting in an ordinate in this period range about 6 times higher than that for the Mt. Lewis event.

Results of the structural analyses are presented in Table 5.5 and Fig. 5.20. Extremely large deformations were calculated in the elastic analysis (e.g., 180 cm (71 inches) of lateral displacement and 0.0101 radian of torsional rotation at the twelfth floor). The computed base shear for the SCT record was 12 times the value obtained for the Morgan Hill event and 7 times the value obtained for the Mt. Lewis event. As expected, the response was severely amplified because of the near concurrence of predominant input and structural periods.

The strong response calculated for the model would not necessarily be that of the structure under similar ground motion conditions because a considerable amount of element yielding would be expected for this level of shaking, as will be shown in the following chapter.

5.9.3 Comments

El Centro and SCT ground motion records are more severe than the events recorded at the building site to date. Also the base shears resulting from the records are significantly higher than those currently used in code-based design. It would be desirable to assess the response of the structure with the excitation scaled to code design levels. For instance, the 1988 UBC in Section 2312 (f) 5 C indicates that base shears obtained from dynamic analyses for regular structures need not exceed 90% of the value found from the static force procedure presented in Section 2312 (e) of the Code. If this procedure is followed for the El Centro or SCT records, the interstory drift ratios and the member forces would satisfy relevant UBC criteria. The values obtained would also be lower than those obtained from an equivalent static lateral load analysis conforming to the 1988 UBC.

5.10 Conclusions

The following conclusions can be drawn from these elastic analyses.

1. **Analytical Models**

   The response of the building derived from the recorded accelerograms (i.e. periods, displacement, interstory drift, base shear, etc.) can be reproduced adequately using simple elastic computer models. A good match was found for models that included the center-to-center member dimensions, no rigid element zones, the magnitude and distribution of mass as estimated from structural plans, nominal element properties, and a modal damping ratio typically associated with steel structures responding in the linear range. By further adjusting the actual mass distribution and incorporating the deck contribution to the beam stiffness, global results were virtually identical to recorded values. Structural factors that did not have a strong effect on the response were the lateral stiffness of light partitions and cladding and P-Δ effects.

   From analyses obtained considering different loading conditions, it was found that both horizontal components of the ground motion records were needed to reproduce the building response. Bi-directional effects accounted for nearly 22% of the maximum response amplitude in orthogonal directions and had a large effect on the shape of the time histories. Torsional input motion was found to have a relatively small effect on the overall response of the structure.

   The viscous damping ratio had an important effect on the computed responses of the models. Because of the rapid fluctuation of spectral acceleration with period in lightly-damped

systems, the responses of the models with low damping were very sensitive to modeling uncertainties that influenced period estimates.

The models also showed a strong sensitivity to the position of floor center of mass. Increasing the eccentricity by 5% of the largest plan dimension of the building reduced the NS displacements at the center of mass by 3%, increased the NS displacements at the SW corner by 18%, increased floor rotations by nearly 144%, reduced the NS base shear in 6%, and base torque by 160%. The ratio of maximum base torque to maximum sum of inertial forces was increased by 180% when this additional eccentricity was included. This is consistent with observations made on the basis of analyses of simpler structures.

The modal coupling was quite sensitive to model parameters. Small changes of stiffness in one direction reduced the coupling in some modal components by nearly 75%. This points out the difficulty of accurately reproducing the coupled behavior of such structures. Also, this sensitivity suggests that the response characteristics of the real structure might change significantly as a result of small nonlinearities.

2. Response of the Model to Other Ground Motions

Markedly different responses were obtained from analyses of the computer models subjected to the NS component of the 1940 El Centro earthquake, the N90W (transverse) component of the 1985 Mexico City SCT record and the building base records. Differences in the response characteristics were caused mainly by the different frequency content of the input motions. This indicates the importance of selecting for design dynamic analyses several ground motions that correspond to the expected input signal at the site, especially when the predominant periods of the ground motion at the location could be similar to one of the fundamental periods of the structure.

3. Code Recommendations

The steel moment-resisting space frame system used in the structure is very flexible. Predominant periods observed (near 2.2 seconds) and computed were well above those estimated using Code-type empirical formulae (i.e., 0.1 N = 1.3 sec. or $0.035(h)^{3/4} = 1.8$ sec.). Such code relations will result in conservative base shear design values for Code-type design spectra. Nevertheless, this will not necessarily be the case for site dependent spectra, nor will lateral displacement be conservatively predicted.

The building was identified by the 1988 Uniform Building Code design recommendations as a regular structure. The static procedures, specified by the UBC were not able to identify the unusual response developed by this structure. It is significant that the design base shear

coefficient required by the 1988 UBC was only 25% of the one actually developed by the building during the minor (0.04 g) Mt. Lewis event. The drifts experienced by the building were 240% larger than accepted by the Code ($0.03/R_w$) for nonfactored design loads. If the response values were scaled proportionally, so that the base shear obtained from the models (or derived from the building records) corresponded to the Code recommended design base shear (as allowed by the 1988 UBC according to Section 2312 (f) 5 C), then drifts and drift ratios would satisfy recommended UBC limitations. Similar observations can be made with the ATC provisions.

4. Computed Building Response

The analytical models confirmed the conclusions developed from the interpretation of the building records. They indicate that the unusual behavior of the building was related to the relatively low amount of structural damping, the lateral-torsional coupling, the three-dimensional modes of the building constructively reinforcing one another during portions of the motion, the resonance effect on the building caused by the agreement of the site input ground motion characteristics and the structure, and the relatively large flexibility of the structure.

From the small set of parametric studies performed herein, it was observed that a moderate amount of modal viscous damping (i.e. 5% of critical), substantially reduced the effective duration of the response. The peak values, nevertheless, were not considerably affected by the small increase in the amount of viscous damping.

Table 5.1: **Model Periods (sec) and Effective Mass Factors.**

MODEL	1	2	3-4	5	6	7	8	RECORDED
T_1	1.93	2.21	2.19	2.23	2.25	2.19	2.09	2.15-2.20
T_2	1.87	2.15	2.10	2.12	2.14	2.14	1.99	2.05-2.10
T_3	1.40	1.63	1.68	1.71	1.70	1.65	1.59	1.65-1.70
T_4	0.70	0.80	0.80	0.80	0.80	0.79	0.76	0.65-0.75
T_5	0.68	0.77	0.76	0.77	0.77	0.77	0.72	0.60-0.70
$EMF_{(1x)}$	0.528	0.538	0.697	0.696	0.699	0.657	0.698	-
$EMF_{(1y)}$	0.249	0.236	0.077	0.079	0.077	0.118	0.077	-
$EMF_{(1z)}$	0.000	0.000	0.002	0.002	0.002	0.001	0.002	-
$EMF_{(2x)}$	0.246	0.232	0.074	0.076	0.074	0.114	0.074	-
$EMF_{(2y)}$	0.521	0.531	0.689	0.689	0.691	0.604	0.691	-
$EMF_{(2z)}$	0.008	0.009	0.010	0.010	0.010	0.056	0.009	-
$EMF_{(3x)}$	0.004	0.005	0.005	0.005	0.005	0.005	0.005	-
$EMF_{(3y)}$	0.004	0.005	0.007	0.007	0.007	0.051	0.006	-
$EMF_{(3z)}$	0.769	0.764	0.764	0.765	0.764	0.719	0.765	-

Table 5.2: **Building and Model Response Values, Morgan Hill Earthquake.**

CASE	RECORDED[i]	1-MH-BT	2-MH-BT	3-MH-BT	3-MH-B	3-MH-NS	5-MH-BT	6-MH-BT	7-MH-NS	8-MH-BT
12^{th} Floor Drift										
EW (cm)	16.41	8.51	17.86	17.65	17.63	3.76	18.64	18.97	2.41	13.16
NS (cm)	16.12	6.73	13.89	17.04	16.99	13.56	17.55	17.32	13.16	9.70
ROT (rad.)	0.0017	0.006	0.0012	0.0012	0.0012	0.0009	0.0012	0.0012	0.0022	0.0008
Max. Drift Coeff.										
EW (%)	0.37(2-7)	0.24(3)	0.44(5)	0.44(5)	0.44(5)	0.09(3-7)	0.47(3-5)	0.47(3-5)	0.32(5)	0.33(3-5)
NS (%)	0.39(2-7)	0.15(2-10)	0.34(5)	0.42(3-5)	0.42(5)	0.33(5)	0.44(5)	0.43(5)	0.06(3-7)	0.24(5)
Base Shear										
EW (10^3 kN)	10.45	8.87	11.93	12.03	12.02	2.66	12.36	12.72	1.69	9.01
NS (10^3 kN)	10.68	5.57	9.60	11.98	11.93	9.66	12.04	12.31	9.05	6.82

Values in parenthesis indicate level where maximum drift index was obtained.

i Derived values at Center of Mass.

Table 5.3: **Building and Model Response Values, Mt. Lewis Earthquake.**

CASE	RECORDED[i]	2-ML-BT	3-ML-BT	4-ML-BT	4-ML-B
12^{th} Floor Drift					
EW (cm)	13.51	12.98	13.06	14.83	13.51
NS (cm)	29.90	24.61	26.44	34.59	34.54
Rot. (rad.)	0.0026	0.0015	0.0015	0.0017	0.0018
Max. Drift Coeff.					
EW (%)	0.30(2-7)	0.31(5 - 7)	0.31(5-7)	0.36(3 & 5)	0.36(3 & 5)
NS (%)	0.67(2-7)	0.60(5)	0.64(5)	0.85(5)	85(5)
Base Shear					
EW (10^3 kN)	8.01	7.92	7.91	9.88	9.90
NS (10^3 kN)	18.24	16.29	18.75	24.59	24.55

Numbers in parenthesis indicate level where maximum drift index was obtained.

i Derived values at Center of Mass.

Table 5.4: **Building and Model Response Values, Loma Prieta Earthquake.**

CASE	RECORDED[i]	2-LP-BT	3-LP-BT	4-LP-BT	4-LP-B
12^{th} Floor Drift					
EW (cm)	30.58	33.43	32.92	38.51	38.56
NS (cm)	34.85	37.21	30.73	33.86	33.71
Rot. (rad.)	0.0027	0.0016	0.0015	0.0018	0.0016
Max. Drift Coeff.					
EW (%)	0.74(2-7)	0.86(5)	0.84(3-5)	1.00(3)	1.00(3)
NS (%)	0.81(2-7)	0.90(5)	0.74(5)	0.78(5-6)	0.79(7)
Base Shear					
EW (10^3 kN)	22.69	22.80	22.78	27.22	27.26
NS (10^3 kN)	21.35	24.29	21.64	22.73	22.64

Numbers in parenthesis indicate level where maximum drift index was obtained.

i Derived values at Center of Mass.

Table 5.5: **Model 3 Response Values, SCT Mexico and 1940 El Centro Earthquake.**

EARTHQUAKE	SCT	EL CENTRO
12^{th} Floor Drift		
EW (cm)	32.64	6.55
NS (cm)	180.34	28.70
Rot. (rad.)	0.0101	0.0020
Max. Drift Coeff.		
EW (%)	0.80(5)	0.17(3)
NS (%)	4.42(5)	0.82(3)
Base Shear		
EW (10^3 kN)	23.40	4.97
NS (10^3 kN)	129.24	25.21

Numbers in parenthesis indicate level where maximum drift index was obtained.

i Derived values at Center of Mass.

Table 5.6: **Model 9 Response Values, Building Code Static Loads. Applied in the NS Direction.**

CODE	UBC-88	ATC 3-06
12^{th} Floor Drift		
EW (cm)	0.20	0.25
NS (cm)	7.52	9.32
Rot. (rad.)	0.0004	0.0005
Max. Drift Coeff.		
EW (%)	0.01	0.01
NS (%)	0.18	0.22
Base Shear		
EW (10^3 kN)	0	0
NS (10^3 kN)	4.69	5.54

1988 UBC Coefficients: Z=0.4, S=1.5, T=2.2 sec., I=1.0 and R_w=12.

ATC 3-06 Coefficients: $A_v = A_a$=0.4, S=1.2, T=2.12 sec., I=1.0 and R=8.

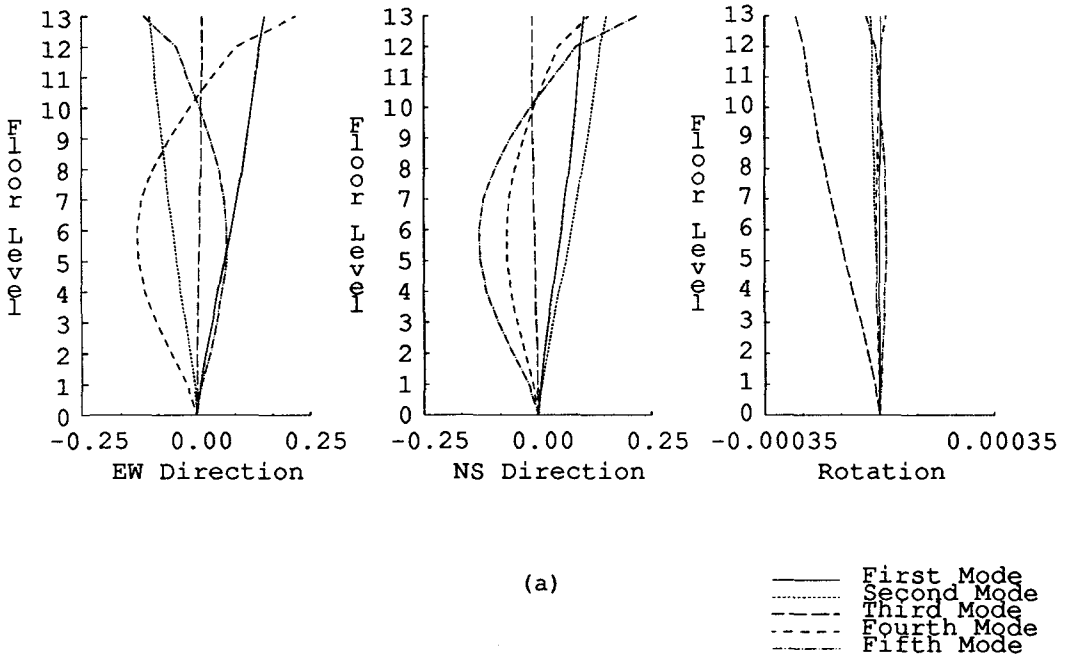

(a)

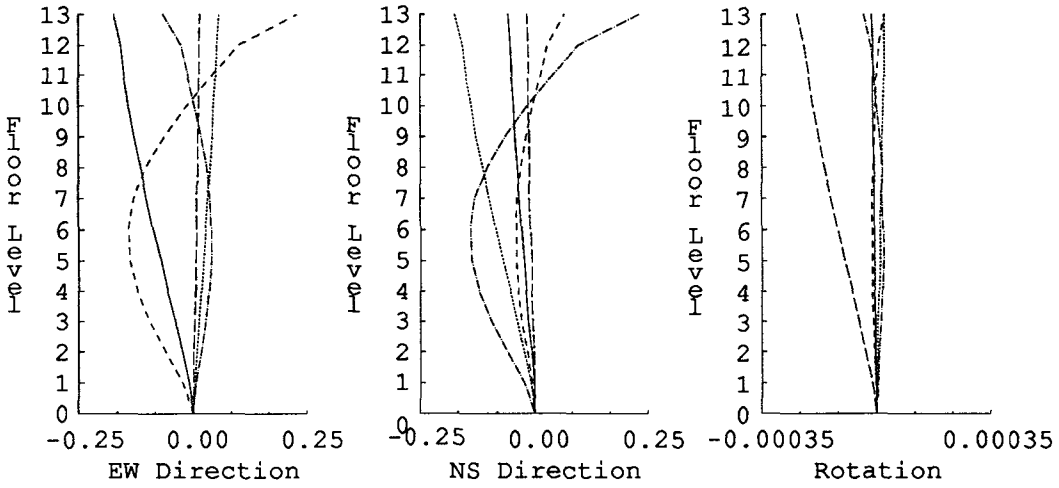

(b)

Figure 5.1: Modal shapes. (a) Model 1. (b) Model 3.

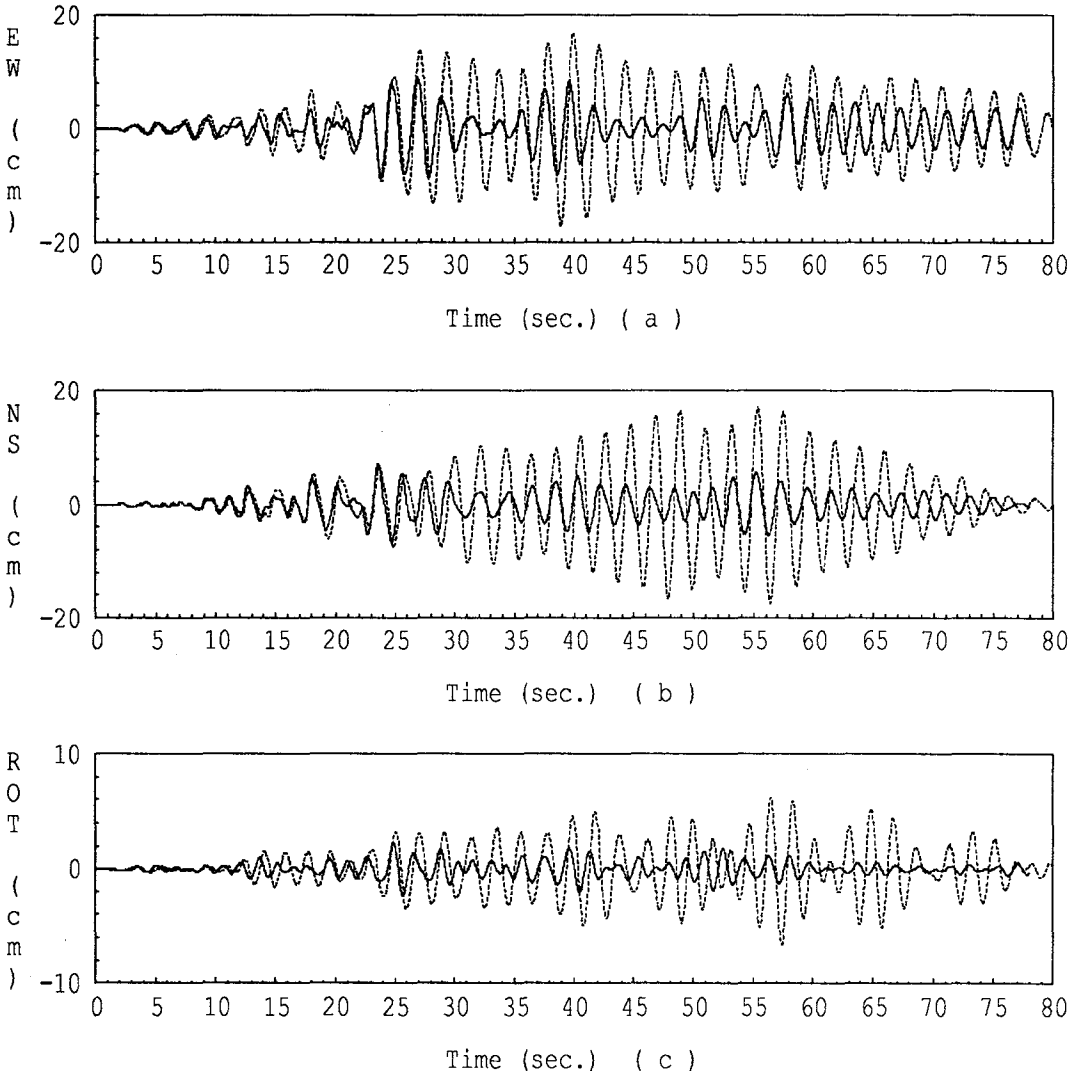

Figure 5.2: CASE 1-MH-BT. Twelfth floor motion. (a) EW relative displacement, SW corner. (b) NS relative displacement, SW corner. (c) Derived torsion, SW-NW corner relative displacement. Model —— Record ·····.

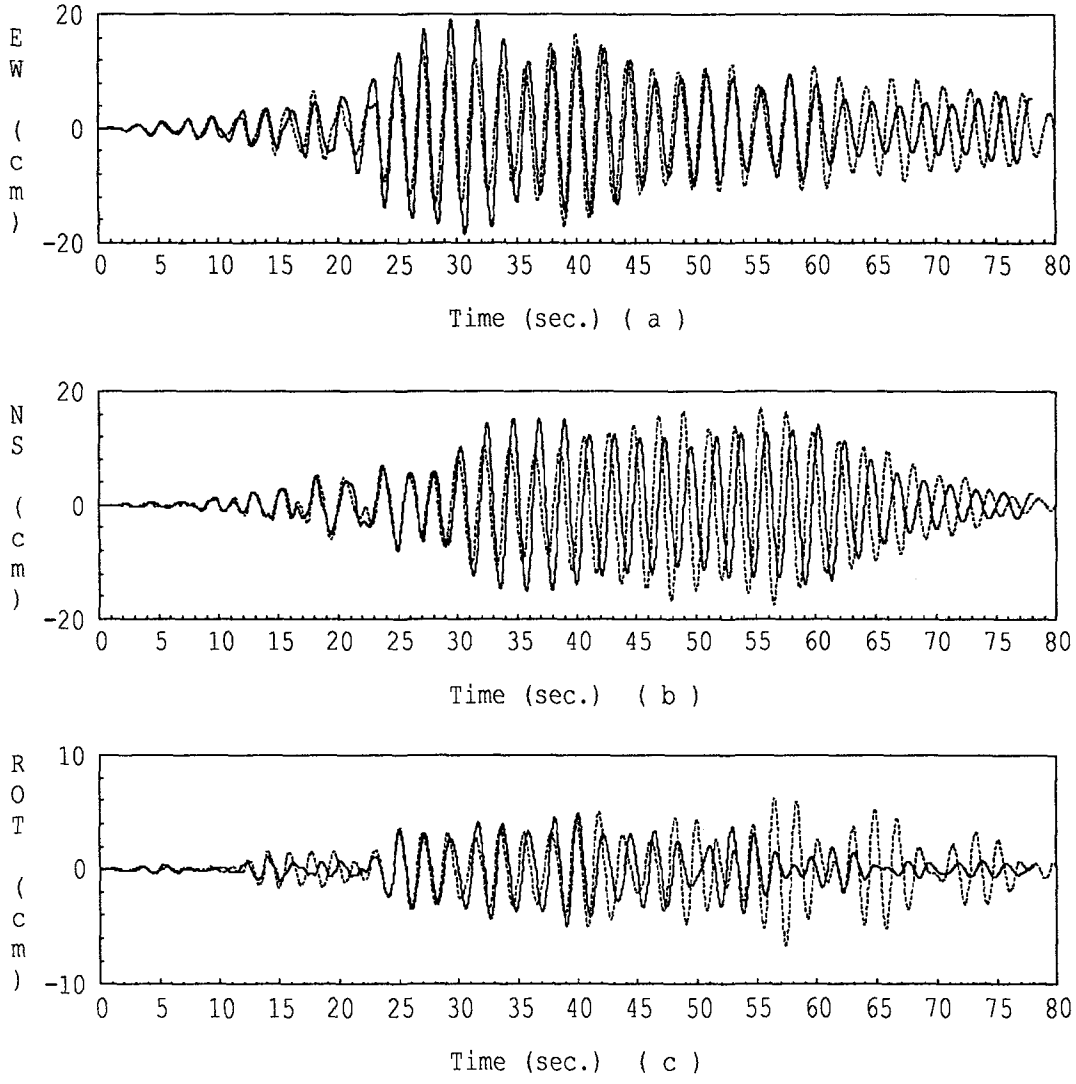

Figure 5.3: CASE 2-MH-BT. Twelfth floor motion. (a) EW relative displacement, SW corner. (b) NS relative displacement, SW corner. (c) Derived torsion, SW-NW corner relative displacement. Model —— Record ·····.

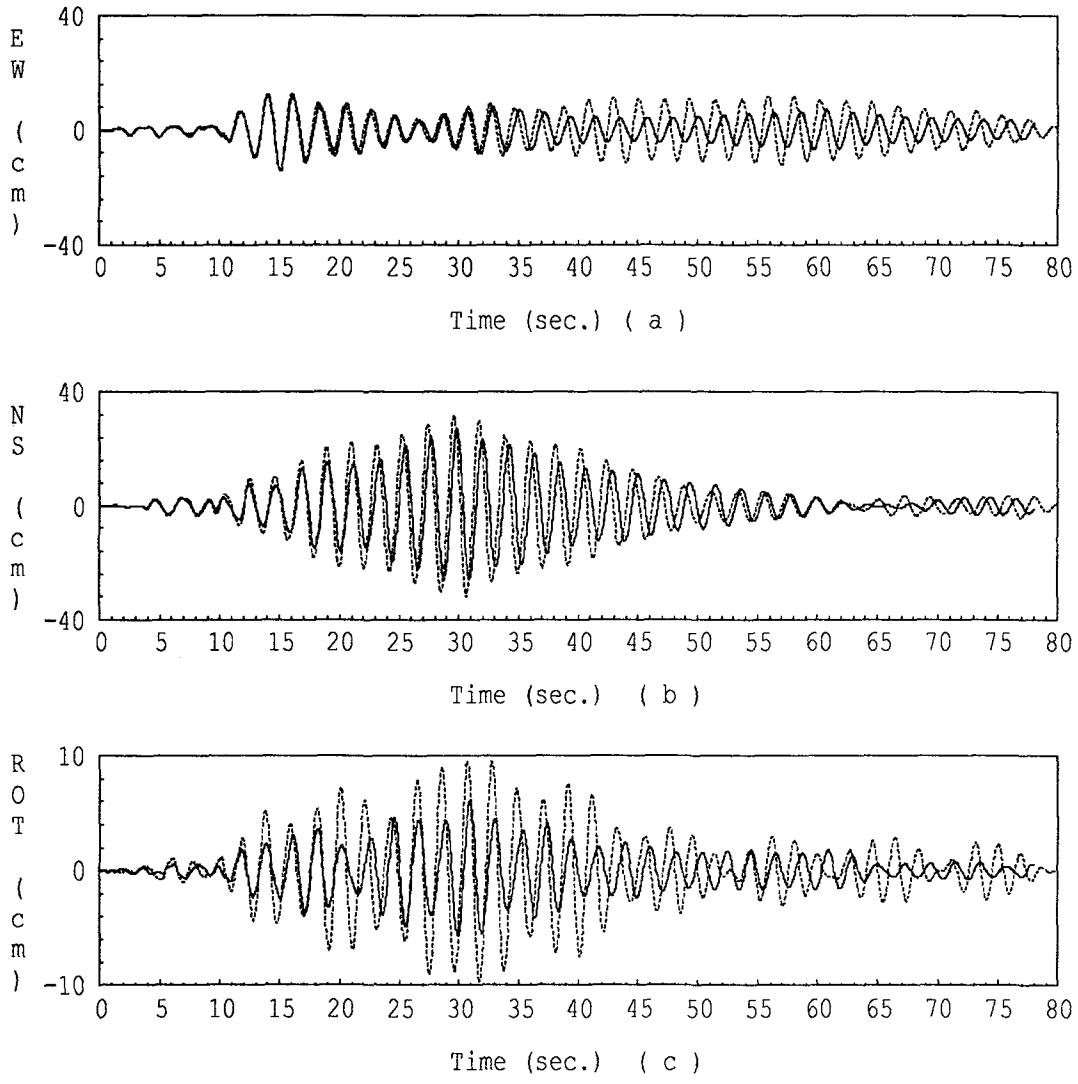

Figure 5.4: CASE 2-ML-BT. Twelfth floor motion. (a) EW relative displacement, SW corner. (b) NS relative displacement, SW corner. (c) Derived torsion, SW-NW corner relative displacement. Model —— Record ·····.

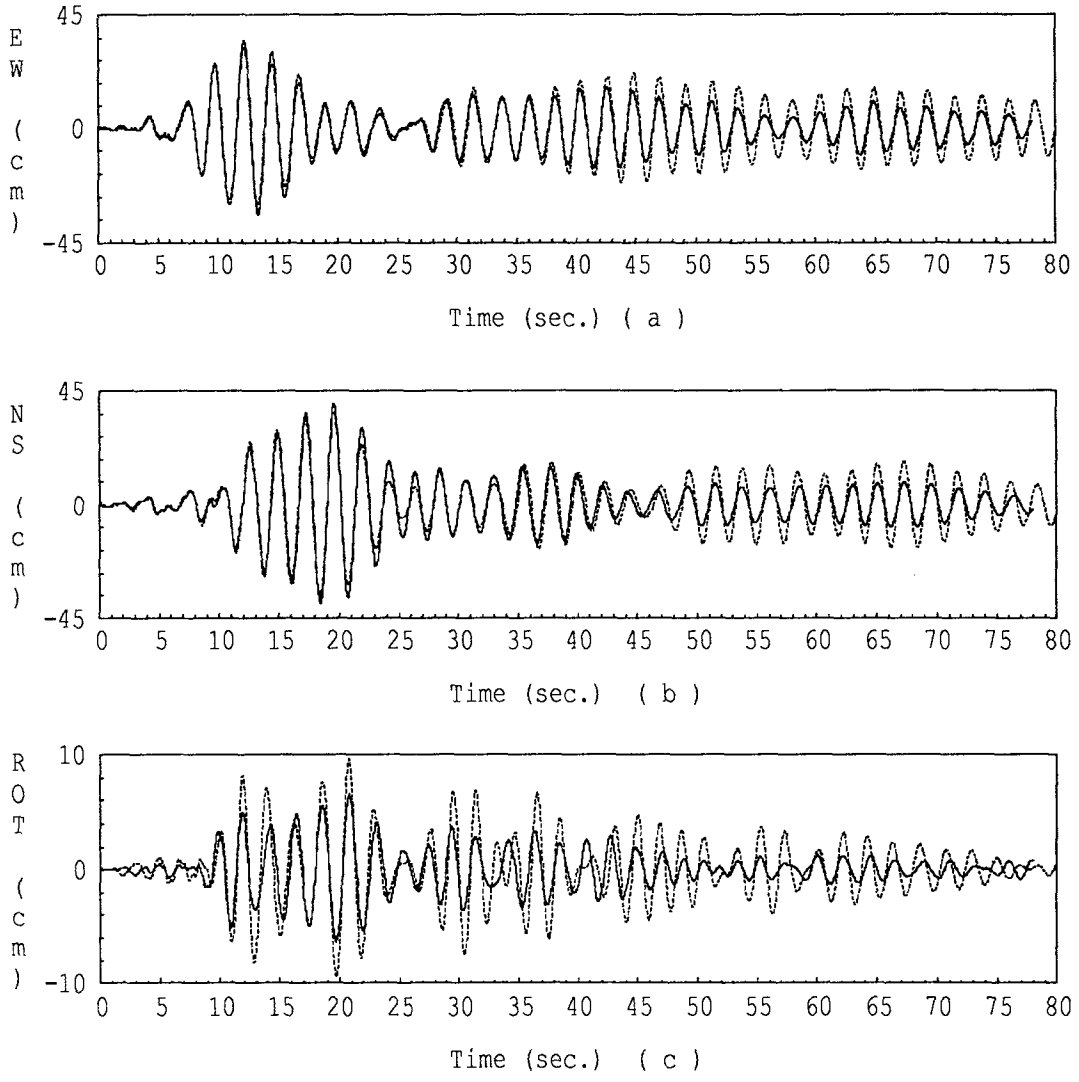

Figure 5.5: CASE 2-LP-BT. Twelfth floor motion. (a) EW relative displacement, SW corner. (b) NS relative displacement, SW corner. (c) Derived torsion, SW-NW corner relative displacement. Model —— Record ·····.

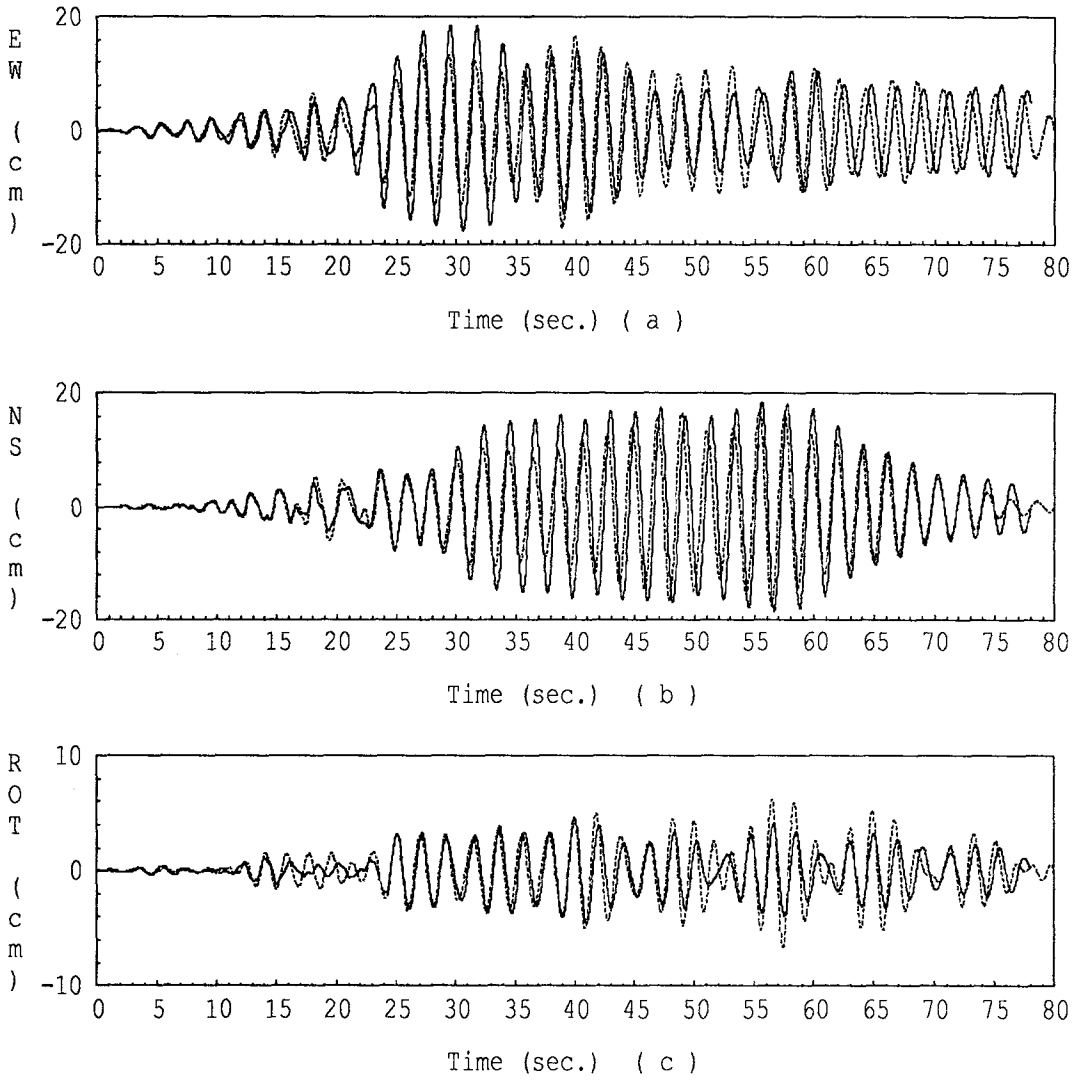

Figure 5.6: CASE 3-MH-BT. Twelfth floor motion. (a) EW relative displacement, SW corner. (b) NS relative displacement, SW corner. (c) Derived torsion, SW-NW corner relative displacement. Model —— Record ·····.

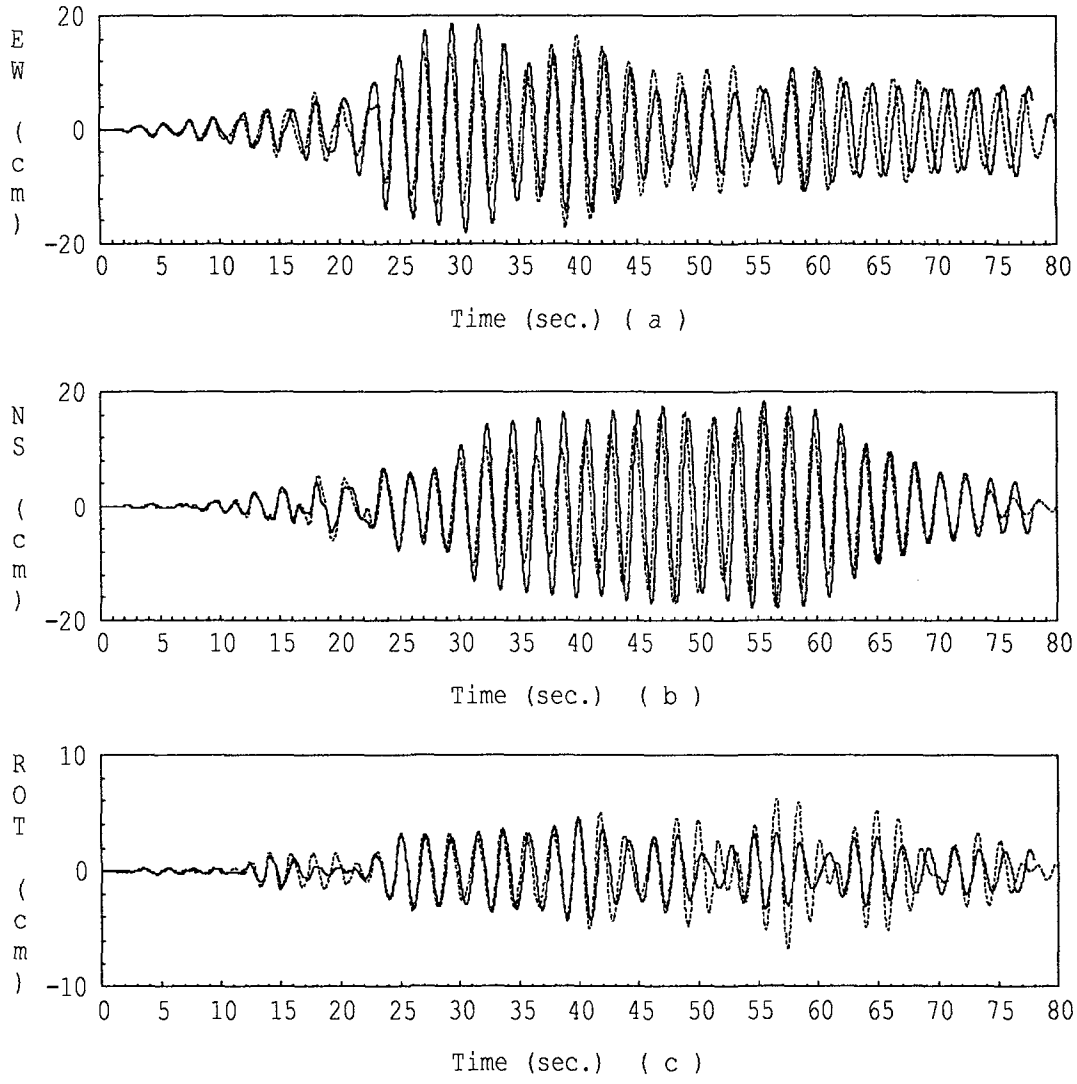

Figure 5.7: CASE 3-MH-B. Twelfth floor motion. (a) EW relative displacement, SW corner. (b) NS relative displacement, SW corner. (c) Derived torsion, SW-NW corner relative displacement. Model —— Record ·····.

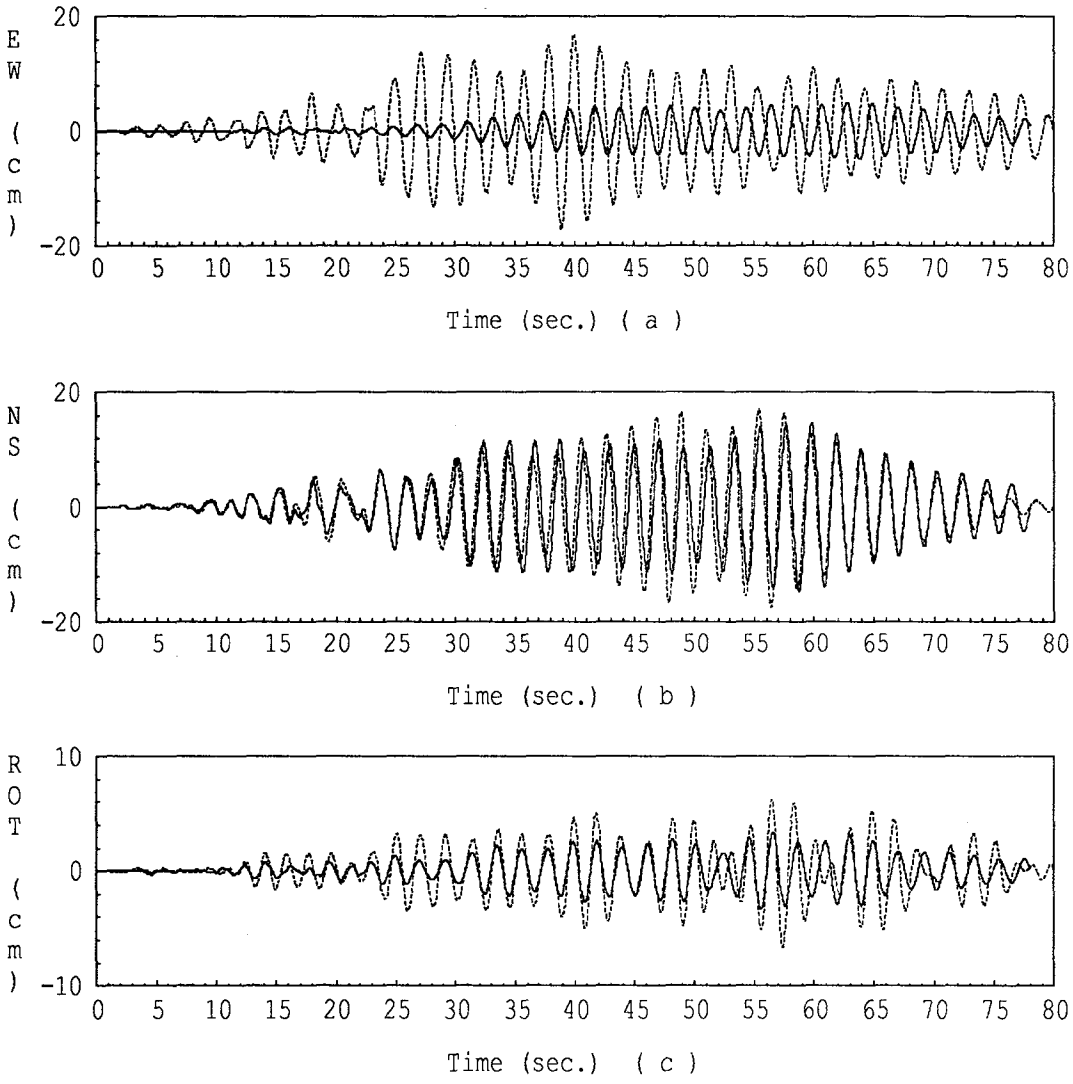

Figure 5.8: CASE 3-MH-NS. Twelfth floor motion. (a) EW relative displacement, SW corner. (b) NS relative displacement, SW corner. (c) Derived torsion, SW-NW corner relative displacement. Model —— Record ·····.

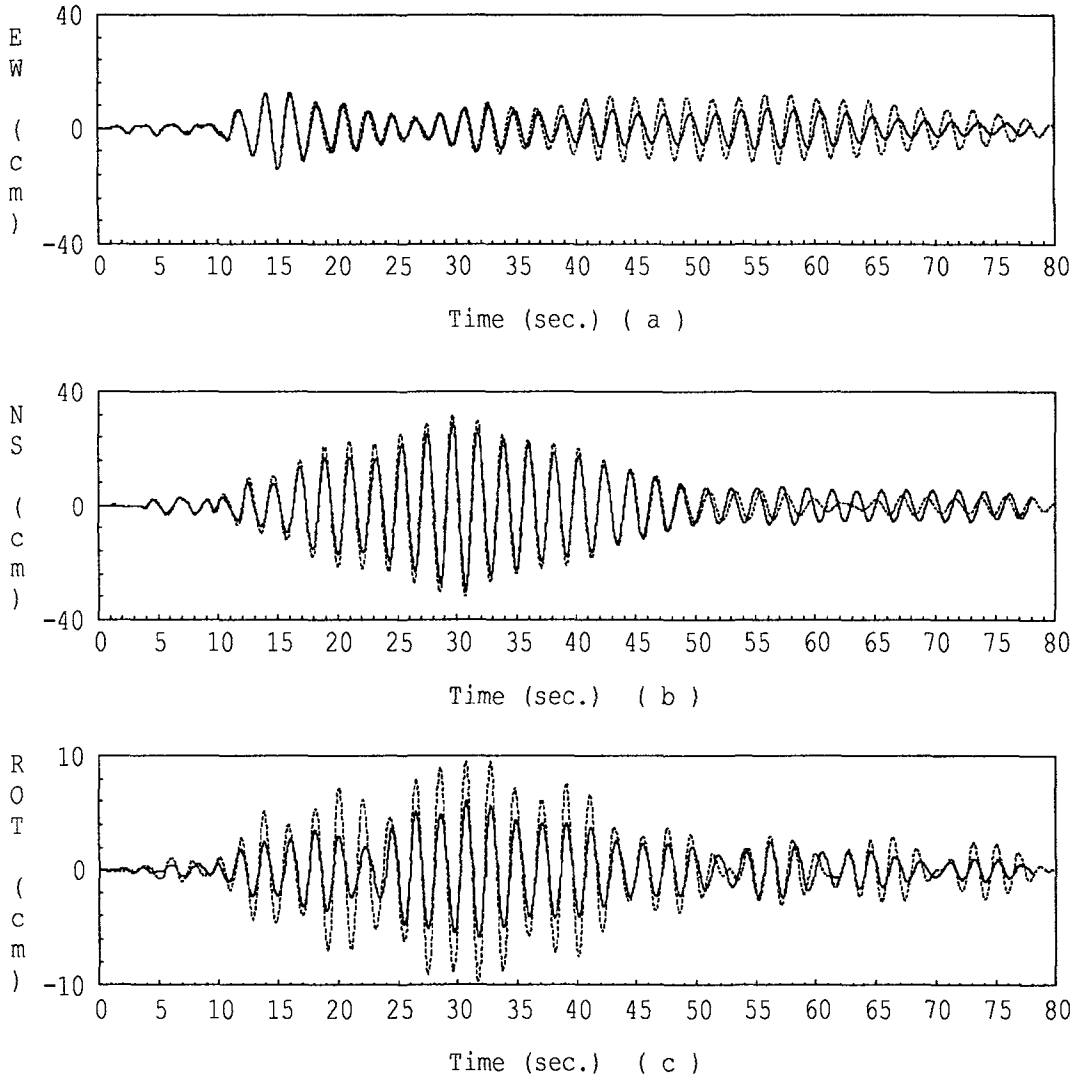

Figure 5.9: CASE 3-ML-BT. Twelfth floor motion. (a) EW relative displacement, SW corner. (b) NS relative displacement, SW corner. (c) Derived torsion, SW-NW corner relative displacement. Model —— Record ·····.

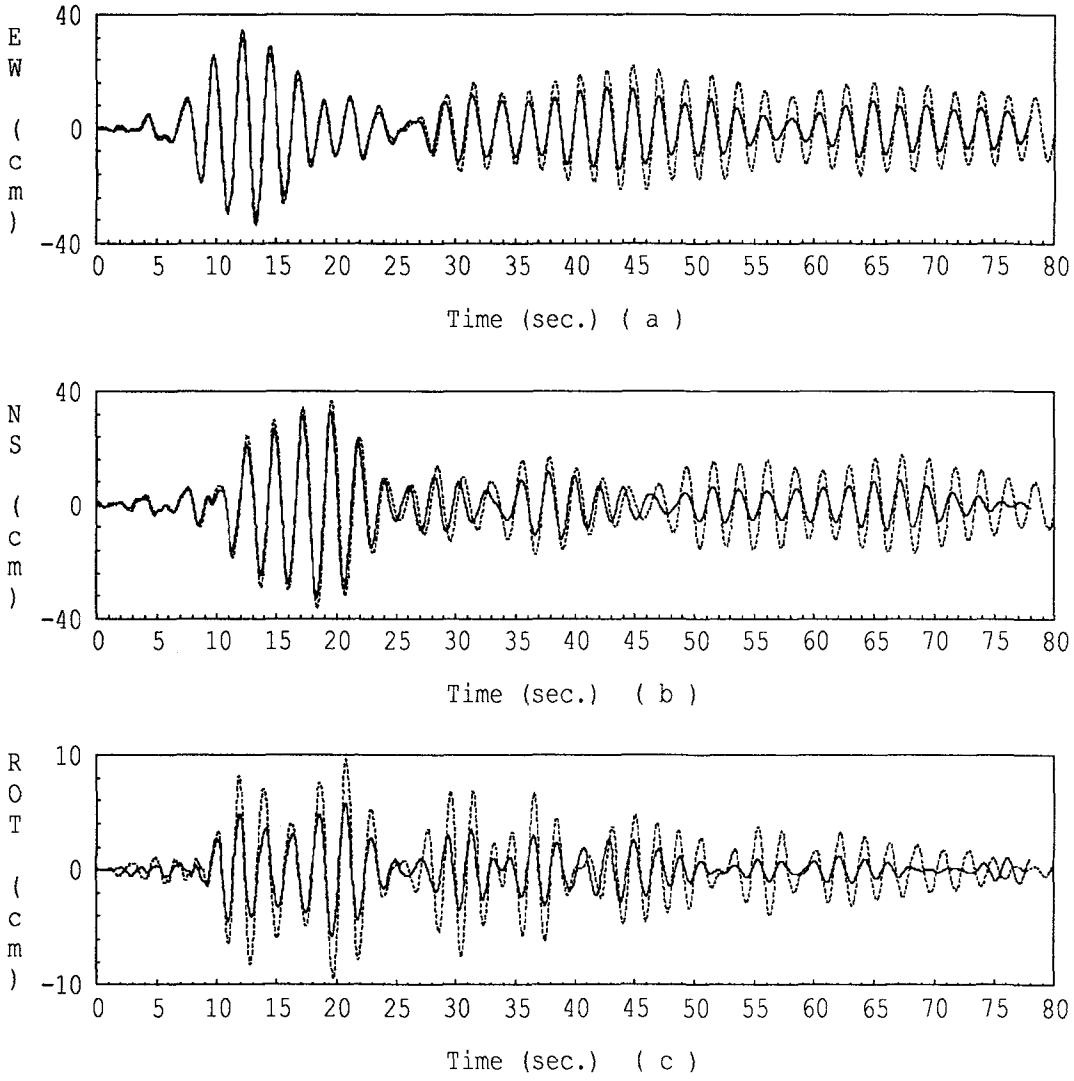

Figure 5.10: CASE 3-LP-BT. Twelfth floor motion. (a) EW relative displacement, SW corner. (b) NS relative displacement, SW corner. (c) Derived torsion, SW-NW corner relative displacement. Model —— Record ·····.

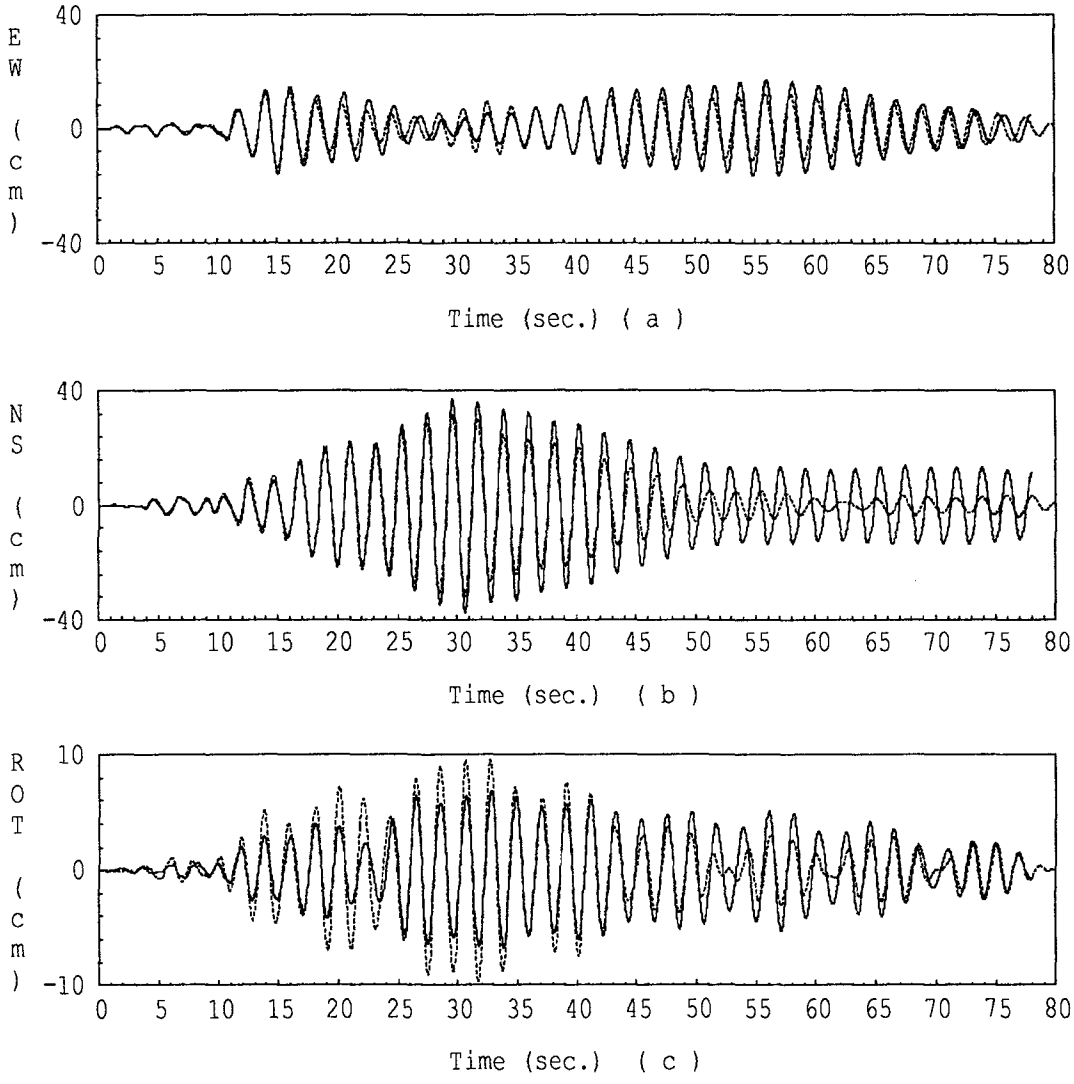

Figure 5.11: CASE 4-ML-BT. Twelfth floor motion. (a) EW relative displacement, SW corner. (b) NS relative displacement, SW corner. (c) Derived torsion, SW-NW corner relative displacement. Model —— Record ·····.

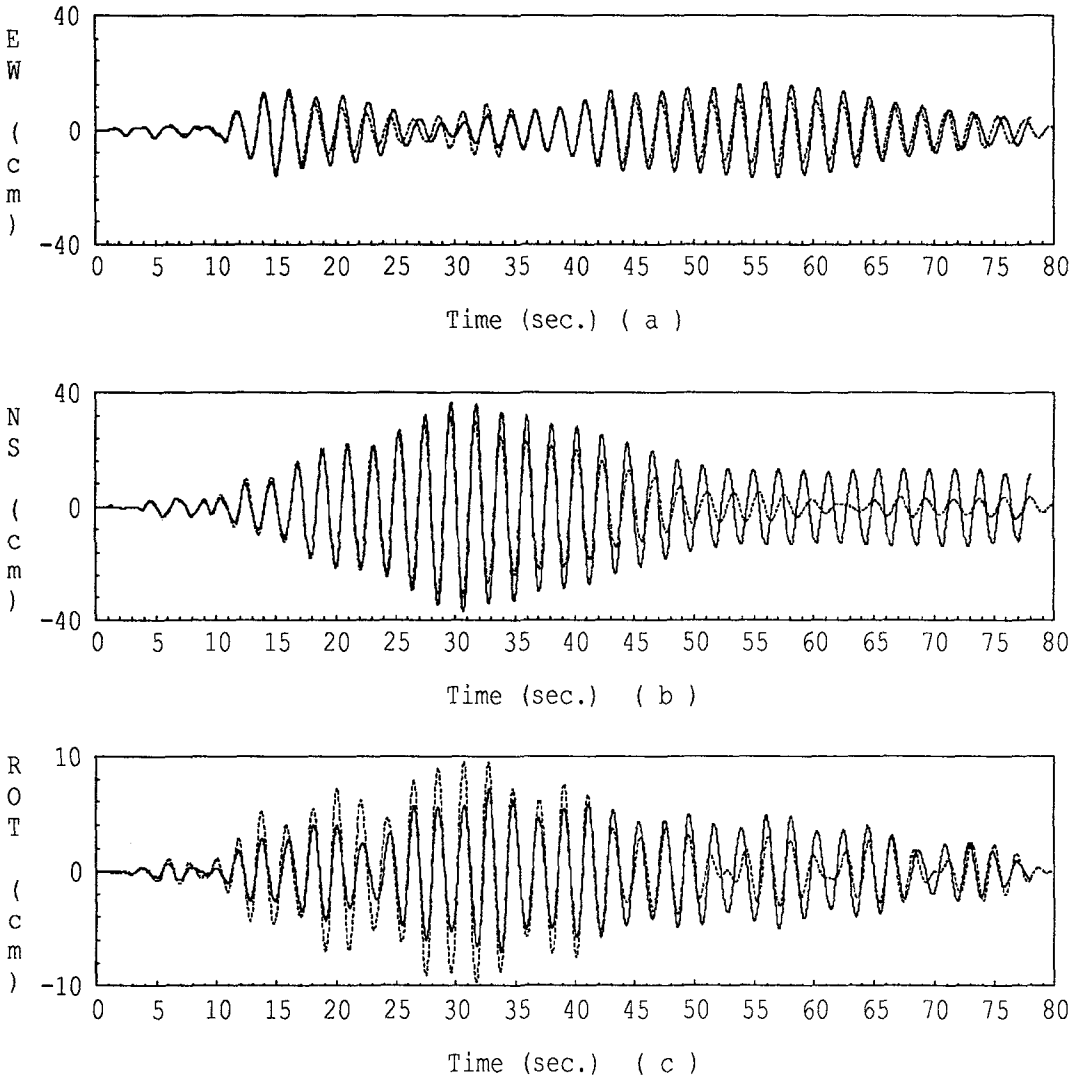

Figure 5.12: CASE 4-ML-B. Twelfth floor motion. (a) EW relative displacement, SW corner. (b) NS relative displacement, SW corner. (c) Derived torsion, SW-NW corner relative displacement. Model —— Record ·····.

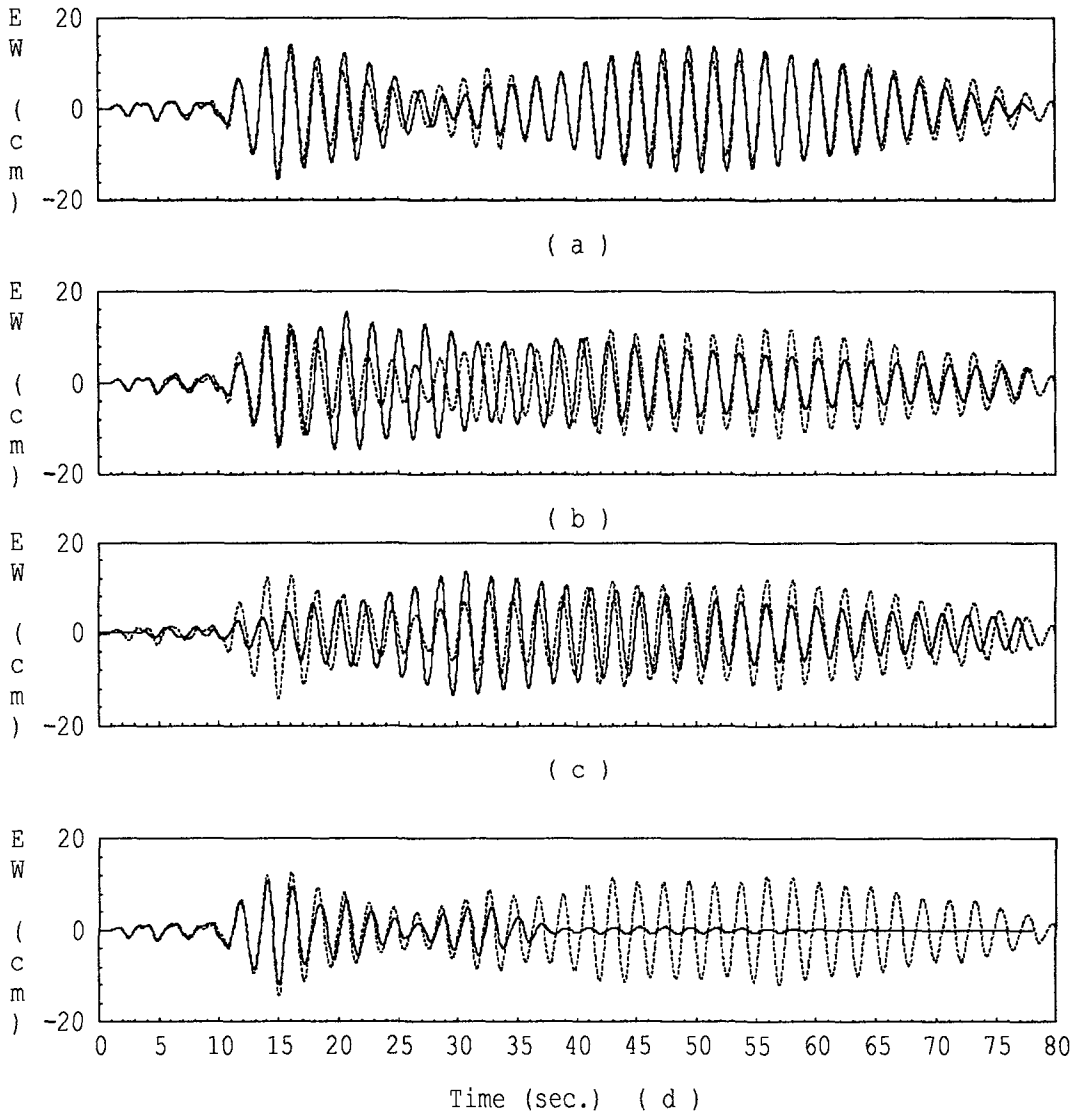

Figure 5.13: CASE 4-ML-B. Twelfth floor motion. Input ground motion 0-40 seconds. EW relative displacement, SW corner. (a) First three modes, low damping model (1 %). (b) First mode, low damping model. (c) Second mode, low damping model. (d) First three modes, moderate damping model (5 %). Model —— Record ·····.

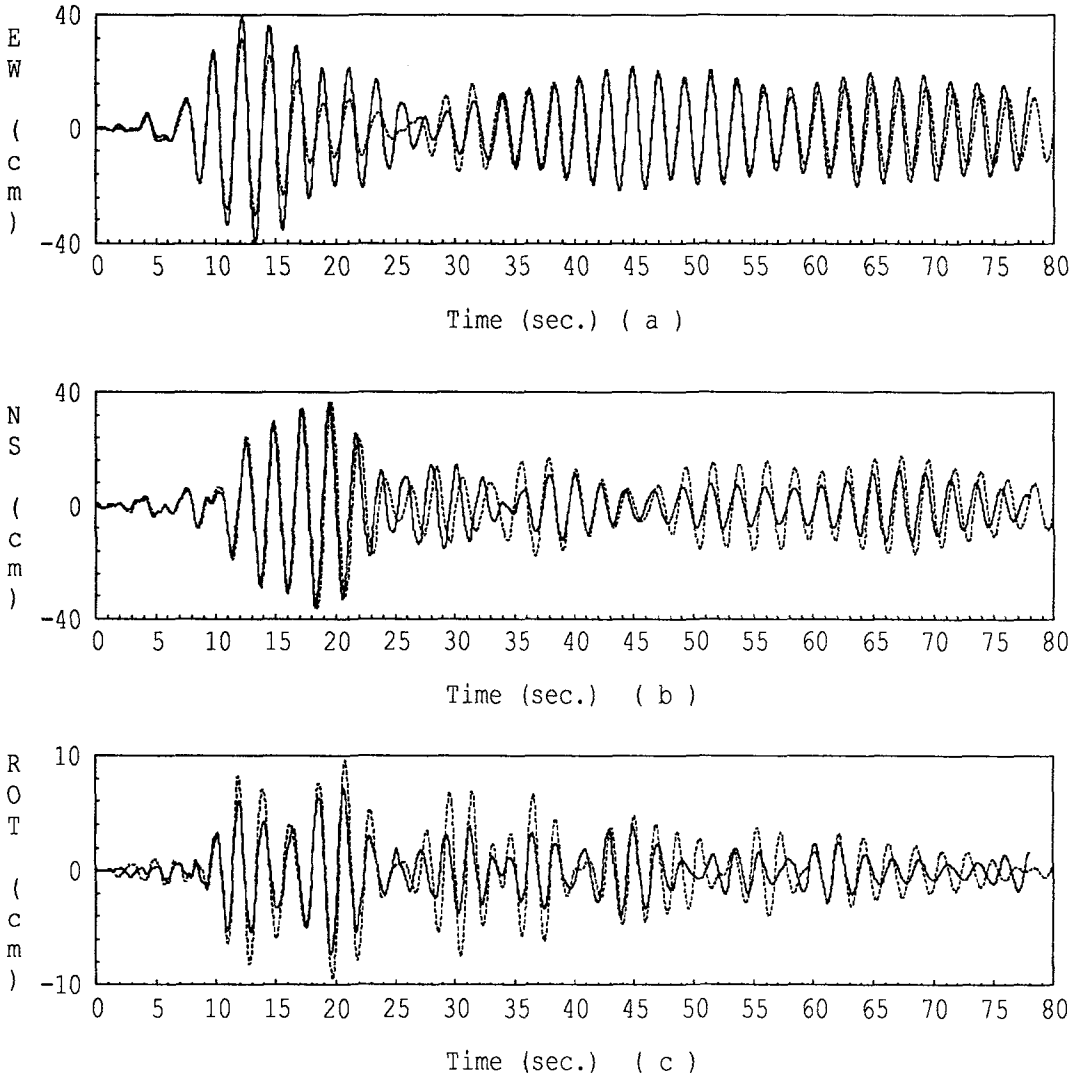

Figure 5.14: CASE 4-LP-BT. Twelfth floor motion. (a) EW relative displacement, SW corner. (b) NS relative displacement, SW corner. (c) Derived torsion, SW-NW corner relative displacement. Model —— Record ·····.

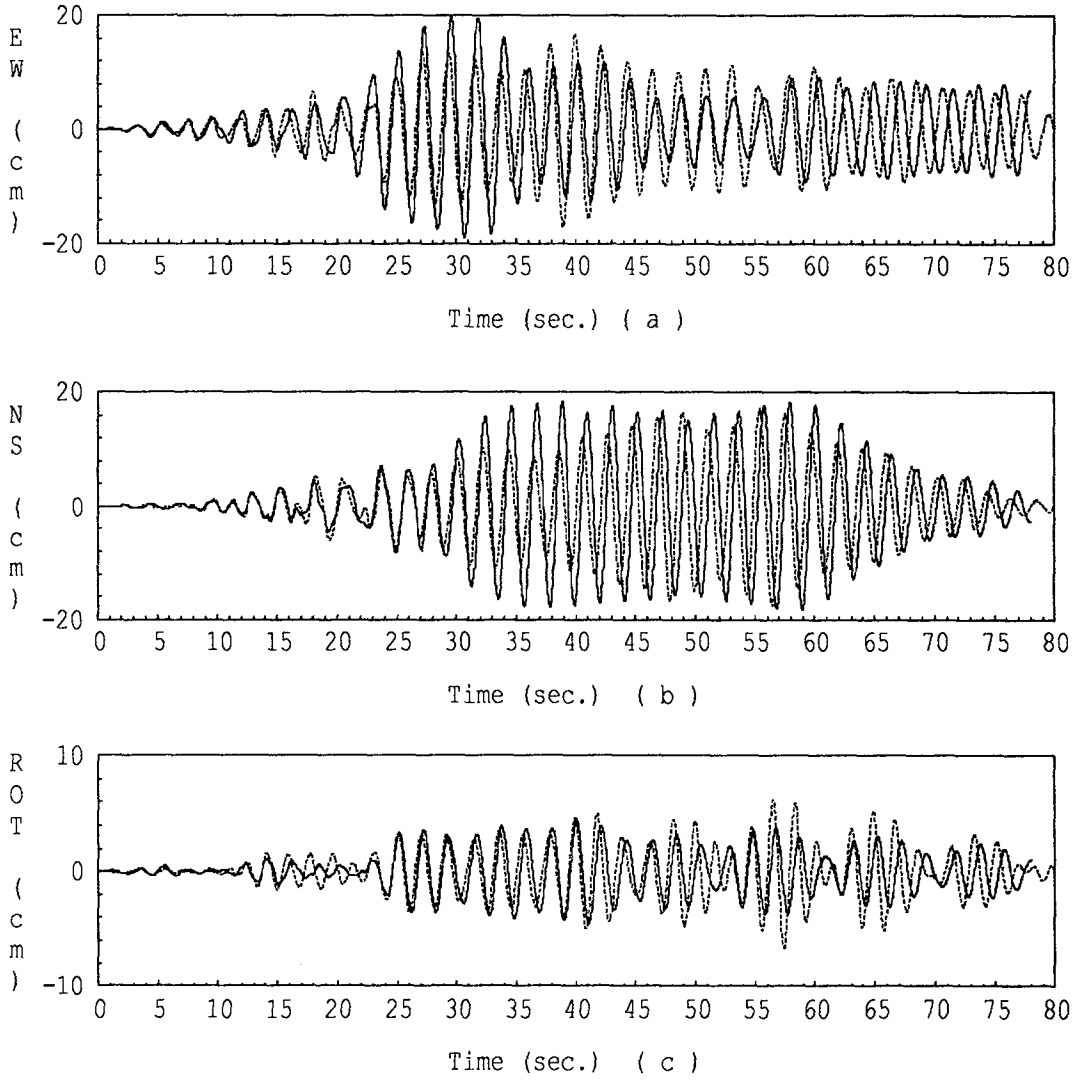

Figure 5.15: CASE 5-MH-BT. Twelfth floor motion. (a) EW relative displacement, SW corner. (b) NS relative displacement, SW corner. (c) Derived torsion, SW-NW corner relative displacement. Model —— Record ·····.

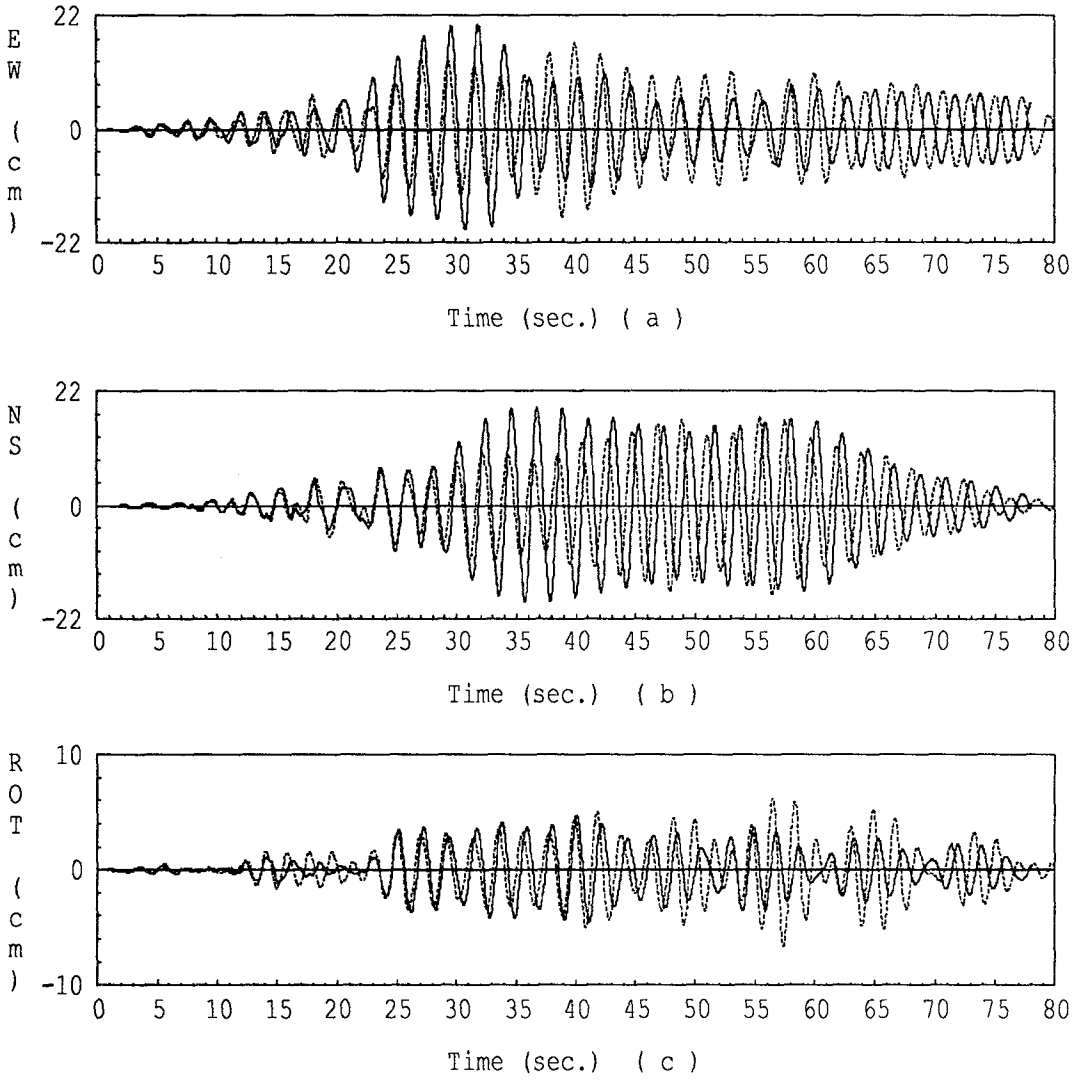

Figure 5.16: CASE 6-MH-BT. Twelfth floor motion. (a) EW relative displacement, SW corner. (b) NS relative displacement, SW corner. (c) Derived torsion, SW-NW corner relative displacement. Model —— Record ·····.

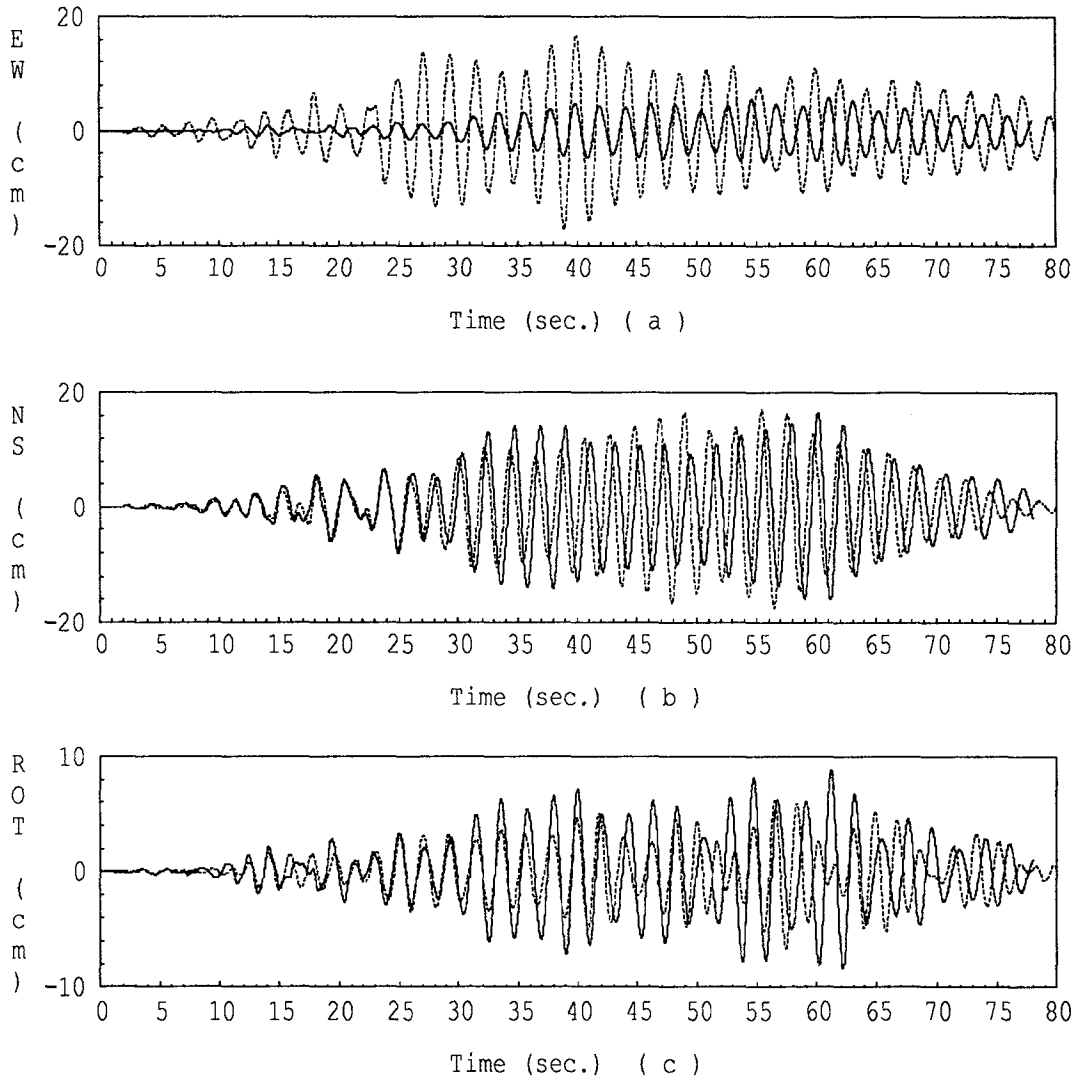

Figure 5.17: CASE 7-MH-NS. Twelfth floor motion. (a) EW relative displacement, SW corner. (b) NS relative displacement, SW corner. (c) Derived torsion, SW-NW corner relative displacement. Model —— Record ·····.

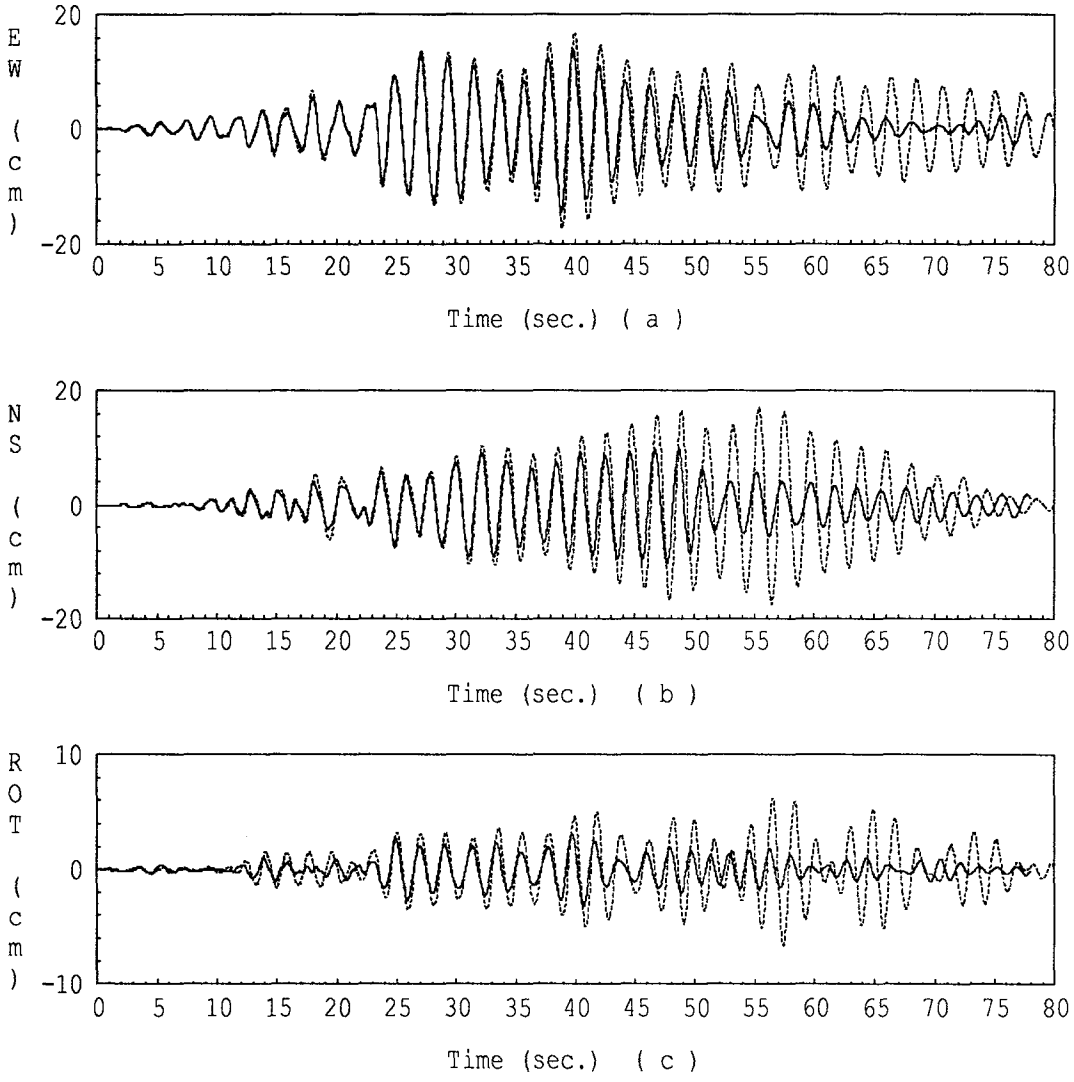

Figure 5.18: CASE 8-MH-BT. Twelfth floor motion. (a) EW relative displacement, SW corner. (b) NS relative displacement, SW corner. (c) Derived torsion, SW-NW corner relative displacement. Model —— Record ·····.

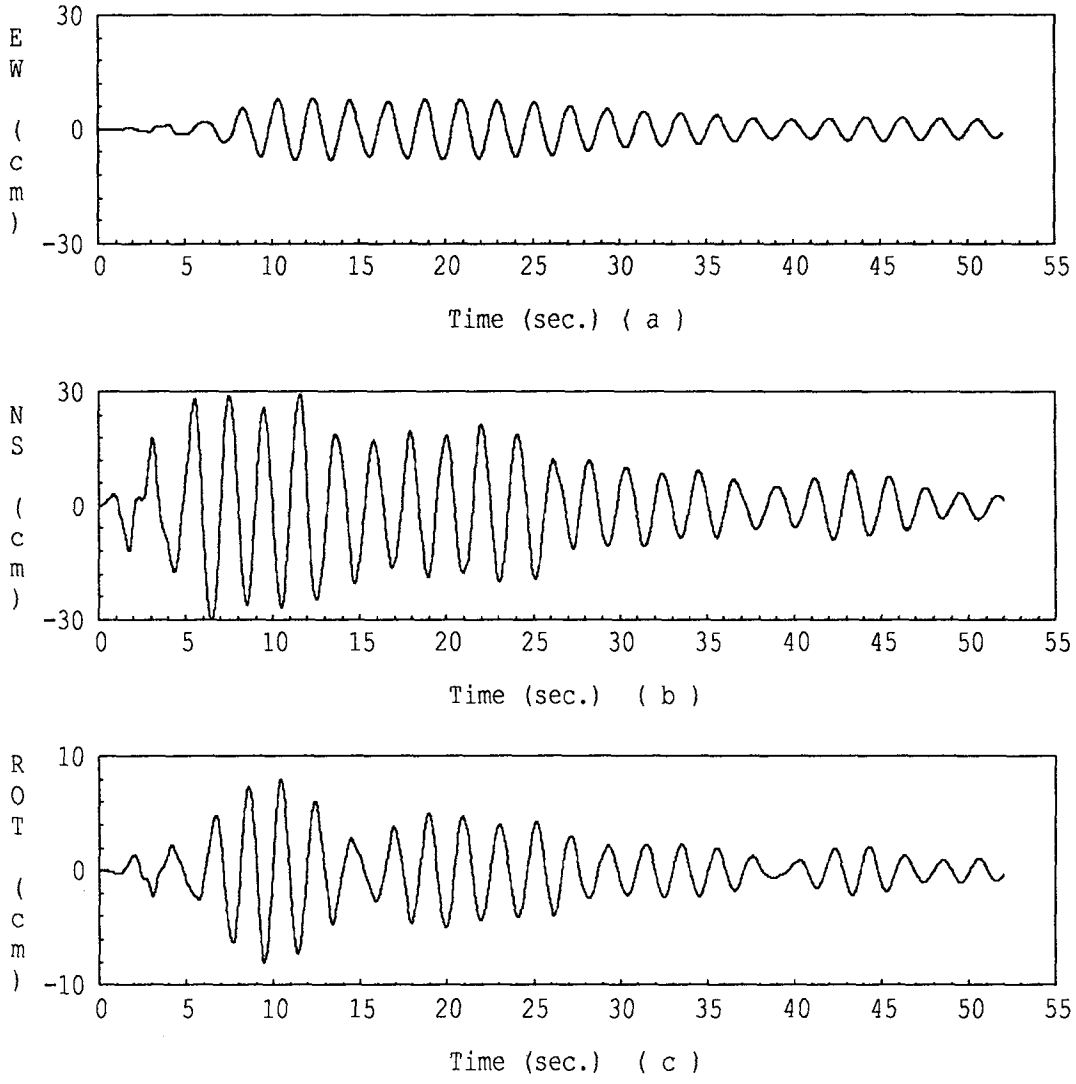

Figure 5.19: CASE 3-CENT-NS. Twelfth floor motion. (a) EW relative displacement, SW corner. (b) NS relative displacement, SW corner. (c) Derived torsion, SW-NW corner relative displacement.

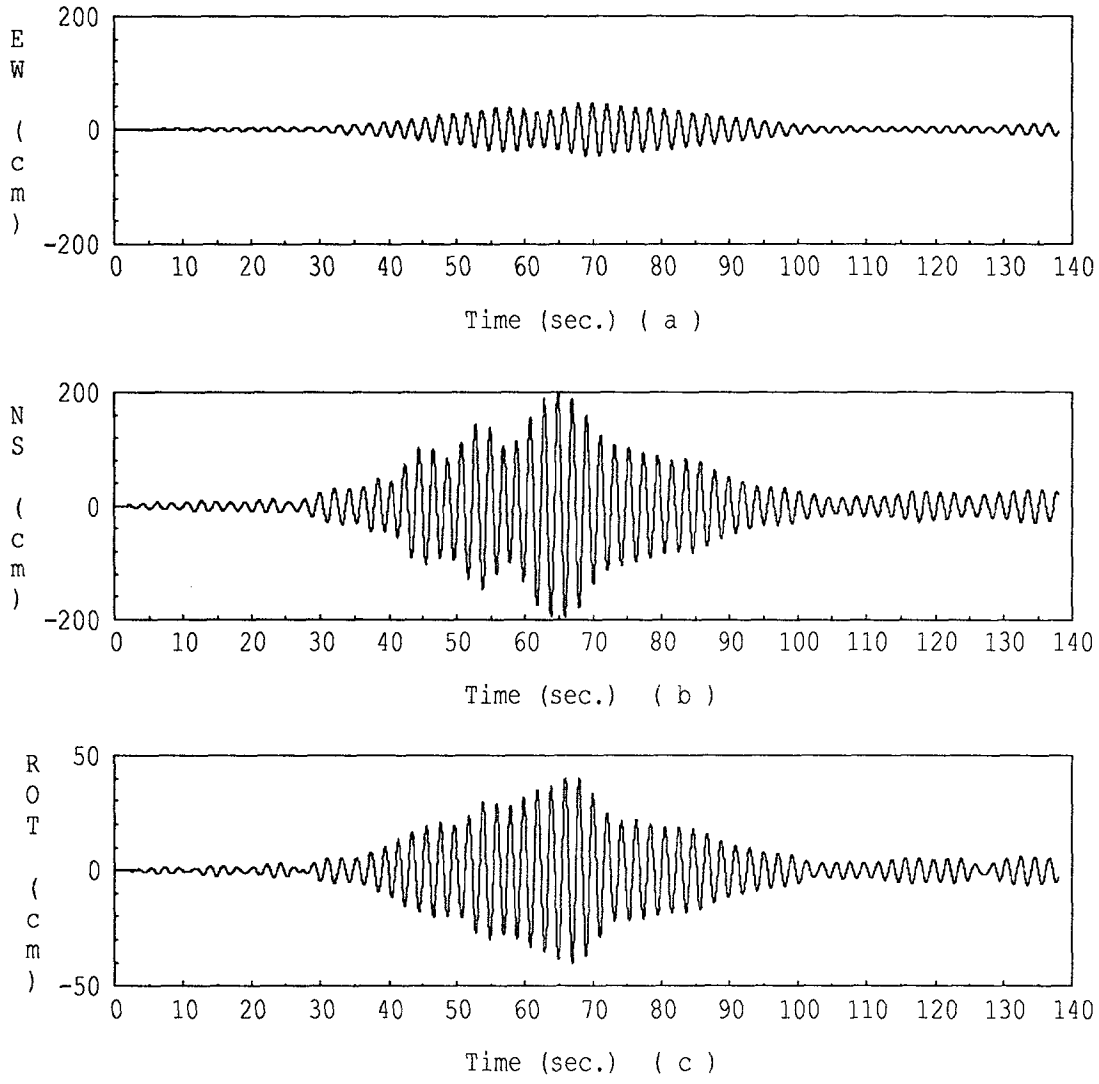

Figure 5.20: CASE 3-SCT-NS. Twelfth floor motion. (a) EW relative displacement, SW corner. (b) NS relative displacement, SW corner. (c) Derived torsion, SW-NW corner relative displacement.

CHAPTER 6

ANALYTICAL MODELS AND RESPONSE: NONLINEAR CASE

6.1 General

Several nonlinear models were developed to evaluate the behavior of the building and to perform parametric studies under severe loading conditions. A modified version of the ANSR-I program was used for the nonlinear analyses [36]. ANSR-I is a general purpose computer program for three-dimensional, nonlinear, dynamic and static analysis of structures. In the program, a structure can be idealized as a three-dimensional assemblage of discrete finite elements connected at nodes. Several elements are provided with the program.

Static and/or dynamic loads can be applied at the nodes. For dynamic loading, the structural mass is assumed to be lumped at the nodes. Damping can be assigned at the element or structure level, and can be specified as a function of the mass or the initial or tangent stiffness. Ground motions can be specified for the three global axes of the structure. In this case all "base" nodes are constrained to move in phase.

Several solution strategies are available in the program. These are based on combinations of the Newton-Raphson and constant stiffness iteration schemes.

Because of the complexity of the computer input for this problem, a graphic interface was developed, which allows the input geometry and member properties to be graphically verified. Examples of the interface output are presented later.

6.2 The Nonlinear Model

The basic characteristics of the best fit linear elastic model, presented in Chapter 5, were utilized to formulate the nonlinear analytical model. Thus, the structure was modeled three-dimensionally, with three degrees of freedom per story, using element center-line dimensions (no rigid element zones), partial composite action of the NS oriented girders (in stiffness, but not in strength), an average translational inertial weight of 9450 kN (2100 kips) per story, an average rotational floor inertial mass of 1.0×10^6 kg-m^2 (3.1×10^9 lb-in^2) and an average gravity load of 6703 N/m^2 (140 psf) [dead $\approx$ 4788 N/m^2 (100 psf) and live $\approx$ 1915 N/m^2 (40 psf)]. The stiffness and strength of the exterior siding and interior partitions were not considered in the nonlinear model, because of their small effects on the linear model and uncertainties in their properties.

Because of differences between the computer programs and modeling constraints, the linear

response envelopes obtained from the ETABS and ANSR-I programs are not identical. Differences in the responses can be related, in part, to the elimination of the nonstructural panel elements and the torsional input in the ANSR-I model, and the different modeling assumptions for the element stiffness and structural damping. The results indicate that these differences are generally less than 10%.

In consideration of the size of the problem and the limitations on computer time and memory, the rather simple, three-dimensional beam and beam-column elements developed by Riahi et al. [44] were used to model the structure. The basic characteristics of these elements are presented below, but a more detailed presentation is given by Riahi et al.

6.2.1 Initial Capacity Analysis

A simple static lateral load capacity analysis of the structure and members was carried out using nominal element properties and assuming no element strain hardening. Gravity load effects were included in the analyses. The analyses indicate the following

- If inelastic action occurs in the structure, plastic hinges in the interior frame girders will typically form at the element ends. In the perimeter frames, hinging occurs in the reduced section of the built-up members, at the ends of the taper. Main elements were found to have compact sections. Some of the EW oriented girders in the interior frame could have lateral stability problems at large inelastic deformations since no lateral bracing was provided at plastic hinge locations.

- The maximum axial load that can be transferred to a column (not located at a corner), is limited to approximately 15% of the its nominal axial load capacity (F_yA). This estimate is based on girder yielding and tributary gravity loads. Similarly, for the perimeter frame corner columns, the maximum axial load is about 31% of their nominal axial capacity, when all girders above the column in one direction and the tributary weight are considered. For bi-directional loading this value could nearly double.

- A strong column-weak girder design philosophy, considering expected ultimate axial loads, was implemented for the interior and perimeter frames.

- The yielding capacity of joints located in the interior and perimeter frames was estimated using the following simplified formula

$$V_{y\,capacity} = 0.55 d_c F_y t \tag{6.1}$$

where

$V_{y\,capacity}$ is the yielding capacity of the joint,
d_c is the column depth,
F_y is the specified minimum yield stress, and
t is the total thickness of the joint panel zone, including doubler plates.

Values obtained using this formula indicate that the joint yield capacities for the interior frames are from 1.0 to 1.5 times those demanded by the nominal plastic moment capacities of the girders connected at the joint. Higher values are found at the lower floors. For the perimeter frame connections, values between 0.92 and 0.98 were found from the first to the seventh floor, 0.85 for the eighth and ninth floor and 1.33 from the tenth to thirteenth floors.

Thus, plastic hinging would be expected in the girders for the interior frames. For the perimeter frames, yielding would be expected to initiate in the girders but would spread, especially in the lower floors, to the joints as the plastic moment capacity of the girders is approached.

6.2.2 Beam Elements

Girder and beam members in the structure were modeled with the simplified beam-column elements developed by Riahi et al. [44]. While these line elements can be oriented arbitrarily in the space, yielding is allowed in only one plane. Deformation hardening is taken into account by assuming that the element consists of elastic and elasto-plastic components acting in parallel. With this procedure, a moment-rotation relationship, instead of a moment-curvature relation, is achieved. Inelastic axial and shear deformations are not allowed in this element. Two types of yield surfaces are provided with the element: a "beam" type in which no interaction exists between axial and moment capacity, and a "column" interaction curve where simplified axial load-moment interaction is considered.

Elastic axial, flexural and shear stiffness corresponding to the plane in which yielding is permitted can be specified directly. Torsional and minor axis stiffness properties are derived from the major axis stiffness terms using scaling factors. Elements with variable cross sections can be accounted for by specifying appropriate stiffness and carry-over factors.

In the computer model of the building, the girders were modeled using nominal plastic capacities ($Z\,F_y$) and the "beam" yield surface provided by the program. The deformation hardening was considered to be 5% of the initial elastic stiffness. Under seismic excitations yielding in the built-up girder elements on the perimeter frame will occur at the end of the reduced section. Therefore, the capacity specified at the ends of the built-up girders on the perimeter frame was derived from the capacity of the reduced section of the girder, considering equilibrium under

anti-symmetrical loading and the location of the hinges along the length. A total of 1,456 beam elements were used in the analyses.

6.2.3 Column Elements

Taking into account the low axial load expected in the columns, the strong column-weak girder condition present in all the important elements, and the results of the linear analyses, columns were also modeled above the second floor using the two dimensional beam-column elements. For these elements a "beam" yield interaction surface was again prescribed. The major axis for these elements was oriented in the direction in which nonlinearities could occur in the elements, considering the beam arrangement, higher mode effects or beam-element strain hardening. A deformation hardening ratio of 5% was assumed for these elements. An additional 814 elements were used to model these columns.

For the first two floors, three-dimensional beam-column elements were employed to model the columns. These column elements, developed by Riahi et al. [44], are an extension of the two dimensional beam-column elements presented above. However, tri-linear relationships can be prescribed directly for the moment-rotation characteristics in both principal axes as well as for the torque-twist and force-extension characteristics. Parabolic and elliptical interaction surfaces are employed to formulate a generalized plastic hinge.

These columns were modeled using their nominal plastic properties and a parabolic interaction surface which had the following form:

$$\theta = \left[\left(\frac{M_{yy}}{M_{yp}}\right)^2 + \left(\frac{M_{zz}}{M_{zp}}\right)^2\right]^{1/2} + \left(\frac{P}{P_p}\right)^2 \tag{6.2}$$

No torsional stiffness was specified for individual columns. A 5% deformation hardening ratio was assumed. For the first two floors, 148 three-dimensional beam-column elements were employed.

6.2.4 Beam-Column Connections

Beam-column connection yielding was not considered directly. To approximate the elastic joint deformation, element center-to-center dimensions were specified.

6.3 Response Parameters Monitored

Because of the size of the model, only selected response parameters will be presented for the different analyses. These include:

- the twelfth story displacement and rotations at the model's center of mass;

- the displacement at the SW corner of the twelfth floor;

- the difference between the SW and NS corner displacements at the twelfth floor;

- the inter-story drift indices computed at the centers of mass for floors 1 to 12;

  In cases where additional eccentricities were added, the initial center-of-mass locations are still used for comparison.

- the maximum rotational ductility (μ) and cumulative rotational ductility (μ_c) demands for the perimeter frame built-up girders (these elements are located between floors 1 and 9);

  The ductility demand μ on the girder elements was derived by dividing the maximum plastic rotation and cumulative plastic rotation by the yield rotation of the element, assuming that the element acted in double curvature in the absence of gravity loads.

  $$\mu = \theta_{mp}/\theta y + 1 \tag{6.3}$$

  $$\mu_c = 1 + \sum_i |\Delta\theta_{pi}|/\theta y \tag{6.4}$$

  where

  θ_y is the yield rotation of the element assuming the element acts under double curvature with a maximum elastic moment equal to the nominal plastic moment,
  θ_{mp} is the maximum plastic rotation of the element, and
  $\Delta\theta_{pi}$ is the plastic rotation increment at time step i.

  For elastic behavior the ratio of maximum computed moment to plastic moment is used as the ductility ratio instead of the rotation ratio, and cumulative values are not considered.

- the sum of the squared displacements (for a given constant time step);

  $$\mathrm{SSD}_v = \sum_i^N d_{iv}^2 \tag{6.5}$$

  where d_{iv} is the displacement at time step i in the global v direction, and N is the number of recording points considered. This parameter will be used to compare the effects of different variables on the amplitude and duration of the response. The SSD values were evaluated for the SW corner displacements at the twelfth floor.

- the axial load and moments at the base of the first story column at the SE corner of the building (Column M-12, Fig. 3.1);

  The values obtained are presented normalized with respect to their respective nominal plastic capacities.

- the number of elements that exhibited inelastic behavior.

The final model mesh used in the analysis is presented in Figs. 6.1 to 6.4. Summaries of the global response characteristics are presented in Tables 6.1 to 6.7 and in Figs. 6.13 to 6.59.

6.3.1 Static Load-to-Collapse Analysis

Static lateral loads on the model were monotonically increased to estimate the lateral capacity of the building and typical deformed shapes. Analyses were performed for both principal directions of the building. The forces were applied at the center of mass of each floor and distributed in elevation as defined by the pattern of design lateral loads in ATC 3-06 [38]. Dead and live gravity loads were included in the analyses. Models with and without P-Δ effects were considered. Figures 6.5 to 6.12 present relations between base shear and twelfth floor displacement, building deflected shapes, ductility demand distribution and inter-story drift distribution. The results of the static analyses confirm that the structure is quite flexible and deformable.

If the base shear-twelfth floor displacement relation (Fig. 6.5) is associated with that of a single degree-of-freedom system then several observation can be made.

- The initial slope observed from the base shear-twelfth floor displacement, Figure 6.5, is 578 kN/cm (326.5 kips/inch), which is similar to that found from the analysis of the earthquake records (see Section 4.5.5).

- When P-Δ effects were not considered, appreciable deviation from linear behavior (local yielding) was detected when the twelfth floor displacement plots, in the EW direction, exceeded 48 cm (19 inches). This corresponds to a base shear coefficient of 0.22.

  An equivalent yield displacement (or global yielding displacement) for the model was defined as the intersection of the initial elastic and average post-yielding slope of the force-deflection relation. The equivalent yield displacement found in this manner was 64 cm (25 inches, 1.3% average drift). This corresponds to an effective base-shear yield coefficient of 0.29. A complete energy dissipation ("collapse") mechanism had apparently not formed at a base shear coefficient of 0.48 and a displacement of 644 cm (253 inches) (corresponding to a 13.0% average drift and displacement ductility of 10). At this point the post-yielding tangent stiffness had a slope corresponding to approximately 6.1% of the initial elastic stiffness (indicating that some of the elements required for a complete energy dissipation mechanism still remained elastic). The structure did not reach an unstable condition, even for higher displacements, because of the absence of P-Δ effects in this analysis, the 5% deformation hardening ratio prescribed for all elements of the structure and the unlimited plastic rotation capacity assumed in the analysis for the members.

- The results indicate that there is a 32% increase in base shear between local and global yielding and a 118% increase between local yielding and the formation of the energy dissipation mechanism. The characteristics and capacity of the model were similar in both directions, as shown in Fig. 6.5.

Building deflected shapes for different load levels are presented in Fig. 6.6. The deflected shape changes with increased loading concentrating deformations in the lower half of the building. Because of the characteristics of the deformed shapes, higher inter-story drifts and, consequently, higher rotational ductility demands in the girders were found between the second and seventh floors.

Figures 6.7 and 6.8 present the inter-story drift and rotational ductility demands at a building global displacement ductility demand (μ_d) of about 3 (i.e., a twelfth floor displacement of 2.03 meters (80 inches)). For this level of deformation the maximum rotational ductility demand and maximum inter-story drift index were found at the fifth floor. The maximum plastic hinge rotation ductility was 8.5, 2.6 times larger than the global displacement ductility of 3. Similarly, the fifth story drift was 6%, 71% larger than the average inter-story drift at this stage.

A total of 903 elements of the model had yielded at a displacement ductility of 3. Of these, 615 were beam elements (out of a total of 1456 beam elements), 181 were two-dimensionally modeled columns (out of a total of 814) and 102 were three-dimensionally modeled columns in the bottom two stories (out of a total of 148). Because there are 74 column lines per story, the numbers presented above indicate that nearly all columns in the first two stories and 22% of columns between the third and thirteenth stories yielded at a global building displacement ductility of 3. This is due to (*i*) the deformation hardening in the girders which increased moments to a level sufficient to yield columns despite the strong column-weak girder behavior expected, (*ii*) inelastic load redistribution and (*iii*) yielding in columns in the exterior frame.

The large lateral displacements that corresponds to a global displacement ductility demand of 3 make it unlikely that the building could reach this level of inelastic behavior for the earthquakes expected at the site. Nonetheless, the analyses indicate several interesting characteristics of steel frames at these large displacement amplitudes.

It was observed from the static load-to-collapse analyses that yielding reduced the apparent coupling between translational and rotation motions and between the translational motions in the two orthogonal directions. For example, Figure 6.9 presents the normalized (to a maximum value of one) ratio of orthogonal displacements (Δ_{NS}/Δ_{EW}) and the normalized ratio of in-plane rotation to displacement in the loading direction (θ/Δ_{EW}). Both ratios are computed at the center of mass of the twelfth floor.

This figure shows that while the system is elastic these ratios are constant (the increase in rotation is in the same proportion as the increase in displacement). When yielding occurs, the

ratio of orthogonal displacements decreases monotonically with increasing deformation, indicating an apparent decoupling between the two directions. The displacement orthogonal to the direction of loading results from the difference between the locations of the centers of mass and rotation. The "center of rotation" actually changes during the loading because of yielding. Thus, the shape of this curve depends on the point being monitored. The decrease in Δ_{NS}/Δ_{EW} as Δ_{EW} increases indicates that, when significant yielding occurs, displacements increase much faster in the direction of loading than in the orthogonal direction. The decrease does not reflect an actual decrease in the orthogonal displacements.

The normalized ratio of in-plane rotation to EW displacement is constant while the system remains elastic. The ratio then initially grows reaching a maximum near the point of global yielding, and then decreases for higher displacements. Thus, as yielding initiates torsional effects increase at a faster rate than lateral displacements because of the irregular location of plastic hinging and a sudden shift of the "center of rotation". As a lateral collapse mechanism begins to form, the rate of increase in the lateral displacements becomes greater than that for the in-plane rotation, Figs. 6.10 and 6.11.

Building models including P-Δ effects indicate that this condition has consequences mainly on the post-yielding behavior of the structure, Fig. 6.12. The initial effective elastic stiffness is only 3.2% lower than the case where P-Δ effects were disregarded. Nevertheless, the post-yield stiffness is 4.6% of the initial stiffness at 2 meters (80 inches) twelfth floor displacement, a 52% reduction compared with the case without P-Δ effects. Furthermore, these results are based on 5% deformation hardening and a smaller value might be appropriate for these large deformation levels.

If the deformation hardening values used for all elements of the model are reduced from 5 to only 1% of the initial elastic stiffness of the member, then P-Δ effects produce a sudden static failure of the structure under monotonic loading after the equivalent global yield displacement (64 cm [25 inches]) has been reached. P-Δ effects can have important consequences on the global inelastic behavior of such types of structures.

In the previous chapter it was found that the 1988 UBC required a base shear coefficient of 0.037 at working stress levels for the structure studied. An approximation to the yield base shear coefficient prescribed by the Code can be obtained by multiplying this value by 1.5 ($1.5 \times 0.037 = 0.056$). ATC 3-06 recommends a yield base coefficient of 0.049. From the results of the static load-to-collapse analysis, it is clear that the capacity of the structure is considerably higher than expected by the design recommendations. The base shears for local yielding, global yielding and formation of the energy dissipation mechanism are approximately 4.2, 5.6 and 9.1 times the 1988 UBC design base shear, respectively. Codes in force at the time the structure was designed would have required an even smaller design base shear. Nevertheless, it should be recalled that the linear

dynamic analyses of the building indicated that several structural elements were close to yield for earthquake events with peak ground accelerations of only 0.04 g.

6.3.2 Model Response to Earthquakes Recorded at the Site

The studies of the linear models presented in the previous chapter indicated the possibility that some element yielding might have occurred in the structure during the Mt. Lewis and Loma Prieta events. To evaluate the effect of these nonlinearities two models with different amounts of viscous damping (1 and 3% of critical) were considered. Rayleigh damping was incorporated into the model as a combination of the mass and initial stiffness matrices. The first and third structural fundamental periods were used to specify the desirable amount of damping.

The nonlinear model was subjected to the building base ground records of these earthquakes, in both directions. For the EW direction an average of the base corner records was used. P-Δ effects were not considered; a time step of 0.02 second was used. The duration of the records considered for the analyses was 80 seconds, resulting in 4000 time steps. Step-by-step integration without iteration was used to solve the equation of motion. Results of the analyses are summarized in Table 6.1.

6.3.2.1 The Mt. Lewis Event

The linear model studies showed that the 1% viscous damping model overestimated some aspects of the response of the system, but captured the basic behavioral characteristics observed during the recorded events. Thus, this model is used herein to represent an upper bound for the response of the nonlinear model of the structure. The global response parameters obtained from this low damping model for the Mt. Lewis event are presented in Figs. 6.13 to 6.15 and Table 6.1.

Comparison of the SW corner displacement in the model with the recorded response, Fig. 6.13, corroborates that the model overestimates the response, especially during the latter portion where the input motion is small and the decay of the response is dominated by the free decay of the modes. However, there is general agreement with the basic response characteristics during the more intense force vibration portion of the response.

Figure 6.15a shows the vertical distribution of maximum inter-story drift indices at the story center of mass, for the NS and EW building directions. The NS deformations were considerably larger than those computed for the EW direction. This model predicts a maximum inter-story drift index (IDX) of 0.89%, located at the fifth level.

A small amount of element yielding occurred in the model. Figure 6.14 shows the times at which the program detected yielding in the structure. The figure shows that yielding was concentrated between 26 and 42 seconds of the response. This time agrees with the time of strong

deformations in the NS direction. For this earthquake, only 36 girder elements yielded, Table 6.1. The distributions with elevation of the maximum (μ) and cumulative (μ_c) rotational ductility demands for the perimeter frame built-up girders are presented in Fig. 6.15b. This type of element was present in the perimeter frame only from the first to the ninth floor. Above this level wide flange beams were used (W21x82). Figure 6.15b shows that element yielding in the built-up girders was limited to the fifth floor and that the maximum rotational ductility demands on these elements were small, μ= 1.06. Because of the limited present in the structure, only a few cycles of inelastic behavior occurred in the perimeter frame girders. As a consequence, the maximum cumulative rotational ductility observed was also small, μ_c=1.09. For the built-up girders that remained elastic, maximum normalized moments are highest between floors 3 and 6 corresponding to the levels with high drift. It should be recalled from Section 6.2.1 that beam-column joint yielding could occur at these levels for moment ratios between 0.92 and 0.98. Similarly, since plastic moment capacities are used to define yielding in the girders, girder yielding would be expected for moment ratios less than 0.88.

Figures 6.15c, d and e present the axial load-moment and bi-directional moment interactions for the monitored column (first story, Column M-12). Column forces and moments are normalized to their nominal plastic capacities. Sections shown in these figures are as follows:

P/P_p-M_{yy}/M_{yp} with $M_{zz}/M_{zp} = 0$,
P/P_p-M_{zz}/M_{zp} with $M_{yy}/M_{yp} = 0$, and
M_{zz}/M_{zp}-M_{yy}/M_{yp} with P/P_p=0.

The force diagrams for the monitored columns show a regular pattern similar to that observed from particle plots of the twelfth floor displacements, see Fig. 4.25.

The model with 3% damping exhibited reduced deformation and no yielding (μ = 0.69) in the structure. Envelope characteristics were closer to those observed from the records. Other response envelopes for this analysis are presented in Table 6.1.

It is concluded from these analyses that little significant yielding occurred in the main elements of the building during the Mt. Lewis event, despite the severe displacement response of the structure.

6.3.2.2 The Loma Prieta Event

During the Loma Prieta event it appears that yielding occurred in the structure. According to the model with 3% damping, 16 elements suffered moderate yielding. None of these were part of the perimeter frame. Girders on the perimeter frame, nevertheless, were close to their plastic capacity (μ = 0.92), Table 6.1. These demands may have been sufficient to initiate yielding in the

perimeter girders and panel zones. The ductility demand (i.e. normalized moment) distribution for the perimeter frame girders is presented in Fig. 6.16b. This figure shows that the demands were again highest between the second and sixth floors.

Figure 6.17 presents displacement histories of the SW corner at the twelfth floor from the analysis and the earthquake response records. The correlation is good. Because a good agreement was also found for the linear models, it is concluded that yielding had only minor effects on the overall response of the structure. Figure 6.18 shows the times when the yielding occurred in the structure. This figure indicates that yielding was concentrated between 13 and 22 seconds of the response when a strong response occurred in the NS direction.

Inter-story drift indices indicate that the EW and NS deformations were similar for this event, with concentration between the second and sixth floors, Fig. 6.16a. This agrees with the concentration of nonstructural damage observed in the building after the earthquake. The maximum inter-story drift index (IDX) computed was 0.89% at the fifth floor.

The axial load-moment interaction plots for the monitored column show a clear directionality and several cycles of moderate stress intensity, Figs. 6.16c, d and e.

The model with 1% damping shows an increase in the number of elements that yield (47). Perimeter frame girders yielded for this model, with a maximum ductility demand of 1.13. Because this model overestimates the response of the structure, it is believed that the model with 3% damping is more representative of what actually happened in the building during this event.

6.3.3 Parametric Studies

A number of parametric studies were performed on the complete three-dimensional nonlinear model to identify the effects of damping, nonlinearities, eccentricities and earthquake loading on the global response.

Five earthquake records were considered in these analyses: the recorded base building records during the Morgan Hill (1984), Mt. Lewis (1986) and Loma Prieta (1989) events, as well as the Mexico SCT (1985) and El Centro (1940) events. Both horizontal components of these earthquakes were used in all the analyses. Because it was observed from these records that maximum structural responses could occur long after the strong phase of the earthquake input ended and in order to evaluate cumulative damage effects, 80 seconds of input were considered in all the analyses, with the exception of those involving the El Centro records for which durations of 40 seconds were considered. Linear response spectra of the records used are presented in Chapter 4, Fig. 4.8 and Appendix C, Figs. C.1 and C.2.

Different effective peak accelerations (EPA) were used in the analyses. The effective peak accelerations were obtained by increasing the peak record acceleration by a scaling factor so that

the 5% viscous damping peak spectral acceleration of the record divided by 2.5 was equal to the desirable EPA value. In each analysis the scaling factor was applied to both components of the input earthquake records. Values of EPA used were 5, 15, 25, 40, 60 and 180% of g. The latter value is unrealistic but was used to assess the ultimate inelastic behavior of the structure. Because of the bi-directional input, these values were adjusted for only one direction of motion as follows:

- El Centro 1940: NS direction.
- Mexico SCT 1985: N90W (transverse) direction.
- Building base record, Morgan Hill 1984: NS direction.
- Building base record, Mt. Lewis 1986: NS direction.
- Building base record, Loma Prieta 1989: NS direction.

The orthogonal components were then scaled by the same factors.

To study the effects of the position of the floor center of mass, two different additional mass eccentricities were considered. These were expressed as a percentage of the building plan dimension (e/D). Values used were 0, 10 and 25%: the value of 0 means that only the original model eccentricities were considered. No additional stiffness or strength eccentricities were added to those already present in the model. Care should be taken when interpreting the results presented below, because several other investigations [14, 50] observed that the inelastic response characteristics of stiffness eccentric and strength eccentric structures differ from those of mass eccentric structures.

To evaluate the effect of viscous damping on the response, models were analyzed with 1, 5, 10, 20 and 40% of critical damping. This damping was incorporated in the model as a combination of the mass and initial stiffness matrices. Again, the latter models are unrealistic, but can be used to assess the effectiveness of retrofitting the structure by adding devices to increase the effective viscous damping.

Because of the large computing cost of each nonlinear analysis, a complete combination of these parameters was not feasible for this investigation. Nevertheless, some general trends in the response can be observed from the limited set of data.

As a way to obtain an upper bound on the response, most of the studies were performed using the low damping models (1% of critical). This should be considered in the interpretation of the results because the response spectra for the records studied change considerably with period for such a low damping value.

The results of these analyses are summarized in Tables 6.2 to 6.12 and in Figs. 6.19 to 6.59. In these figures the following denomination of model damping and ground motion input is used:

- Model with 1% viscous damping subjected to the Mt. Lewis event building base records: ML-1.

- Model with 5% viscous damping subjected to the Mt. Lewis event building base records: ML-5.
- Model with 1% viscous damping subjected to the Morgan Hill event building base records: MH-1.
- Model with 1% viscous damping subjected to the Loma Prieta event building base records: LP-1.
- Model with 1% viscous damping subjected to the Mexico SCT records: SCT-1.
- Model with 1% viscous damping subjected to the El Centro records: CENT-1.

Results of Parametric Studies

6.3.3.1 Effect of Different Ground Motions on the Response

Five different ground motions were studied in this part of the investigation. On the basis of the frequency content characteristics of the ground motions studied, the building base records and the Mexico SCT record can be classified as a "soft soil" record. The El Centro ground motion, corresponds to a "firm soil" record.

The effect of the different ground motions on the response of the structure was found to be dependent on the level of inelastic behavior of the model. Figures 6.40, 6.41 and 6.42 present the maximum twelfth floor displacement at the center of mass, the maximum in-plane rotation of the twelfth floor and the maximum inter-story drift index for an elastic and an inelastic model, respectively, for the same earthquake intensity (EPA=60% g). Figures 6.43 through 6.47 present other response parameters for the inelastic models subjected also to ground motions with 60% g effective peak acceleration.

Analyses of the results indicate the following:

- There is a clear difference in the severity of the response between the soft soil records and the firm soil record. The El Centro record, with its relatively high frequency content and short strong motion duration, has a relatively small effect on the structure. On the contrary, the soft site ground motions, with their predominant frequencies close to the natural periods of the building and with their long durations, produce larger displacements, inter-story drifts and ductility demands on the structure.
- The difference between earthquakes is more pronounced for structures responding in the linear range. This could be attributed to the resonance effect present in these lightly-damped

models. The most severe responses were obtained in the linear models subjected to the Mt. Lewis event. The elastic analysis indicates global displacement 6 times greater than the yield displacement for this scaled record. The behavior changes considerably in the inelastic range for relatively large earthquake intensities (EPA=60% g). At this level of intensity, the difference in response for different input ground motions is greatly reduced, especially for soft-site records.

For example, inelastic global ductility demands are very similar for the earthquakes studied, and in general much smaller than predicted by elastic analyses. The marked reduction in this parameter can be associated with the limiting of resonance effects because of structural nonlinearities. Similar observations can be made regarding in-plane torsion and inter-story drift. Local element rotation ductilities, while larger than global displacement ductilities, are also relatively small, about 4, Fig. 6.43. Cumulative rotational ductilities vary more among the different ground motions, but results indicate that the cumulative effects are equivalent to only 2 to 3 complete cycles of reversals at the maximum rotational ductility, Fig. 6.44. Many elements have inelastic excursions, Figs. 6.45 and 6.46.

The earthquake causing the severest response depends on the particular parameter:

- the Morgan Hill event is the most severe in terms of the number of yielding elements and cumulative rotational ductility demands, Figs. 6.44, 6.45 and 6.46;
- the Mt. Lewis event is the most severe in terms of the maximum in-plane story rotations, Fig. 6.41;
- and the Mexico SCT event is the most severe in terms of the maximum rotational ductility demands; maximum inter-story drift index and twelfth floor displacements, Figs. 6.40, 6.42 and 6.43.

- There is a strong difference in torsional response to the various ground motions studied, Figs. 6.41 and 6.47. A discussion of this behavior is presented in Sections 6.3.3.3 and 6.3.3.4.

6.3.3.2 Effect of Acceleration Level on the Response

The effect of peak ground acceleration on the response of the building was investigated by studying the response of several models to effective peak ground accelerations (EPA) of 5, 15, 25, 40, 60 and 180% g. Models with 1 and 5% damping were considered in these analyses. The effects of effective acceleration level on several response parameters are presented in Figs. 6.48 through 6.50.

Figure 6.48 shows the relation between the global ductility demand, μ_d, (maximum twelfth floor center-of-mass displacement divided by global yield displacement found from the static load-to-collapse analyses) and the EPA. This figure shows that the effective global ductility demands are quite small (less than 2) for relatively large EPA (60% g). Even for the unrealistic EPA=180% g, global ductility demands have values lower than 5. Correspondingly, values of maximum and cumulative rotational ductility demands for individual members are relatively small ($\mu < 5$ and $\mu_c < 60$) for EPA=60% g, Figs. 6.43, 6.44 and 6.49.

This response characteristic can be attributed to the relatively large flexibility and strength of the structure for which even small global ductilities imply large deformations. For example, a 3% inter-story drift index corresponds to global ductility demands of 1.5 (observed for the model subjected to the Mt. Lewis and Loma Prieta earthquakes for a 60% EPA, Fig. 6.50a.) Larger displacements are not attainable with the ground motions recorded thus far at the building site, or with the two other ground motions used in this study, at credible values of EPA. Similarly, if one were to limit drift indices to 1.5%, the EPA for the motions considered can not exceed 25% g.

Because of the weak girder-strong column design present in the structure, only a few columns yield even for large values of EPA. For example, for the 1% damping model subjected to the Mt. Lewis event with an EPA of 60% g, only 92 columns yielded (37 between the third and thirteenth story and 55 in the first two stories) and 1196 girders yielded, Figs. 6.46 and 6.50b and c. Most of the girder elements yield for EPA values greater than 60% g, Figs. 6.45 and 6.50b.

In some cases the structure benefits from this small amount of inelastic behavior. For example, Figs. 6.40 and 6.42 show significant reductions in maximum twelfth floor displacement and inter-story drift index when compared with an elastic system subjected to the same earthquake intensity. These figures show that considerable reductions are obtained for even small global ductility demands (1.5) or EPA (60% g). Nevertheless, the benefit of this reduction depends on the earthquake used and the viscous damping present in the model. As mentioned above these benefits can be associated in part with the limiting effect that nonlinearities have on structural resonance.

6.3.3.3 Effect of Yielding on Torsional Response

The effect of yielding on building torsional response was investigated by studying the effect of earthquake intensity on two parameters:

1. the ratio of the computed in-plane rotation of the twelfth floor in the nonlinear model to that of an equivalent linear model for the same level of earthquake intensity:

$$\frac{\theta_{inelastic}}{\theta_{elastic}} \tag{6.6}$$

2. the ratio of the in-plane rotation to the maximum displacement at the twelfth floor, for elastic and inelastic models at the same level of earthquake intensity:

$$\frac{\theta_{inelastic}}{\Delta_{inelastic}} \text{ or } \frac{\theta_{elastic}}{\Delta_{elastic}} \tag{6.7}$$

These ratios are presented in Tables 6.8 and 6.9 and Figs. 6.41 and 6.47.

The results indicate that these ratios are quite sensitive to input ground motion characteristics, effective peak acceleration, and damping. The reason for these differences could relate to different of the properties of the ground motion (predominant direction, frequency content, etc.) and to the different sensitivities of response parameters to inelastic behavior and damping (e.g., displacements are more sensitive than rotation to different levels of inelastic behavior).

Despite the different behavior observed in the models for the ground motions studied, the results show that inelastic torsional rotations are generally smaller in amplitude than those predicted using elastic models, and that ratios of nonlinear to linear elastic torsional rotation consistently decreases with increasing nonlinearity. Nevertheless, ratios of maximum in-plane rotation to maximum lateral displacement are greater for the nonlinear models than for the linear idealizations, at least for EPA=60% g. For other intensities a clear trend in these data was not identified. For example, results of the models subjected to the Mt. Lewis event indicate that torsional deformation increased with respect to translational deformation with increasing levels of effective peak acceleration, Table 6.9. On the other hand, results from the Loma Prieta event indicate that this ratio could grow or decrease depending on the level of EPA.

Also, it was observed from some of model responses that the history of the torsional behavior changes considerably when nonlinearities are introduced in the response. Figure 6.51 shows the torsional response at the twelfth floor (normalized to a value of 1) of several elastic and inelastic (EPA=60% g) models. The elastic and inelastic response histories differ considerably. For example, in the case of the 1% damping model subjected to the Mt. Lewis earthquake, the nonlinear torsional response tends to decrease considerably after yielding has occurred in the structure, Fig. 6.51a (after 34 seconds). This effect was not as clearly observed in the other cases, but it implies that torsional behavior could be considerably reduced in some cases when nonlinearities occur in the system. These effects may be associated with yielding which changes and separates the effective "modal periods" of the structure, thereby reducing the coupling, and breaking up the elastic resonance.

6.3.3.4 Effect of Additional Eccentricities on the Response

The effect of additional mass eccentricities was studied by displacing the center of mass at each floor towards the SW corner of the building by an equal amount (10 and 25% of the maximum

building plan dimension) in both directions. No attempts was made to move the center of stiffness or the center of strength of the floor. Because of the regular geometry of the building and the member locations and properties, the "center of stiffness and resistance of the floor" is located approximately in the geometric center of the square formed by the perimeter frame.

The movement of the center of mass by 10% and 25% of the building dimension increased the floor rotations by more than 100% in most of the analyses, Fig. 6.52 and Table 6.10. Other observations are as follows:

- The increase in eccentricity produced a reduction in the center of mass displacement in one direction and an increase in the orthogonal direction for the Mt. Lewis, Mexico SCT, and Loma Prieta events, a reduction in both directions for the El Centro event and an increase in both directions for the Morgan Hill event. Because the additional eccentricity was provided by moving the floor "center of mass", the comparison between these displacements was not strictly evaluated at the same position. To evaluate the displacement at a common point for all models and to consider the combined effect of rotations and displacements, the twelfth floor displacements at the SW corner (which was found from analysis of the building records to have the most severe response) were derived from the center-of-mass displacements and rotations. For this case, a reduction in one direction and an increase in the orthogonal direction were found for the Mt. Lewis event only, an increase for both directions was found for the Morgan Hill, Mexico SCT and El Centro events, and a reduction in both directions was found for the Loma Prieta event. These results indicate the strong dependence of the torsional response of the building on the dynamic characteristics of the structure and properties of the input ground motion. A similar pattern was observed for inter-story drifts, see Figs. 6.19 to 6.39.

- Also, the increase in eccentricity produces a reduction in the ratio of inelastic to elastic rotation and an increase in the ratio of rotation to maximum displacement at the twelfth floor for most of the records, Tables 6.8 and 6.9. In the case of the Mexico SCT record the rotation ratio ($\theta_{inelastic}/\theta_{elastic}$) increases and for El Centro it does not change. For the large additional eccentricity, e/D=25, there was considerable change in the initial period of the structure so the apparent change in rotational amplification is likely very dependent on the shape of the earthquake response spectrum.

- From response tables for the different earthquakes and Table 6.10 it can be seen that the change in eccentricity had the effect of consistently increasing the maximum ductility demand of the perimeter frame girders (maximum increment was 22%) and reducing the cumulative rotational ductility demand on these same elements (maximum reduction was 58%) and the SSD values (maximum reduction was 56%). For the elastic modes, the moment ratios of the

perimeter girders increased (up to 40%) or decreased (25%) depending on the ground motions studied. Similar trends were observed for inter-story drifts.

One explanation for the behavior of the maximum and cumulative rotational ductility demands can be deduced by examining Figs. 6.54 to 6.59. These figures show the distribution of maximum ductility and maximum cumulative ductility for the fifth floor perimeter frame built-up girders. Each value on the horizontal axes represents a column position (there are 10 columns on each side of the perimeter frame), Fig. 6.53. Each side of the building is represented in these figures by a different type of line. The cases of 0 and 10% additional eccentricities are presented. These figures show that when additional eccentricity was considered (which in all cases increased torsional rotations and maximum girder rotational ductilities) there usually was a redistribution of inelastic demand between orthogonal directions. This redistribution generally caused an increase in maximum ductility demand and a reduction in cumulative damage (the demands tended to average out). For example, in the case of the Mt. Lewis event shown in Fig. 6.55, the addition of eccentricity shifted the maximum ductility demand from the West side to the South side of the building.

- Despite the large increase in torsional deformations caused by the additional mass eccentricities considered, increases in maximum rotational ductility demands and moment ratios were relatively small. This effect can be related to the presence of a relatively strong and stiff perimeter frame that creates a torsionally stiff structural system, (i.e. the first predominant torsional period is shorter than the predominant translational period).

- Column forces also changed when the position of the center of mass was displaced: moments increased or decreased depending on the earthquake and column section orientation and the peak axial load generally decreased with increasing eccentricity.

6.3.3.5 Effect of Additional Damping on the Response

Several nonlinear analyses were initially performed on inelastic single degree-of-freedom oscillators to investigate the effect of viscous damping on yielding systems (see Appendix C). An elasto-perfectly-plastic model was selected for the analyses. Eleven different ground motions were used in the studies, six obtained on relatively firm soils and five on relatively soft soils. Damping values studied were 0, 1, 2, 5, 10, 20, 40 and 80% of critical. Five different structural strengths and 20 different structural periods were considered. Response parameters considered were the maximum and cumulative displacement ductility demands, the sum of the squared accelerations and the apparent strong motion duration. A detailed description of the analyses and results may be found in Appendix C.

From these analyses it was found that increasing the amount of damping generally reduced the amount of yielding in the system.

- Maximum ductility demand and cumulative damage decrease with increasing viscous damping.
- The total accelerations (related to base shear and overturning moments) could increase or decrease in the system depending on the period and capacity of the structure. Generally, an increase in inertial forces was found for weak systems and for structures with periods below the predominant period of the ground. This could be expected because weak and short period structures generally have high ductility demands. Damping forces may thus be large in comparison with the structural yield force.
- Strong motion duration, based on acceleration histories, can also increase or decrease with increasing damping, depending on the system capacity and period. Nonetheless, in most cases duration decreases with increasing damping and, if it increases, it is only by a small amount.
- A general conclusion of the study in Appendix C, was that there is an optimum value of viscous damping after which further increases have relatively little influence on the response. This value is between 20 and 30% for maximum and cumulative ductility, between 10 and 20% for the sum of the squared accelerations and around 10% for response duration. The apparent "optimal-limit damping" for all parameters studied would be 30% of critical.

The effect of additional damping on the response of the complete three-dimensional model was studied using the Mt. Lewis and Loma Prieta events. Results showing the effect of damping on inelastic responses are presented in Tables 6.1 through 6.7 and Tables 6.11 through 6.12. Additional parameters were monitored for this part of the study:

- The maximum inertial force at the base of the building:

$$\mathrm{V}_i = \mathrm{MAX}_t \left(\sum_{j=1}^{N=12} m_j \, a_j^i(t) \right) \tag{6.8}$$

where

V_i is the base inertial shear in the i direction,
m_j is the translational mass of floor j, and
$a_j^i(t)$ is the total acceleration at floor j, in the i direction, at time t.

This parameter is a measure of the total inertial forces in the building. For low levels of viscous damping it is similar to the base shear obtained by summing element shears at the base of the structure, at the time of maximum response. For high levels of damping, the damping forces are considerably larger, so it will overestimate the shears present in the elements at the base of the building. However, this parameter may reflect the actual base shear and overturning moments if damping forces are introduced in the building by means of mechanical devices.

- The square root of the floor sum of the squared total acceleration values for the first to the twelfth story:

$$\mathrm{RSA}_i = \sqrt{\sum_{j=1}^{N=12} \sum_{t} \left(a_j^i(t)\right)^2 \Delta t} \tag{6.9}$$

RSA will be used to compare the effects of different amounts of damping on the amplitude and duration of the response for a given direction i.

Results indicate similar behavior to that found for the one degree-of-freedom studies, Table 6.11. In general, those parameters that are related to displacement values decreased with increasing amounts of damping. The decrease was smaller for large inelastic behavior in the structure and was larger for cumulative values (μ_c and SSD) than for maximum values (maximum displacement at twelfth floor, IDX and μ), see Table 6.11. Maximum in-plane rotation of the twelfth floor was, nevertheless, affected more by the amount of viscous damping than cumulative values. The response of the model to Mt. Lewis event illustrates clearly the effect of viscous damping for different levels of inelastic behavior. In this case the ratio of the maximum rotational ductility and maximum cumulative rotational ductility between models with 1 and 5% damping (i.e , $[(\mu)_{\xi=5\%}/(\mu)_{\xi=1\%}]$, $[(\mu_c)_{\xi=5\%}/(\mu_c)_{\xi=1\%}]$) were 20 and 49% larger for EPA=60% g than that for EPA=25% g, respectively (i.e., benefit of viscous damping decreased with increasing level of nonlinearities). The different effect of viscous damping on cumulative and maximum values can be observed from the response of the models with 1 and 5% for EPA = 25% g subjected to the Mt. Lewis event. For this case the reduction in cumulative rotational ductility demand ($[(\mu_c)_{\xi=5\%}/(\mu_c)_{\xi=1\%}]$=0.42) was nearly three times that in the maximum rotational ductility demand ($[(\mu)_{\xi=5\%}/(\mu)_{\xi=1\%}]$=0.80).

For parameters depending on maximum acceleration values (inertial base shear) increases or decreases were found depending on the level of nonlinearities present in the structure, Table 6.12. For parameters depending on the complete acceleration history (RSA) a decrease was observed with increasing damping. Again, the reduction is smaller for higher levels of nonlinearities. For example, for the Loma Prieta event and the model with 10% damping the base shears due to inertial forces and RSA values were 20 and 47% larger for EPA = 180% g than those for EPA=60% g, respectively.

The structural response improves when additional viscous damping is included in the model. From the linear analysis of the full structural model it was found that small amounts of viscous damping (5% of critical) substantially reduced the apparent duration of the response. As presented above, studies from the nonlinear model indicate that viscous damping, as provided in the computer models, generally reduces the response (peak and cumulative parameters) of the structure. The benefits are, nevertheless, much greater for cumulative values than for peak values of the response, and the benefits are reduced with increasing inelastic behavior in the system.

6.4 Summary and Conclusions

A nonlinear model of the building was generated to evaluate the behavior of the structure during the recorded earthquakes and to perform parametric studies. The following conclusions were found from these analyses:

1. **Static Load-To-Collapse Analysis**

   The structure was found to be relative strong, flexible and deformable. The mode of behavior in the main elements of the structure is strong column-weak girder. Column axial loads at the ultimate load level are relatively small. Apparently, care was taken in the design to provide for strong columns in the perimeter frame, especially at the corners. Girder-column joints, nevertheless, have yield strengths that are on average 10% below the plastic strength of the connecting girders.

   Several observations can be made by comparing the base shear-twelfth floor displacement relation obtained from these analyses with that of a single degree-of-freedom system. Appreciable departure from linear behavior (local yielding) occurred for a base shear coefficient (V/W) of 0.22 and a twelfth floor displacement of 48 cm (19 inches). This corresponds to a 1% average drift index. The effective twelfth floor yield displacement (global yielding) for the structure was estimated to be 64 cm (25 inches, 1.3% average drift); the base shear coefficient at this point was 0.29. A nearly complete energy dissipation ("collapse") mechanism, in the absence of P-Δ effects, was not formed until a base shear coefficient of 0.48 and a displacement of 644 cm (253 inches, 13.0% average drift) were achieved.

   Models including P-Δ effects indicated that this condition has consequences mainly on the post-yielding tangent stiffness of the structure. The initial effective elastic stiffness was only 3.2% lower than the case where P-Δ effects were disregarded. Nevertheless, the post-yield stiffness was reduced by 52% in comparison with the case without P-Δ effects. These geometric effects make the response of the computer model sensitive to the selection of the deformation

hardening modulus, since this parameter controls the post-yielding tangent stiffness of the structure. For the models studied, when deformation hardening ratios were changed in all elements from 5% to 1% of the elastic stiffness, a sudden "static failure" was observed in the model after the equivalent yield displacement of the model was reached (1.3% average drift).

Also, it was observed from the static load-to-collapse analyses that the high levels of yielding had the effect of reducing the ratio of the in-plane floor rotation to the translational displacement in the direction of loading, and of the displacements in the two orthogonal translational directions at the center of mass. The reduction of these ratios, or apparent de-coupling, indicates that after severe yielding occurs in the structure rotations and orthogonal displacements do not increase as fast as the displacements in the direction of loading.

The ATC 3-06 and 1988 UBC base shear design values are considerably lower than the capacities estimated from the static load-to-collapse analyses of the structure.

2. **Response of the Building Models to Recorded Earthquakes**

Several nonlinear models were subjected to the Mt. Lewis and Loma Prieta events to investigate nonlinear behavior on the structure. It was observed from studies of the computed responses that some elements may have yielded, especially during the stronger Loma Prieta event. Nevertheless, these nonlinearities had only a small effect on the overall response of the structure.

3. **Parametric Studies**

- Analyses using different ground motion records indicated that the frequency content and the duration of input motion have a strong effect on the response of the models. These effects, however, are more pronounced for elastic than for inelastic response (not taking into account cumulative damage parameters). Of the ground motions considered, the amplified Mt. Lewis event (because of its frequency content and duration) presented the most severe demands on linear models. For nonlinear models, the Morgan Hill and the Mexico SCT events were generally more severe, but the variations in response to different ground motions was relatively small.
- Several analysis with more severe ground motions than those recorded in the structure were performed. They indicate that large displacement and inter-story drift could be expected under these events. Nevertheless, inelastic ductilities demands remained relatively small for effective peak accelerations lower than 60% g because of the relatively large flexibility and strength of the structure. However, drifts may become excessive because EPA values greater than 25% g resulted in average drift indices exceeding 1.5%

- The ratio of in-plane torsional rotations to lateral displacements ("apparent coupling") could increase or decrease depending on the level of inelastic behavior and the characteristics of the input ground motion. The scatter of the results indicates that more analyses are needed to identify definitively the factors controlling the response. The efficacy of observations regarding potential decoupling of torsional and lateral motions made on the basis of the static load-to-collapse studies in this chapter, and the effect of input motion predominant direction observed from the simple models in Chapter 2, need to be more thoroughly investigated.

- Results from the analyses that considered added mass eccentricities indicate that, contrary to what has been found for models subjected to unidirectional inputs (Refs. [25, 17, 14]), displacement at the center of mass (or at a fixed distance from the center of mass) could decrease or increase depending on the building characteristics and the properties of the input ground motion.

  An increase in eccentricity, from e/D=0 to e/D=10%, in models that responded inelastically had the effect of increasing the maximum rotational ductility demand on the perimeter frame girders (maximum increment was 22%), and reducing the cumulative ductility demand on these same elements (maximum reduction was 58%) and the SSD values (maximum reduction was 56%). On the other hand, for the elastic models, moment demands for the perimeter girders increased (up to 40%) or decreased (25%) depending on the ground motion studied. Similar trends were observed for the inter-story drifts.

  Also, the addition of this mass eccentricity redistributed inelastic demands between orthogonal directions. In some cases, the maximum ductility demand for a given earthquake changed from one direction to the orthogonal direction when the additional eccentricity was included.

  The results of this part of the investigation agree with findings from the analyses of simple mass eccentric structures developed in Chapter 2 and in other investigations. In general, increased torsional response increases the stress or ductility demands in elements located far away from the center of rotation and changes the maximum translational displacements. These effects are more severe for elastic structures than inelastic structures and are highly dependent on the characteristics of the input ground motion.

- It was found that increasing the amount of damping reduces the amount of yielding in the system. This implies that maximum ductility demands, cumulative damage, the sum of the squared displacements and generally the strong motion duration decrease

with increasing viscous damping. However inertial forces in the structure could increase or decrease depending on the period and strength of the structure.

From analyses of single degree-of-freedom systems it was found that there is a value of the critical damping ratio after which increased damping does not affect the response very much. This value is between 20 and 30% for maximum ductility and cumulative ductility demands, between 10 and 20% for the sum of the squared accelerations and around 10% for duration of the response. The benefits of increased damping are, nevertheless, much greater for cumulative values than for peak values of the response, and they are reduced with increasing inelastic behavior in the system.

Table 6.1: **Model Response to the Recorded Earthquakes**

Earthquake	Mt. Lewis		Loma Prieta	
Damping	1%	3%	1%	3%
12^{th} Level Drifts				
Center of Mass				
EW (cm)	16.45	13.13	40.12	34.22
NS (cm)	36.20	23.71	36.77	30.97
Rot. (rad)	0.0023	0.0016	0.0022	0.0016
Disp. SW Corner				
EW (cm)	19.56	14.29	41.50	36.06
NS (cm)	39.68	26.04	40.41	33.53
Tors. Rot. (cm)	9.113	6.340	8.598	6.340
Max. IDX[i]	0.0089	0.0058	0.0105	0.0089
Max. μ^{ii}	1.06	0.69	1.13	0.92
Max. ${\mu_c}^{ii}$	1.09	0.00	1.15	0.00
SSD x10^6				
EW (cm^2)	0.2802	0.0604	0.7135	0.3640
NS (cm^2)	0.9649	0.2587	0.4220	0.2831
Normalized Max.				
Column Forces				
$M_{yy}/M_{p\,yy}$	0.42	0.28	0.45	0.38
$M_{zz}/M_{p\,zz}$	0.25	0.17	0.56	0.48
P/P_p	0.16	0.13	0.18	0.15
Number of Inelastic				
Elements				
Columns	0	0	0	0
Beams	36	0	47	16

(*i*) Inter-story drift index at the position of the center of mass of models with no additional eccentricity.

(*ii*) For perimeter frame built-up girders.

Table 6.2: **Model Response to the Mt. Lewis Record**

Effective Peak Accel.	60[i]	60[i]	60 [i]	25	25	25	40	60	60	60
Damping	1%	1%	1%	1%	1%	1%	1%	1%	1%	1%
Added Eccentricity	0	10	25	0	10	25	0	0	10	25
12^{th} Level Drifts										
Center of Mass										
EW (cm)	197.11	250.89	249.01	60.05	68.51	65.61	73.15	77.69	82.33	83.22
NS (cm)	429.89	282.59	235.60	64.22	63.17	58.94	76.25	87.17	77.16	75.58
Rot. (rad)	0.0266	0.0518	0.0545	0.0084	0.0144	0.0210	0.0110	0.0158	0.0288	0.0314
D. SW Corner										
EW (cm)	234.22	291.38	264.40	66.50	78.26	69.66	81.28	86.79	121.30	100.72
NS (cm)	470.82	334.96	257.40	72.33	71.83	60.11	83.50	96.17	92.43	76.96
Tors. Rot. (cm)	105.25	205.07	215.95	33.244	57.059	83.171	44.62	62.53	114.04	124.30
Max. IDX[ii]	0.1053	0.0733	0.0733	0.0178	0.0199	0.0208	0.0232	0.0288	0.0291	0.0325
Max. μ	12.78	9.57	7.60	2.78	2.87	2.36	3.57	4.16	4.86	4.16
Max. μ_c	0.00	0.00	0.00	27.08	19.27	15.52	38.17	50.07	47.57	40.60
SSD x10^6										
EW (cm^2)	38.9400	46.930	39.137	2.1378	2.2516	2.7733	3.0069	4.1860	4.9443	4.4076
NS (cm^2)	134.3700	64.563	41.898	3.6271	3.0926	2.9397	4.4080	5.3412	5.2096	4.4309
Normalized Max.										
Column Forces										
$M_{yy}/M_{p\,yy}$	4.92	3.05	2.82	0.68	0.69	0.68	0.75	0.83	0.87	0.79
$M_{zz}/M_{p\,zz}$	3.03	3.61	3.54	0.75	0.79	0.86	0.93	0.96	0.98	0.99
P/P_p	3.61	3.00	2.93	0.31	0.26	0.21	0.35	0.36	0.36	0.26
Number of Inelastic										
Elements										
Columns	0	0	0	0	7	9	14	92	123	114
Beams	0	0	0	866	882	817	1061	1196	1137	1181

(i) Linear analysis.

(ii) Inter-story drift index at the position of the center of mass of models with no additional eccentricity.

Table 6.3: **Model Response to the Mt. Lewis Record**

Effective Peak Accel.	60[i]	60[i]	25	60	60	60	60	60
Damping	5%	5%	5%	5%	5%	10%	20%	40%
Added Eccentricity	0	10	0	0	10	0	0	0
12^{th} Level Drifts								
Center of Mass								
EW (cm)	134.45	149.92	52.37	75.38	81.86	71.66	60.21	38.04
NS (cm)	200.74	161.68	58.44	89.55	71.92	81.94	59.20	37.35
Rot. (rad)	0.0141	0.0348	0.0060	0.0104	0.0220	0.0065	0.0037	0.0016
D. SW Corner								
EW (cm)	145.91	187.46	56.56	83.79	102.50	76.95	63.25	39.93
NS (cm)	221.70	192.59	64.30	94.85	85.41	85.85	62.68	39.46
Tors. Rot. (cm)	55.750	137.92	23.893	41.328	87.292	25.716	14.502	6.221
Max. IDX[ii]	0.0488	0.0411	0.0151	0.0260	0.0263	0.0228	0.0158	0.0100
Max. μ	6.00	5.73	2.23	4.00	3.98	3.33	2.08	1.00
Max. μ_c	0.00	0.00	11.27	30.10	26.13	18.98	7.28	1.00
SSD x10^6								
EW (cm^2)	4.5062	5.1011	0.7113	2.3396	3.0413	1.4296	0.7377	0.2654
NS (cm^2)	16.159	4.9740	1.7193	3.7424	3.2874	2.4584	1.2582	0.4213
Normalized Max.								
Column Forces								
$M_{yy}/M_{p\,yy}$	2.33	1.43	0.64	0.79	0.80	0.78	0.72	0.51
$M_{zz}/M_{p\,zz}$	1.74	2.17	0.70	0.96	0.97	0.90	0.82	0.58
P/P_p	1.34	2.77	0.27	0.36	0.32	0.34	0.29	0.21
Number of Inelastic								
Elements								
Columns	0	0	0	36	67	26	0	0
Beams	0	0	624	1082	1023	964	725	50

(i) Linear analysis. (ii) Inter-story drift index at the position of the center of mass of models with no additional eccentricity.

Table 6.4: **Model Response to the Morgan Hill Record**

Effective Peak Accel.	60[i]	60[i]	60	60
Damping	1%	1%	1%	1%
Added Eccentricity	0	10	0	10
12^{th} Level Drifts				
Center of Mass				
EW (cm)	314.12	272.78	91.55	105.47
NS (cm)	372.54	253.04	77.66	79.73
Rot. (rad)	0.0237	0.0532	0.0129	0.0268
Disp. SW Corner				
EW (cm)	345.14	342.30	96.53	131.64
NS (cm)	383.03	289.82	75.42	87.48
Tors. Rot. (cm)	93.968	210.956	51.036	106.350
Max. IDX[ii]	0.0920	0.0748	0.0309	0.0327
Max. μ	10.99	9.34	4.40	5.17
Max. μ_c	0.00	0.00	60.23	49.22
SSD x10^6				
EW (cm^2)	24.0880	9.3540	6.6376	5.6924
NS (cm^2)	24.7800	7.6170	3.8175	4.7496
Normalized Max.				
Column Forces				
$M_{yy}/M_{p\,yy}$	4.70	2.59	0.98	0.91
$M_{zz}/M_{p\,zz}$	4.44	4.79	0.99	0.96
P/P_p	3.73	3.33	0.44	0.39
Number of Inelastic				
Elements				
Columns	0	0	167	147
Beams	0	0	1251	1200

(*i*) Linear analysis.

(*ii*) Inter-story drift index at the position of the center of mass of models with no additional eccentricity.

Table 6.5: **Model Response to the SCT Mexico Record**

Effective Peak Accel.	60^{i}	60^{i}	60	60
Damping	1%	1%	1%	1%
Added Eccentricity	0	10	0	10
12^{th} Level Drifts				
Center of Mass				
EW (cm)	241.32	157.55	78.06	76.99
NS (cm)	226.73	244.60	93.32	103.82
Rot. (rad)	0.0219	0.0452	0.0080	0.0224
Disp. SW Corner				
EW (cm)	277.51	183.54	79.01	85.94
NS (cm)	245.62	300.85	105.27	133.26
Tors. Rot. (cm)	86.645	178.908	31.739	88.639
Max. IDX^{ii}	0.0603	0.0643	0.0330	0.0357
Max. μ	6.77	8.13	4.97	5.91
Max. μ_c	0.00	0.00	42.54	42.24
SSD $x10^6$				
EW (cm^2)	4.4818	4.1200	3.6942	3.7706
NS (cm^2)	5.03747	4.6400	4.4733	4.1707
Normalized Max.				
Column Forces				
$M_{yy}/M_{p\,yy}$	2.75	2.09	0.80	0.74
$M_{zz}/M_{p\,zz}$	3.55	2.32	0.80	0.87
P/P_p	1.73	1.16	0.38	0.32
Number of Inelastic				
Elements				
Columns	0	0	60	81
Beams	0	0	1048	1031

(i) Linear analysis.

(ii) Inter-story drift index at the position of the center of mass of models with no additional eccentricity.

Table 6.6: **Model Response to the El Centro Record**

Effective Peak Accel.	60^{i}	60^{i}	60	60
Damping	1%	1%	1%	1%
Added Eccentricity	0	10	0	10
12^{th} Level Drifts				
Center of Mass				
EW (cm)	79.73	54.46	56.11	43.70
NS (cm)	74.51	52.53	44.76	43.51
Rot. (rad)	0.0084	0.0234	0.0075	0.0208
Disp. SW Corner				
EW (cm)	88.55	82.60	65.69	69.42
NS (cm)	78.74	80.51	51.63	67.89
Tors. Rot. (cm)	34.097	92.780	29.678	82.339
Max. IDX^{ii}	0.0214	0.0203	0.0147	0.0150
Max. μ	2.33	2.56	2.07	2.50
Max. μ_c	0.00	0.00	10.06	4.27
SSD x10^6				
EW (cm^2)	1.3560	0.1903	1.9346	0.8414
NS (cm^2)	1.2300	0.2006	1.1339	1.0360
Normalized Max.				
Column Forces				
$M_{yy}/M_{p\,yy}$	0.94	0.54	0.60	0.55
$M_{zz}/M_{p\,zz}$	1.38	1.57	0.77	0.82
P/P_p	0.75	0.61	0.36	0.25
Number of Inelastic				
Elements				
Columns	0	0	5	27
Beams	0	0	655	577

(i) Linear analysis.

(ii) Inter-story drift index at the position of the center of mass of models with no additional eccentricity.

Table 6.7: **Model Response Loma Prieta Building Record**

Effective Peak Accel.	60[i]	60[i]	60	60	60	60	60	180	180	180
Damping	1%	1%	1%	1%	10%	20%	40%	1%	10%	20%
Added Eccentricity	0	10	0	10	0	0	0	0	0	0
12^{th} Level Drifts										
Center of Mass										
EW (cm)	154.12	185.15	80.01	93.69	71.13	50.20	38.67	287.10	206.07	155.04
NS (cm)	141.79	105.40	77.82	73.64	64.85	51.75	33.00	180.33	136.98	116.00
Rot. (rad)	0.0086	0.0459	0.0073	0.0190	0.0037	0.0019	0.0010	0.0149	0.0072	0.0046
Disp. SW Corner										
EW (cm)	159.45	239.60	86.65	111.00	70.56	61.20	39.73	292.61	207.84	155.04
NS (cm)	153.40	132.92	76.21	83.18	67.96	54.14	34.24	171.96	137.16	116.79
Tors. Rot. (cm)	33.877	181.875	29.044	75.325	14.700	7.45	3.804	59.119	28.529	18.148
Max. IDX[ii]	0.0405	0.0525	0.0312	0.0350	0.0210	0.0156	0.0103	0.0955	0.0688	0.0514
Max. μ	4.30	6.06	4.31	5.25	2.78	1.92	1.09	12.38	8.88	6.45
Max. μ_c	0.00	0.00	35.12	37.45	9.41	3.58	1.09	92.17	54.20	33.00
SSD x10^6										
EW (cm^2)	10.4290	11.0970	5.2637	5.1176	1.5634	0.7763	0.2777	14.2250	7.2852	4.4220
NS (cm^2)	6.1920	3.9951	3.1808	4.3911	1.5403	0.8356	0.3119	11.0800	7.1237	4.6863
Normalized Max.										
Column Forces										
$M_{yy}/M_{p\,yy}$	1.73	1.83	0.85	0.79	0.77	0.70	0.48	1.00	0.96	0.96
$M_{zz}/M_{p\,zz}$	2.13	3.33	0.92	0.94	0.85	0.82	0.59	0.98	0.98	0.94
P/P_p	1.25	1.53	0.33	0.29	0.26	0.22	0.16	0.42	0.40	0.38
Number of Inelastic										
Elements										
Columns	0	0	100	126	39	1	0	515	392	366
Beams	0	0	1159	1181	839	616	32	1301	1213	1134

(*i*) Linear analysis.

(*ii*) Inter-story drift index at the position of the center of mass of models with no additional eccentricity.

Table 6.8: **Ratio of Inelastic to Elastic Torsional Rotations at 12^{th} Floor, $(\theta_{inelastic}/\theta_{elastic})$.**

Record	Damping	EPA	e/D		
			0	10	25
Mt. Lewis	1%	25	0.76	0.67	0.92
Mt. Lewis	1%	40	0.63	–	–
Mt. Lewis	1%	60	0.60	0.55	0.57
Mt. Lewis	5%	25	1.03	–	–
Mt. Lewis	5%	60	0.74	0.63	–
Mt. Lewis	5%	180	0.11	–	–
Morgan Hill	1%	60	0.54	0.50	–
Mexico SCT	1%	60	0.37	0.50	–
El Centro	1%	60	0.89	0.89	–
Loma Prieta	1%	60	0.85	0.41	–
Loma Prieta	1%	180	0.58	–	–

Table 6.9: **Ratio of Torsional Rotations to Maximum Lateral Displacement at 12^{th} Floor, (θ/Δ).**

Record	Damping	EPA	e/D		
			0	10	25
Mt. Lewis	1%	elastic	0.62	1.83	2.19
Mt. Lewis	1%	5.2	0.64	–	–
Mt. Lewis	1%	25	1.31	2.11	2.10
Mt. Lewis	1%	40	1.44	–	–
Mt. Lewis	1%	60	1.81	3.50	3.77
Mt. Lewis	5%	elastic	0.70	2.15	–
Mt. Lewis	5%	25	0.70	–	–
Mt. Lewis	5%	60	1.03	2.69	–
Mt. Lewis	5%	180	1.52	–	–
Morgan Hill	1%	elastic	0.64	1.95	–
Morgan Hill	1%	60	1.41	2.54	–
Mexico SCT	1%	elastic	0.90	1.85	–
Mexico SCT	1%	60	0.86	2.16	–
El Centro	1%	elastic	1.05	4.30	–
El Centro	1%	60	1.34	4.76	–
Loma Prieta	1%	elastic	0.56	2.48	–
Loma Prieta	1%	15.7	0.55	–	–
Loma Prieta	1%	60	0.91	2.03	–
Loma Prieta	1%	180	0.52	–	–

Table 6.10: **Ratio of Model Response Parameters (e/D=10)/(e/D=0).**

Record	Damping	EPA	θ_{10}/θ_0	μ_{10}/μ_0	$\mu_{c\ 10}/\mu_{c\ 0}$	SSD_{10}/SSD_0	$IDX_{10}/\ IDX_0$	$(\theta/\Delta)_{10}/(\theta/\Delta)_0$
Mt. Lewis	1%	elastic	1.95	0.75	–	0.48	0.70	2.95
Mt. Lewis	1%	25	1.71	1.03	0.71	0.85	1.12	1.61
Mt. Lewis	1%	60	1.82	1.14	0.95	0.98	1.01	1.93
Mt. Lewis	5%	elastic	2.47	0.96	–	0.31	0.84	3.07
Mt. Lewis	5%	60	2.11	1.00	0.87	0.88	1.01	2.61
Morgan Hill	1%	elastic	2.24	0.85	–	0.38	0.81	3.04
Morgan Hill	1%	60	2.07	1.18	0.82	0.86	1.06	1.80
Mexico SCT	1%	elastic	2.23	1.20	–	0.92	1.06	2.04
Mexico SCT	1%	60	2.86	1.19	0.99	0.93	1.08	2.51
El Centro	1%	elastic	3.78	1.10	–	0.14	0.95	4.10
El Centro	1%	60	2.77	1.21	0.42	0.44	1.02	3.55
Loma Prieta	1%	elastic	1.30	1.40	–	1.06	1.30	4.43
Loma Prieta	1%	60	2.60	1.22	1.07	0.97	1.12	2.23

(*i*) Linear analysis.

(*ii*) Inter-story drift index at the position of the center of mass of models with no additional eccentricity.

Table 6.11: **Ratio of Model Response Parameters. Damping Effects. e/D=0.**

Record	Parameter	EPA	Damping Ratio			
			5/1	10/1	20/1	40/1
Mt. Lewis	SSD	elastic	0.12	–	–	–
Mt. Lewis	IDX^{i}	elastic	0.46	–	–	–
Mt. Lewis	$\mu_d{}^{ii}$	elastic	0.47	–	–	–
Mt. Lewis	Rotation^{iii}	elastic	0.53	–	–	–
Mt. Lewis	μ	25	0.80	–	–	–
Mt. Lewis	μ_c	25	0.42	–	–	–
Mt. Lewis	SSD	25	0.47	–	–	–
Mt. Lewis	IDX^{i}	25	0.84	–	–	–
Mt. Lewis	$\mu_d{}^{ii}$	25	0.91	–	–	–
Mt. Lewis	Rotation^{iii}	25	0.71	–	–	–
Mt. Lewis	μ	60	0.96	0.80	0.50	0.24
Mt. Lewis	μ_c	60	0.60	0.38	0.15	0.02
Mt. Lewis	SSD	60	0.70	0.46	0.24	0.19
Mt. Lewis	IDX^{i}	60	0.90	0.79	0.55	0.35
Mt. Lewis	$\mu_d{}^{ii}$	60	1.03	0.94	0.69	0.44
Mt. Lewis	Rotation^{iii}	60	0.66	0.41	0.23	0.10
Loma Prieta	μ	60	–	0.65	0.45	0.25
Loma Prieta	μ_c	60	–	0.27	0.10	0.03
Loma Prieta	SSD	60	–	0.30	0.17	0.05
Loma Prieta	IDX^{i}	60	–	0.67	0.46	0.33
Loma Prieta	$\mu_d{}^{ii}$	60	–	0.89	0.75	0.48
Loma Prieta	Rotation^{iii}	60	–	0.51	0.24	0.14
Loma Prieta	μ	180	–	0.72	0.52	–
Loma Prieta	μ_c	180	–	0.59	0.36	–
Loma Prieta	SSD	180	–	0.51	0.33	–
Loma Prieta	IDX^{i}	180	–	0.72	0.53	–
Loma Prieta	$\mu_d{}^{ii}$	180	–	0.72	0.54	–
Loma Prieta	Rotation^{iii}	180	–	0.48	0.31	–

(i) Inter-story drift index at the position of the center of mass of models with no additional eccentricity.

(ii) Global ductility demand: maximum twelfth floor displacement divided by global yield displacement from static load to collapse studies (64 cm (25 inches)).

(iii) Maximum in-plane rotation at twelfth floor.

Table 6.12: **Ratio of Model Acceleration Response Parameters. Damping Effects. e/D=0.**

Record	Parameter	EPA	Damping Ratio			
			5/1	10/1	20/1	40/1
Mt. Lewis	Max. Base Shear (EW)	60	0.93	0.99	1.03	0.81
Mt. Lewis	Max. Base Shear (NS)	60	0.92	0.98	1.01	0.83
Mt. Lewis	RSA (EW)	60	0.76	0.62	0.52	0.43
Mt. Lewis	RSA (NS)	60	0.84	0.73	0.60	0.46
Loma Prieta	Max. Base Shear (EW)	60	–	1.00	0.99	0.84
Loma Prieta	Max. Base Shear (NS)	60	–	0.99	0.97	0.77
Loma Prieta	RSA (EW)	60	–	0.55	0.44	0.34
Loma Prieta	RSA (NS)	60	–	0.67	0.54	0.41
Loma Prieta	Max. Base Shear (EW)	180	–	1.18	1.38	–
Loma Prieta	Max. Base Shear (NS)	180	–	1.20	1.42	–
Loma Prieta	RSA (EW)	180	–	0.81	0.76	–
Loma Prieta	RSA (NS)	180	–	0.84	0.79	–

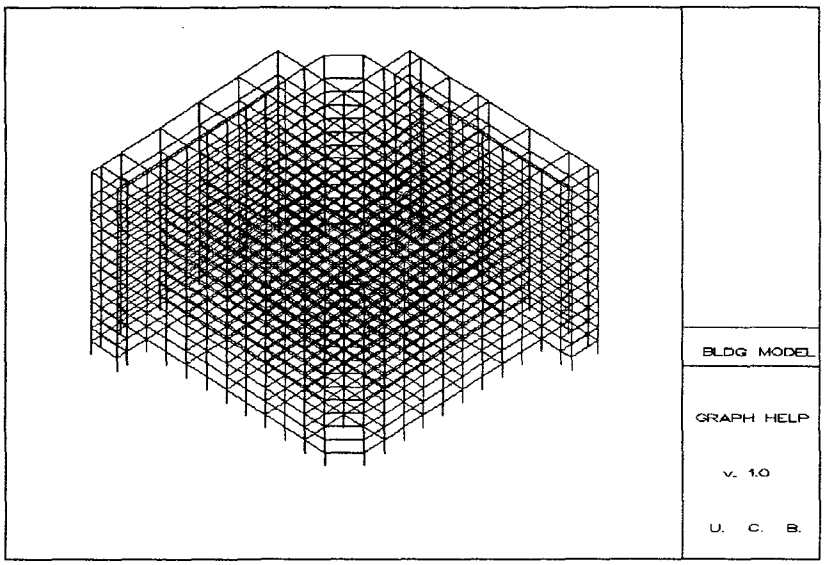

Figure 6.1: Building model. NE corner view.

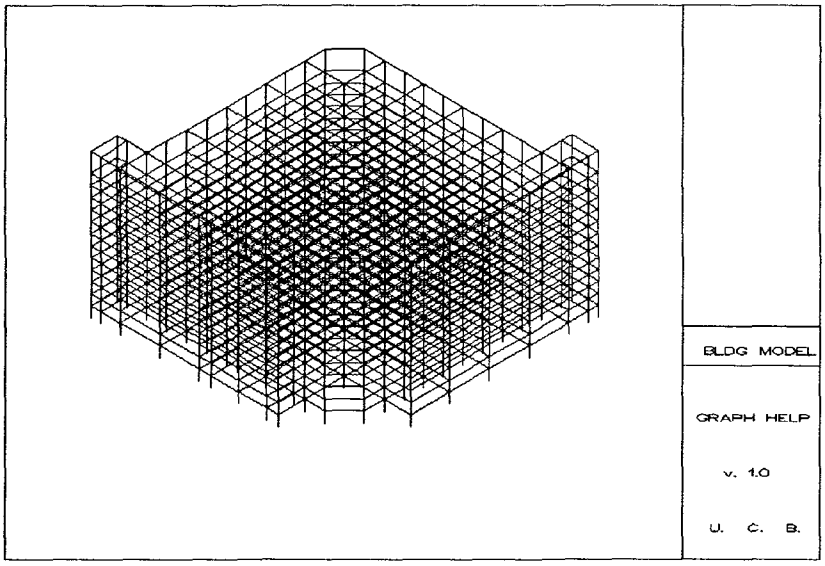

Figure 6.2: Building model. SW corner view.

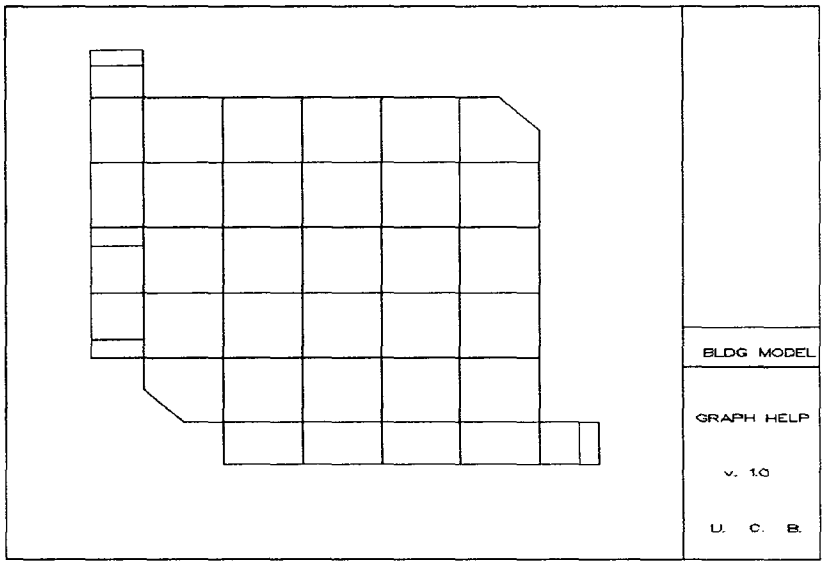

Figure 6.3: Building model. Plan view.

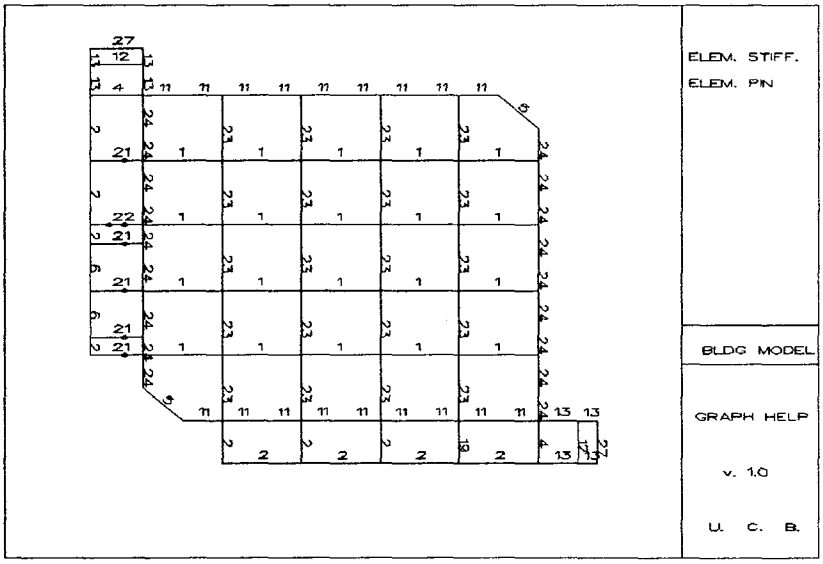

Figure 6.4: Building model. Fourth level element stiffness distribution.

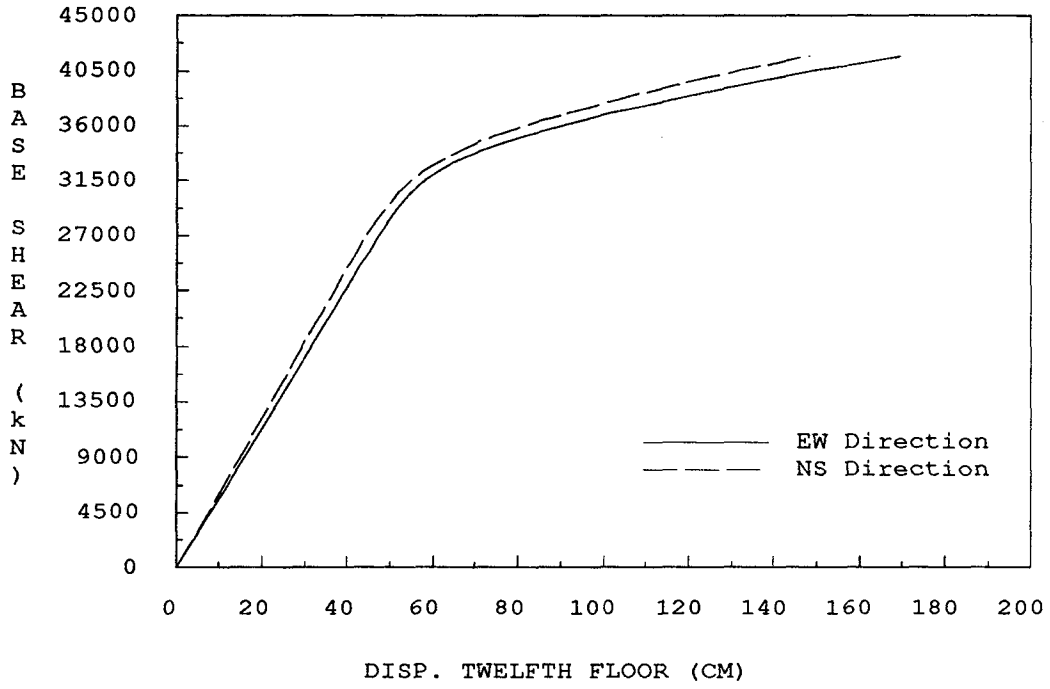

Figure 6.5: Base shear-twelfth floor displacement. EW and NS directions. P-Δ effects ignored.

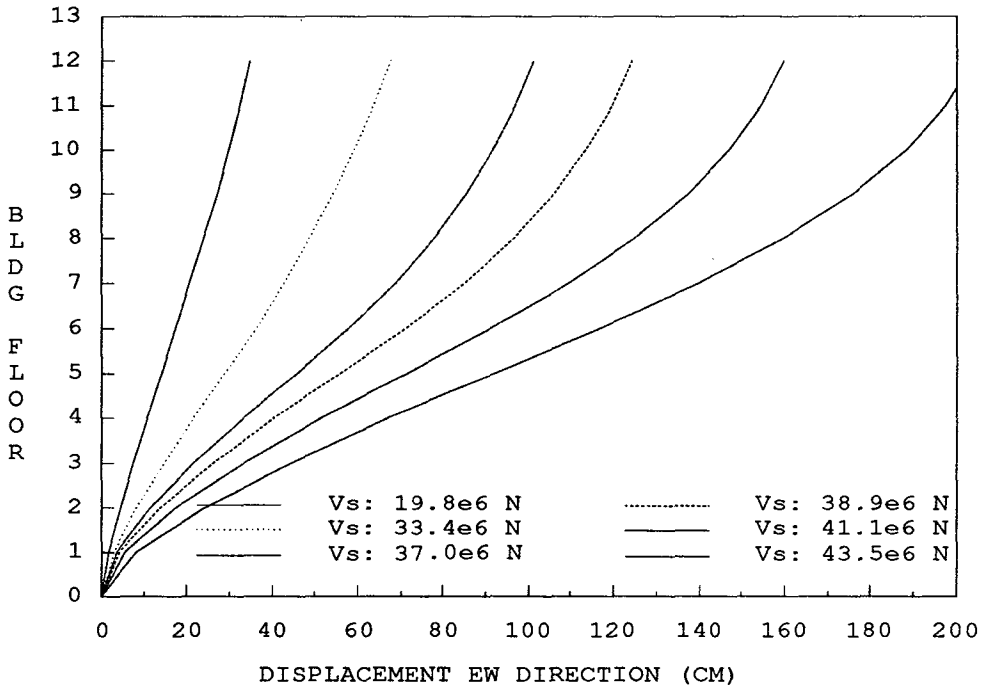

Figure 6.6: Building deformed shape for different base shear levels (Vs). EW direction. P-Δ effects ignored.

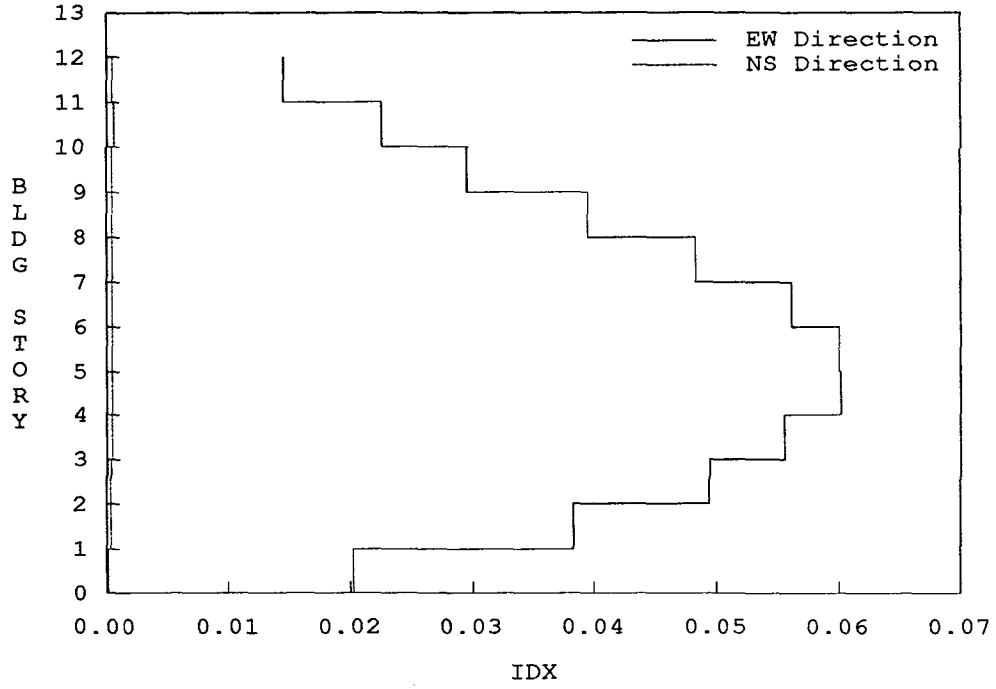

Figure 6.7: Building interstory drift ratios at 2.03 m (80 inches, 4.1% average drift) twelfth floor displacement. P-Δ effects ignored.

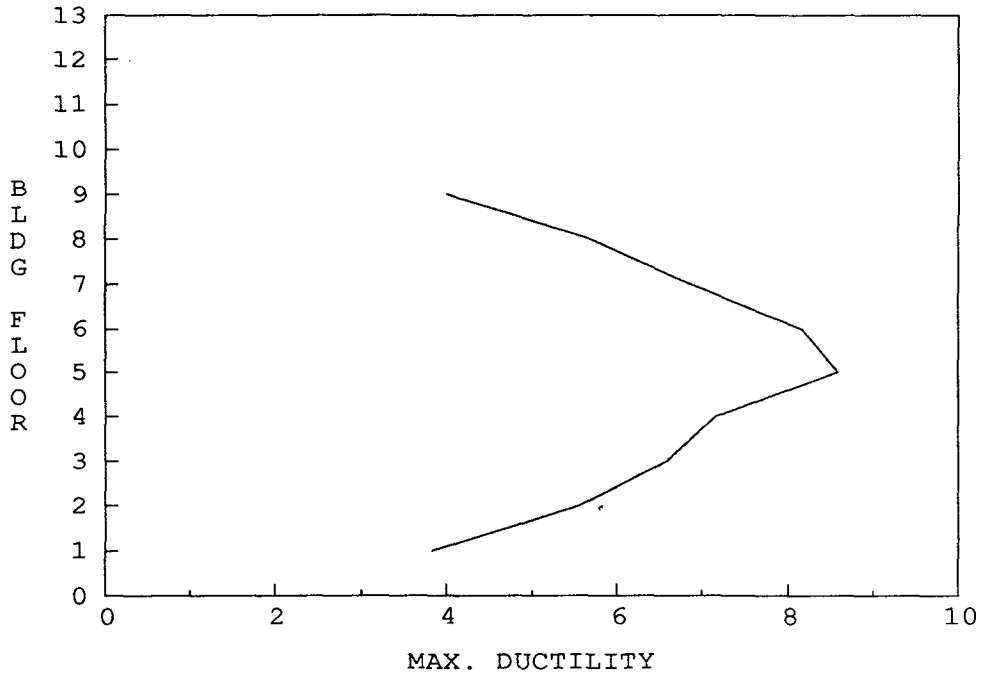

Figure 6.8: Building girder rotational ductility demand at 2.03 m (80 inches, 4.1% average drift) twelfth floor displacement. P-Δ effects ignored.

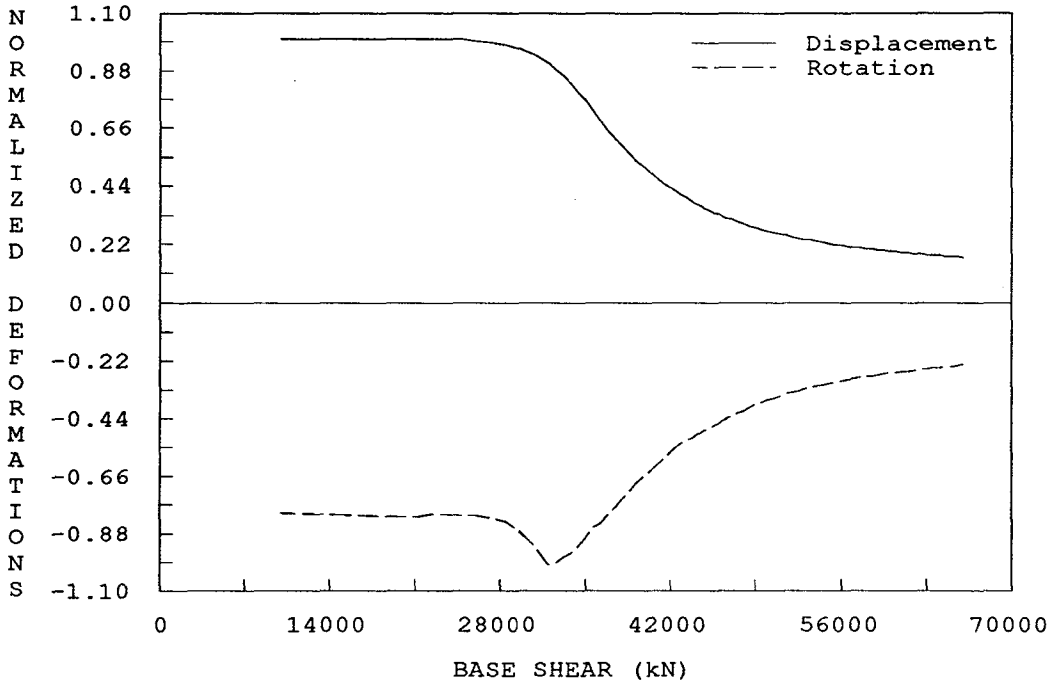

Figure 6.9: Normalized twelfth floor NS displacement (Δ_{NS}/Δ_{EW}) and torsional rotations (θ/Δ_{EW}) at Center of Mass. Static-to-collapse analysis for the EW direction. P-Δ effects ignored.

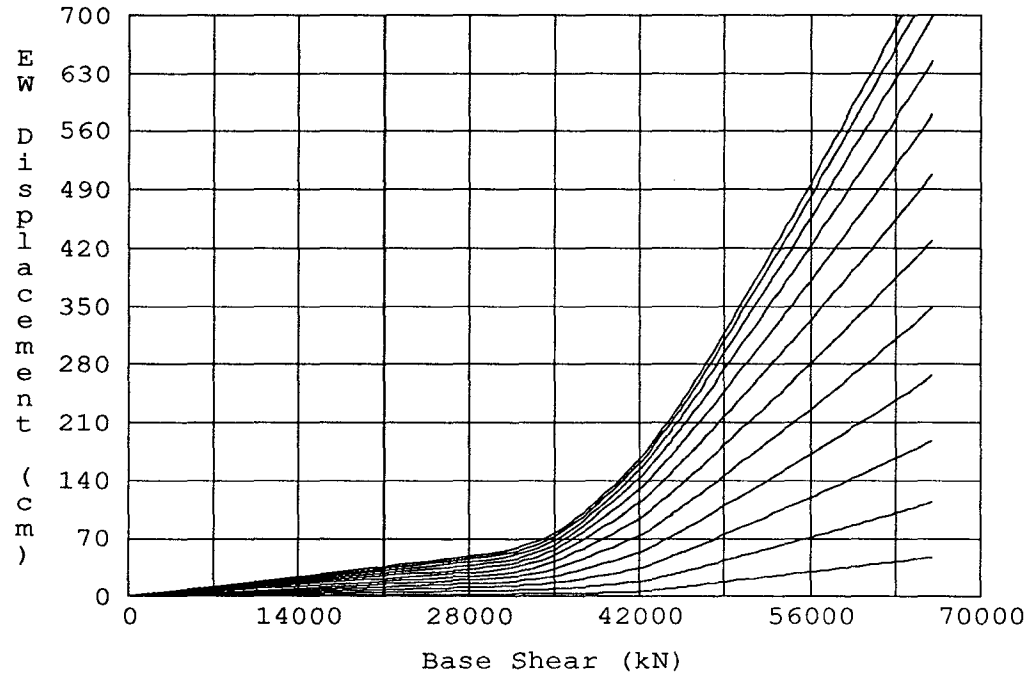

Figure 6.10: Lateral displacement, EW direction. Floors 1 to 12 (bottom to top) at Center of Mass. Static-to-collapse analysis for the EW direction. P-Δ effects ignored.

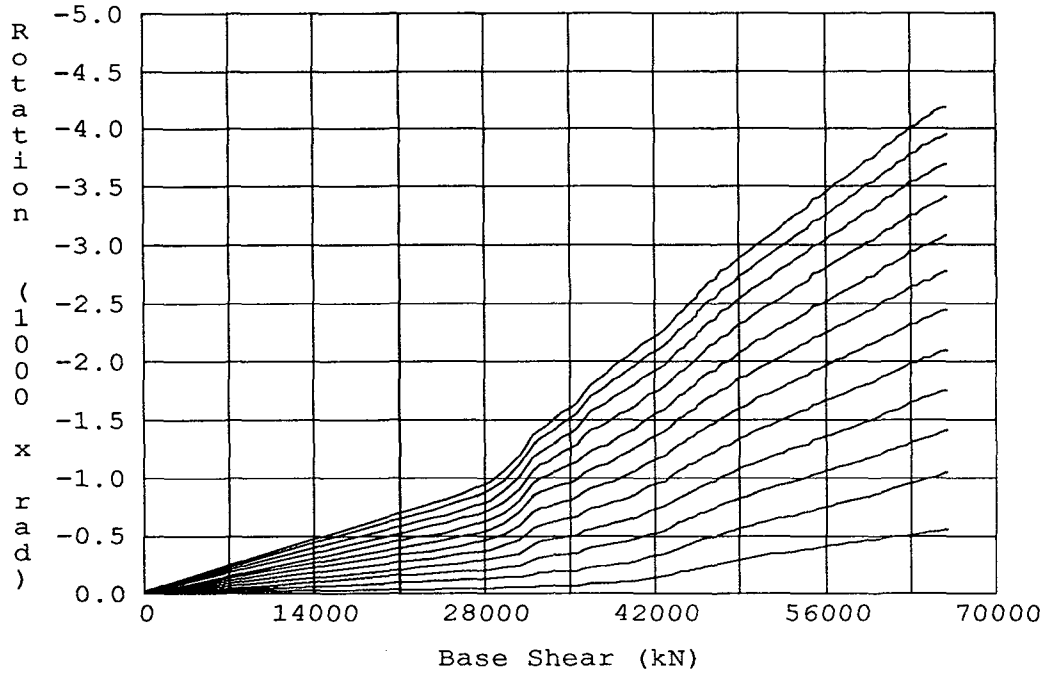

Figure 6.11: In-plane rotations. Floors 1 to 12 (bottom to top). at Center of Mass. Static-to-collapse analysis for the EW direction. P-Δ effects ignored.

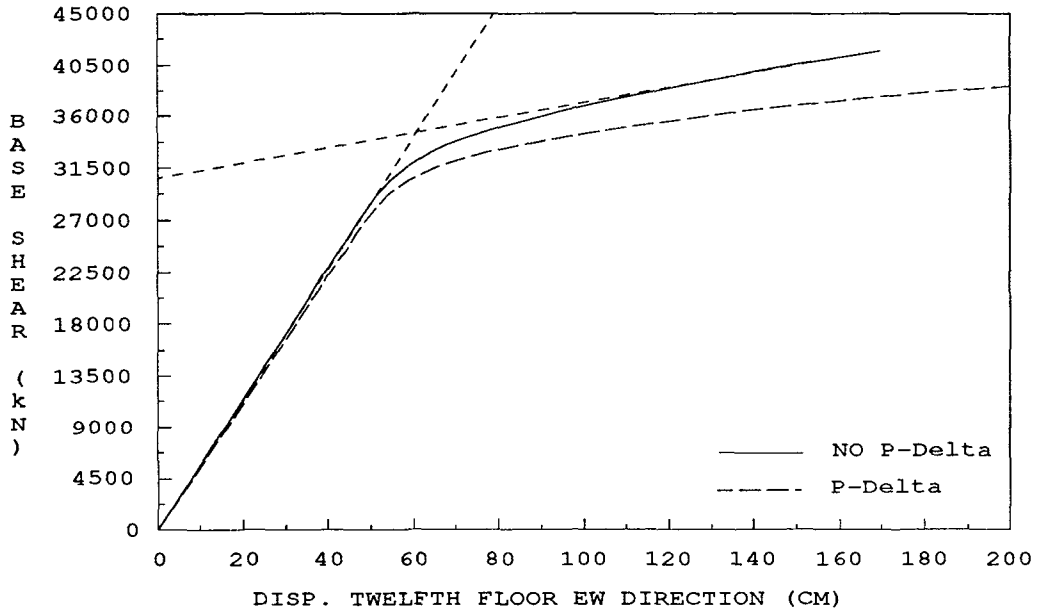

Figure 6.12: Base shear-twelfth floor displacement, EW direction. With and without P-Δ effects

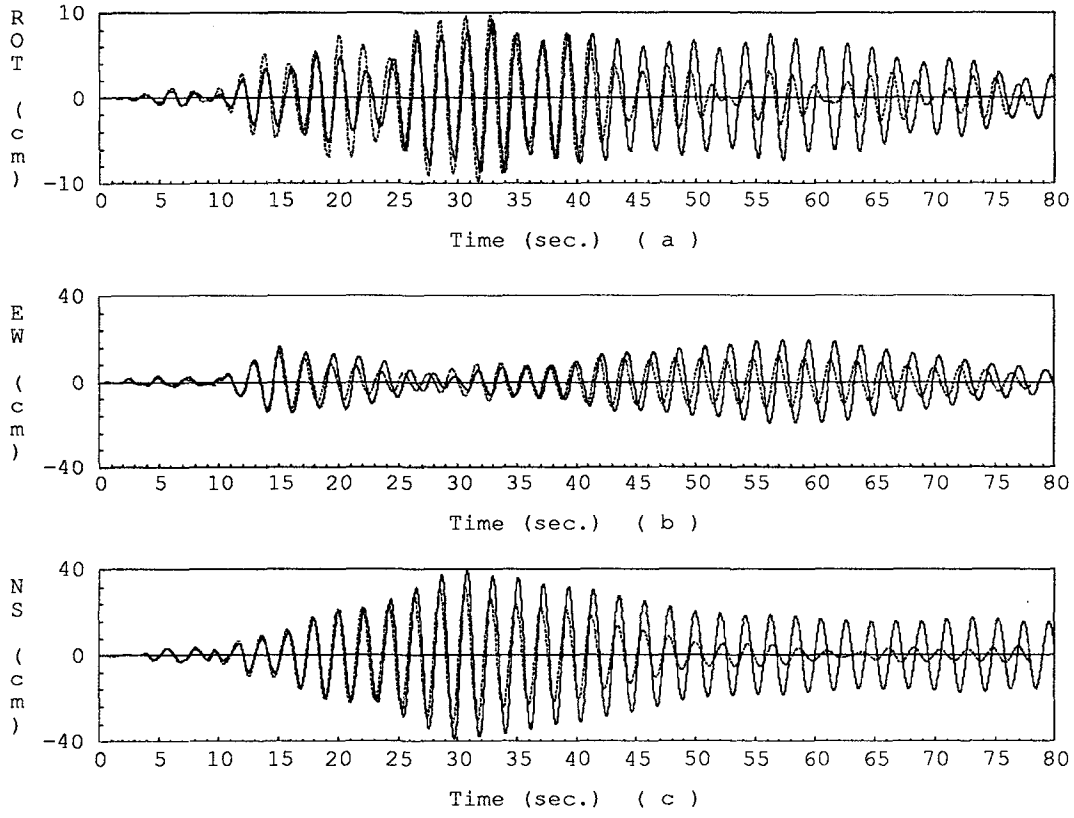

Figure 6.13: Twelfth floor SW corner nonlinear response. Mt. Lewis event, 1% damping model. Model —— Record ·····.

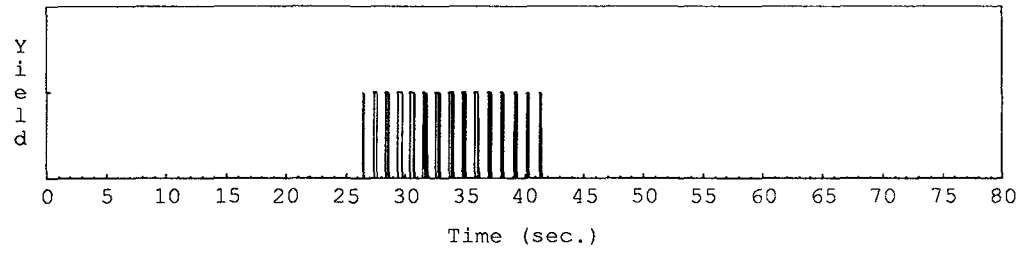

Figure 6.14: Model yield events. Mt. Lewis event, 1% damping model.

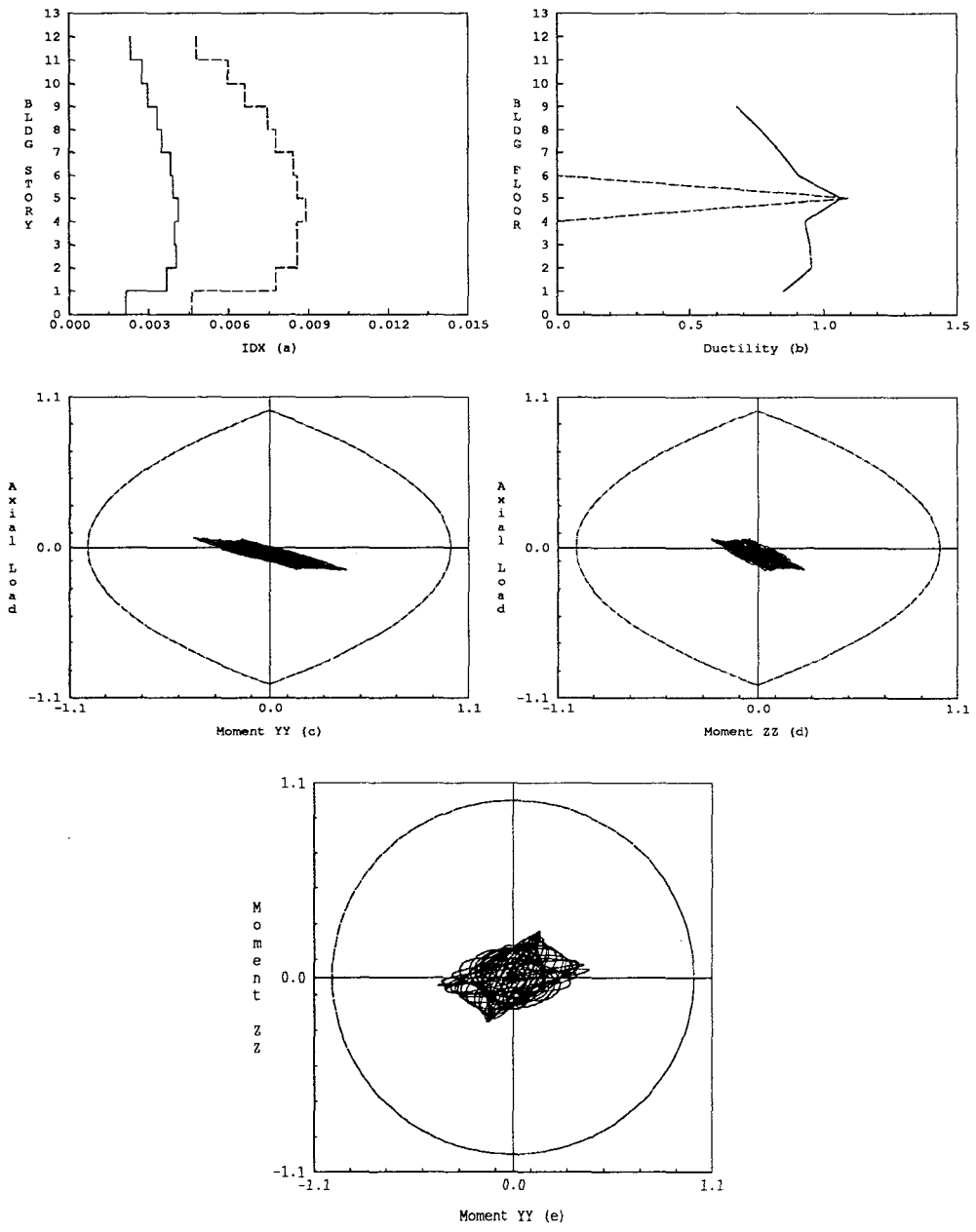

Figure 6.15: Global model parameters. Mt. Lewis event, 1% damping model. (a) Maximum inter-story drift. EW —— NS - - - - -. (b) Perimeter frame girder ductility. Maximum ————, Cumulative - - - - -. (c) Normalized column forces, P-M_{yy}. (d) Normalized column forces, P-M_{zz}. (e) Normalized column forces, M_{zz}-M_{yy}.

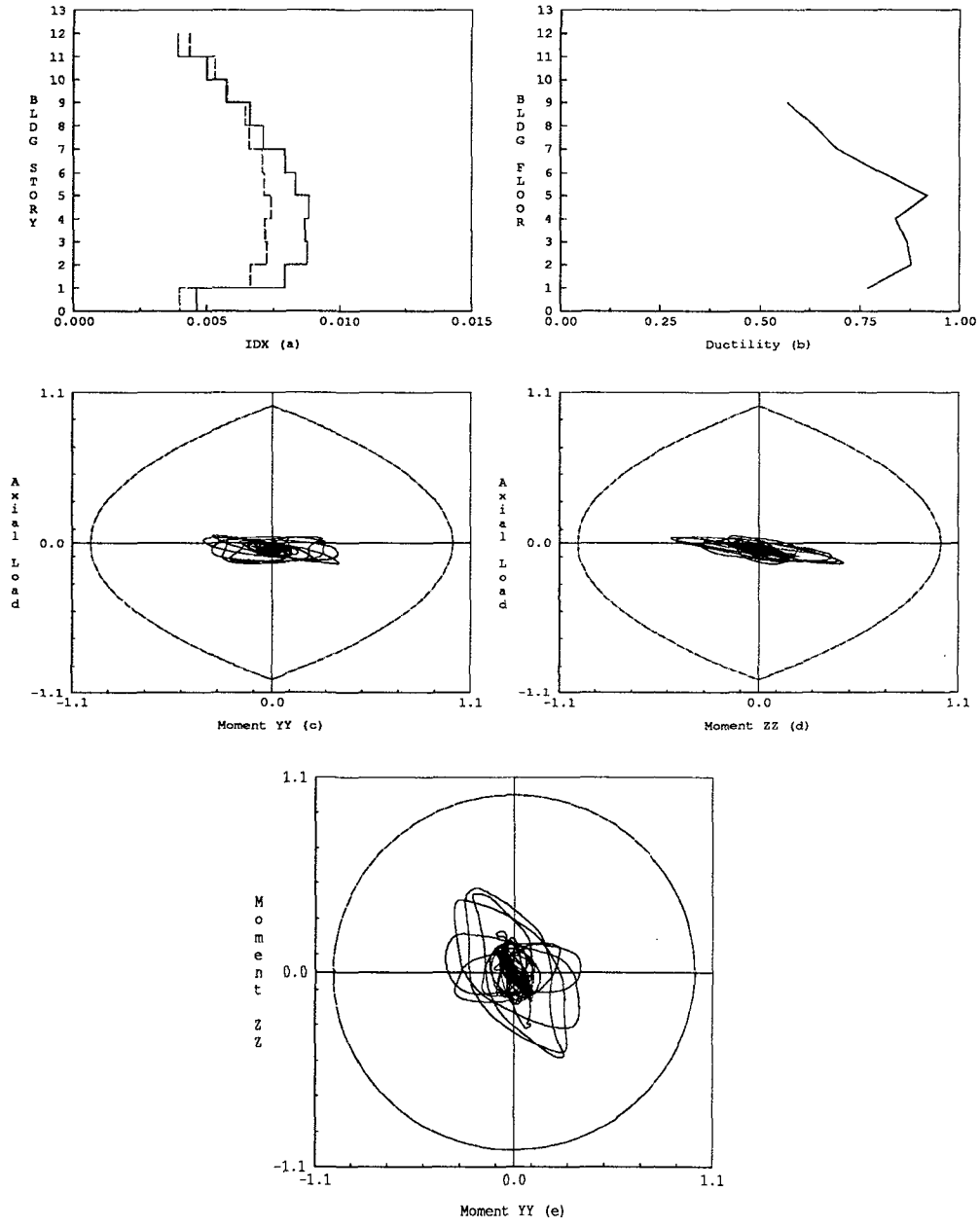

Figure 6.16: Global model parameters. Loma Prieta event, 3% damping model. (a) Maximum inter-story drift. EW —— NS - - - - -. (b) Perimeter frame girder ductility. Maximum ————, Cumulative - - - - -. (c) Normalized column forces, P-M_{yy}. (d) Normalized column forces, P-M_{zz}. (e) Normalized column forces, M_{zz}-M_{yy}.

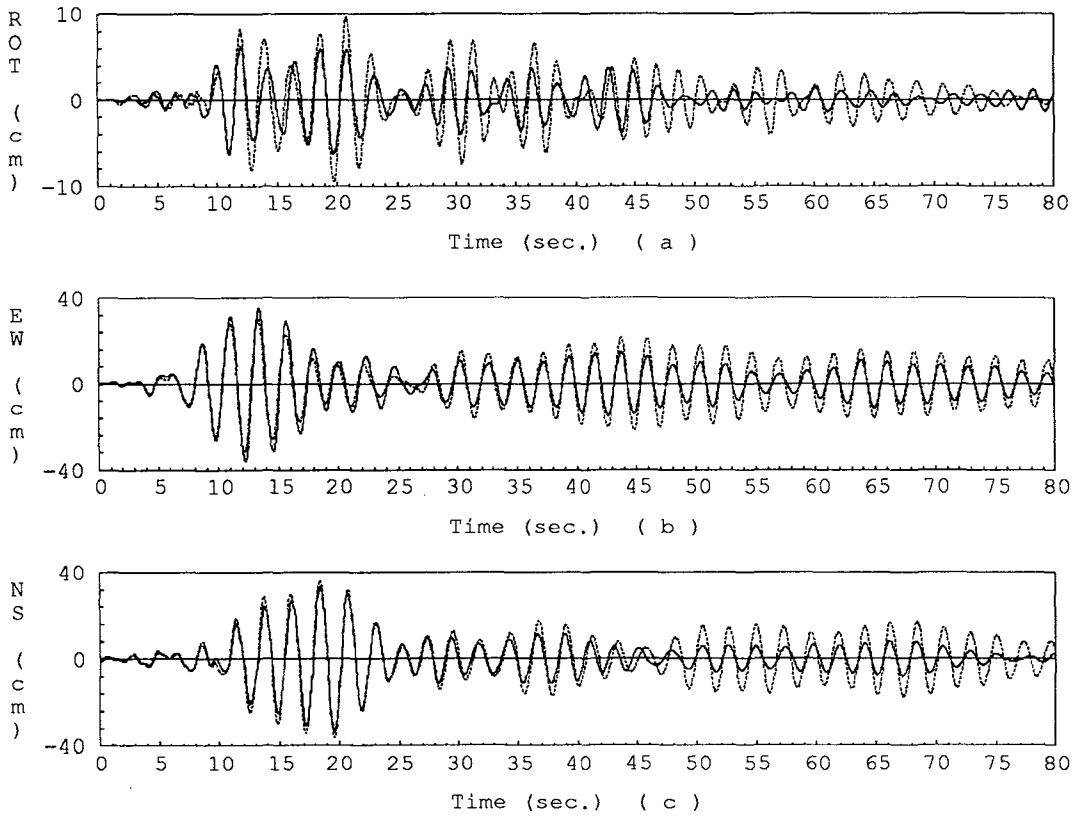

Figure 6.17: Twelfth floor SW corner nonlinear response. Loma Prieta event, 3% damping model. Model —— Record ·····.

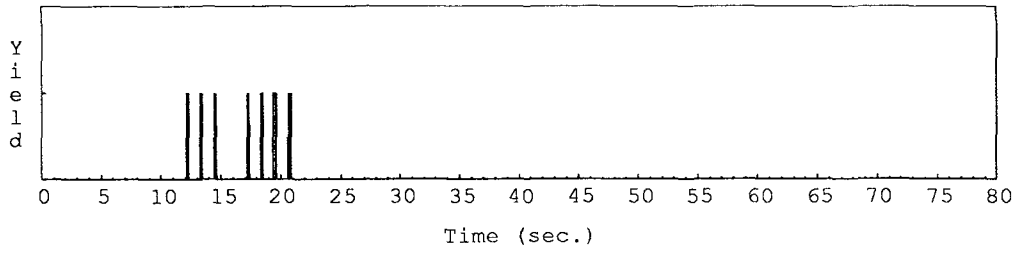

Figure 6.18: Model yield events. Loma Prieta event, 3% damping model.

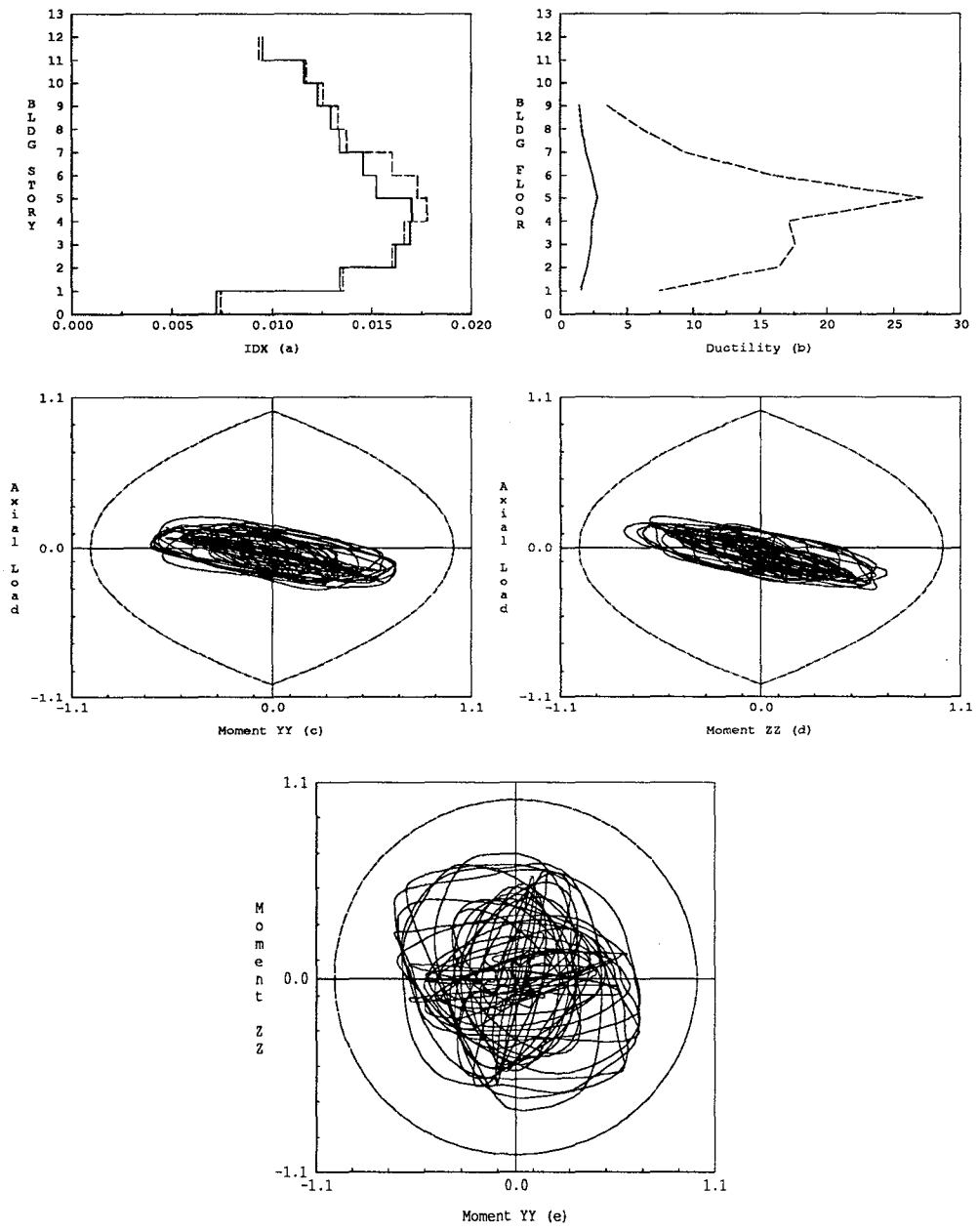

Figure 6.19: Global model parameters. Mt. Lewis event, 1% damping model, EPA=25, e/D=0. (a) Maximum inter-story drift. EW —— NS - - - - -. (b) Perimeter frame girder ductility. Maximum ————, Cumulative - - - - -. (c) Normalized column forces, P-M_{yy}. (d) Normalized column forces, P-M_{zz}. (e) Normalized column forces, M_{zz}-M_{yy}.

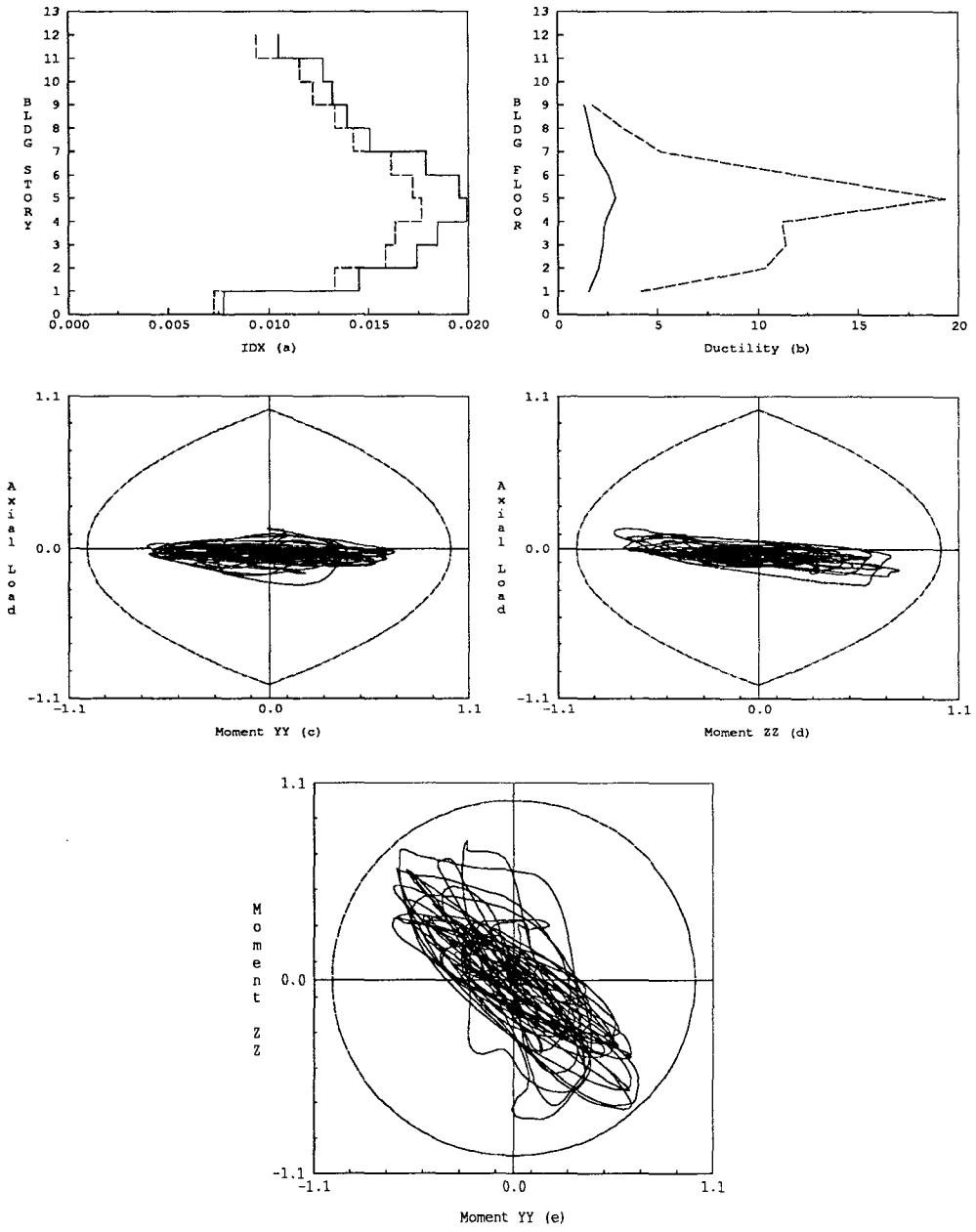

Figure 6.20: Global model parameters. Mt. Lewis event, 1% damping model, EPA=25, e/D=10. (a) Maximum inter-story drift. EW —— NS - - - - -. (b) Perimeter frame girder ductility. Maximum ————, Cumulative - - - - -. (c) Normalized column forces, P-M_{yy}. (d) Normalized column forces, P-M_{zz}. (e) Normalized column forces, M_{zz}-M_{yy}.

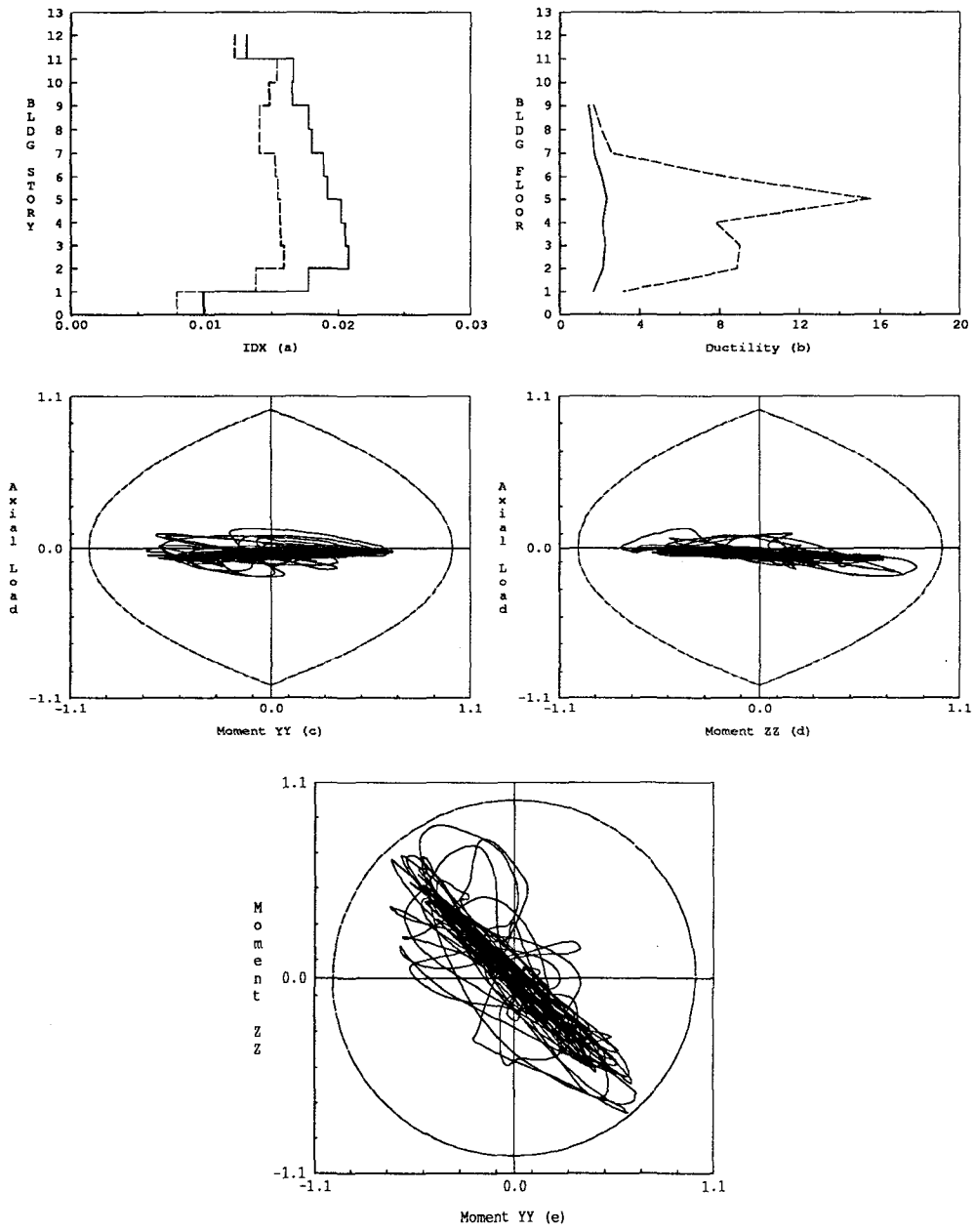

Figure 6.21: Global model parameters. Mt. Lewis event, 1% damping model, EPA=25, e/D=25. (a) Maximum inter-story drift. EW —— NS - - - - -. (b) Perimeter frame girder ductility. Maximum ————, Cumulative - - - - -. (c) Normalized column forces, P-M_{yy}. (d) Normalized column forces, P-M_{zz}. (e) Normalized column forces, M_{zz}-M_{yy}.

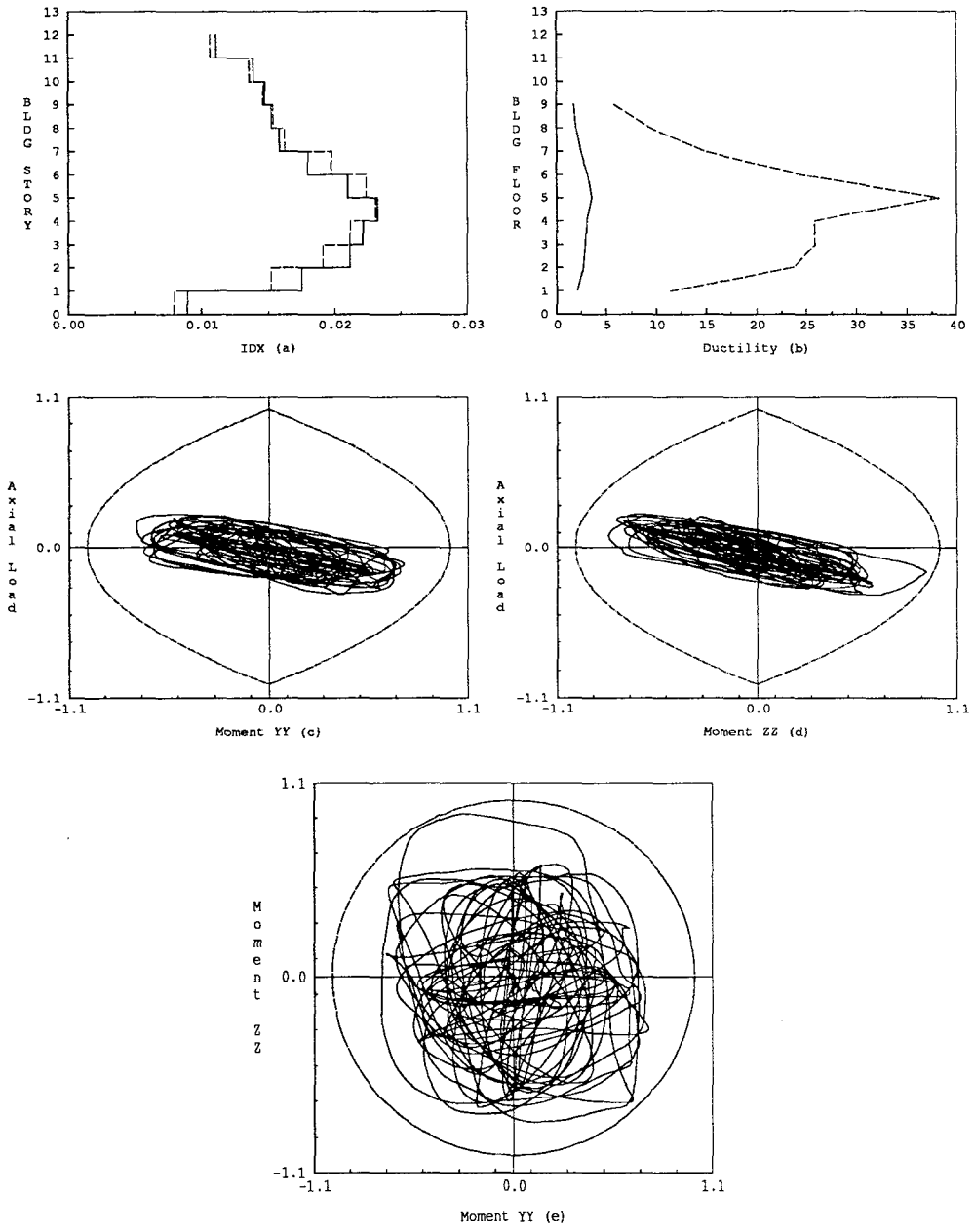

Figure 6.22: Global model parameters. Mt. Lewis event, 1% damping model, EPA=40, e/D=0. (a) Maximum inter-story drift. EW —— NS - - - - -. (b) Perimeter frame girder ductility. Maximum ————, Cumulative - - - - -. (c) Normalized column forces, P-M_{yy}. (d) Normalized column forces, P-M_{zz}. (e) Normalized column forces, M_{zz}-M_{yy}.

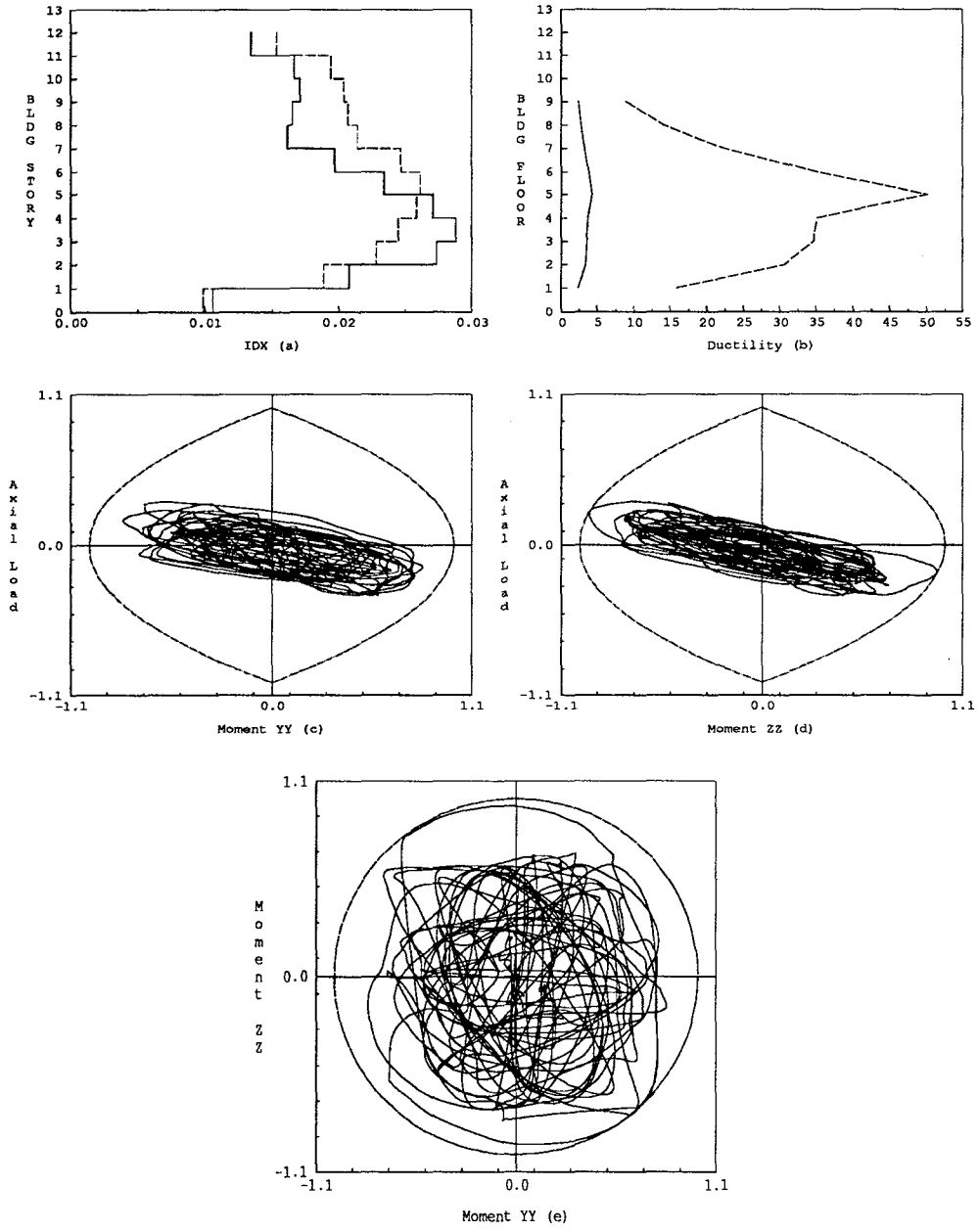

Figure 6.23: Global model parameters. Mt. Lewis event, 1% damping model, EPA=60, e/D=0. (a) Maximum inter-story drift. EW —— NS - - - - -. (b) Perimeter frame girder ductility. Maximum ————, Cumulative - - - - -. (c) Normalized column forces, P-M_{yy}. (d) Normalized column forces, P-M_{zz}. (e) Normalized column forces, M_{zz}-M_{yy}.

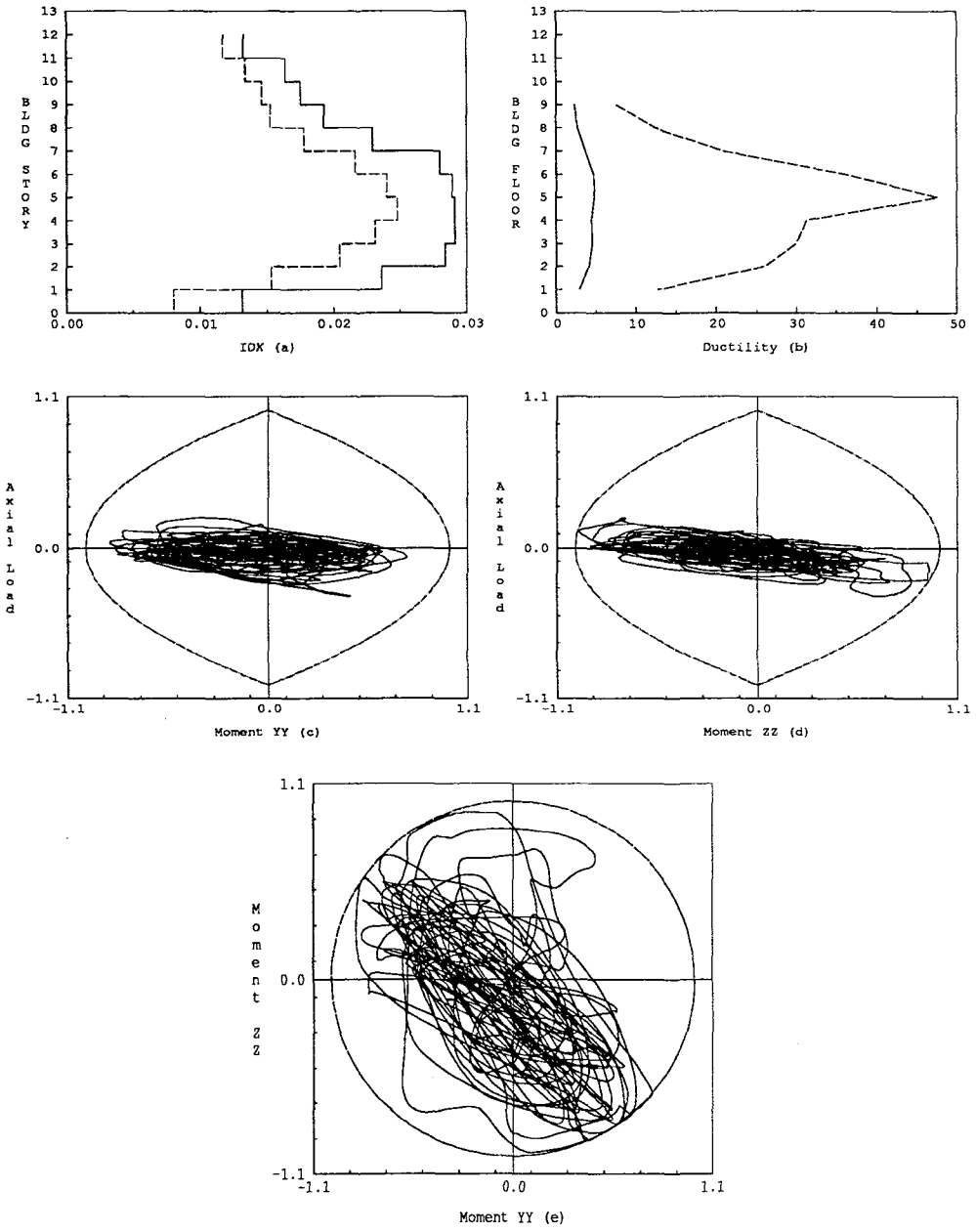

Figure 6.24: Global model parameters. Mt. Lewis event, 1% damping model, EPA=60, e/D=10. (a) Maximum inter-story drift. EW —— NS - - - - -. (b) Perimeter frame girder ductility. Maximum ————, Cumulative - - - - -. (c) Normalized column forces, P-M_{yy}. (d) Normalized column forces, P-M_{zz}. (e) Normalized column forces, M_{zz}-M_{yy}.

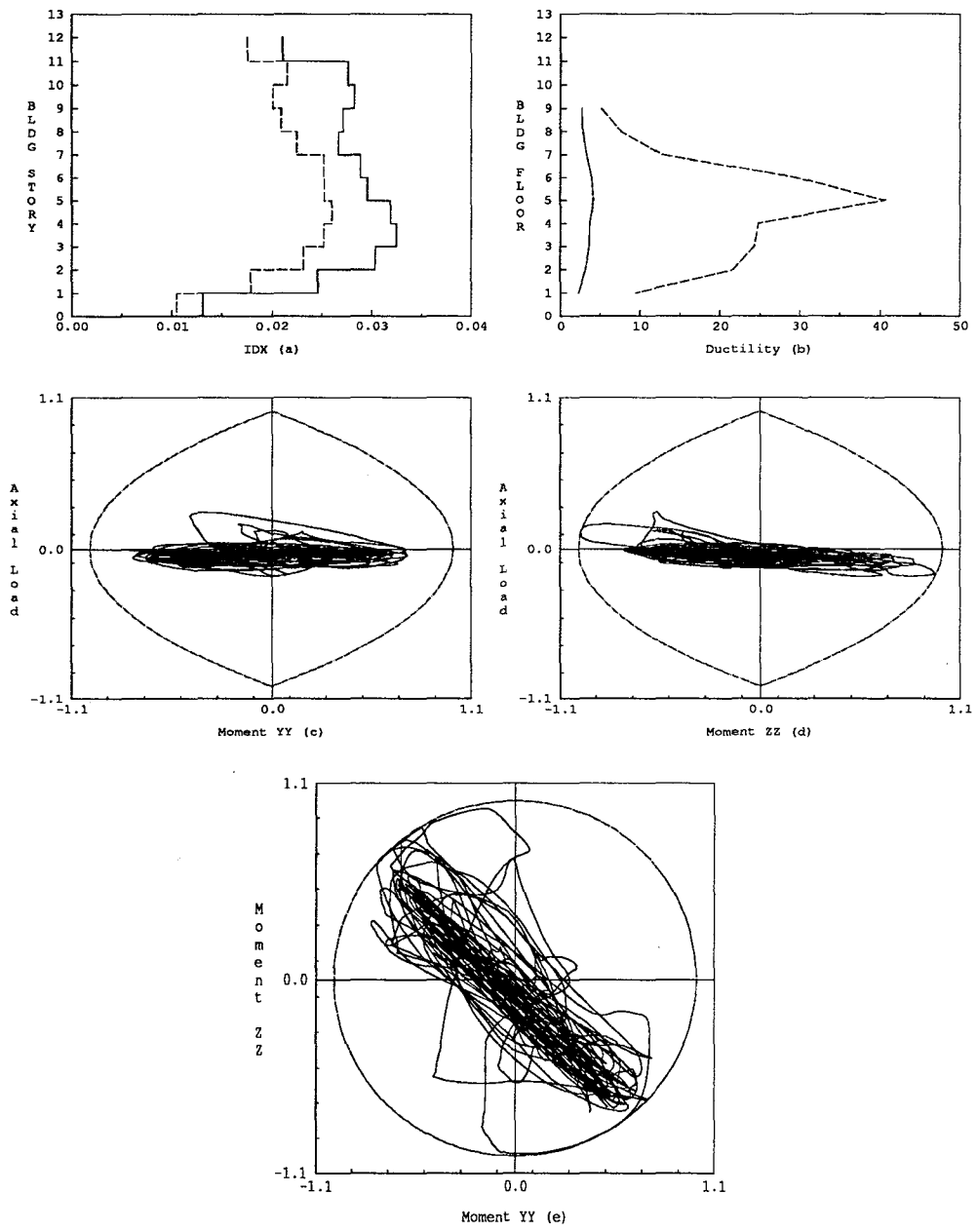

Figure 6.25: Global model parameters. Mt. Lewis event, 1% damping model, EPA=60, e/D=25. (a) Maximum inter-story drift. EW —— NS - - - - -. (b) Perimeter frame girder ductility. Maximum ————, Cumulative - - - - -. (c) Normalized column forces, P-M_{yy}. (d) Normalized column forces, P-M_{zz}. (e) Normalized column forces, M_{zz}-M_{yy}.

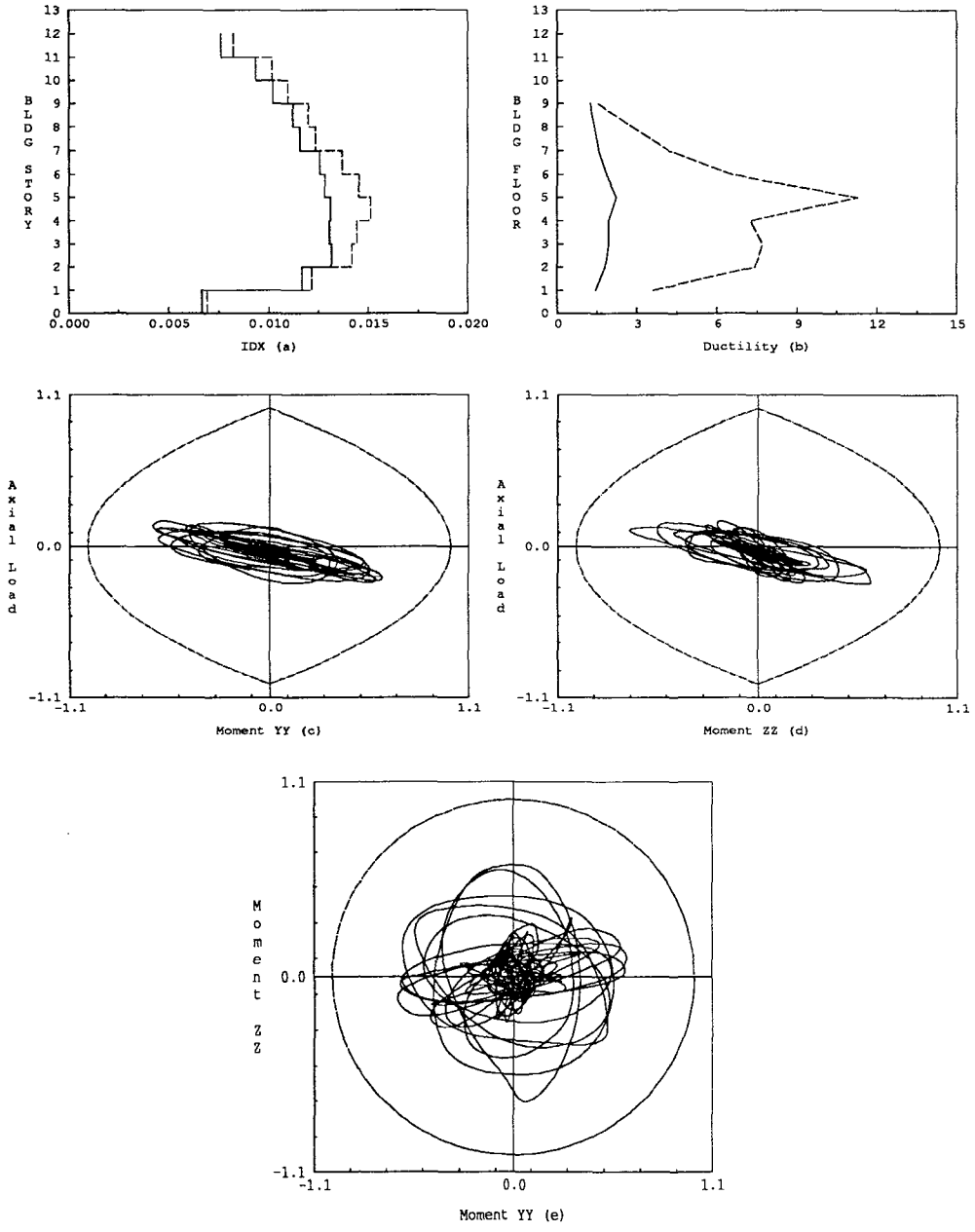

Figure 6.26: Global model parameters. Mt. Lewis event, 5% damping model, EPA=25, e/D=0. (a) Maximum inter-story drift. EW —— NS - - - - -. (b) Perimeter frame girder ductility. Maximum ————, Cumulative - - - - -. (c) Normalized column forces, P-M_{yy}. (d) Normalized column forces, P-M_{zz}. (e) Normalized column forces, M_{zz}-M_{yy}.

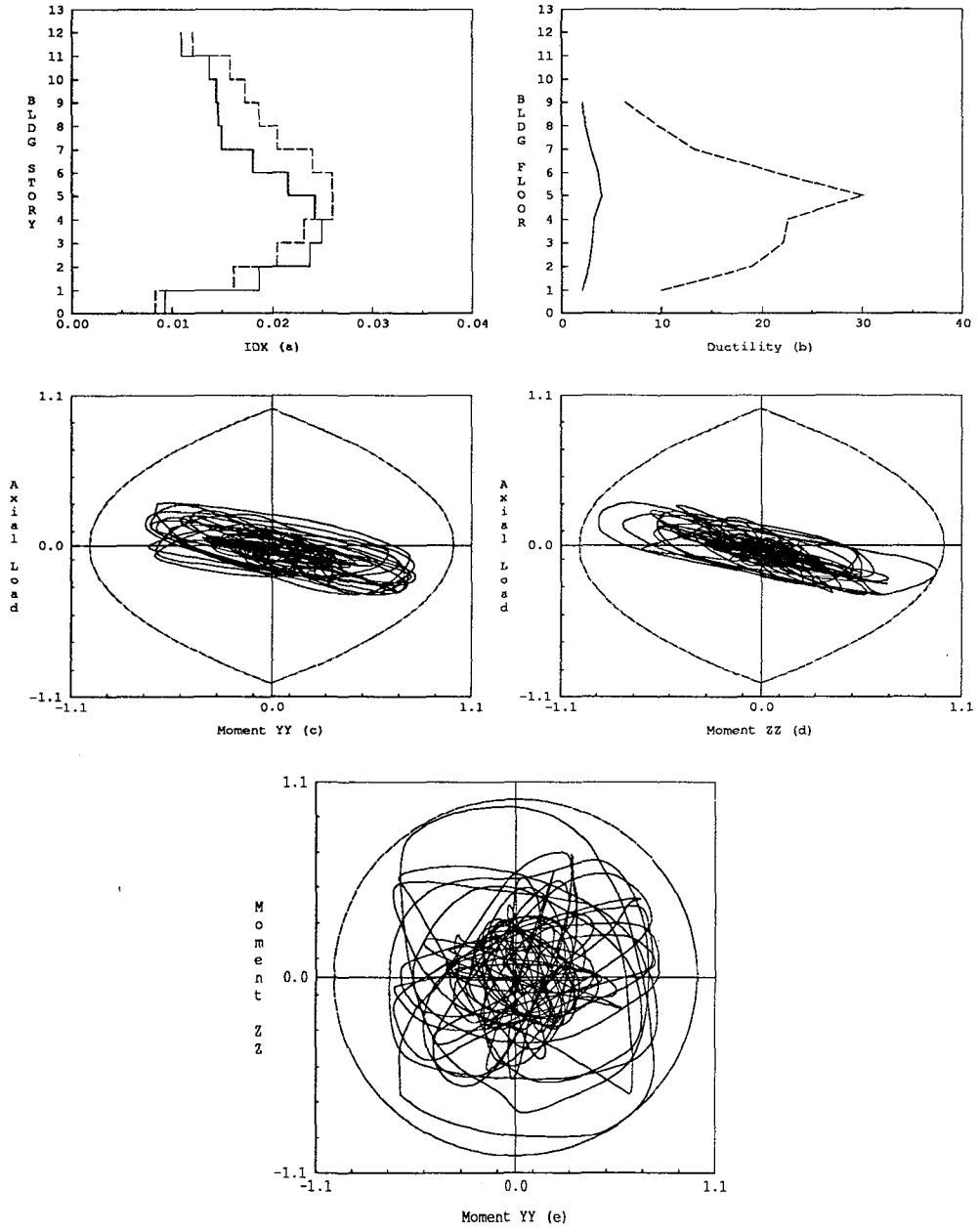

Figure 6.27: Global model parameters. Mt. Lewis event, 5% damping model, EPA=60, e/D=0. (a) Maximum inter-story drift. EW —— NS - - - - -. (b) Perimeter frame girder ductility. Maximum ————, Cumulative - - - - -. (c) Normalized column forces, P-M_{yy}. (d) Normalized column forces, P-M_{zz}. (e) Normalized column forces, M_{zz}-M_{yy}.

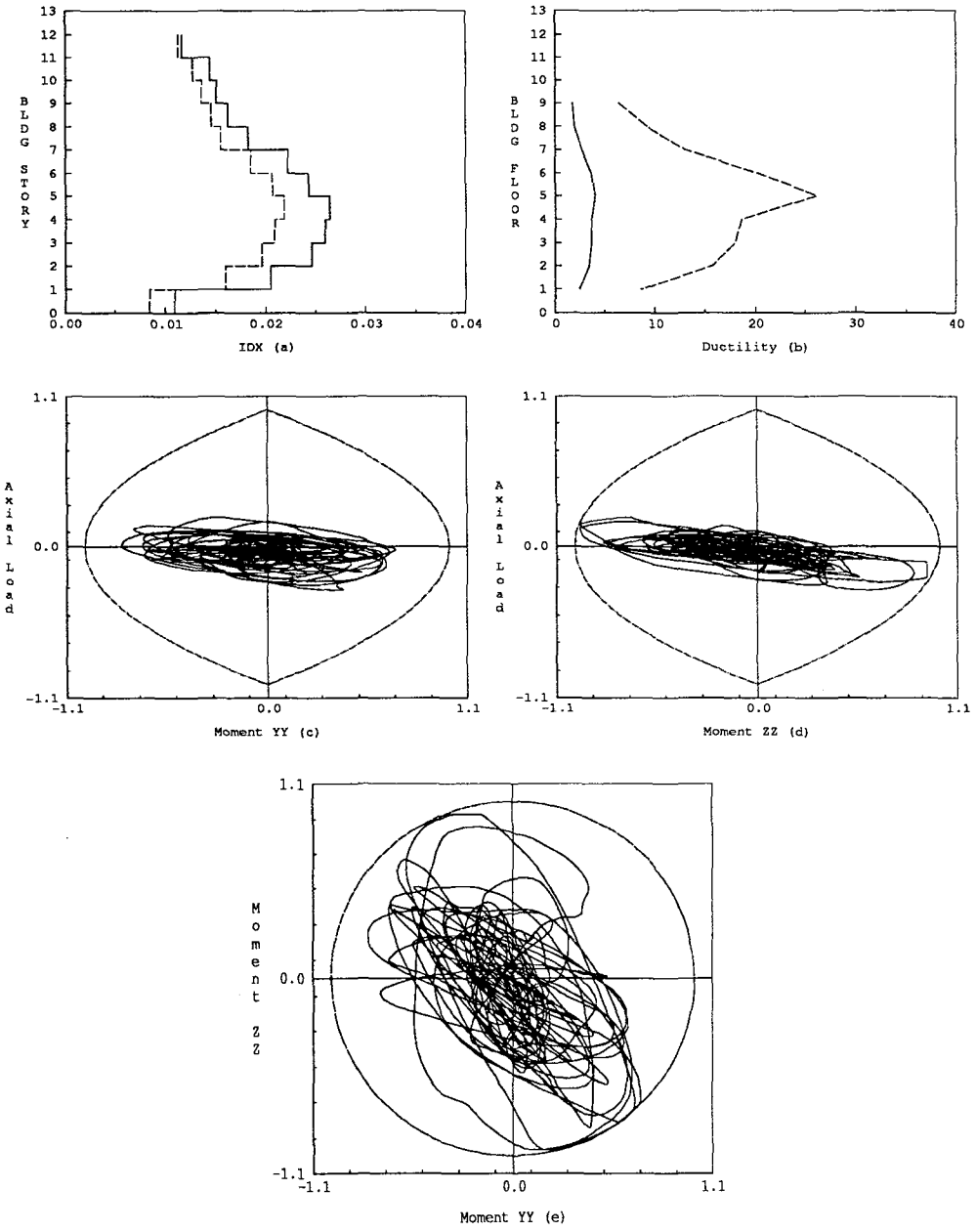

Figure 6.28: Global model parameters. Mt. Lewis event, 5% damping model, EPA=60, e/D=10. (a) Maximum inter-story drift. EW —— NS - - - - -. (b) Perimeter frame girder ductility. Maximum ————, Cumulative - - - - -. (c) Normalized column forces, P-M_{yy}. (d) Normalized column forces, P-M_{zz}. (e) Normalized column forces, M_{zz}-M_{yy}.

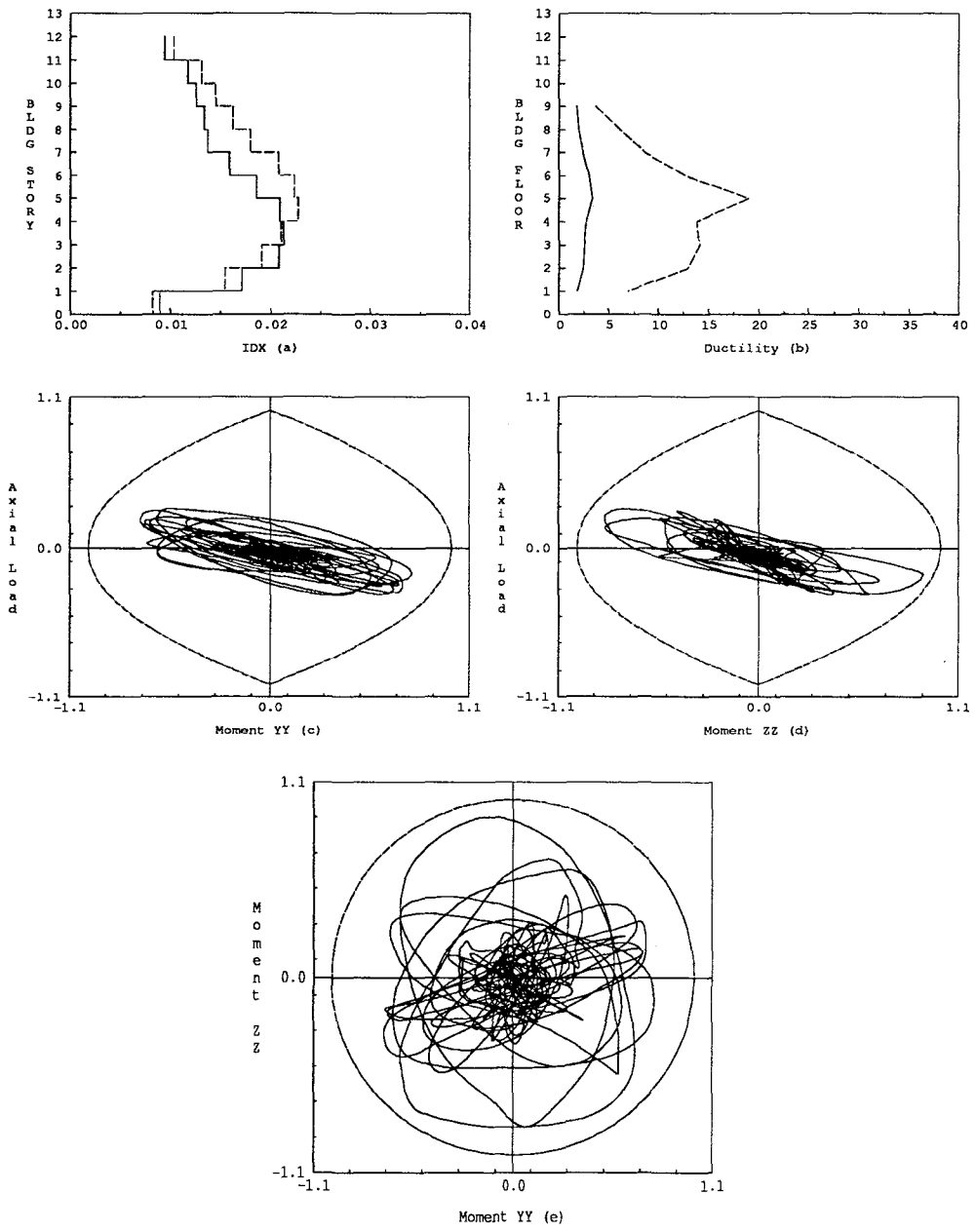

Figure 6.29: Global model parameters. Mt. Lewis event, 10% damping model, EPA=60, e/D=0. (a) Maximum inter-story drift. EW —— NS - - - - -. (b) Perimeter frame girder ductility. Maximum ————, Cumulative - - - - -. (c) Normalized column forces, P-M_{yy}. (d) Normalized column forces, P-M_{zz}. (e) Normalized column forces, M_{zz}-M_{yy}.

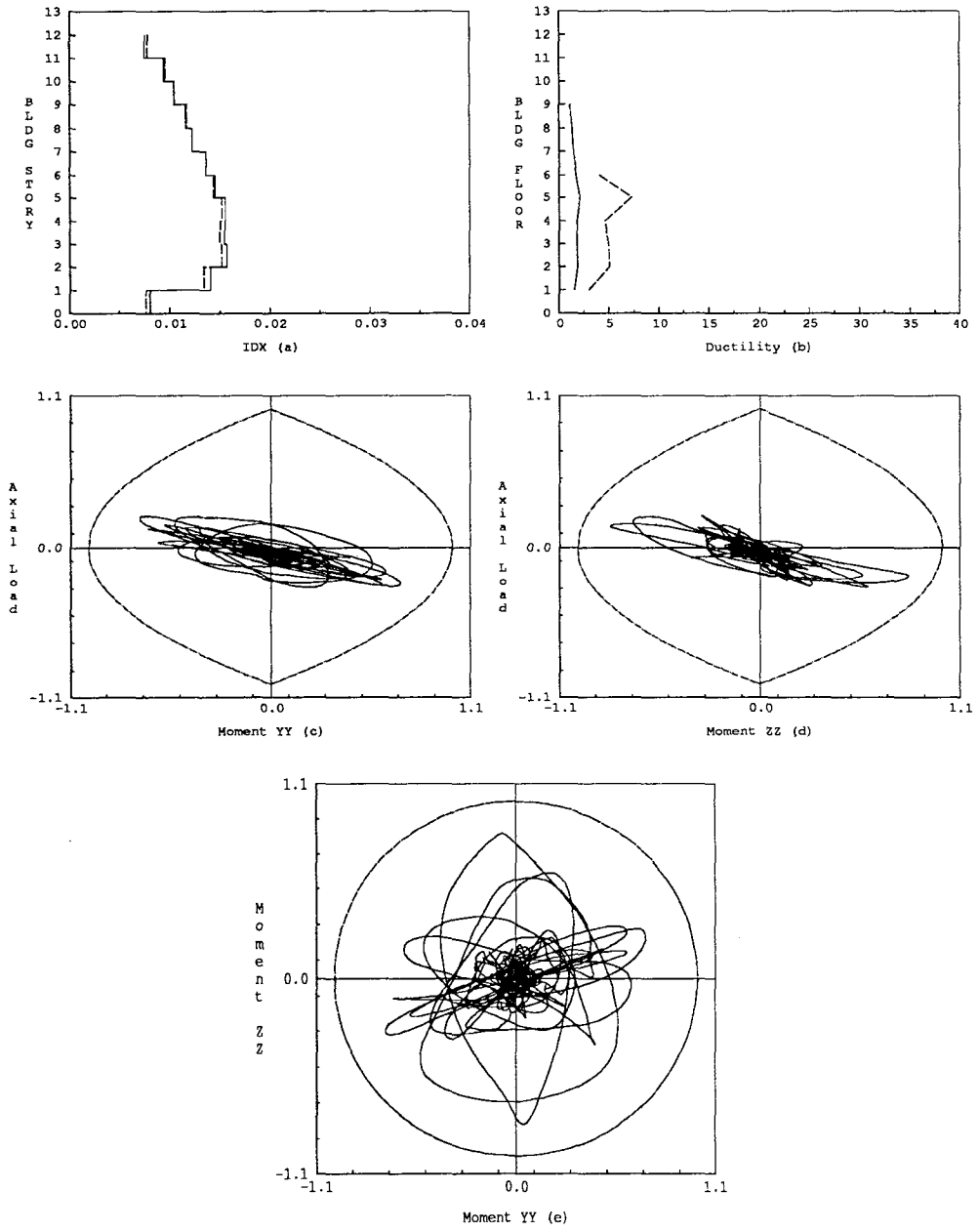

Figure 6.30: Global model parameters. Mt. Lewis event, 20% damping model, EPA=60, e/D=0. (a) Maximum inter-story drift. EW —— NS - - - - -. (b) Perimeter frame girder ductility. Maximum ————, Cumulative - - - - -. (c) Normalized column forces, P-M_{yy}. (d) Normalized column forces, P-M_{zz}. (e) Normalized column forces, M_{zz}-M_{yy}.

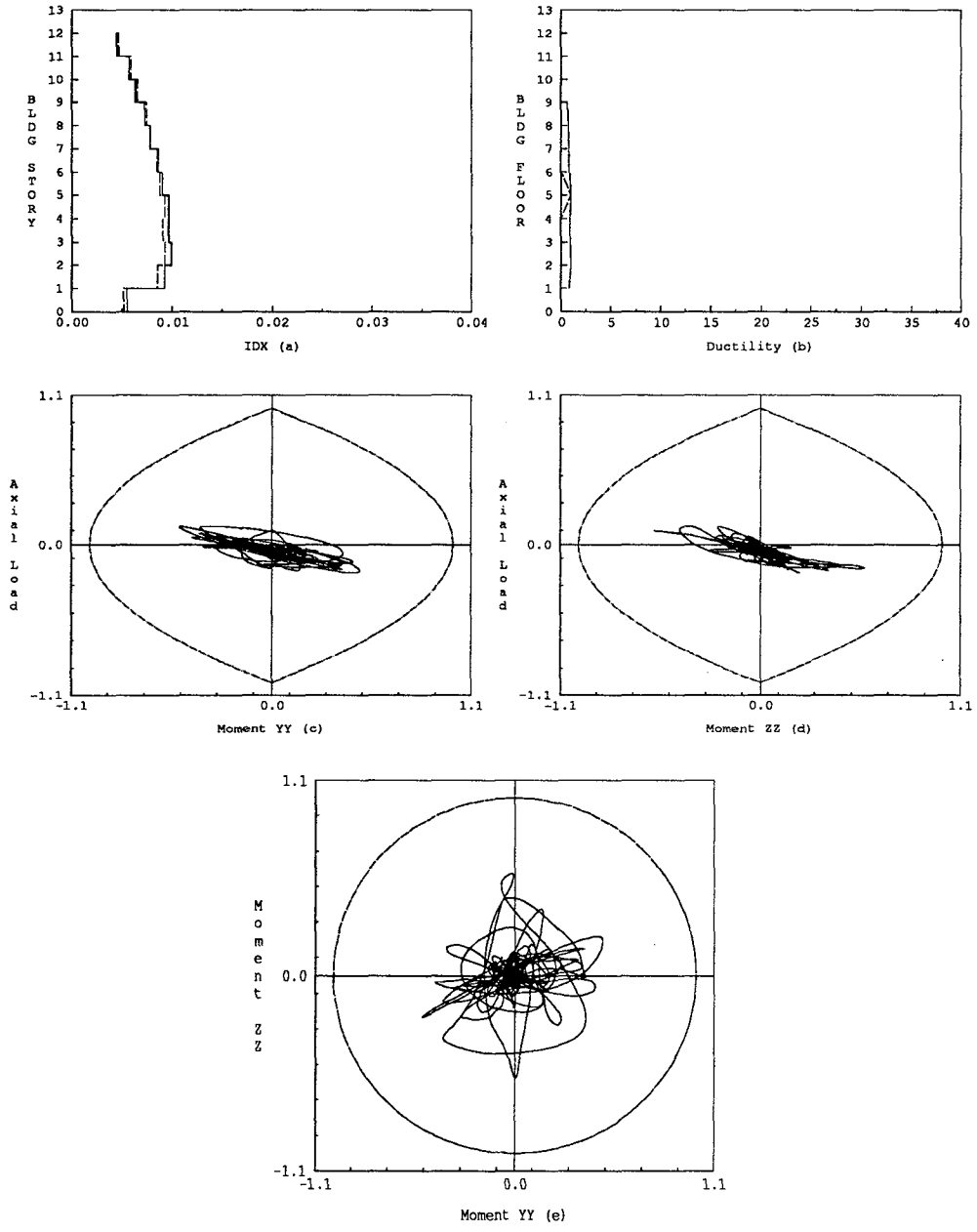

Figure 6.31: Global model parameters. Mt. Lewis event, 40% damping model, EPA=60, e/D=0. (a) Maximum inter-story drift. EW —— NS - - - - -. (b) Perimeter frame girder ductility. Maximum ————, Cumulative - - - - -. (c) Normalized column forces, P-M_{yy}. (d) Normalized column forces, P-M_{zz}. (e) Normalized column forces, M_{zz}-M_{yy}.

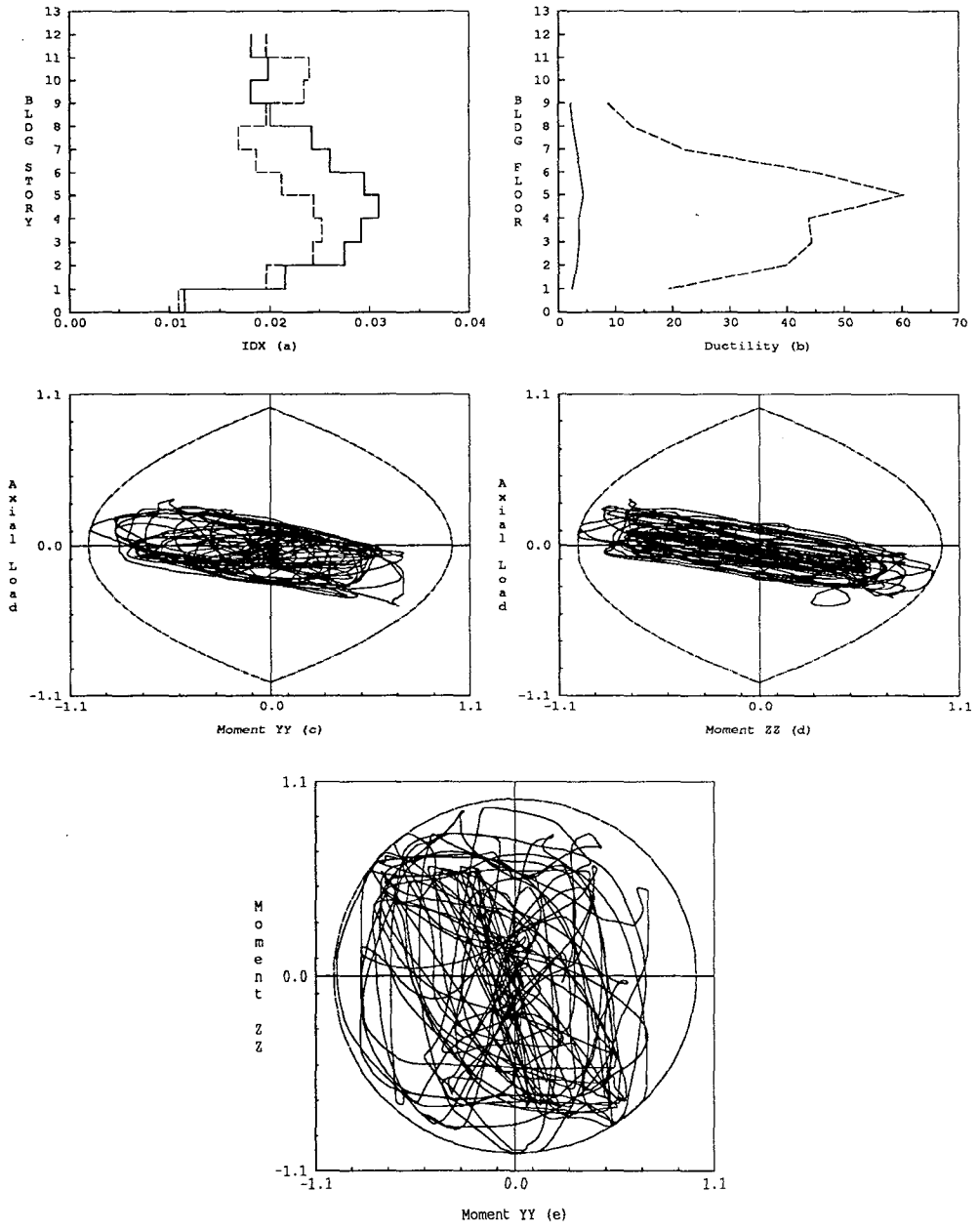

Figure 6.32: Global model parameters. Morgan Hill event, 1% damping model, EPA=60, e/D=0. (a) Maximum inter-story drift. EW —— NS - - - - -. (b) Perimeter frame girder ductility. Maximum ————, Cumulative - - - - -. (c) Normalized column forces, P-M_{yy}. (d) Normalized column forces, P-M_{zz}. (e) Normalized column forces, M_{zz}-M_{yy}.

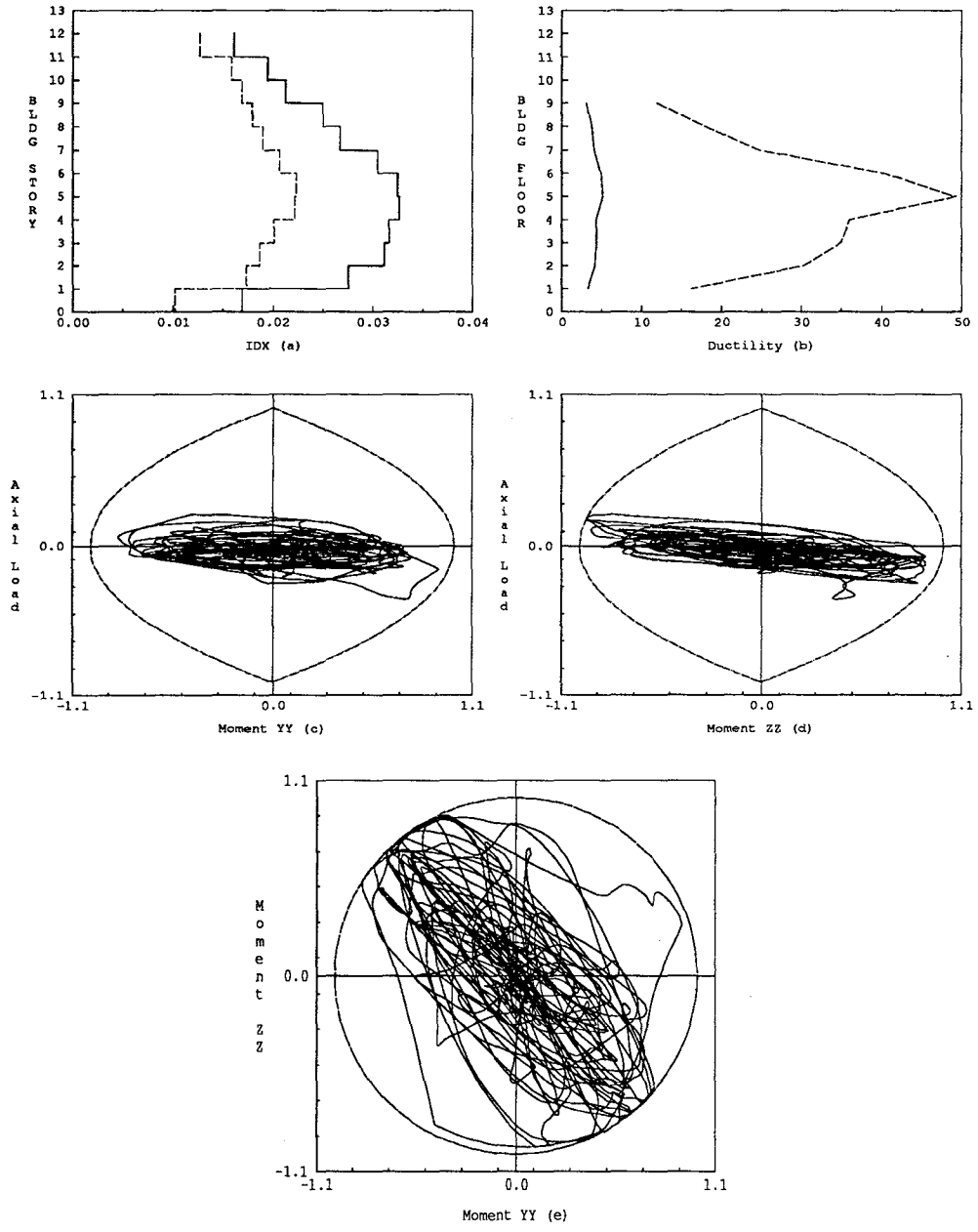

Figure 6.33: Global model parameters. Morgan Hill event, 1% damping model, EPA=60, e/D=10. (a) Maximum inter-story drift. EW —— NS - - - - -. (b) Perimeter frame girder ductility. Maximum ————, Cumulative - - - - -. (c) Normalized column forces, P-M_{yy}. (d) Normalized column forces, P-M_{zz}. (e) Normalized column forces, M_{zz}-M_{yy}.

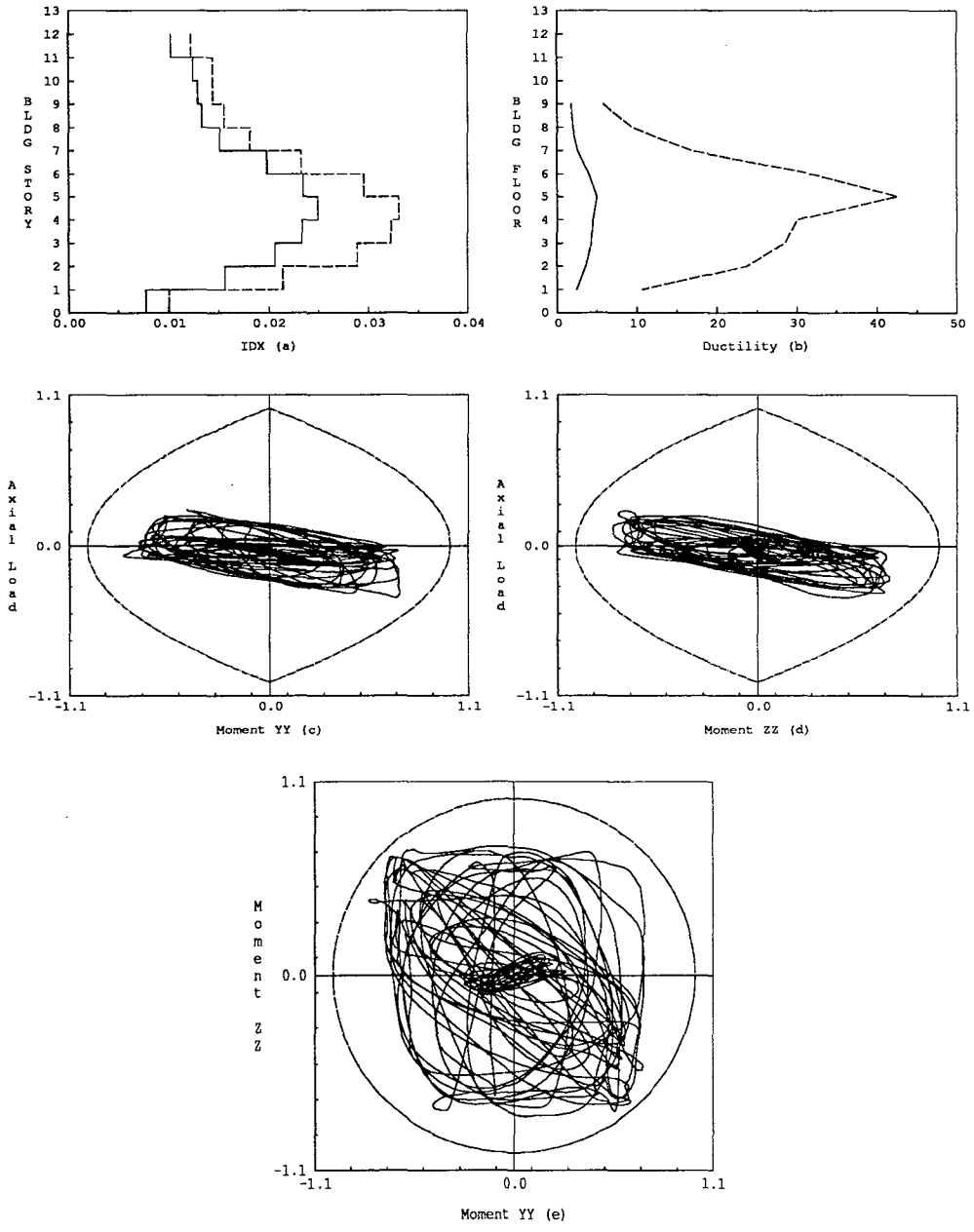

Figure 6.34: Global model parameters. Mexico SCT event, 1% damping model, EPA=60, e/D=0. (a) Maximum inter-story drift. EW —— NS - - - - -. (b) Perimeter frame girder ductility. Maximum ————, Cumulative - - - - -. (c) Normalized column forces, P-M_{yy}. (d) Normalized column forces, P-M_{zz}. (e) Normalized column forces, M_{zz}-M_{yy}.

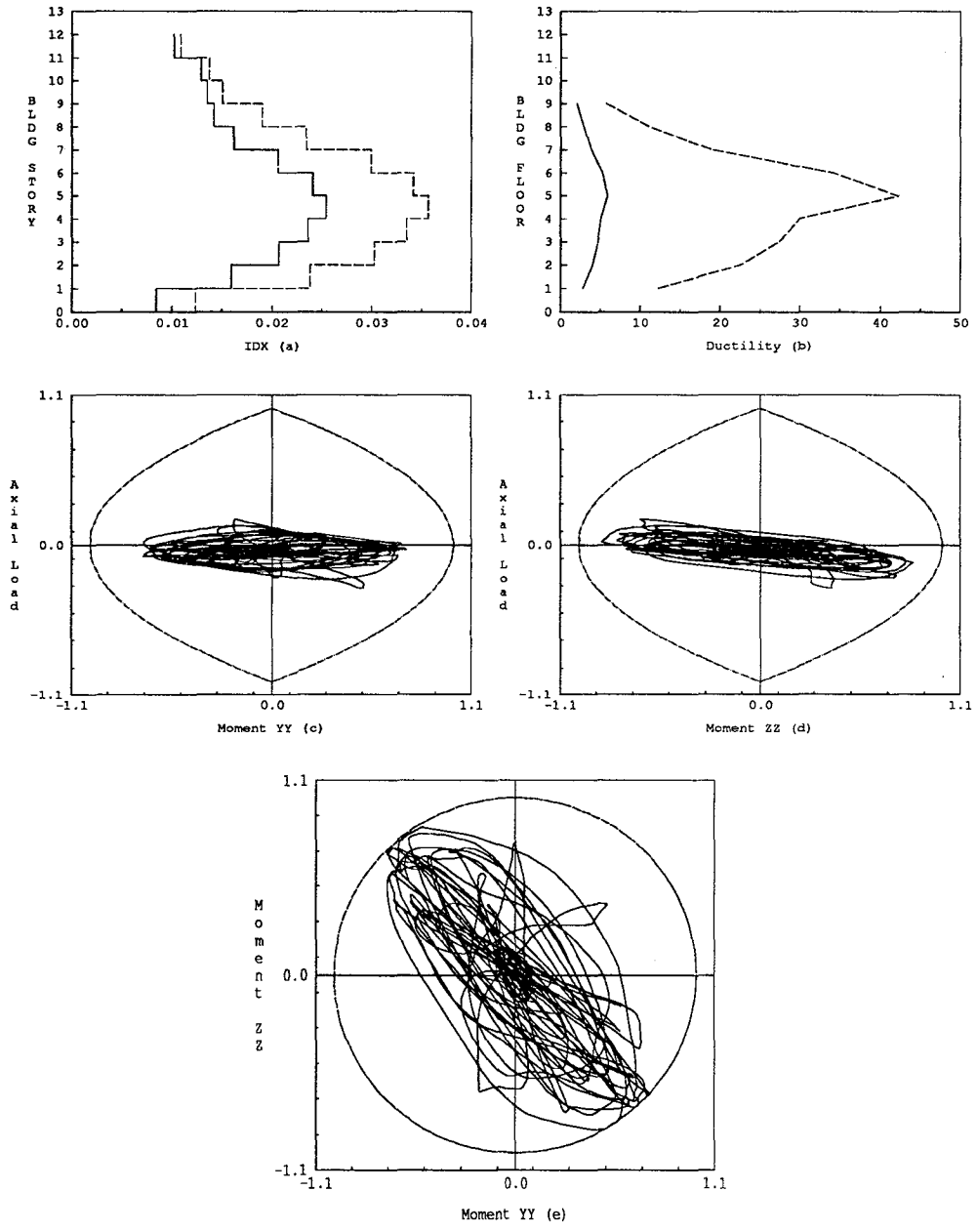

Figure 6.35: Global model parameters. Mexico SCT event, 1% damping model, EPA=60, e/D=10. (a) Maximum inter-story drift. EW —— NS - - - - -. (b) Perimeter frame girder ductility. Maximum ————, Cumulative - - - - -. (c) Normalized column forces, P-M_{yy}. (d) Normalized column forces, P-M_{zz}. (e) Normalized column forces, M_{zz}-M_{yy}.

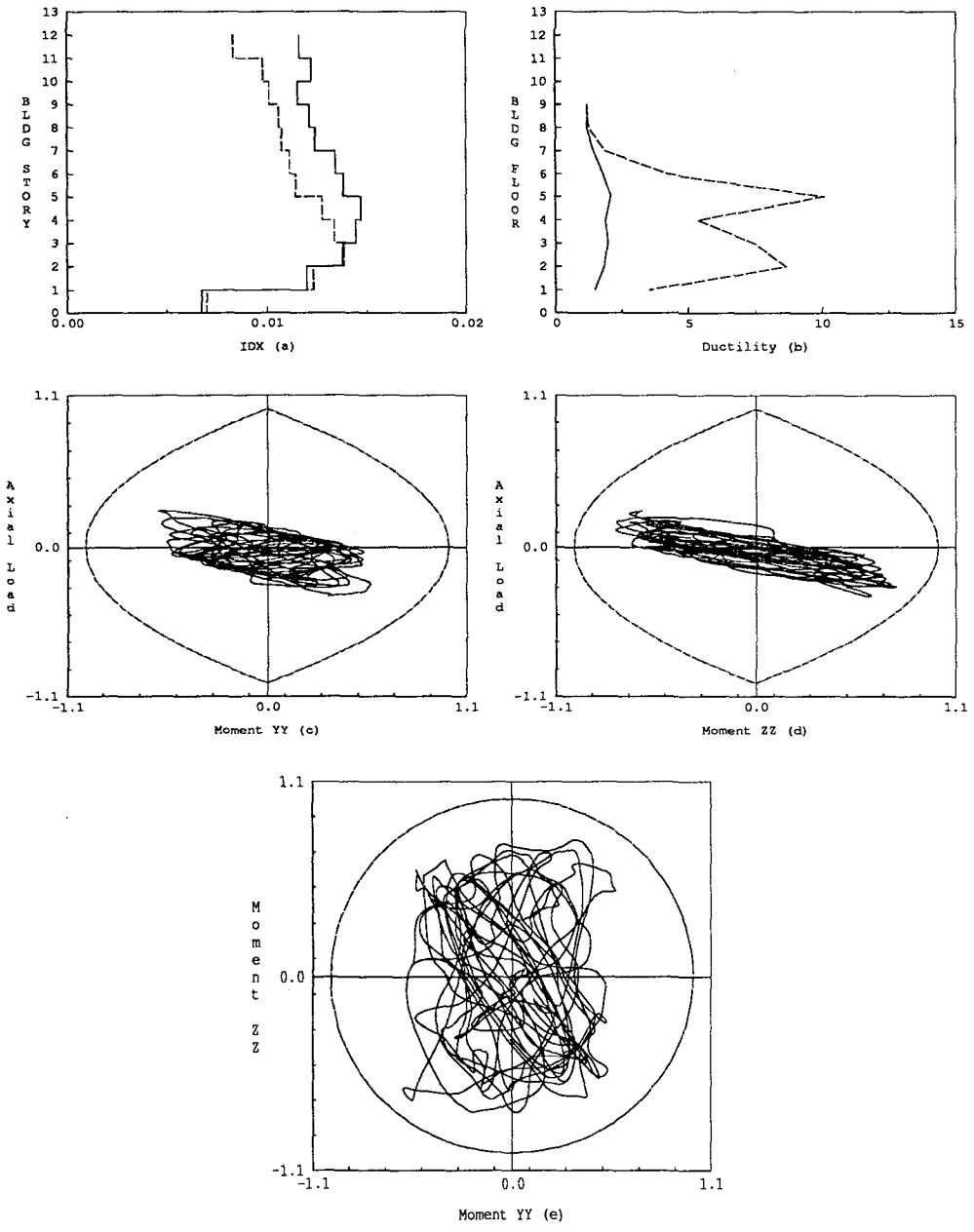

Figure 6.36: Global model parameters. El Centro NS 1940, 1% damping model, EPA=60, e/D=0. (a) Maximum inter-story drift. EW —— NS - - - - -. (b) Perimeter frame girder ductility. Maximum ————, Cumulative - - - - -. (c) Normalized column forces, P-M_{yy}. (d) Normalized column forces, P-M_{zz}. (e) Normalized column forces, M_{zz}-M_{yy}.

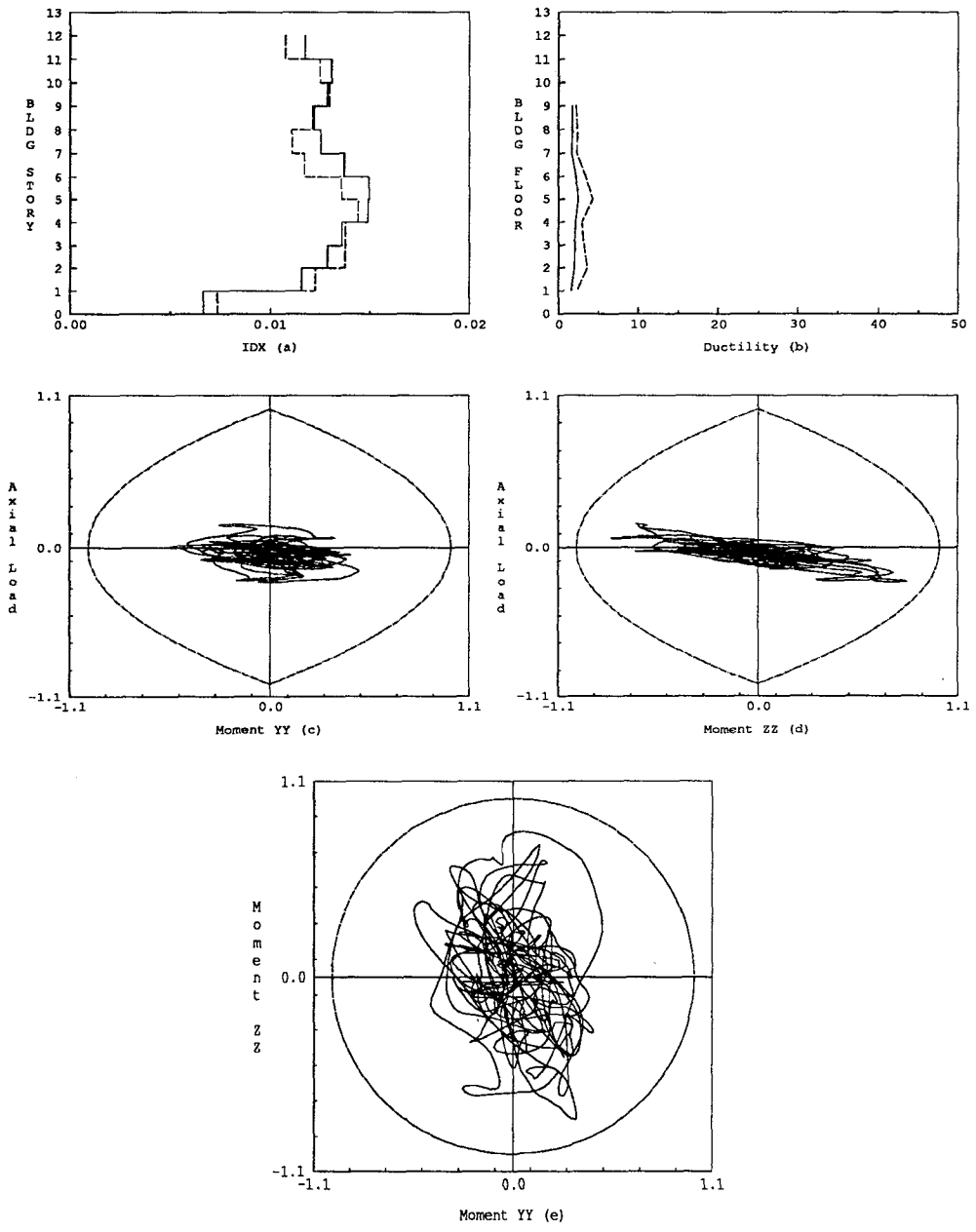

Figure 6.37: Global model parameters. El Centro NS 1940, 1% damping model, EPA=60, e/D=10. (a) Maximum inter-story drift. EW —— NS - - - - -. (b) Perimeter frame girder ductility. Maximum ————, Cumulative - - - - -. (c) Normalized column forces, P-M_{yy}. (d) Normalized column forces, P-M_{zz}. (e) Normalized column forces, M_{zz}-M_{yy}.

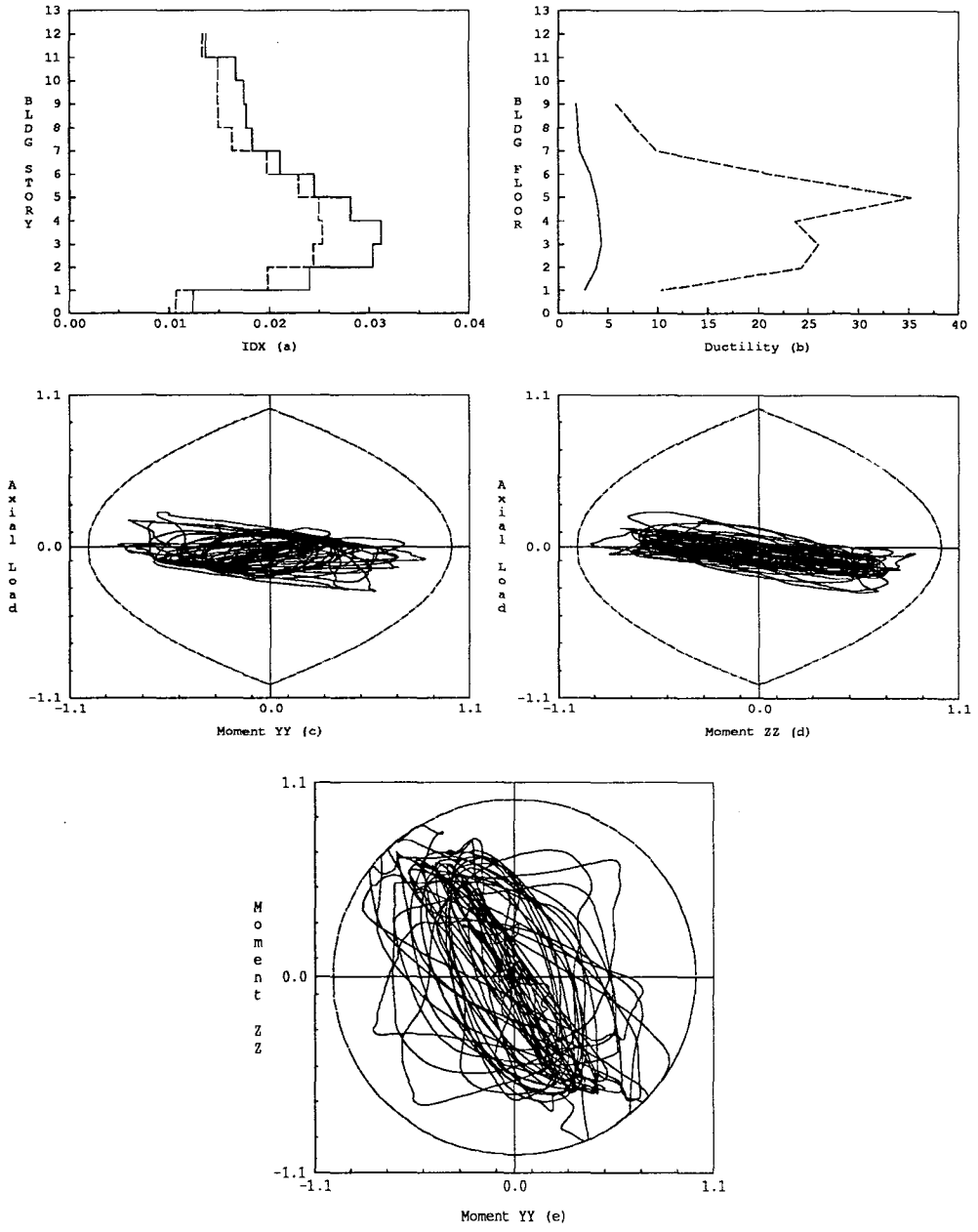

Figure 6.38: Global model parameters. Loma Prieta event, 1% damping model, EPA=60, e/D=0. (a) Maximum inter-story drift. EW —— NS - - - - -. (b) Perimeter frame girder ductility. Maximum ————, Cumulative - - - - -. (c) Normalized column forces, P-M_{yy}. (d) Normalized column forces, P-M_{zz}. (e) Normalized column forces, M_{zz}-M_{yy}.

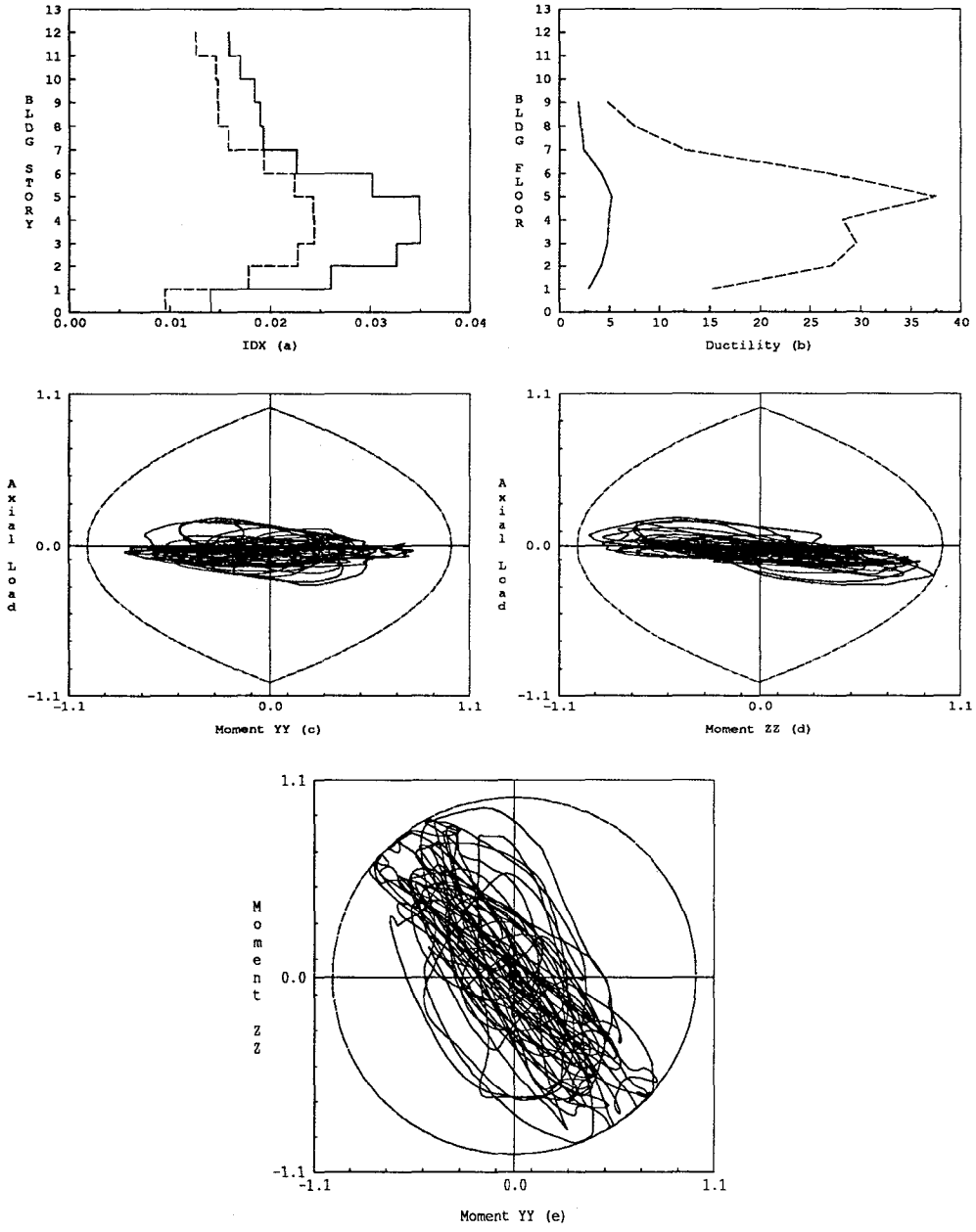

Figure 6.39: Global model parameters. Loma Prieta event, 1% damping model, EPA=60, e/D=10. (a) Maximum inter-story drift. EW —— NS - - - - -. (b) Perimeter frame girder ductility. Maximum ————, Cumulative - - - - -. (c) Normalized column forces, P-M_{yy}. (d) Normalized column forces, P-M_{zz}. (e) Normalized column forces, M_{zz}-M_{yy}.

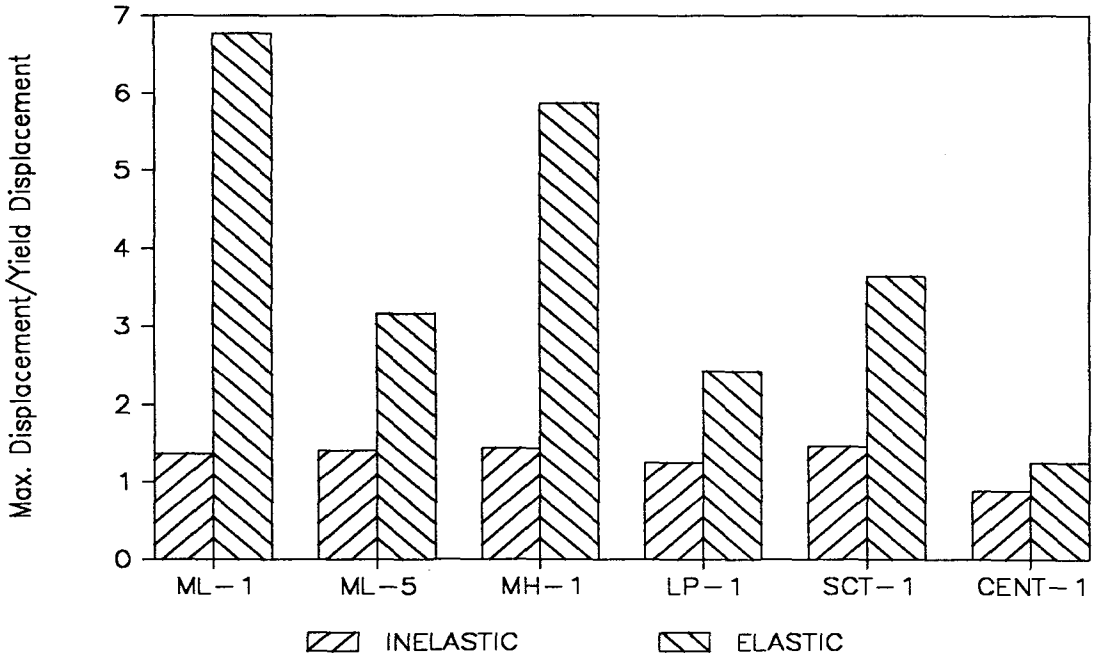

Figure 6.40: Normalized maximum twelfth floor displacement, EPA=60%, e/D=0. All records.

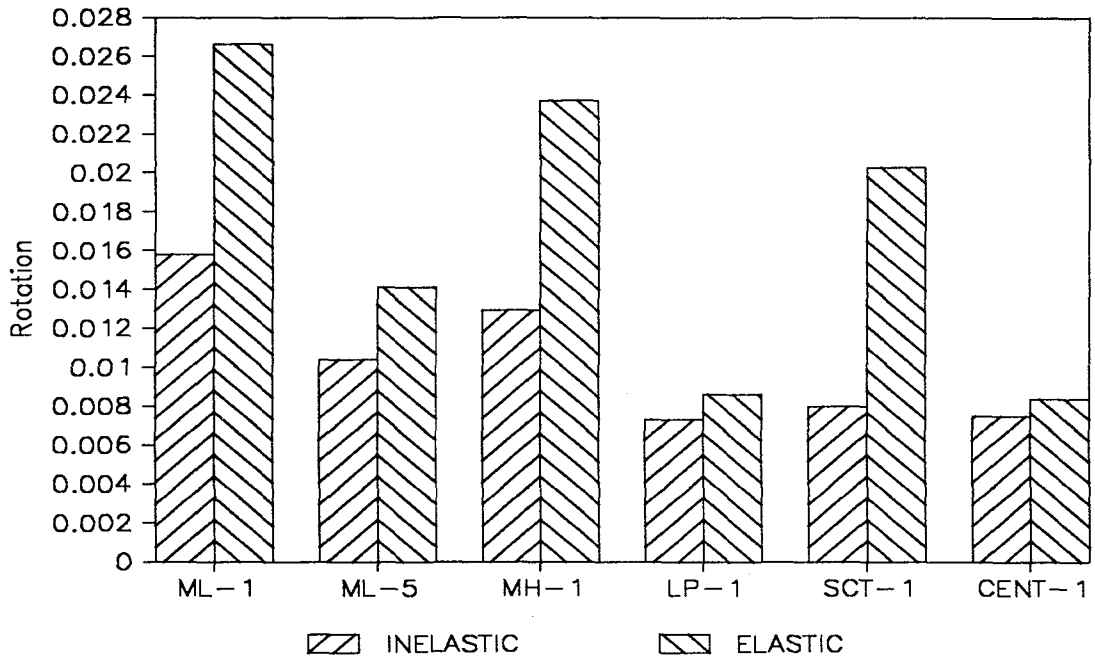

Figure 6.41: Twelfth floor in-plane rotations, EPA=60%, e/D=0. All records.

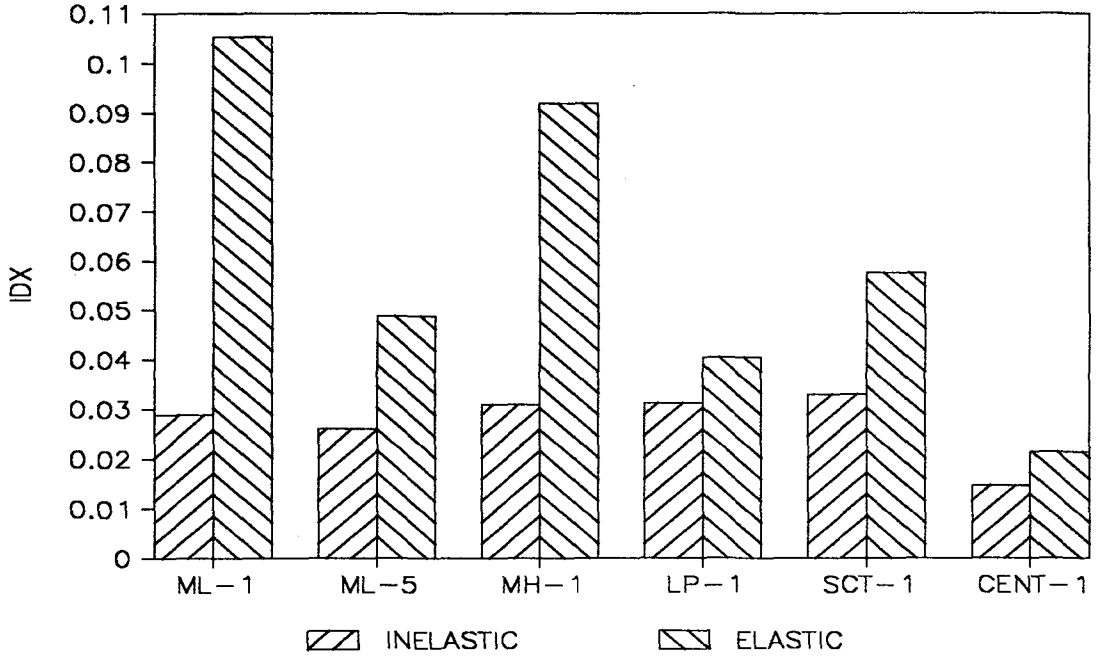

Figure 6.42: Maximum inter-story drifts, EPA=60%, e/D=0. All records.

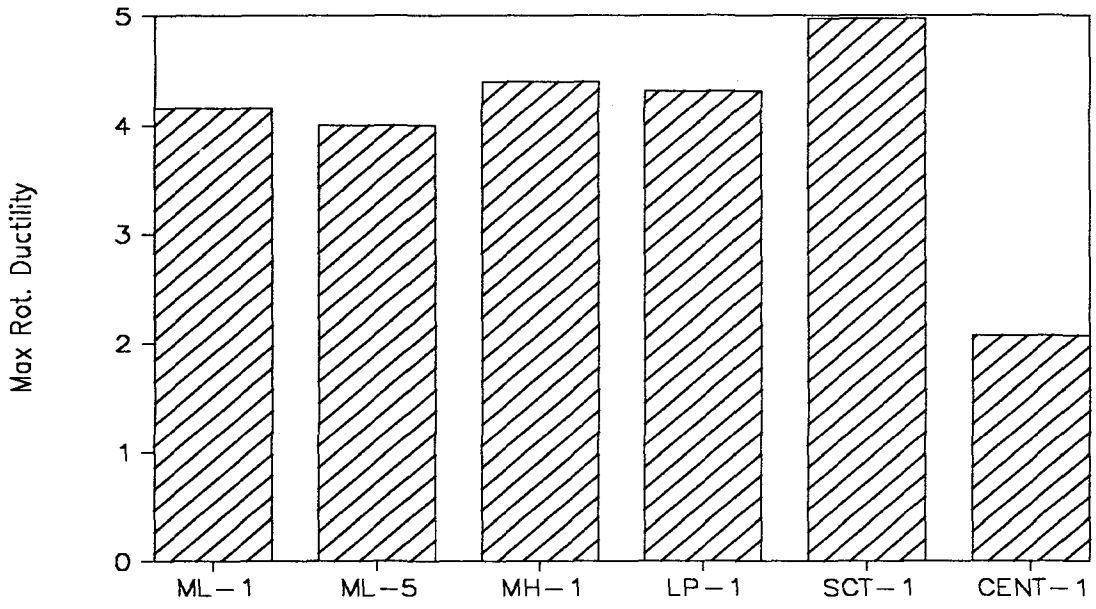

Figure 6.43: Maximum rotational ductility demand, EPA=60%, e/D=0. All records.

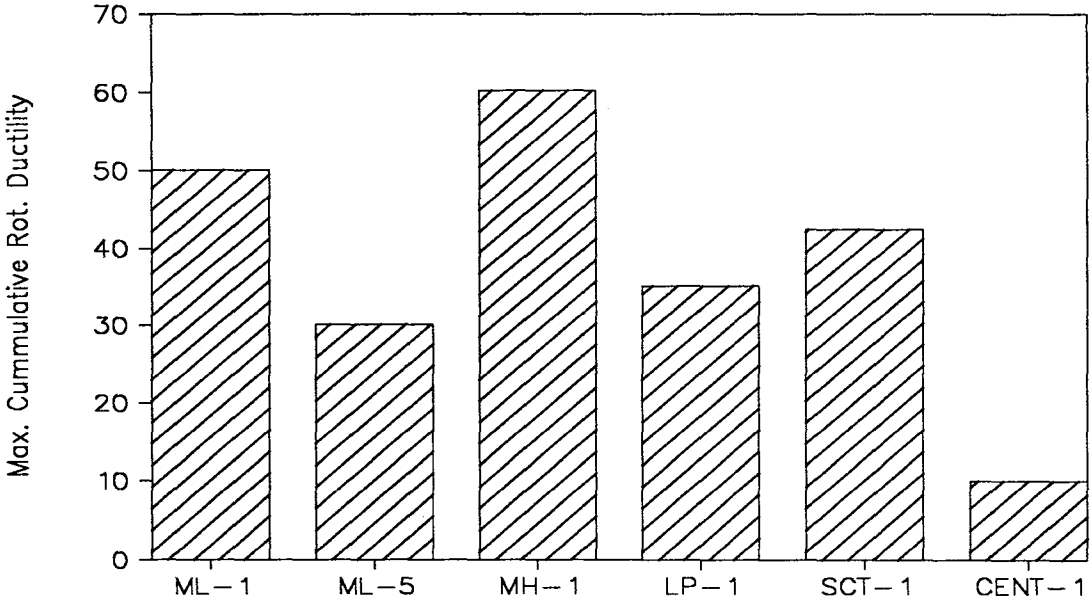

Figure 6.44: Maximum cumulative rotational ductility demand, EPA=60%, e/D=0. All records.

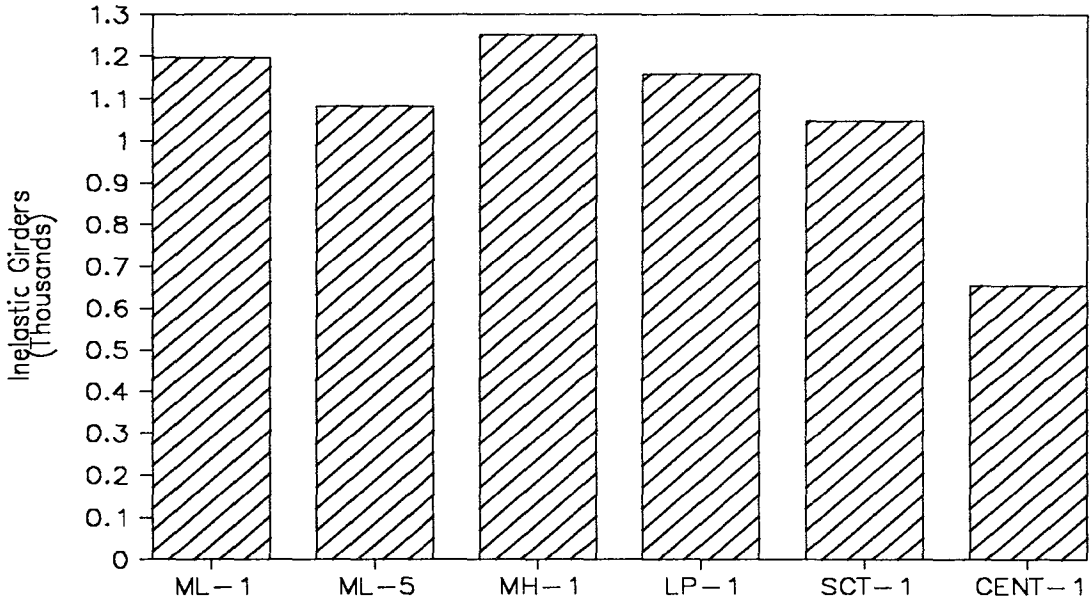

Figure 6.45: Maximum number of inelastic girder elements, EPA=60%, e/D=0. All records.

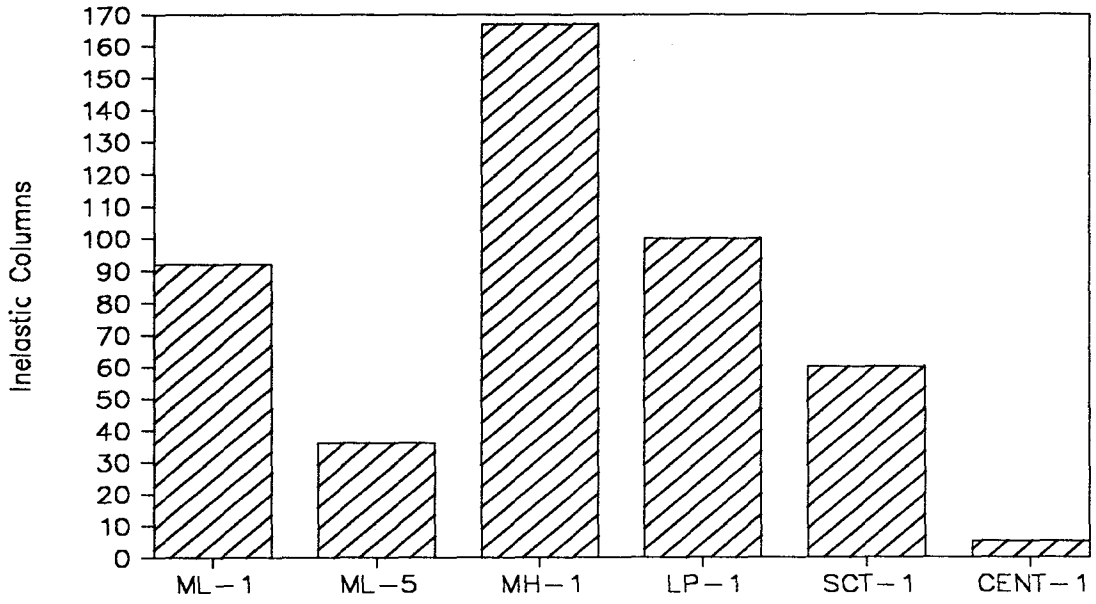

Figure 6.46: Maximum number of inelastic column elements, EPA=60%, e/D=0. All records.

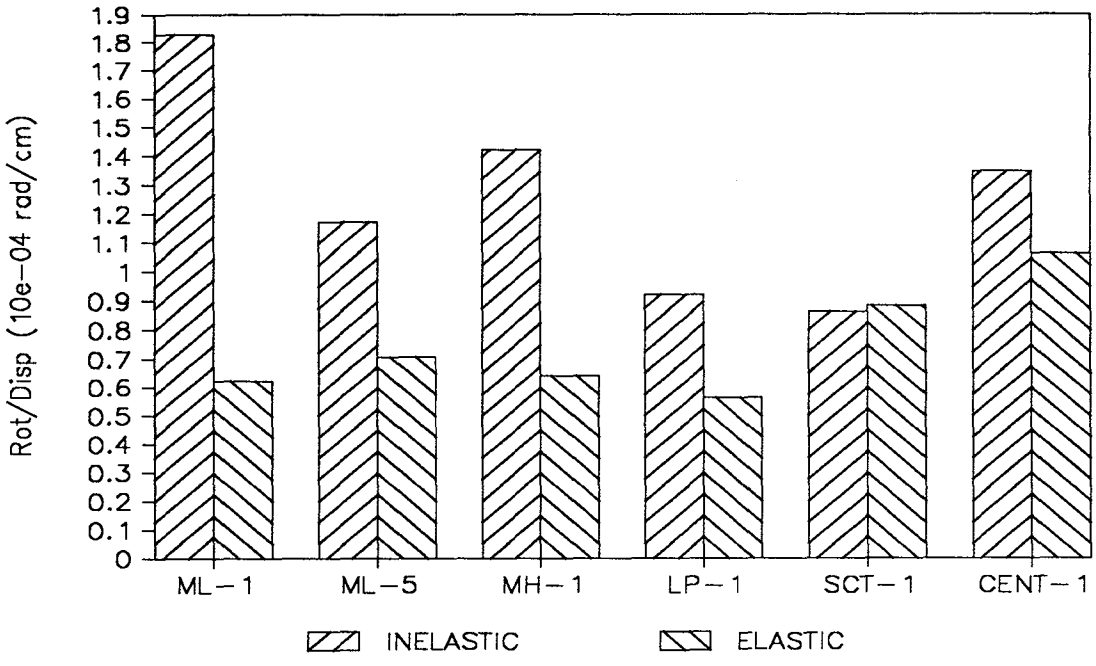

Figure 6.47: Ratio of twelfth floor in-plane rotation to maximum displacement, EPA=60%, e/D=0. All records.

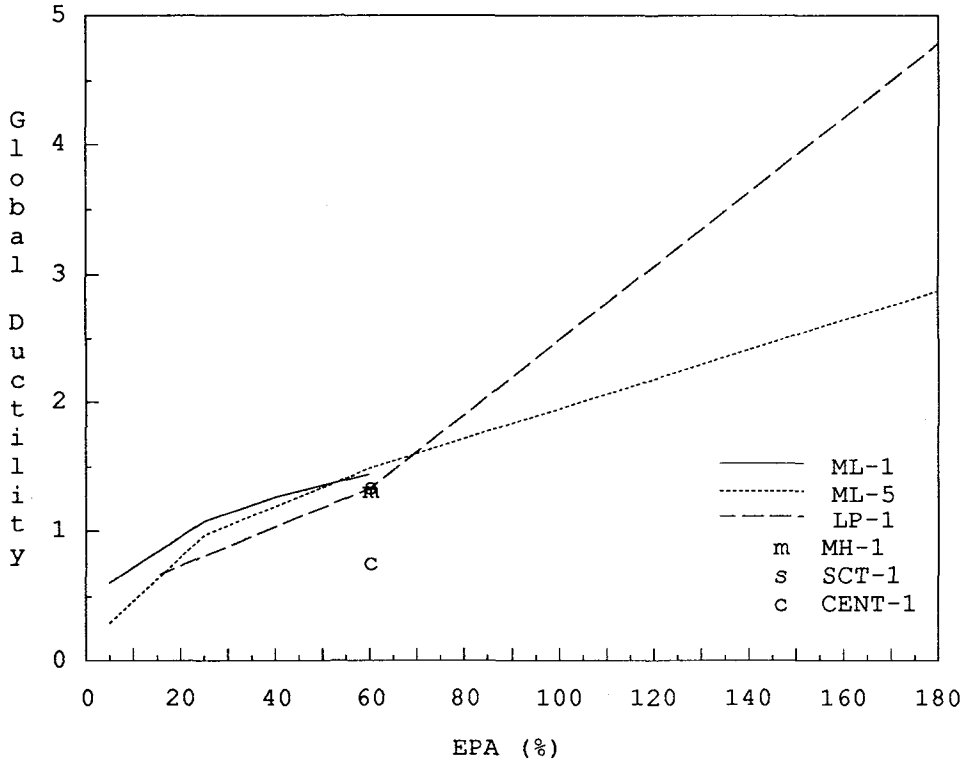

Figure 6.48: Relation between global ductility demand and EPA, e/D=0. All records.

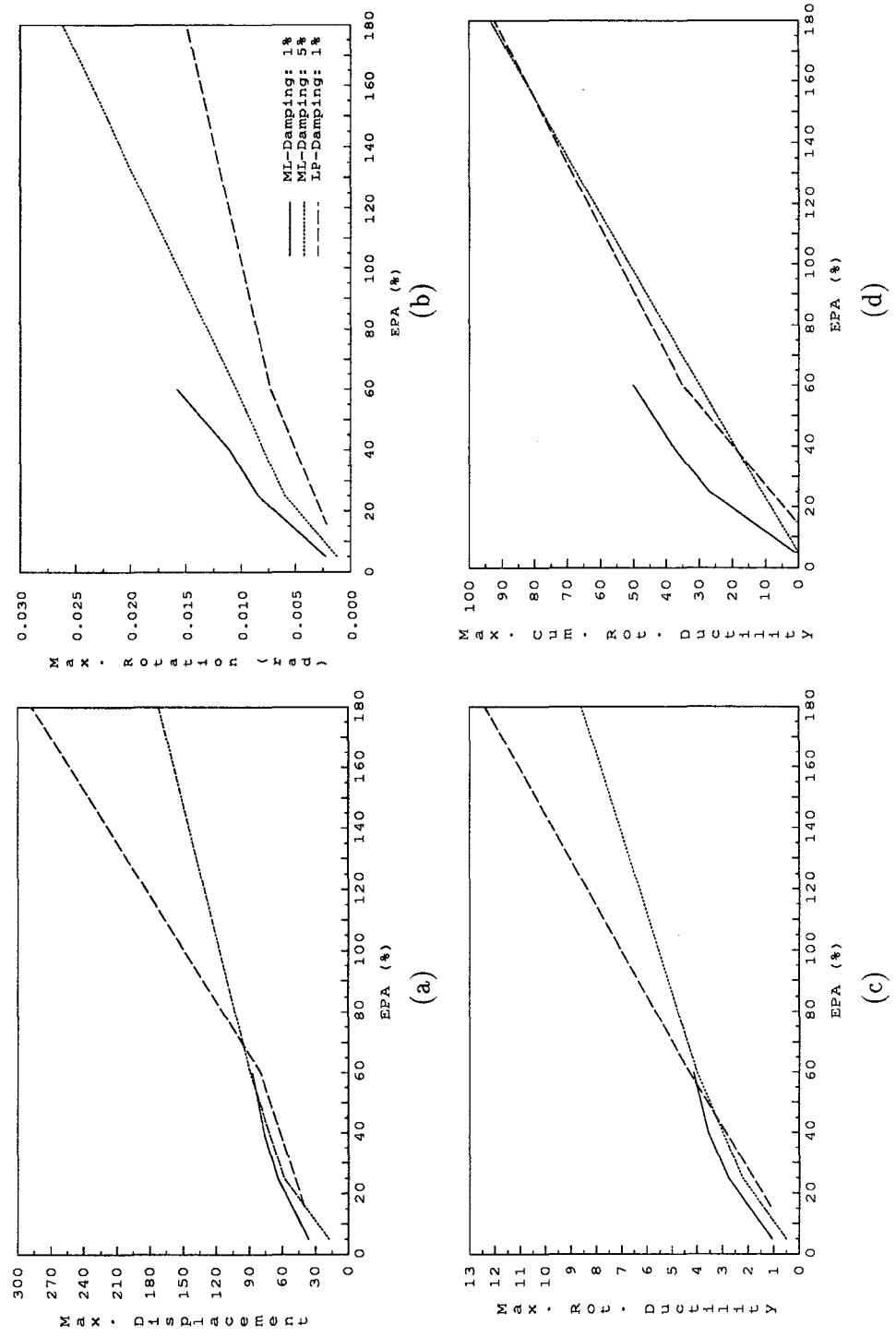

Figure 6.49: Effect of Acceleration Level on the Response. (a) Maximum twelfth floor center of mass displacement. (b) Maximum twelfth floor in-plane rotation. (c) Maximum perimeter frame girder rotational ductility. (d) Maximum perimeter frame girder cumulative rotational ductility. e/D=0

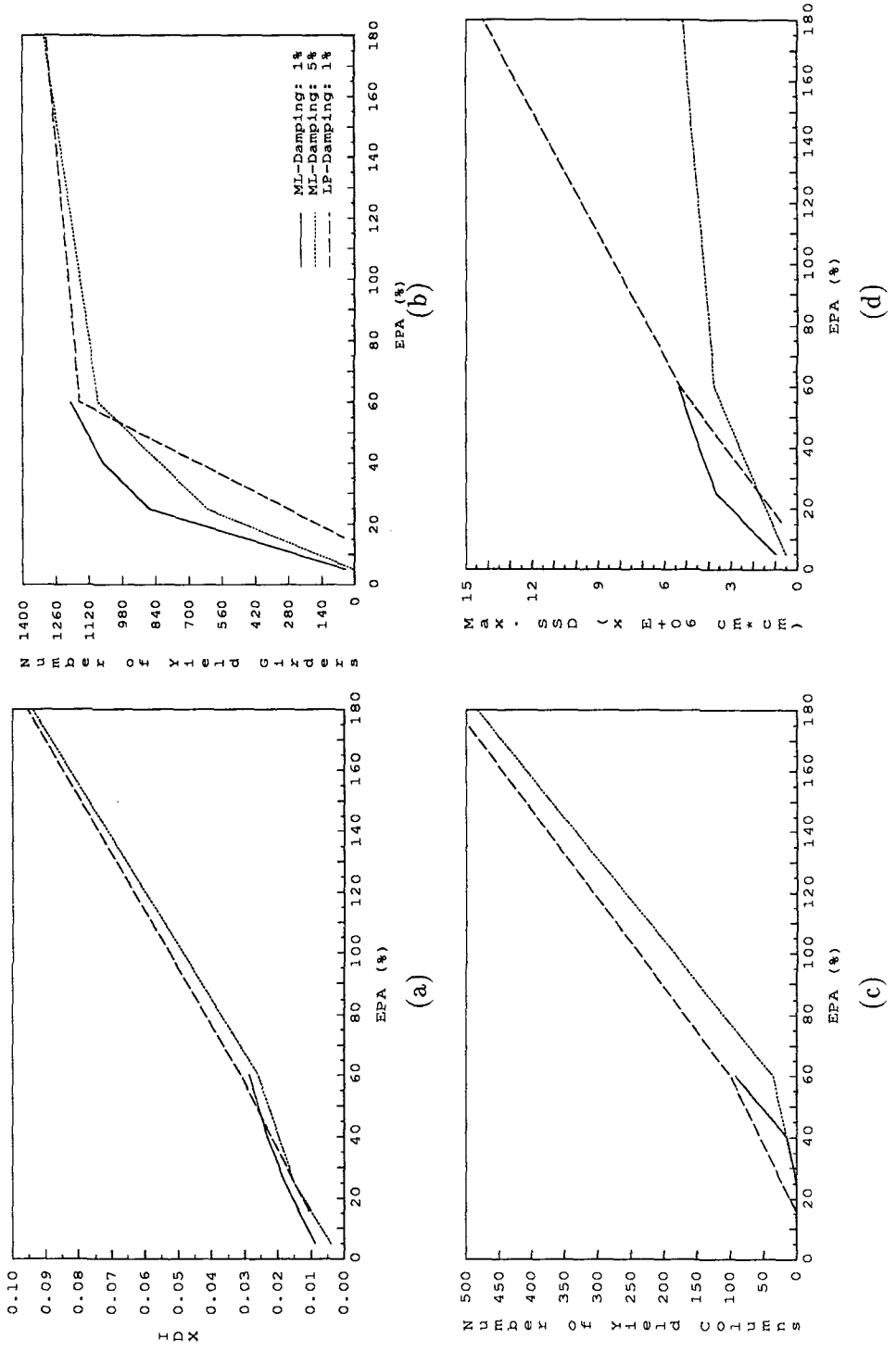

Figure 6.50: Effect of Acceleration Level on the Response, continuation. (a) Maximum inter-story drift index. (b) Number of yielded girder elements. (c) Number of yielded column elements. (d) Maximum SSD values. e/D=0

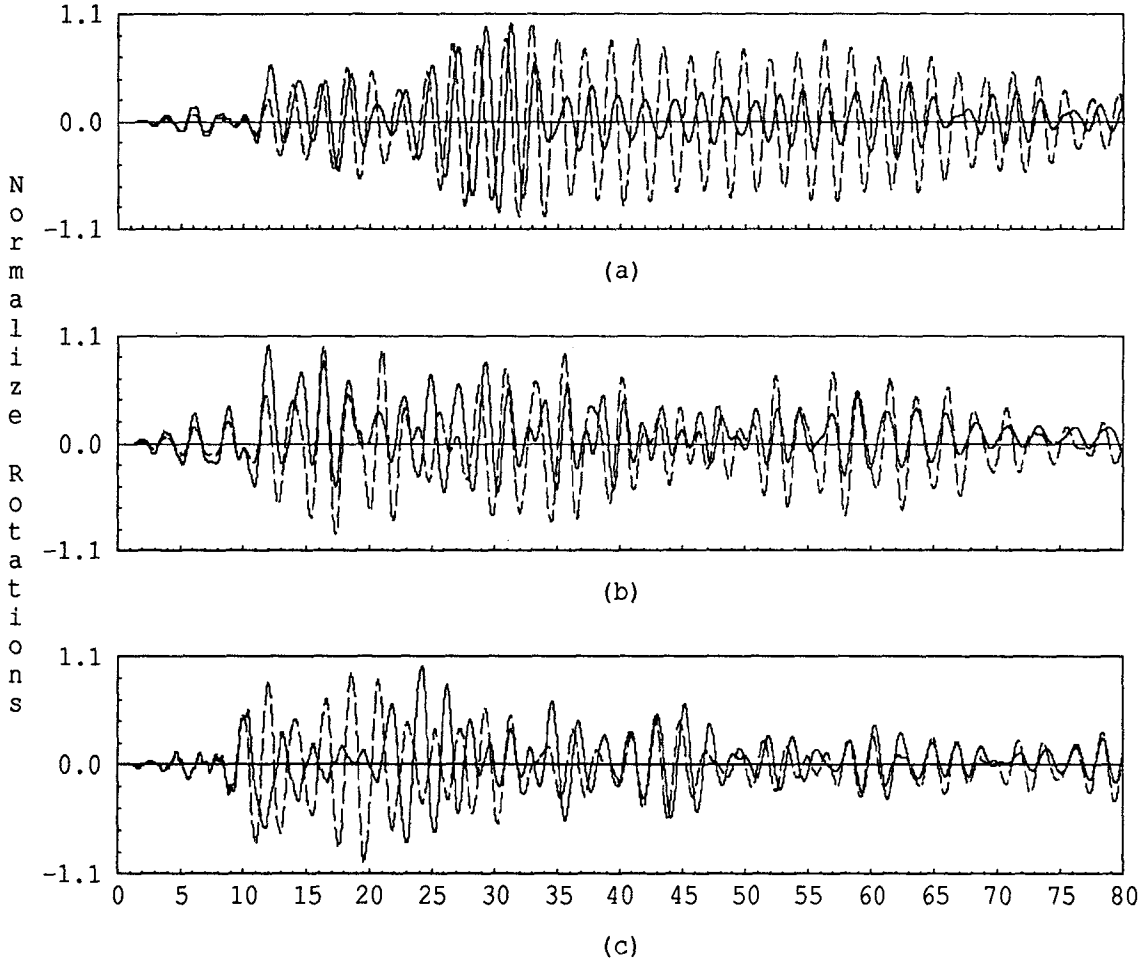

Figure 6.51: Normalized twelfth floor in-plane rotations. Elastic and inelastic (EPA=60) response. (a) Mt. Lewis event, 1% damping model. (b) Mt. Lewis event, 5% damping model. (c) Loma Prieta event, 1% damping model. Inelastic ——, Elastic - - - - -.

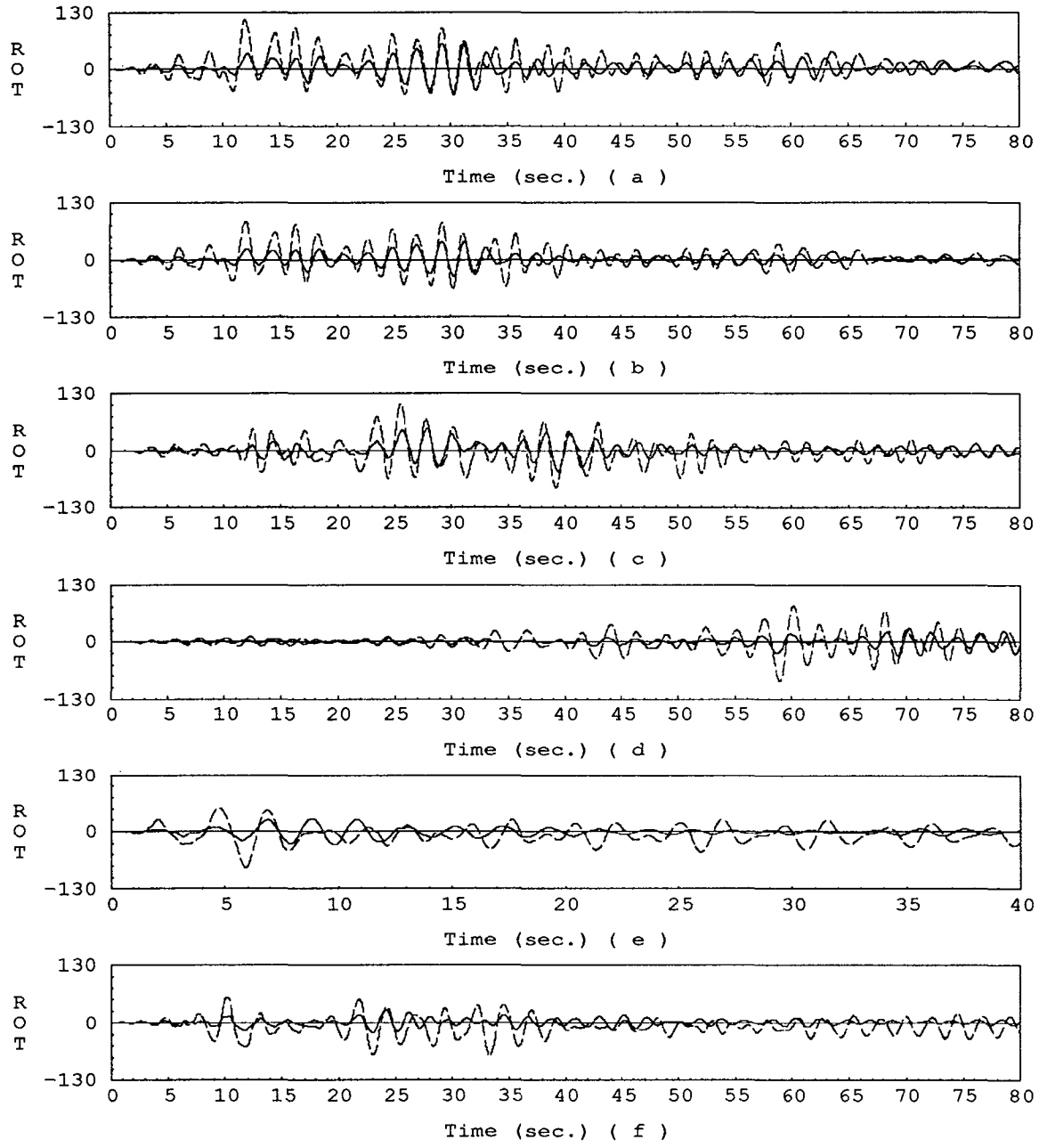

Figure 6.52: Twelfth floor torsional deformations (difference between SW and NW perimeter frame corners (cm)). (a) Mt. Lewis event, 1% damping model. (b) Mt. Lewis event, 5% damping model. (c) Morgan Hill event, 1% damping model. (d) SCT-Mexico event, 1% damping model. (e) El Centro event, 1% damping model. (f) Santa Cruz Mountains Loma Prieta event, 1% damping model. e/D=0% —— e/D=10% - - - - -.. EPA=60% g.

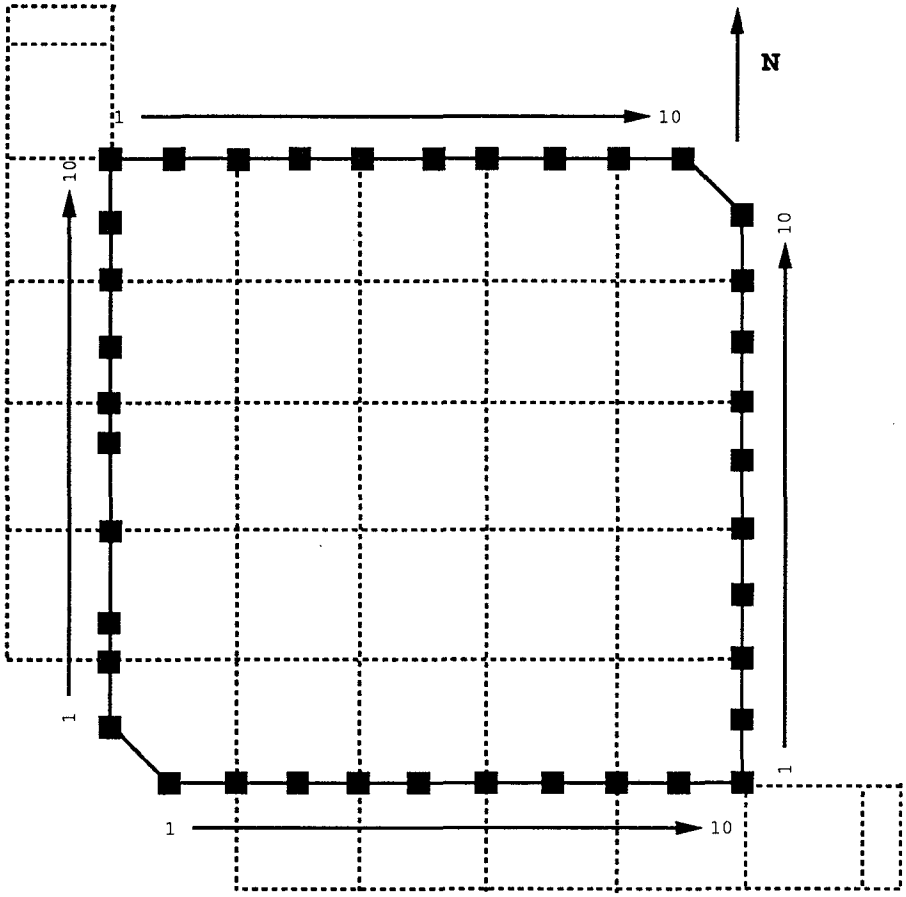

Figure 6.53: Column position for description of ductility distribution figures.

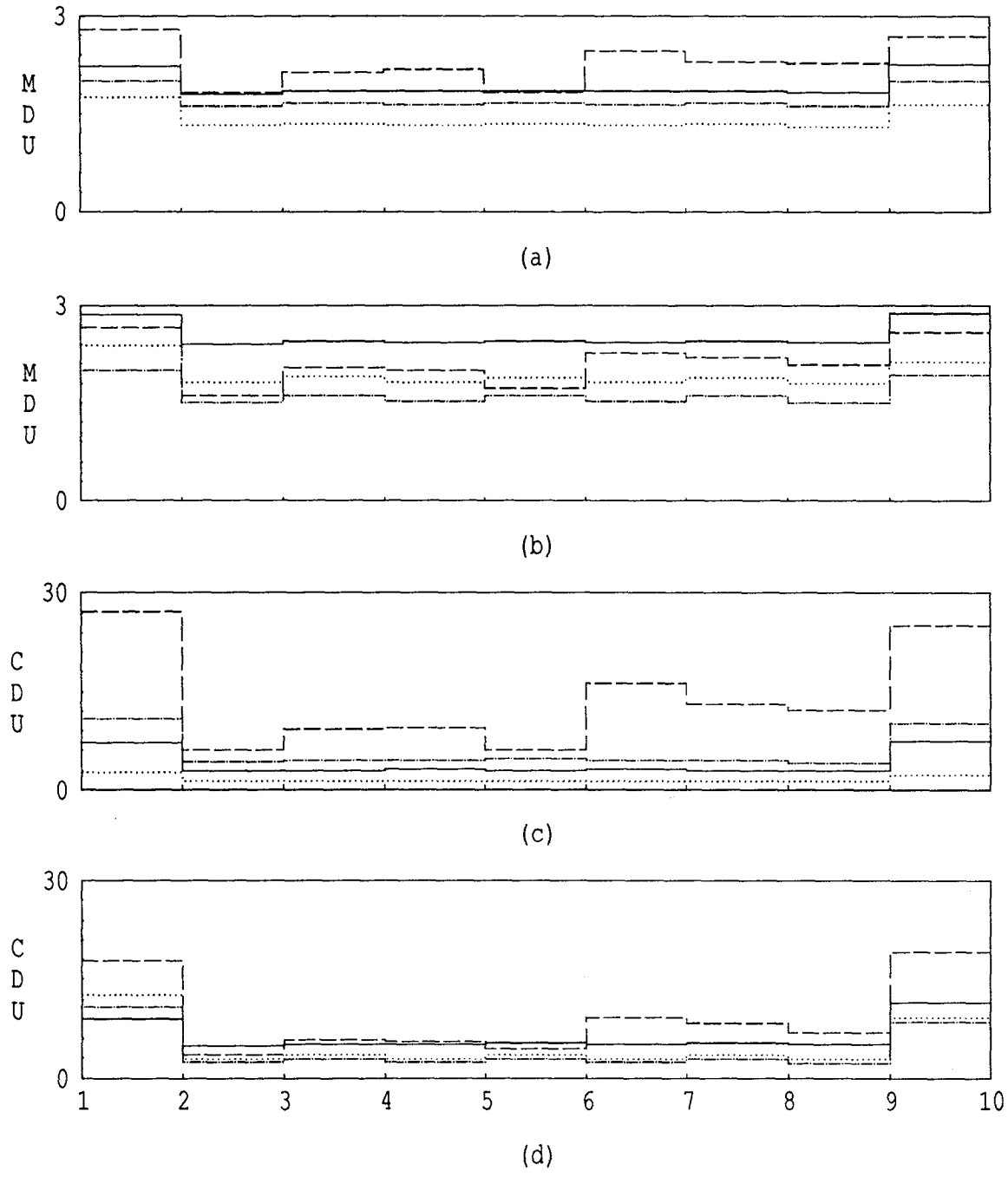

Figure 6.54: Fifth floor built-up girder rotational ductility distribution. Mt. Lewis event, 1% damping, EPA=25%. (a) Maximum ductility distribution, e/D=0%. (b) Maximum ductility distribution, e/D=10%. (c) Cumulative ductility distribution, e/D=0%. (d) Cumulative ductility distribution, e/D=10%. South side ——, North side · · · · ·, West side - - - - -, East side —·—·— . Horizontal axis show column position. Refer to Fig. 6.53 for column position.

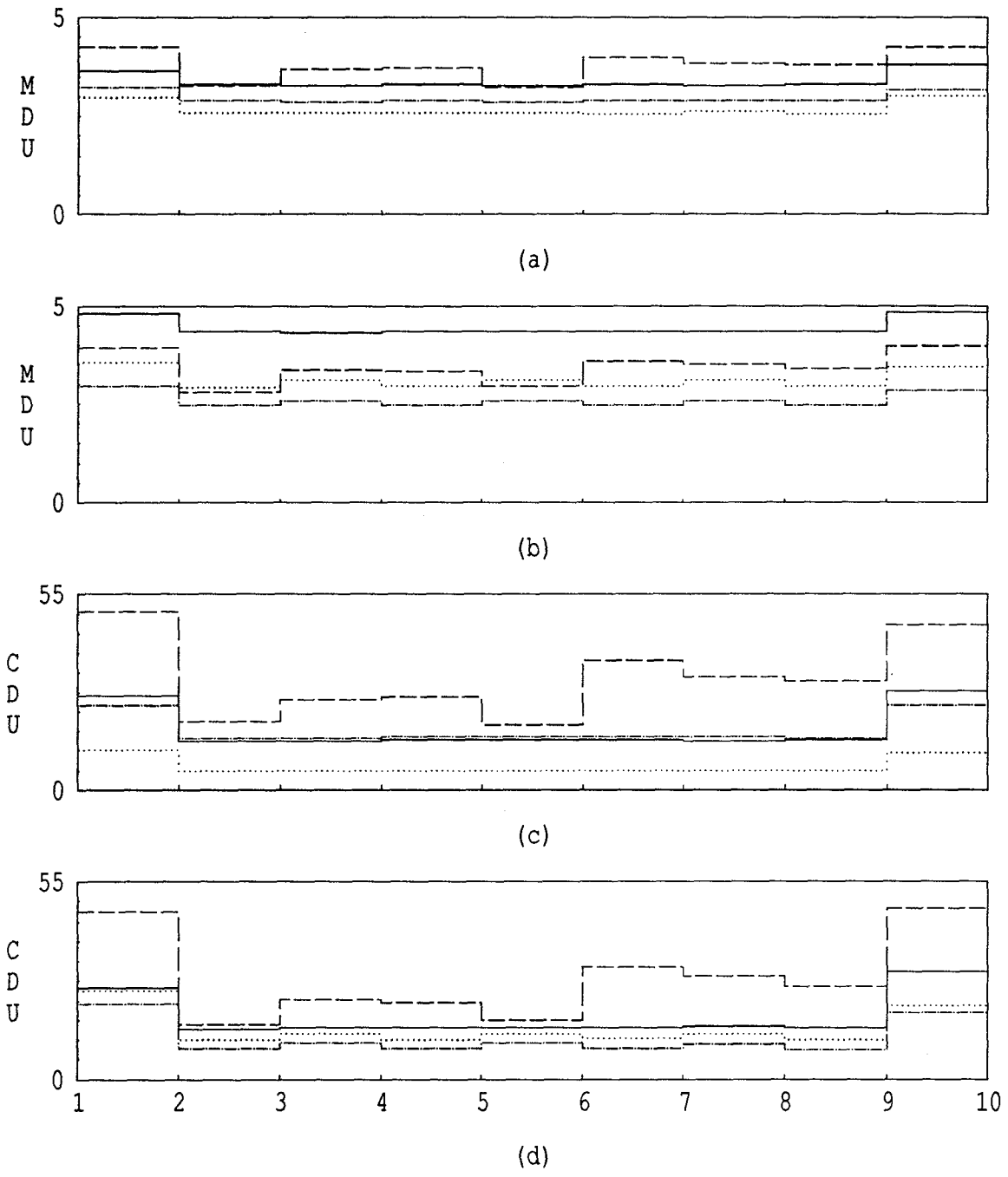

Figure 6.55: Fifth floor built-up girder rotational ductility distribution. Mt. Lewis event, 1% damping, EPA=60%. (a) Maximum ductility distribution, e/D=0%. (b) Maximum ductility distribution, e/D=10%. (c) Cumulative ductility distribution, e/D=0%. (d) Cumulative ductility distribution, e/D=10%. South side ——, North side · · · · ·, West side - - - - -, East side —·—·— . Horizontal axis show column position. Refer to Fig. 6.53 for column position.

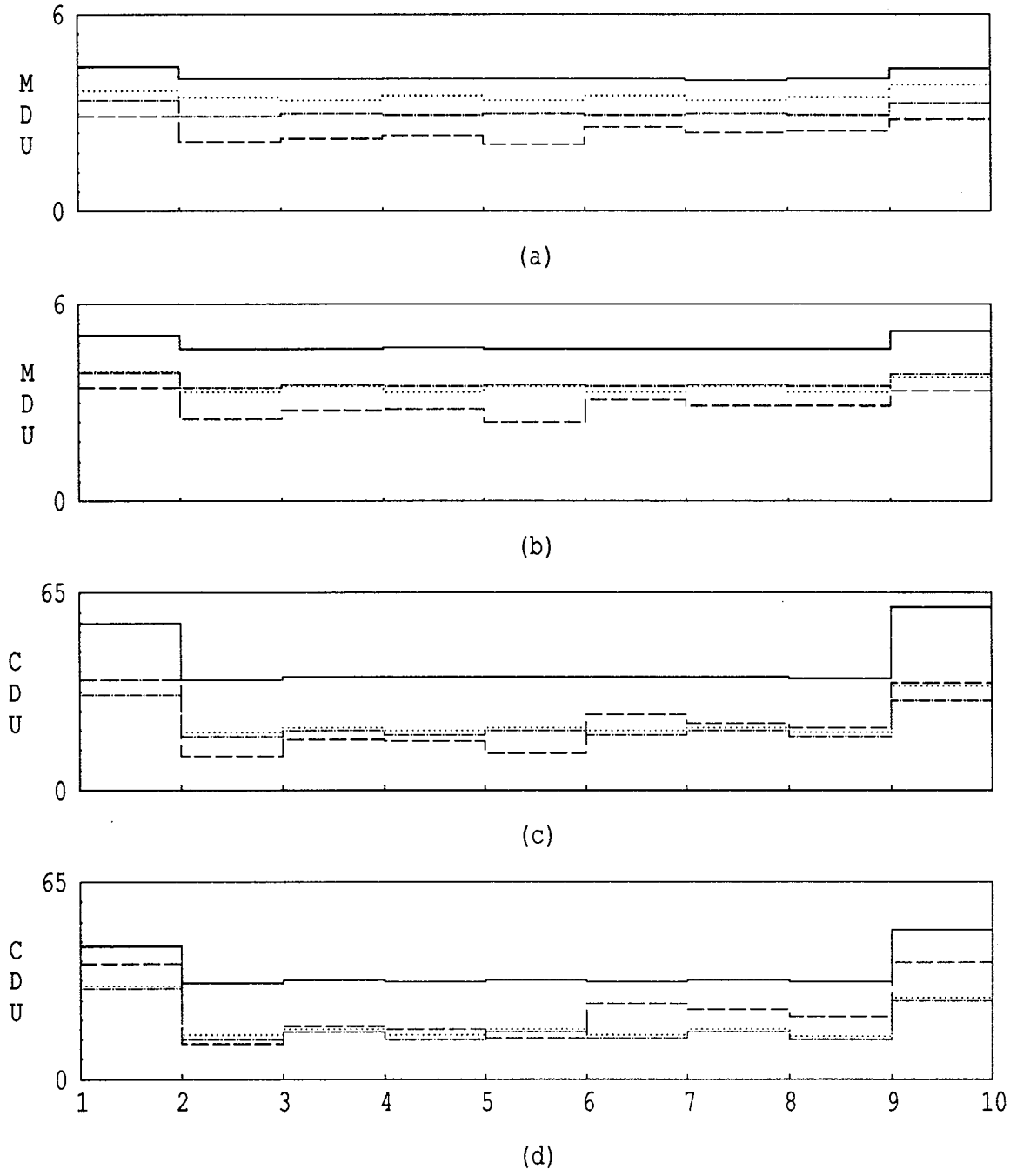

Figure 6.56: Fifth floor built-up girder rotational ductility distribution. Morgan Hill event, 1% damping, EPA=60%. (a) Maximum ductility distribution, e/D=0%. (b) Maximum ductility distribution, e/D=10%. (c) Cumulative ductility distribution, e/D=0%. (d) Cumulative ductility distribution, e/D=10%. South side ——, North side · · · · · ·, West side - - - - -, East side —·—·— . Horizontal axis show column position. Refer to Fig. 6.53 for column position.

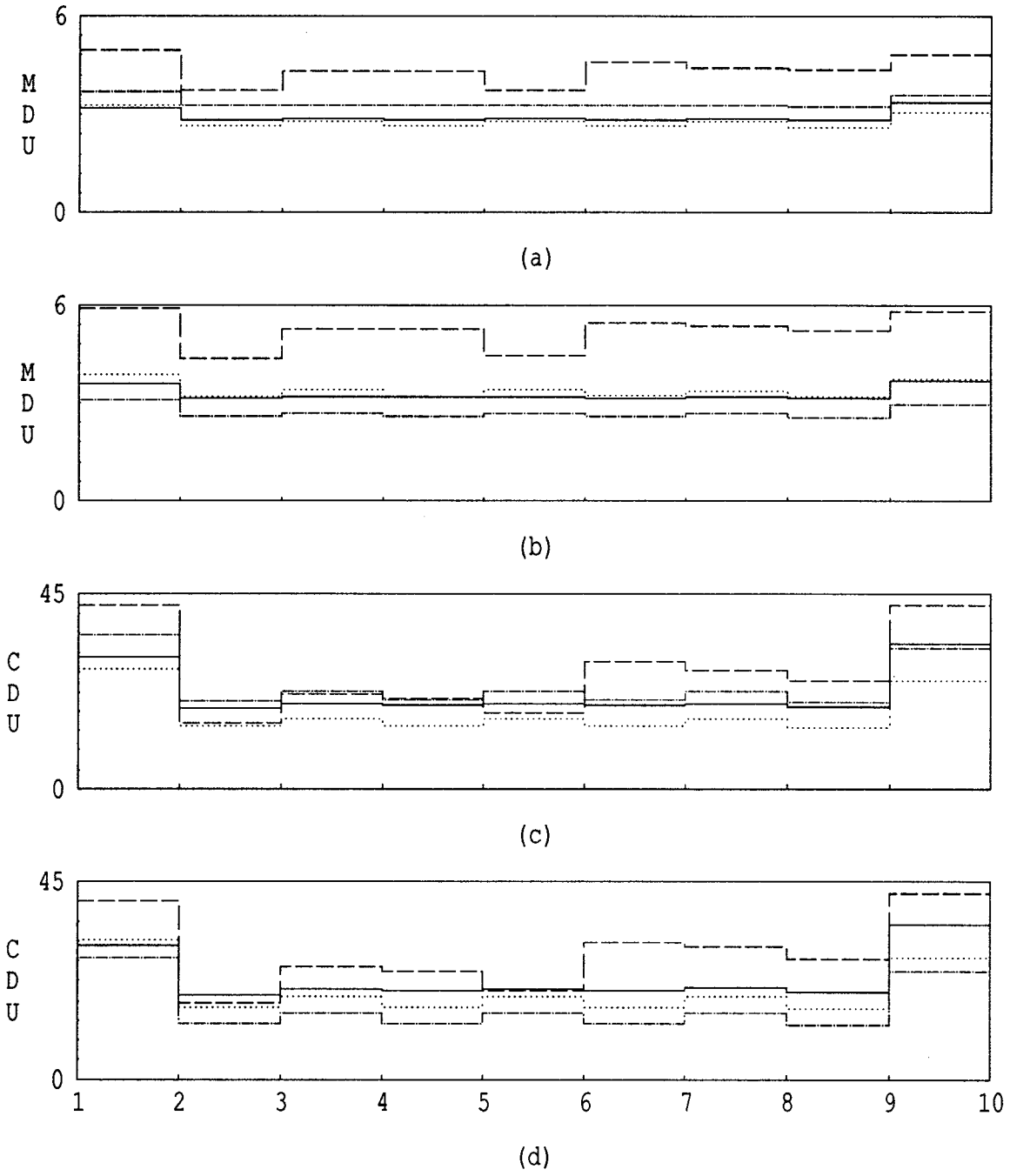

Figure 6.57: Fifth floor built-up girder rotational ductility distribution. SCT-Mexico event, 1% damping, EPA=60%. (a) Maximum ductility distribution, e/D=0%. (b) Maximum ductility distribution, e/D=10%. (c) Cumulative ductility distribution, e/D=0%. (d) Cumulative ductility distribution, e/D=10%. South side ——, North side · · · · · ·, West side - - - - -, East side —·—·— . Horizontal axis show column position. Refer to Fig. 6.53 for column position.

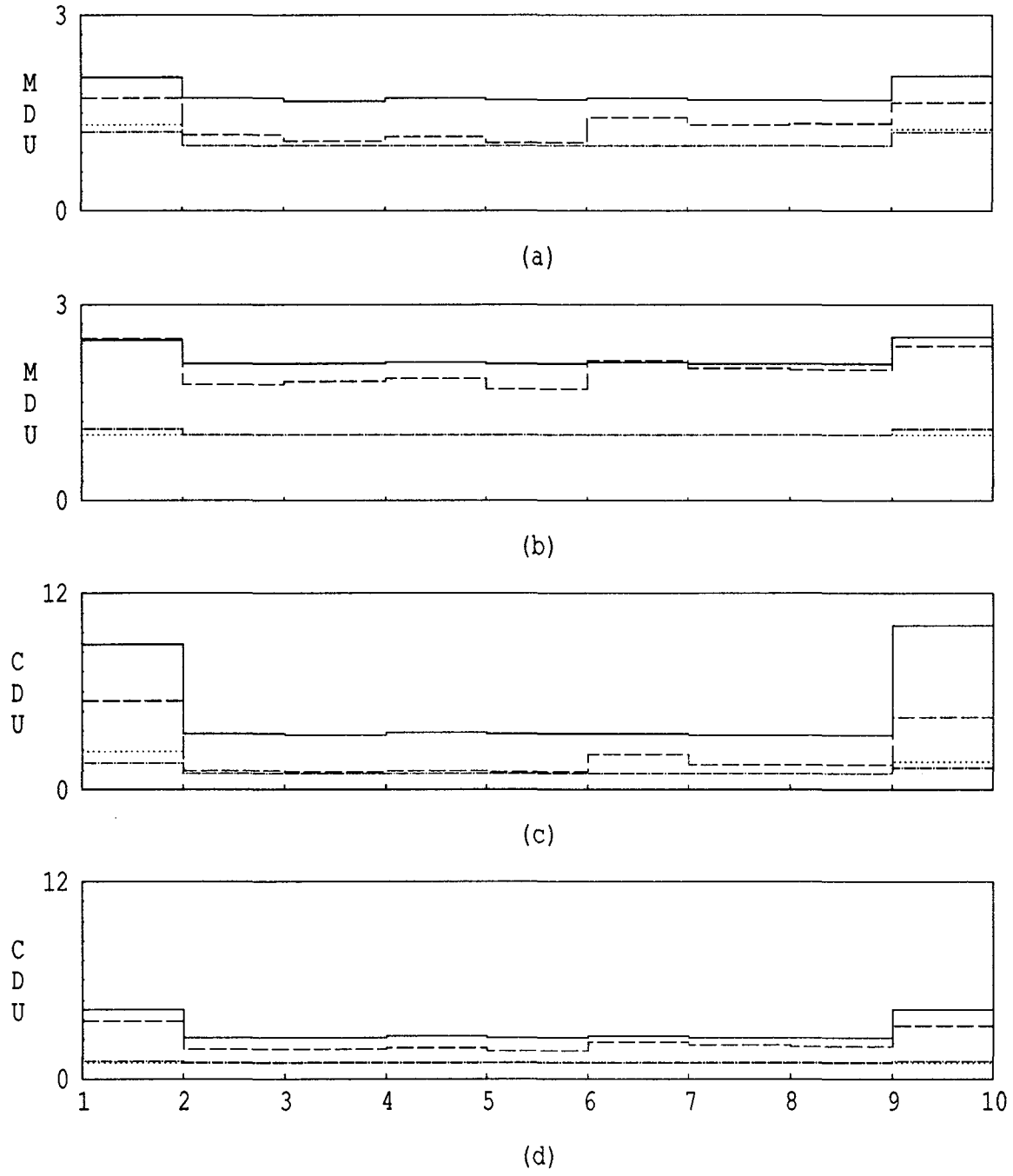

Figure 6.58: Fifth floor built-up girder rotational ductility distribution. El Centro event, 1% damping, EPA=60%. (a) Maximum ductility distribution, e/D=0%. (b) Maximum ductility distribution, e/D=10%. (c) Cumulative ductility distribution, e/D=0%. (d) Cumulative ductility distribution, e/D=10%. South side ——, North side ·····, West side - - - - -, East side —·—·— . Horizontal axis show column position. Refer to Fig. 6.53 for column position.

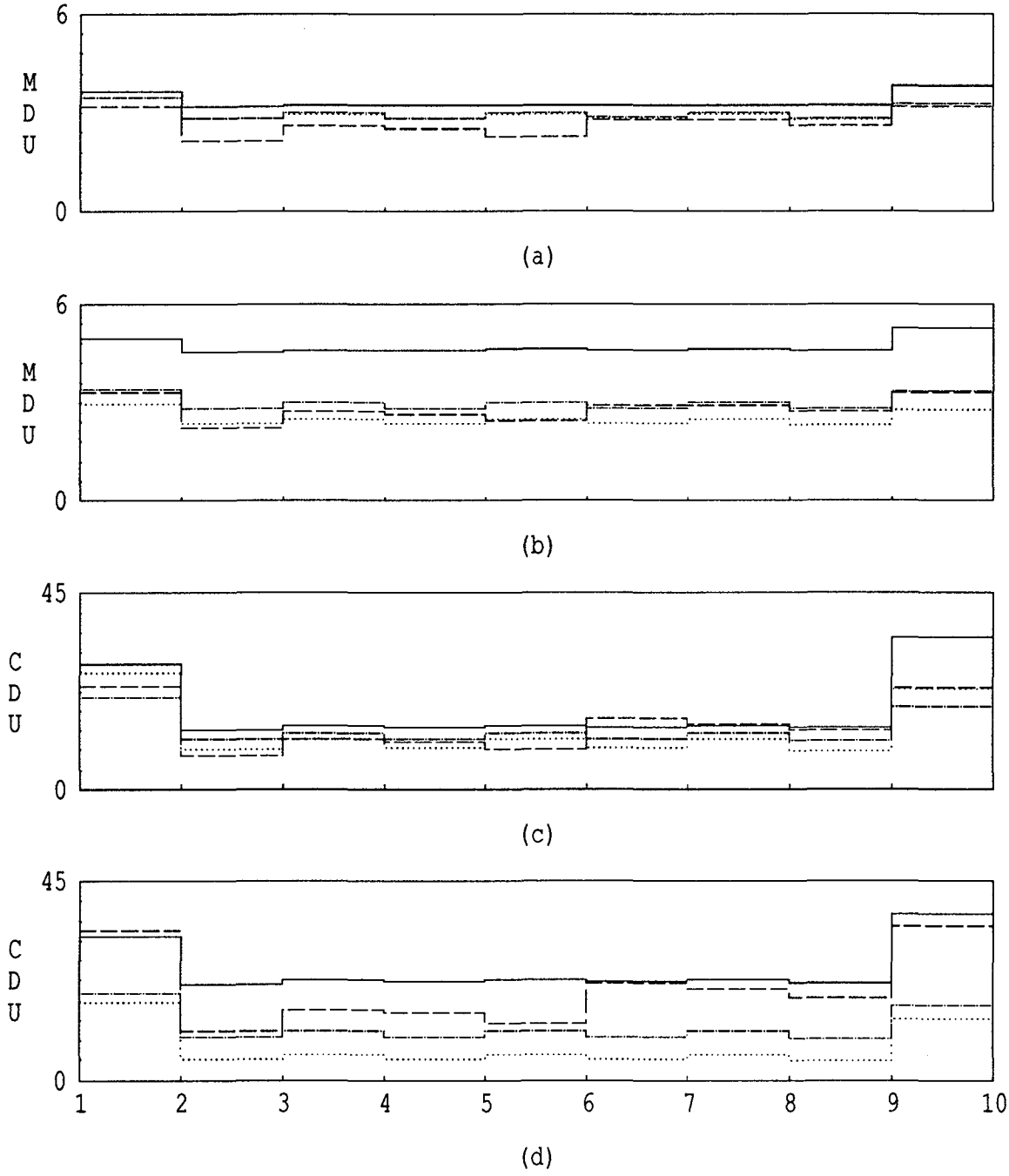

Figure 6.59: Fifth floor built-up girder rotational ductility distribution. Santa Cruz Mountain, Loma Prieta event, 1% damping, EPA=60%. (a) Maximum ductility distribution, e/D=0%. (b) Maximum ductility distribution, e/D=10%. (c) Cumulative ductility distribution, e/D=0%. (d) Cumulative ductility distribution, e/D=10%. South side ——, North side ·····, West side - - - - -, East side —·—·— . Horizontal axis show column position. Refer to Fig. 6.53 for column position.

CHAPTER 7

CONCLUSIONS AND RECOMMENDATIONS FOR FUTURE RESEARCH

7.1 Conclusions

The following are the general conclusions drawn from this investigation. More detailed conclusions are found at the end of each chapter.

1. **Response of the Building to Recorded Ground Motions**

   The recorded seismic behavior of the building studied was unusual and characterized by large amplification of the input motions, large drifts, torsion response, strong amplitude modulation, long durations and slow decay of the amplitude of the response. From analysis of the building response and the computer models it was found that the peculiar response characteristics were caused by the building's low damping, the three-dimensional modes of the building constructively reinforcing one another during portions of the motion, the long input duration and the resonance effect on the building caused by the close match of the dynamic characteristics of the site and the structure. Thus, the unusual behavior of the building during the earthquakes studied can be associated with its structural system and the relation of its dynamic characteristics to those the site,

   - The use of a regular steel moment-resisting space frame, with similar structural properties in orthogonal directions and with a nearly uniform distribution of stiffness in plan, produced a rather flexible system, with similar translational and torsional periods, and low-energy dissipation capacities (when responding in the linear range).
   - The existence of small plan eccentricities coupled the lateral and torsional motions.
   - The separation of the few non-structural elements in the building from the structural system limited their participation in the dissipation of energy in the structure.
   - The use of a flexible structure with low energy dissipation capacities (when responding in the linear range) on a relatively soft soil site allowed a resonance phenomenon in the structure, resulting in high amplifications.

   The results of the linear and nonlinear analyses of the building models and of the building records themselves suggest that the structure remained essentially elastic during the Morgan Hill earthquake. Minor yielding could have occurred in the structure for the other recorded

events, especially during the stronger Loma Prieta motion. Nevertheless, these nonlinearities are believed to have had only a small effect on the overall response of the structure.

From static load-to-collapse analyses, base shear coefficients (V/W) of 0.22, 0.29 and 0.48 were obtained for local and global yielding and for the formation of an energy dissipation mechanism, respectively. Hence, the building is very strong in comparison with current code requirements (e.g., the 1988 UBC design base shear, amplified by a factor of 1.5, is still only 19% of the computed global yielding base shear capacity). Nevertheless, the possibility that yielding occurred during the relatively small recorded earthquakes indicates that substantially worse behavior would have occurred had the structure been designed less conservatively.

From the parametric studies on the building models, it is concluded that the building response, in the linear and nonlinear ranges, can be improved by adding even moderate viscous damping to the system. The linear analyses of the full structural model showed that small amounts of viscous damping (5% of critical) can substantially reduce the apparent duration of the response. From the nonlinear model studies it was found that viscous damping, as provided in the computer models, generally reduced the response (peak and cumulative parameters) of the structure. The benefits are, nevertheless, much greater for cumulative values than for peak values of the response, and the benefits reduce with increasing inelastic behavior in the system.

2. Computer Modeling of the Building

The linear response observed in the building during the recorded events can be adequately reproduced by simple three-dimensional linear elastic computer models. A good match can be found with models that include center-to-center dimensions (with no rigid element zones, to account approximately for the flexibility of the beam-column connections), mass magnitude and distribution as obtained from the plans, nominal element properties and modal damping values typically associated with steel structures responding at low element stress levels (2-3% of critical damping). By further adjusting the actual mass distribution and incorporating a small slab contribution to the beam stiffness, global analytical results can be obtained that are virtually identical to recorded values. Factors that do not have a strong effect on the response of the linear models are the stiffness of the light partitions and cladding used in the building and torsional input motion.

Because of the small amount of damping present in the models, their response is highly susceptible to small variations in those design parameters that affect the fundamental period of the model.

3. Parametric Studies

Parametric studies were performed in the linear and nonlinear ranges to evaluate the effects of ground-motion characteristics, effective peak acceleration, additional mass eccentricities and the amount of viscous damping on the response of the structure.

(a) Ground Motion Characteristics

Frequency content and duration of the input motions have a strong effect on the response of the models. These effects were found to be more pronounced in the elastic (rather than in the inelastic) range of response. Motions representative of soft-soil sites were found to have a particularly severe effect on the structure.

(b) Lateral-Torsional Coupling

The ratio of in-plane torsional rotation to lateral displacement ("apparent coupling") can increase or decrease depending on the level of inelastic behavior and the input ground motion characteristics. From the static lateral load-to-collapse analyses, it was observed that this apparent coupling increases for low levels of yielding and then decreases for increasing levels of nonlinearities when compared with an elastic model. This type of behavior was observed in dynamic analyses for only one of the input ground motions used. More analyses that include other multi-directional motions and different strength, stiffness and mass eccentricities are required to identify controlling factors.

When additional mass eccentricities were incorporated into the models in such a way that torsional rotations increased for all earthquakes, the following results were obtained:

- The displacement at the center of mass (or at a fixed point on the perimeter frame) could decrease or increase depending on the relative orientation of the eccentricity, building characteristics and the properties of the input ground motion.
- The addition of this eccentricity has the effect of re-distributing inelastic demands between frames in orthogonal directions. For most of the cases studied the maximum ductility demand in the monitored elements of the perimeter frame increased (up to 22%), with the increase in eccentricity. In contrast, it was found that cumulative values, such as the cumulative ductility demand and the sum of the squared displacements, tended to decrease when additional eccentricities are added. One explanation for the difference in behavior for maximum and cumulative rotational ductilities is that the addition of the eccentricities apparently tended to balance the inelastic cumulative demands between the two orthogonal directions.

(c) Effect of Acceleration Level on the Response

Analyses of the models to different ground motion intensities also showed that the building can benefit from small nonlinearities in the response by reducing the amplitude of the displacements and torsional rotations observed in the linear models for the same level of earthquake intensity. This is because the nonlinear response is less sensitive to resonant like excitations.

(d) Effect of Additional Damping on the Response

Analyses of single degree-of-freedom oscillators and the building models indicated that increasing the amount of viscous damping present in a structure reduces the inelastic behavior of the system. Maximum ductility demands, cumulative damage, sum of the squared accelerations and generally the strong motion duration decrease with increasing amounts of viscous damping. Inertia forces can increase or decrease in the system depending on the period and capacity of the structure. Analyses of the single degree-of-freedom system showed that there is a critical damping value after which and increase has little effect on the response. This value is between 20 and 30% for maximum ductility and cumulative ductility demands, between 10 and 20% for the sum of the squared accelerations and around 10% for strong motion duration.

4. Code Recommendations

Design seismic recommendations such as the 1988 UBC and ATC 3-06 based on static lateral loads, were unable to predict the unusually severe response in the structure. The building periods, drifts and base shear observed from earthquake records and computer models differed considerably from those "expected" by the code, making an evaluation of the structure by a code approach unreliable. Even code response-spectrum analysis procedures used with standard normalized spectra would not be able to identify the potentially severe response of the building.

The problem is that the unusual behavior of the structure is controlled, in part, by factors that are not addressed directly by these codes. These factors include the low-energy dissipation capacity of the structure (at service-level loads) and the use of a structural system with a fundamental natural period close to the apparent predominant period of the site. Codes in other parts of the world and the more recent 1991 UBC code [23] include recommendations to increment lateral loadings in case of possible site-structure resonance. The effects of these recommendation on the behavior of structures similar to the one studied should be addressed.

Design codes are not intended to be used to simulate the observed response of a structure. Nevertheless, some codes do try to indicate the important factors that affect response. Most

codes try to address the problem of torsional response through accidental and static eccentricities. Nevertheless, as found from this and other investigations, the behavior is also greatly affected by the existence of closely-spaced translational and torsional periods, by the amount of viscous damping, and by the relation between strength, stiffness and mass eccentricities among other variables. The 1986 Costa Rica and the 1987 Mexico design codes try to include at least one of these additional variables. This does not mean that other codes are incorrect. Nevertheless, inclusion of these parameters can guide users of these codes on how to consider variables that could adversely affect the response of the structure.

The building studied herein is a good example of the necessity of performing design analyses considering different levels of structural response. In terms of capacity, the building was found to be adequate. Nevertheless, the behavior under service-level earthquake loading was undesirable. The basic behavioral characteristics of the structure for each level of response should be considered for the analysis. These studies also indicated that care should be taken in design to evaluate the expected site response spectra in relation to the expected building properties. On sites were resonance is possible, evaluations should be undertaken to modify the stiffness of the structure and to provide enough damping, even for a low level of element stress, to limit the severity of the response in the structure.

7.2 Areas of Future Research

This investigation could be extended in several ways. Some of the areas of possible future research are presented below:

- Records from the new free-field instrument outside the building and new earthquake events should be included in a more comprehensive study of soil-structure interaction.
- The responses of the building should be compared with the responses of other buildings with similar structural characteristics to obtain more general conclusions about the behavior of this type of structure.
- A more extensive parametric study should be performed on this type of structure to develop more reliable design procedures. Consideration should be given to other building configurations, larger eccentricities, variation of strength, stiffness and mass eccentricities in multiple directions, different yield capacities and other input motion characteristics.
- Studies should be undertaken to evaluate the effectiveness of improving the response of such buildings by increasing the stiffness and energy dissipation capacities, separating the natural periods and uncoupling the natural modes of the structure.

- P-Δ effects in the nonlinear response of the structure should be assessed more accurately.

BIBLIOGRAPHY

[1] Christopher Arnold. Occupant behavior related to seismic performance in a high-rise office building. In *Proceedings Third US National Conference on Earthquake Engineering*, volume 3, 1986.

[2] Abolhassan Astaneh-Asl, Stephen Mahin, J. Shen, and Ruben Boroschek. Investigation of design and analysis methods for steel framed buildings. In *Seminar on Seismological and Engineering Implications of Recent Strong-Motion Data*. SMIP California, Department of Conservation, 1990.

[3] Pierre Bard. The importance of rocking in building motion: An experimental evidence. In *Proceedings Ninth World Conference on Earthquake Engineering*, Japan, 1988.

[4] James L. Beck. System identification applied to strong motion records from structures. In *Earthquake Ground Motion and its Effect on Structures*. The Applied Mechanics Division, ASME, 1982. Vol. 53.

[5] Ruben Boroschek and Stephen Mahin. Computer program descriptions for analysis and interpretation of building response records. Technical report, Department of Conservation, California Strong Motion Instrumentation Program, 1990.

[6] Ruben Boroschek and Stephen Mahin. Seismic response and analytical modeling of a thirteen story government office building. Technical report, Department of Conservation, California Strong Motion Instrumentation Program, 1990.

[7] Ruben Boroschek, Stephen Mahin, and Christos Zeris. Engineering interpretation of responses of three instrumented buildings in San Jose, California. Technical report, Department of Conservation, California Strong Motion Instrumentation Program, 1990.

[8] Ruben Boroschek, Stephen Mahin, and Christos Zeris. Seismic response and analytical modeling of three instrumented buildings. In *Proceedings of Fourth U.S. National Conference on Earthquake Engineering*, 1990.

[9] Earth Sciences Associates. Soil and foundation investigation for the proposed Santa Clara County Civic Center. Technical report, Earth Sciences Associates, November 1971.

[10] D. G. Elms. Seismic torsional effects on buildings. *Bulletin of the New Zealand National Society for Earthquake Engineering*, 9(1), March 1976.

[11] Federal Emergency Management Agency. *NEHRP Recommended Provisions for the Development of Seismic Regulations for New Buildings*, 1988.

[12] Sigmund A. Freeman. Racking test of high-rise building partitions. *Struc. Div.*, 103(ST8), August 1977.

[13] James F. Gibbs and Roger D. Borcherdt. Effects of local geology on ground motion in the San Francisco Bay Region, California – A continued study. Open-File Report 74-222, USGS, 1974.

[14] Rakesh K. Goel and Anil K. Chopra. Inelastic seismic response of one-story, asymmetric-plan systems: Effects of stiffness and strength distribution. *Earthquake Engineering and Structural Dynamics*, 19:949–1970, 1990.

[15] Rakesh K. Goel and Anil K. Chopra. Some aspects of inelastic earthquake response of one-story asymmetric-plan systems. In *Proceedings of Fourth U. S. National Conference on Earthquake Engineering*, Palm Springs, California, May 1990.

[16] Robert D. Hanson, David M. Bergman, and Samir A. Ashour. Supplemental mechanical damping for improved seismic response of buildings. In *Proc. Third U.S. National Conference on Earthquake Engineering*, August 1986.

[17] R. Hejal and A. K. Chopra. Earthquake response of torsionally-coupled buildings. Report UCB/EERC 87-20, Earthquake Engineering Research Center, University of California at Berkeley, 1987.

[18] J. Brent Hoerner. Modal coupling and earthquake response of tall buildings. Technical Report 71-07, EERL, 1971.

[19] G. W. Housner and P. C. Jennings. Generation of artificial earthquakes. *Engineering Mechanics Division*, 90(EM1):113–150, February 1964.

[20] M. Huang, A. Shakal, D. Parke, R. Sherburne, and R. Nutt. Processed data from the strong-motion records of the Morgan Hill earthquake of 24 April 1984. Part II structural - response records. OSMS 85-05, California Strong Motion Instrumentation Program, 1985.

[21] International Association For Earthquake Engineering. *Earthquake Resistant Regulations a World List-1988*, 1988.

[22] International Conference of Building Officials. *Uniform Building Code*, 1988.

[23] International Conference of Building Officials. *Uniform Building Code*, 1991.

[24] Paul C. Jennings, R. Mathiessen, and J. Brent Hoerner. Forced vibration of a 22-story steel frame building. Technical Report 71-01, EERL, 1971.

[25] C. Kan and A. Chopra. Couple lateral torsional response of buildings to ground shaking. Report UCB/EERC 76 - 13, Earthquake Engineering Research Center, University of California at Berkeley, 1976.

[26] James Kelly. Coupled lateral torsional response of base isolated buildings. Course 290D Notes, University of California, Berkeley, Spring 1990.

[27] Takuji Kobori, Ryoichiro Minai, and Teizo Fujiwara. Earthquake response of framed structures composed of inelastic members. In *Proceedings of the Fifth World Conference on Earthquake Engineering*, 1974.

[28] H. Krawinkler, V. Bertero, and E. Popov. Inelastic behavior of steel beam-to-column subassemblages. Report UCB/EERC 71-7, Earthquake Engineering Research Center, University of California at Berkeley, 1971.

[29] H. Krawinkler and S. Mohasseb. Effect of panel zone deformations on seismic response. *Construction Steel Research*, (8), 1987.

[30] Bing-Chang Lin and Apostolos S. Papageorgiou. Demonstration of torsional coupling caused by closely spaced periods-1984 Morgan Hill earthquake response of the Santa Clara County building. *Earthquake Spectra*, 5(3), 1989.

[31] J. P. Lin and S. A. Mahin. Effect of inelastic behavior on the analysis and design of earthquake resistant structures. Report UCB/EERC 85-08, Earthquake Engineering Research Center, University of California at Berkeley, 1985.

[32] S. A. Mahin and J. Lin. Construction of inelastic response spectra for single-degree-of- freedom systems–Computer program and applications. Report UCB/EERC 83-17, Earthquake Engineering Research Center, University of California at Berkeley, 1983.

[33] Stephen Mahin, Ruben L. Boroschek, and Christos Zeris. Engineering interpretation of responses of three instrumented buildings in San Jose. In *Seminar on Seismological and Engineering Implications of Recent Strong Motion Data.* Strong Motion Instrumentation Program, 1989.

[34] B. Maison and C. Neuss. SUPER-ETABS an enhanced version of the ETABS program. Computer manual, NISEE, 1985.

[35] Martin W. McCann. and Haresh Shah. Determining strong-motion duration of earthquakes. *Bull. Seismological Society of America*, 69(4), August 1979.

[36] Digambar P. Mondkar and Graham H. Powell. Ansr-i general purpose program for analysis of nonlinear structural response. Report UCB/EERC 75-37, Earthquake Engineering Research Center, University of California at Berkeley, December 1975.

[37] Simin Naaseh. The Morgan Hill earthquake of april 24, 1984 - Performance of three engineered structures. *Earthquake Spectra*, 1(3), May 1985.

[38] National Bureau of Standards. *ATC 3-06, Tentative Provisions for the Development of Seismic Regulations for Buildings*, 1978. Special Publication 510.

[39] N. M. Newmark and W. Hall. Procedures and criteria for earthquake resistant design. In *Building Practice for Disaster Mitigation.* NBS, 1973. Building Science Series 45.

[40] Nathan M. Newmark. Torsion in symmetrical buildings. In *Proceedings of Fourth World Conference on Earthquake Engineering*, pages A3 19–32, Chile, 1969.

[41] Nathan M. Newmark and Emilio Rosenblueth. *Fundamentals of Earthquake Engineering.* Prentice Hall, Inc. Englewood Cliffs, New Jersey, 1971.

[42] David A. Pecknold. Inelastic structural response to 2D ground motion. *The Engineering Mechanics Division*, 100(EM5):949–963, October 1974.

[43] B. K. Raghu Prasad and K. S. Jagadish. Inelastic torsional response of a single story framed structure. *Engineering Mechanics Division*, 115(8):1782–1797, August 1989.

[44] Ali Riahi, Dennis G. Row, and Graham H. Powell. ANSR-I : INEL-2 *&* 3. Three Dimensional Inelastic Frame Elements For The ANSR-I Program. Report UCB/EERC 78-06, Earthquake Engineering Research Center, University of California at Berkeley, August 1978.

[45] T. Rogers and J. Williams. Potential seismic hazards in Santa Clara County California. Special Report 107, CDMG, 1974.

[46] Hassan Sedarat and Vitelmo V. Bertero. Effects of torsion on the nonlinear inelastic seismic response of multi-story structures. In *Proceedings of Fourth U. S. National Conference on Earthquake Engineering*, Palm Springs, California, May 1990.

[47] A. Shakal and M. Huang. Torsional response of three instrumented buildings during the 1984 Morgan Hill earthquake. In *Proceedings Third US National Conference Earthquake Engineering*, 1986.

[48] A. Shakal, M. Huang, M. Reichle, C. Ventura, T. Cao, R. Sherburne, et al. CSMIP strong-motion records from the Santa Cruz Mountains (Loma Prieta), California earthquake of 17 October 1989. OSMS 89-06, California Strong Motion Instrumentation Program, 1989.

[49] M. Trifunac and A. Brady. A study on the duration of strong earthquake ground motion. *Bull. Seismological Society of America*, 65(3), June 1975.

[50] W. K. Tso and Hongshan Ying. Additional seismic inelastic deformation caused by structural asymmetry. *Earthquake Engineering and Structural Dynamics*, 19:243–258, 1990.

[51] Erik H. Vanmarcke. Structural response to earthquakes. In C. Lomnitz and E. Rosenblueth, editors, *Seismic Risk and Engineering Decisions*, chapter 8. Elsevier Scientific Publishing Company, 1976.

[52] M. Wakabayashi. *Design of earthquake resistant buildings.* McGraw Hill, 1986.

[53] Woodward-Clyde-Sherard and Associates. Soil investigation for the proposed new Santa Clara County Office Building San Jose, California. Technical report, Woodward-Clyde-Sherard and Associates, 1958.

[54] Woodward-Clyde-Sherard and Associates. Geology and structural engineering. Part 2, Recommendation for land use planning in the Baylands. Technical report, Woodward-Clyde-Sherard and Associates, 1970.

[55] Yutaka Yamazaki. Inelastic torsional response of structures subjected to earthquake ground motions. Report UCB/EERC 80-07, Earthquake Engineering Research Center, University of California at Berkeley, 1980.

[56] Christos Athanassiou Zeris. *Three Dimensional Nonlinear Response of Reinforced Concrete Buildings.* PhD thesis, Structural Engineering Mechanics and Materials. Civil Engineering., University of California at Berkeley, 1986.

Appendix A

THE MODAL BEATING PHENOMENON

A.1 Introduction

A beating phenomenon occurs in linear multiple degree-of-freedom systems having closely-spaced modal periods (and mode shapes that interact). Generally, the response histories of systems thus affected are characterized by a modulated pattern envelope of cyclic responses. For example, the free vibration response of a simple undamped two-mode system is shown in Fig. A.1. If the modes are well-separated the response is as shown in Fig. A.1a. Here, the the effect of the second mode is simply superimposed on top of the first mode response. For this example, the second mode amplitude and period are taken as 1/2 and 1/5 of the values corresponding to the first mode. This type of response is typically observed in structures with well separated (period) planar modes.

However, if the two modes have similar but not identical modal frequencies, the beating phenomenon, as shown in Fig. A.1b, occurs. For this example, the amplitudes are the same and the period of the second mode is taken as 80% of the value corresponding to first mode. The apparent frequency of vibration is similar (but not equal) to the interacting modal frequencies, and the amplitude of peak cyclic motion is modulated with a much larger period.

A simple analogy using trigonometric series will be used here to assess this behavior. The sum of two harmonic waveforms with different periods and amplitudes, varying as cosine functions, can be expressed as

$$A_1 \cos\left(2\pi\frac{t}{T_1}\right) + A_2 \cos\left(2\pi\frac{t}{T_2}\right) = A_1\left[2\cos\left(\pi t\left(\frac{1}{T_1}+\frac{1}{T_2}\right)\right)\cos\left(\pi t\left(\frac{1}{T_1}-\frac{1}{T_2}\right)\right) + \left(\frac{A_2}{A_1}-1\right)\cos\left(2\pi\frac{t}{T_2}\right)\right] \tag{A.1}$$

where

A_i and T_i are the amplitude and period of vibration of the i^{th} interacting wave form, and

t represents time.

By appropriate manipulation of this relation, the beating period can be estimated as

$$T_B \approx \frac{2T_1T_2}{T_1 - T_2} \tag{A.2}$$

with $T_1 > T_2$; and the equivalent natural period of the composite motion can be expressed as

$$T_N \approx \frac{2T_1T_2}{T_1 + T_2} \tag{A.3}$$

Figure A.2 (a and b) shows that the apparent (equivalent) natural period differs from the actual dynamic characteristics of either interacting modes and that the beating period increases rapidly as the two system periods approach one another.

The same approach can be expanded to the case of superimposing three constant (unit) amplitude cosine wave forms with different periods

$$\begin{aligned}\cos(A) + \cos(B) + \cos(C) = \cos\left[\frac{1}{2}(A+B)\right]\cos\left[\frac{1}{2}(A-B)\right] + \\ \cos\left[\frac{1}{2}(A+C)\right]\cos\left[\frac{1}{2}(A-C)\right] + \\ \cos\left[\frac{1}{2}(B+C)\right]\cos\left[\frac{1}{2}(B-C)\right]\end{aligned} \tag{A.4}$$

in which $A = 2\pi\frac{t}{T_1}$, $B = 2\pi\frac{t}{T_2}$, and $C = 2\pi\frac{t}{T_3}$.

The resulting signal has three beating periods

$$T_B = \frac{2T_1T_2}{T_1 - T_2}; \quad T_B = \frac{2T_2T_3}{T_2 - T_3}; \quad T_B = \frac{2T_1T_3}{T_1 - T_3}$$

A.2 A Simple Application for the Building Studied

The use of this trigonometric analysis will help clarify the behavior observed in the building studied. From displacement response records of the building during the 1986 Mt. Lewis earthquake two apparent beating periods (16 and 100 seconds) and two equivalent natural periods (2.2 seconds for translational records and 1.85 seconds for torsional records) were present, Figs. A.4a and A.5a. From Equations A.2 and A.3 and using the 100 second beating period and the 2.2 seconds natural period, it can be estimated that the signals producing this effect have the following periods

$$T_1 = 2.25 \text{ seconds.}$$

$$T_2 = 2.15 \text{ seconds.}$$

These are reasonable estimates of the first two predominantly translational three-dimensional natural periods of the structure, as found from frequency domain studies.

These values are further corroborated by information obtained from torsional records. The average apparent first torsional period is 1.85 seconds, Fig. A.5a, and the beating period observed in the torsional record is approximately 16 seconds, Again, using Equations A.2 and A.3, the two periods of vibration that produce this behavior are calculated to be

$$T_1 = 2.09 \text{ seconds.}$$

$$T_2 = 1.66 \text{ seconds.}$$

Again these are reasonable estimates of the periods of a predominantly translational and a torsional mode of vibration, respectively. The translational period computed here would likely correspond to the value of 2.15 seconds computed earlier. The average could reasonably be taken as an estimate for this mode, considering the crudeness with which the beating periods were estimated from the records.

A reasonable conclusion is that the modulated displacement pattern exhibited by the building time histories mentioned, is the result of the beating of three modes with periods approximately equal to 2.2, 2.1 and 1.7 seconds.

A.3 Simulation of Structural Response.

Following a reverse procedure, time histories were generated using simple trigonometric time series and the results are compared with the measured response. To shape the generated response, a modified Bogdanoff amplitude envelope, as shown in Fig. A.3, was applied to simple harmonic waveforms. The equation of this envelope is as follows

$$amplitude(t) = \sqrt{2b}e^{(0.5-bt^2)} \tag{A.5}$$

where b controls the time of maximum amplitude (t_{max}) and the decay of the signal

$$b = \frac{1}{2t_{max}^2} \tag{A.6}$$

The recorded history that corresponds to the NS/r/W drift during the Mt. Lewis earthquake, Fig. A.4a, was first simulated using two trigonometric series having equal amplitudes of 1.0 and periods of 2.25 and 2.15 seconds. The amplitude of the resulting time series was modified with an envelope with constant b=0.000556 (t_{max}=30 sec., from Eq. A.6). Figure A.4b shows the resulting signal. The agreement with Fig. A.4a is good, considering the simple and restrictive model used. The apparent length of the beating period is difficult to reproduce because it is clearly affected by a third signal that produces the pattern seen near t=22 sec. If a third time series is added, with amplitude 0.2 and a period of 1.66 seconds, and maintaining the same envelope, the agreement is nearly perfect, as shown in Fig. A.4c.

The derived torsional time histories from EW displacement records, Fig. A.5a, again exhibit the high displacement levels in the first part of the records seen in Fig. A.4a showing the great effect that lateral-torsional coupling has on the displacement response. After that, a slowly decaying free torsional motion, affected by beating, occurs. The first part of the records is the effect of three signals and the second part mainly the effect of two signals. This record was simulated using two trigonometric series with periods of 2.1 and 1.66 seconds. The amplitude was modified again with an envelope with constant b=0.000556. Here, also, the agreement is particularly good, Fig. A.5b and c.

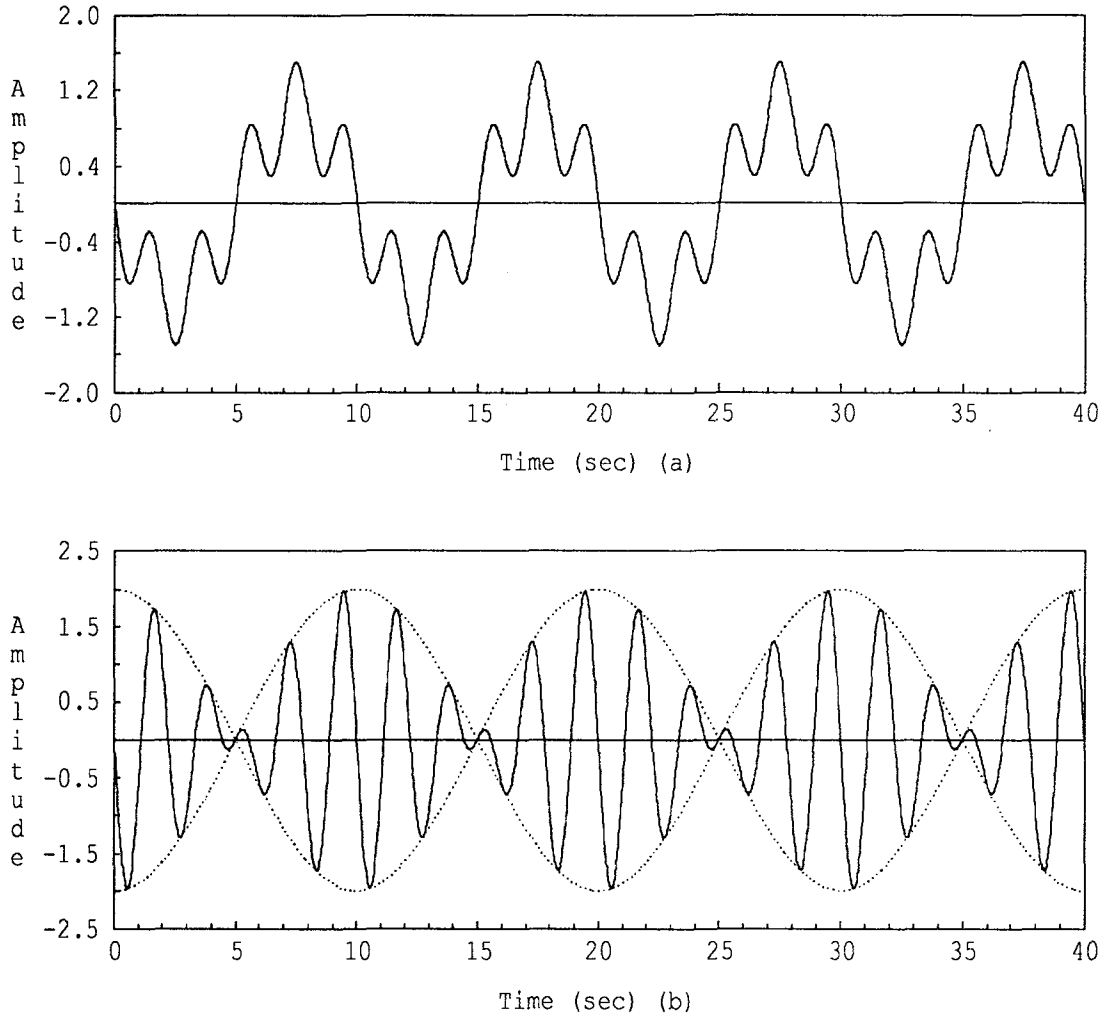

Figure A.1: Beating trigonometric time series. (a) Amplitudes 1.0 and 0.5. Period: 10.0 and 2.0 seconds. (b) Amplitudes 1.0 and 1.0. Period: 2.5 and 2.0 seconds.

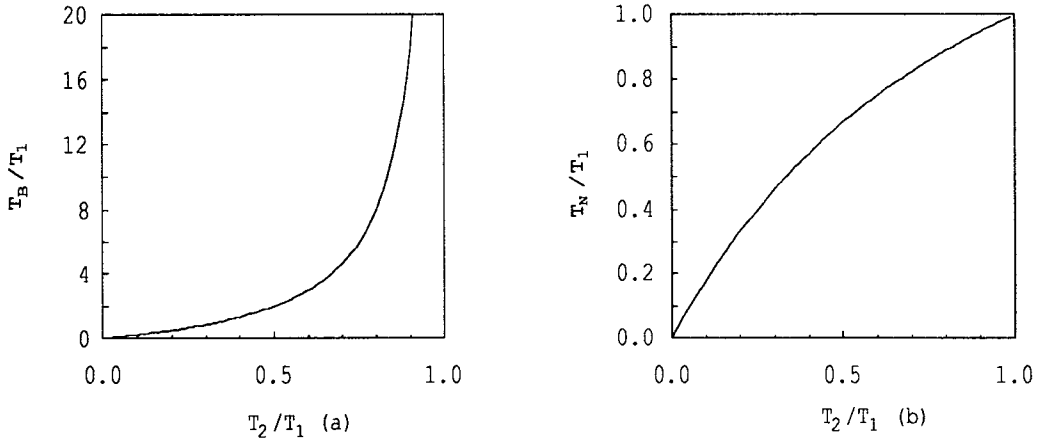

Figure A.2: (a) Relative beating period versus T_2/T_1.(b) Relative equivalent natural period versus T_2/T_1.

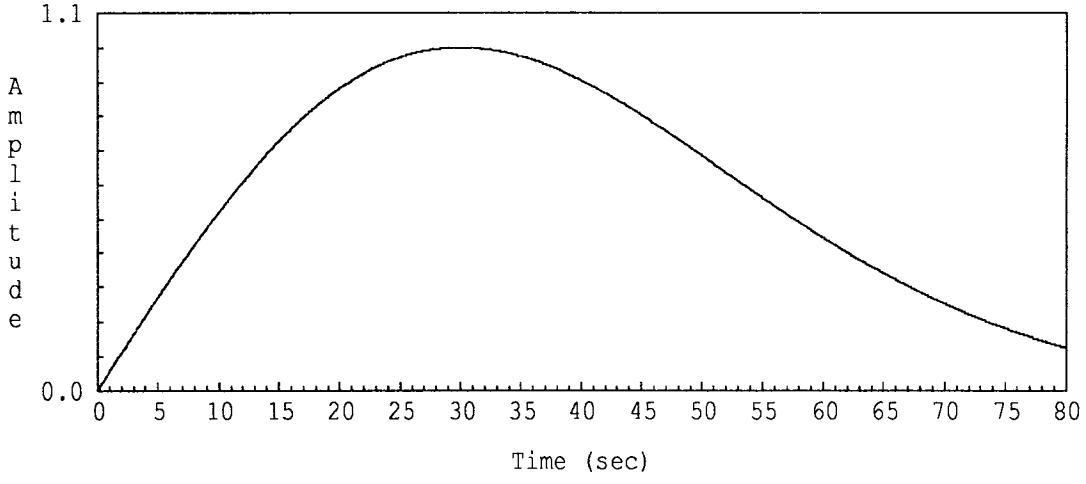

Figure A.3: Bogdanoff envelope (b=0.000556).

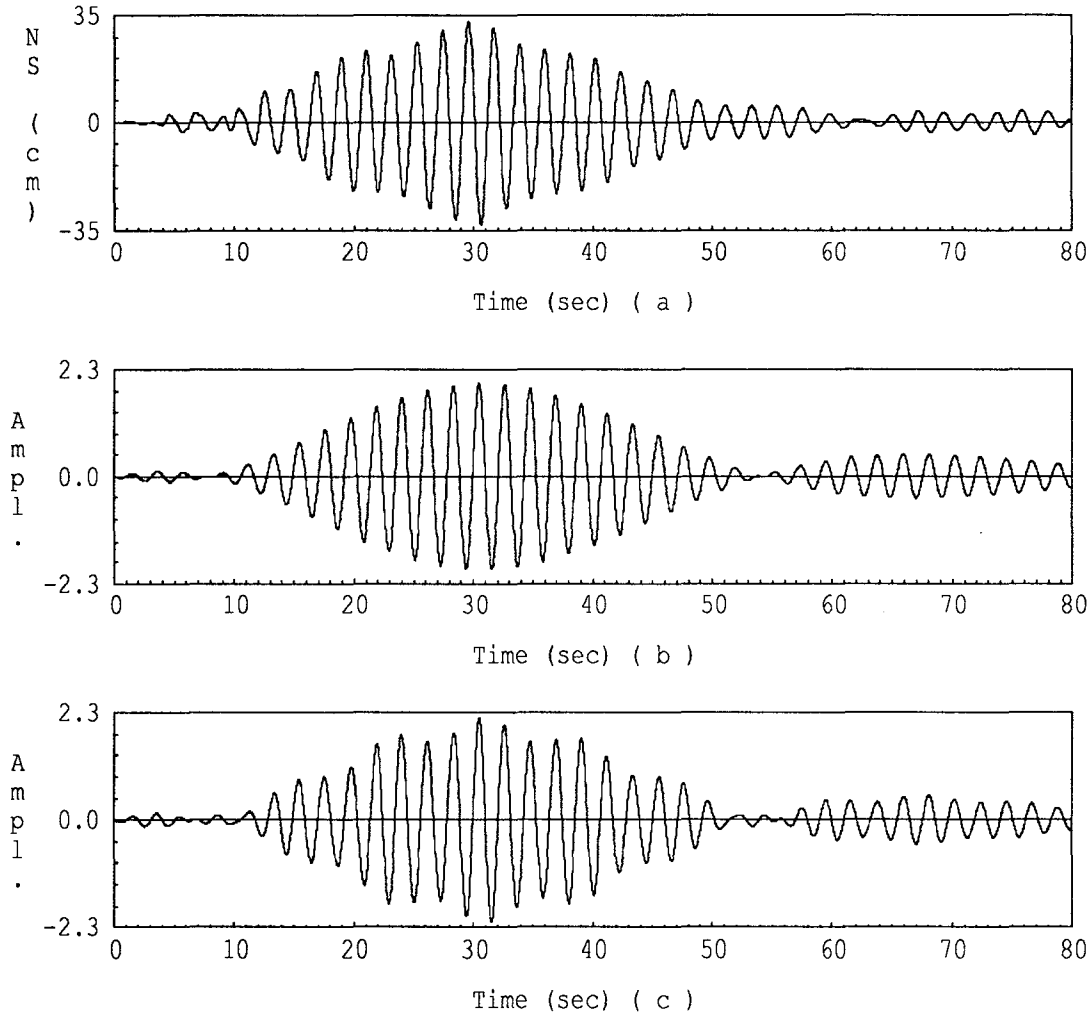

Figure A.4: (a) Building relative drift, NS/roof/W-NS/0/W. Mt. Lewis earthquake. (b) Simulation: two signal beating. Amplitudes: 1.0 and 1.0. Periods: 2.25 and 2.15. Envelope constant b=0.000556. (c) Simulation: three signal beating. Amplitudes: 1.0, 1.0 and 0.2. Periods: 2.25, 2.15 and 1.66. Envelope constant b=0.000556.

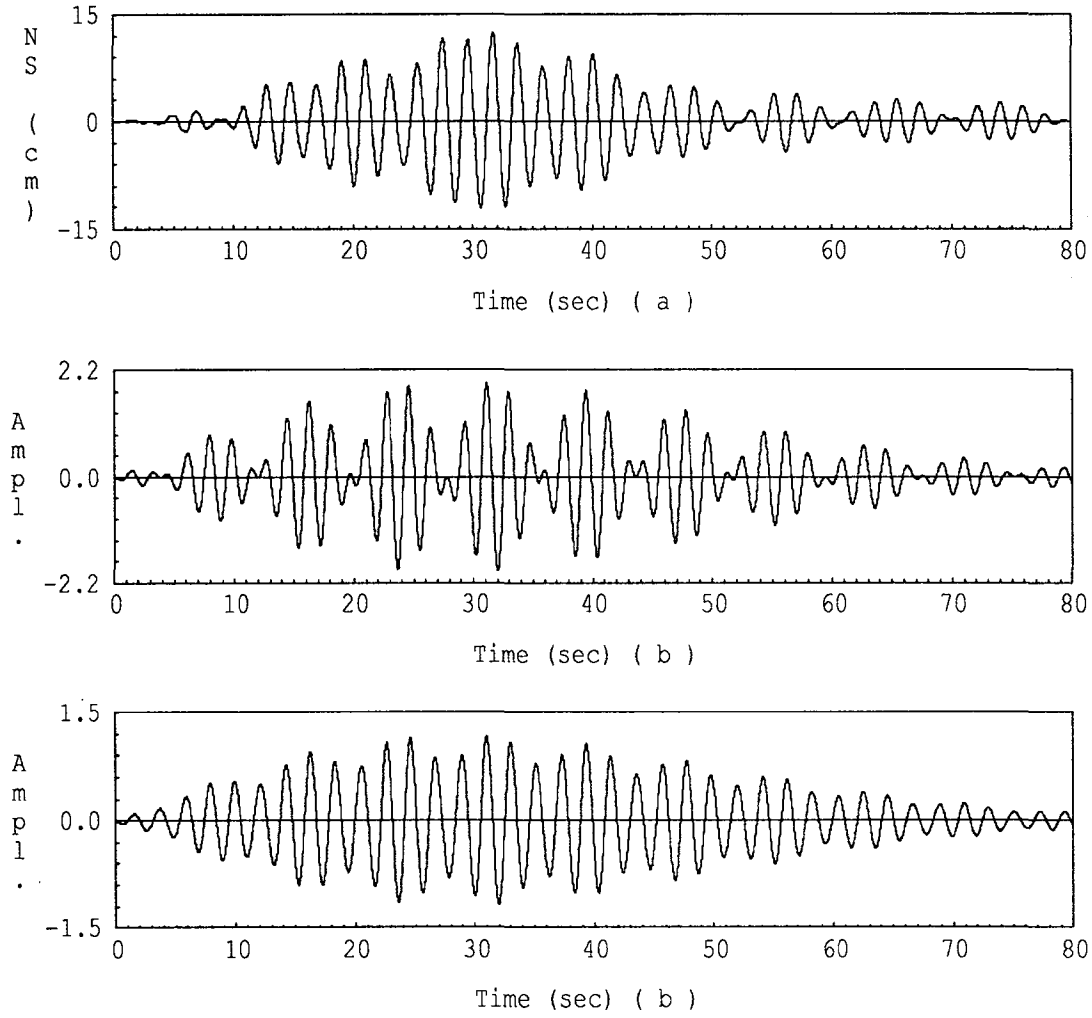

Figure A.5: (a) Building derived total roof torsion, EW/r/N-EW/r/S. Mt. Lewis earthquake. (b) Simulation: two signal beating. Amplitudes: 1.0 and 1.0. Periods: 2.1 and 1.66. Envelope constant b=0.0006. (c) Simulation: two signal beating. Amplitudes: 1.0 and 0.2. Periods: 2.1 and 1.66. Envelope constant b=0.0006.

Appendix B

TRANSLATIONAL TO TORSIONAL UNCOUPLED PERIOD RATIO FOR A ONE STORY SHEAR STRUCTURE

B.1 Introduction

It has been observed from actual buildings and mathematical models that the fundamental torsional and translational periods are often close for structures that have a uniform distribution of stiffness in plan [24, 41]. Uniform distribution of stiffness in plan is typically found in regular space frame structures.

A simple derivation is carried out to study the relation between torsional and translational periods for this type of structure. The solution will be presented for the case of a shear frame building having an odd number of columns in each direction of the structure. Similar results may be found for even, or for even and odd, numbers of columns.

The one-story shear structure must have the following characteristics :

(a) Multiple columns evenly distributed.

(b) Uniform distribution of mass.

(c) Coincident centers of mass and stiffness.

(d) All columns with the same stiffness in a given direction.

(e) Shear building behavior (no beam flexibility effects), with three degrees of freedom per story (two horizontal translations and one in-plane rotation at the center of mass).

(d) Negligible torsional stiffness for all vertical elements.

The notation used is as follows (see Fig. B.1):

$N_{x\ or\ y}$ is the number of column lines in the x or y direction. This value must be greater than one.

$d_{x\ or\ y}$ is the spacing between two consecutive columns in the X or Y direction.

$k_{x\ or\ y}$ is the stiffness of an individual column in the X or Y direction.

K_x is the total story translational stiffness in the X direction.

K_θ is the total story torsional stiffness.

T_{ux} is the uncoupled translational period in the X direction.

$T_{u\theta}$ is the uncoupled torsional period.

$k_{yx} = k_y/k_x$.

$n_{x\ or\ y} = (N_{x\ or\ y} - 1)/2$.

B.2 General Derivation

The story translational stiffness in the X direction and story rotational stiffness can be expressed as

$$K_x = N_x N_y k_x \tag{B.1}$$

and

$$K_\theta = \sum_{i=1}^{N_x N_y} (k_y x_i^2 + k_x y_i^2) = k_x \sum_{i=1}^{N_x N_y} (k_{yx} x_i^2 + y_i^2) \tag{B.2}$$

Because columns are located at regular spacing d_x or d_y

$$\sum_{i=1}^{N_x N_y} x_i^2 = 2N_y d_x^2 \sum_{i=1}^{n_x} i^2 = 2N_y d_x^2 n_x (n_x + 1)\frac{(2n_x + 1)}{6} \tag{B.3}$$

and

$$\sum_{i=1}^{N_x N_y} y_i^2 = 2N_x d_y^2 n_y (n_y + 1)\frac{(2n_y + 1)}{6} \tag{B.4}$$

Then, the story torsional stiffness can be expressed as

$$K_\theta = \frac{1}{3} k_x [k_{yx} N_y d_x^2 n_x (n_x + 1)(2n_x + 1) + N_x d_y^2 n_y (n_y + 1)(2n_y + 1)] \tag{B.5}$$

For a rectangular floor plan with uniform distribution of mass, the radius of gyration can be expressed as

$$r^2 = \frac{1}{12}[(N_x - 1)^2 d_x^2 + (N_y - 1)^2 d_y^2] \tag{B.6}$$

Then, from

$$\left(\frac{T_{ux}}{T_{u\theta}}\right)^2 = \frac{K_\theta}{r^2 K_x} \tag{B.7}$$

and substituting Equations B.1, B.5 and B.6 in B.7

$$\left(\frac{T_{ux}}{T_{u\theta}}\right)^2 = 4\frac{[k_{yx} N_y d_x^2 n_x (n_x + 1)(2n_x + 1) + N_x d_y^2 n_y (n_y + 1)(2n_y + 1)]}{N_x N_y [(N_x - 1)^2 d_x^2 + (N_y - 1)^2 d_y^2]} \tag{B.8}$$

Noting that

$$n_x = \frac{(N_x - 1)}{2} \; ; \; (n_x + 1) = \frac{(N_x + 1)}{2} \; ; \; (2n_x + 1) = N_x \tag{B.9}$$

and similar expressions for n_y and N_y, then

$$\left(\frac{T_{ux}}{T_{u\theta}}\right)^2 = \frac{[(d_x/d_y)^2 (k_y/k_x)(N_x{}^2 - 1) + (N_y{}^2 - 1)]}{(N_x - 1)^2 (d_x/d_y)^2 + (N_y - 1)^2} \tag{B.10}$$

B.3 Special Type of Building

For the special case of buildings with the same number of columns and column stiffness in the principal directions this formula can be simplified as follows:

$N_x = N_y = N$, and $k_x = k_y$,

so that

$$\left(\frac{T_{ux}}{T_{u\theta}}\right)^2 = \frac{(N+1)}{(N-1)} \tag{B.11}$$

It can be seen in Fig. B.2 that this ratio quickly approaches unity as the number of columns increases.

For multiple story shear structures, with identical floor characteristics on all levels and the restrictions shown above, the same formulae apply for each group of modes (i.e. for the first translational and torsional modes, for the second translational and torsional modes, etc.). Also, because these formulae apply to this type of structure, the ratio of the translational to torsional uncoupled periods is the same for all groups of modes.

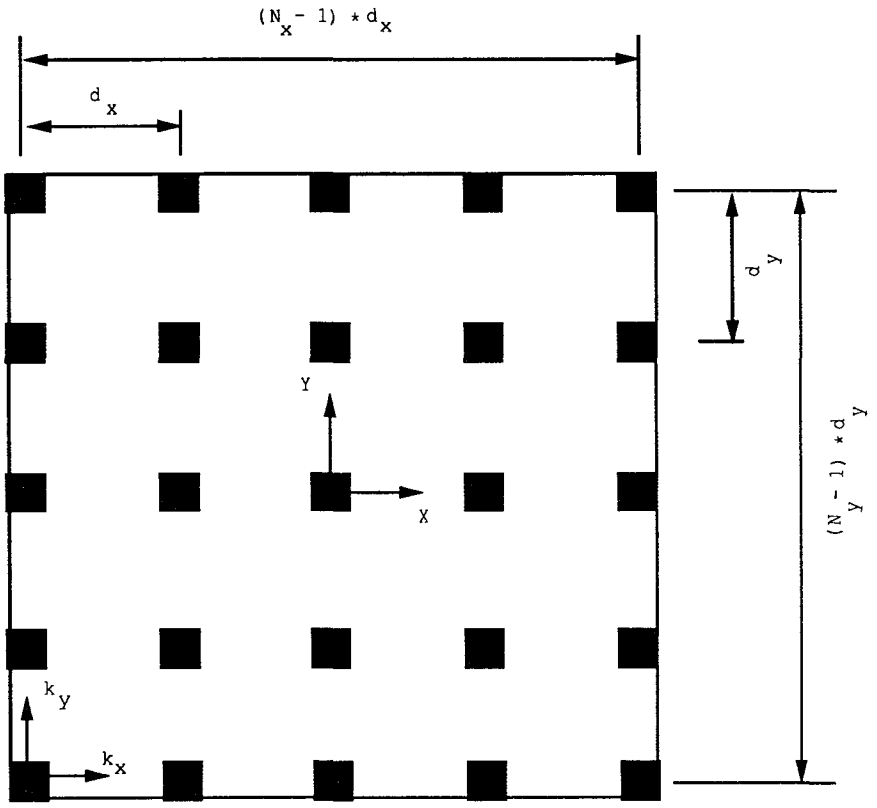

Figure B.1: One story frame plan.

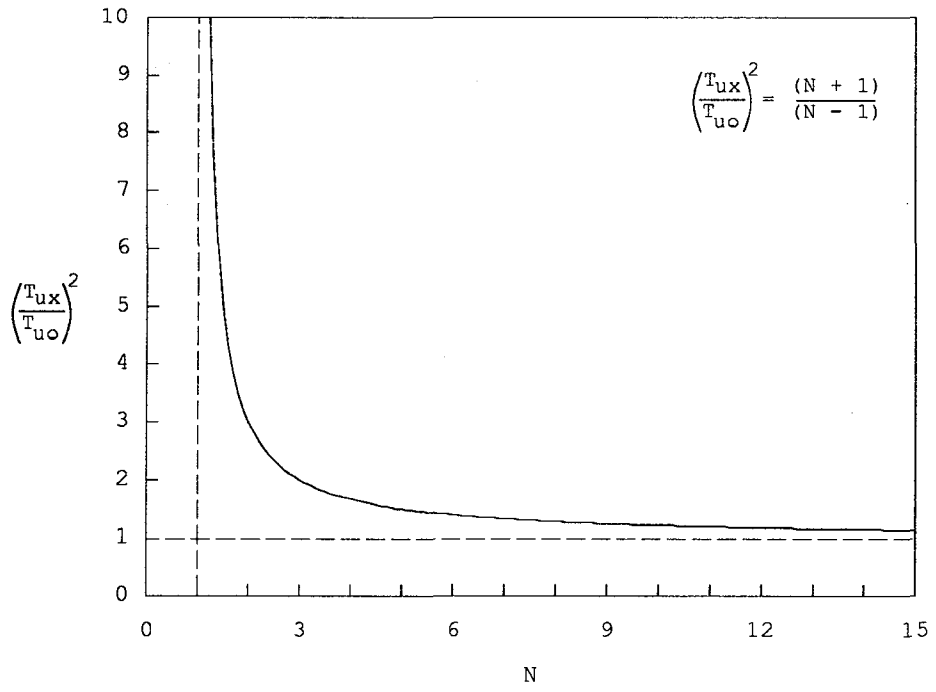

Figure B.2: Ratio of uncoupled translational and torsional periods for a regular one-story structure.

Appendix C

DAMPING EFFECTS ON NONLINEAR STRUCTURES

C.1 General

An attempt is made to evaluate the effect of viscous damping on the response characteristics of one degree-of-freedom nonlinear oscillators, by studying the variation of selected response parameters to variable amounts of viscous damping. The effect of damping on linear oscillators has been studied extensively; see for example Refs. [16, 19, 39, 51].

A modified version of the program NONSPEC [32] was used to compute the inelastic responses. The oscillators considered had elasto-perfectly-plastic (EPP) hysteretic curves. Eleven earthquake records were used in the studies, six on relatively firm soils and five on relatively soft soils; see Table C.1 for a list of ground motions. Linear response spectra for the records and different amounts of viscous damping are presented in Figs. C.1 and C.2. Viscous damping values studied were 0, 1, 2, 5, 10, 20, 40, 80% of critical. Several system capacities were considered. The capacity of the system relative to the earthquake intensity was defined by the nondimensional parameter η (eta) as follows [32]:

$$\eta = \frac{V_y}{M\ PRA} \tag{C.1}$$

where V_y is the yield shear, M is the mass of the system and PRA is the peak record acceleration. Values of η of 2.0, 1.0, 0.8, 0.4, 0.2 were considered in the analyses.

The following parameters were used to evaluate the effect of viscous damping on the response of nonlinear oscillators.

- Maximum displacement ductility demand:

$$\mu_d = \frac{\Delta_{max}}{\Delta_y} \tag{C.2}$$

  where Δ_{max} is the maximum displacement and Δ_y is the yield displacement of the system. This parameter is a measure of the maximum inelastic deformation of the system.

- The maximum cumulative ductility:

$$\mu_c = \sum_j \frac{|\Delta_{inelastic}|_j}{\Delta_y} + 1 \tag{C.3}$$

where $|\Delta_{inelastic}|_j$ is the absolute inelastic displacement at time step j. This definition implies that if the oscillator responds only in the elastic range μ_c has a value of one. This parameter is a good measure of the total hysteretic energy dissipated by EPP systems.

- Sum of the squared accelerations:

$$A^2 = \sum a_i^2 \delta t_i \tag{C.4}$$

where a_i is the acceleration at step i and δt_i is the time step at step i. This is an indicator of the response envelope characteristics (amplitude and duration) and the base for the definition of apparent duration presented below.

- Apparent strong motion duration ($\mathcal{T}$):
Defined as the elapsed time between 5% and 95% of A^2. This definition of strong motion duration has been used previously for ground records by Trifunac and Brady [49] among others, and has given reasonable results. A more detailed description of the procedure can be found in Reference [49].

C.2 Results

To evaluate the effect of viscous damping the nonlinear response spectra for twenty different periods, five capacity values and eight damping values were first obtained. For example, Figures C.3 to C.8. present the 5% of critical viscous damping nonlinear response spectra for the different parameters studied. Next, all spectra were normalized with respect to their respective 0% of critical viscous damping spectra. Finally, the variation of the selected parameter was plotted against the amount of viscous damping. No averaging over the different records was computed. Normalized spectra for each individual record are shown in Figs. C.11 to C.22, for the parameters studied (μ_d, μ_c, $A^2$and $\mathcal{T}$) as functions of damping. Two sets of plots are presented for each spectra: (1) Figures where all capacity values are plotted together differentiated only by undamped periods (0.5, 2.0 and 3.0 seconds) and soil conditions. (2) Figures where two selected undamped periods (0.5 and 2.0 seconds) are plotted for all records (firm soils, [solid lines] and soft soils, [dotted lines], i.e., there are 6 solid and 5 dotted lines in each of these figures) and selected capacities (0.2, 0.8, 1.0, 2.0).

The results are summarized as follows.

1. Figures C.11 to C.13 present the normalized spectra for maximum ductility demands. These plots show the following:

- The displacement ductility (and displacements) demand decreases with increasing amount of viscous damping.
- The decay rates for firm and soft soils are similar with more dispersion on values for firm soil records, Fig. C.11.
- For oscillators with relatively short periods (with respect to the earthquake predominant period) and low capacities, the reduction of the response due to damping was larger for soft than for firm soils. For high strength capacity values, the reduction is larger for firm than for soft soils, Fig. C.12.

  For longer periods, the ratio tends to be the same for both soil types, but larger dispersions are found for the firm soil records, Fig. C.13.
- The incremental effect of viscous damping is strong between 0 and 30% of critical.

2. Figures C.14 to C.16 present the normalized spectra for cumulative ductility demands. The horizontal lines observed in these figures correspond to the cases in which the system, with viscous damping, responded elastically (i.e., the value of μ_c is one); so the normalized value shown is the inverse of μ_c for the the case of 0% viscous damping. These plots show the following:

   - This parameter decays with increasing amount of viscous damping.
   - The decay rates for firm and soft soils are similar. As expected, systems with larger periods tend to behave linearly for most of the firm soil records, Fig. C.14.
   - The incremental effect of viscous damping is strong between 0 and 30% of critical. For the majority of the cases studied, a value of viscous damping higher than 40% tends to produce linear responses for systems in the displacement controlled region of the spectrum (i.e. for system periods larger than the predominant period of the records), Figs. C.15 and C.16.

3. Figures C.17 to C.19 present the normalized spectra for the sum of the squared accelerations. These plots show the following:

   - This parameter can either decay or increase with increasing amounts of viscous damping, Fig. C.17. An explanation for this is that, for large amounts of viscous damping, a considerable portion of the inertial forces is resisted by damping forces. This increase in damping force limits yielding and allows higher accelerations to occur in the system.
   - The rate of change of the sum of the squared accelerations with viscous damping was typically smaller for soft soils than for firm soils. For some records first a decrease and later an increase of the ratio was observed with increasing amounts of viscous damping.

- Large dispersion of the parameter for the different records is observed from these figures.
- Viscous damping has its strongest effect between 0 and 20% of critical for most records.

4. Figures C.20 to C.22 present the normalized spectra for strong motion duration. These plots show the following:

   - This parameter generally, but not always, decreases with increasing amounts of viscous damping. The effect of damping in the different records, Fig. C.20, varies considerably.
   - Damping has a significant effect especially between 0 and 10% of critical, and the ratios for soft soils tend to be slightly higher than for firm soils.

It can generally be concluded from this parametric study that there is a critical value of viscous damping after which an increase in the parameter does not affect the response very much. This value is between 20 and 30% for maximum ductility and cumulative ductility, between 10 and 20% for the sum of squared accelerations and about 10% for strong motion duration. A single value for all parameters studied would be 30% of critical.

Table C.1: **Earthquake Records**

Earthquake	Year	Recording Station	Component	Peak Accel. (g)	Soil Type*
Imperial Valley	1940	El Centro	NS	0.34	firm
Western Washington	1949	Olympia	N86E	0.28	firm
Kern County	1952	Taft	S69E	0.18	firm
Santa Cruz Mountains	1989	Corralitos	NS	0.64	firm
Santa Cruz Mountains	1989	Capitola	EW	0.47	firm
Santa Cruz Mountains	1989	Santa Cruz	EW	0.44	firm
Santa Cruz Mountains	1989	Oakland Wharf	305°	0.27	soft
Santa Cruz Mountains	1989	CSMIP 57357	Channel 22	0.10	soft
Morgan Hill	1984	CSMIP 57357	Channel 22	0.04	soft
Mexico	1985	SCT	N90W	0.17	soft
Mt. Lewis	1986	CSMIP 57357	Channel 22	0.04	soft

* Classification was based on record predominant period.

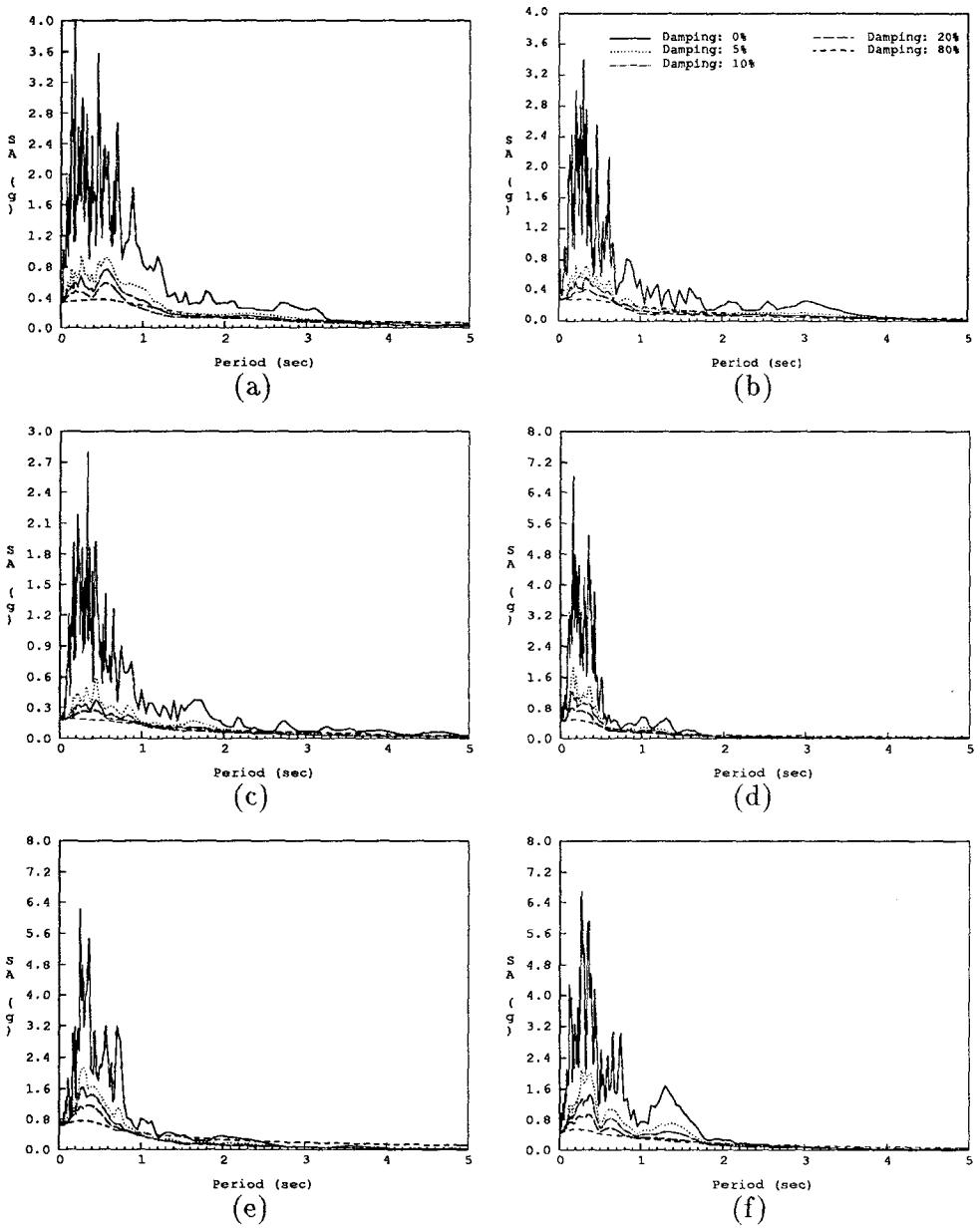

Figure C.1: Linear response spectra, firm soils. (a) El Centro NS 1940. (b) Olympia N86E 1949. (c) Taft S69E 1952. (d) Santa Cruz EW, Santa Cruz Mountains, Loma Prieta 1989. (e) Corralitos NS, Santa Cruz Mountains, Loma Prieta 1989. (f) Capitola EW, Santa Cruz Mountains, Loma Prieta 1989.

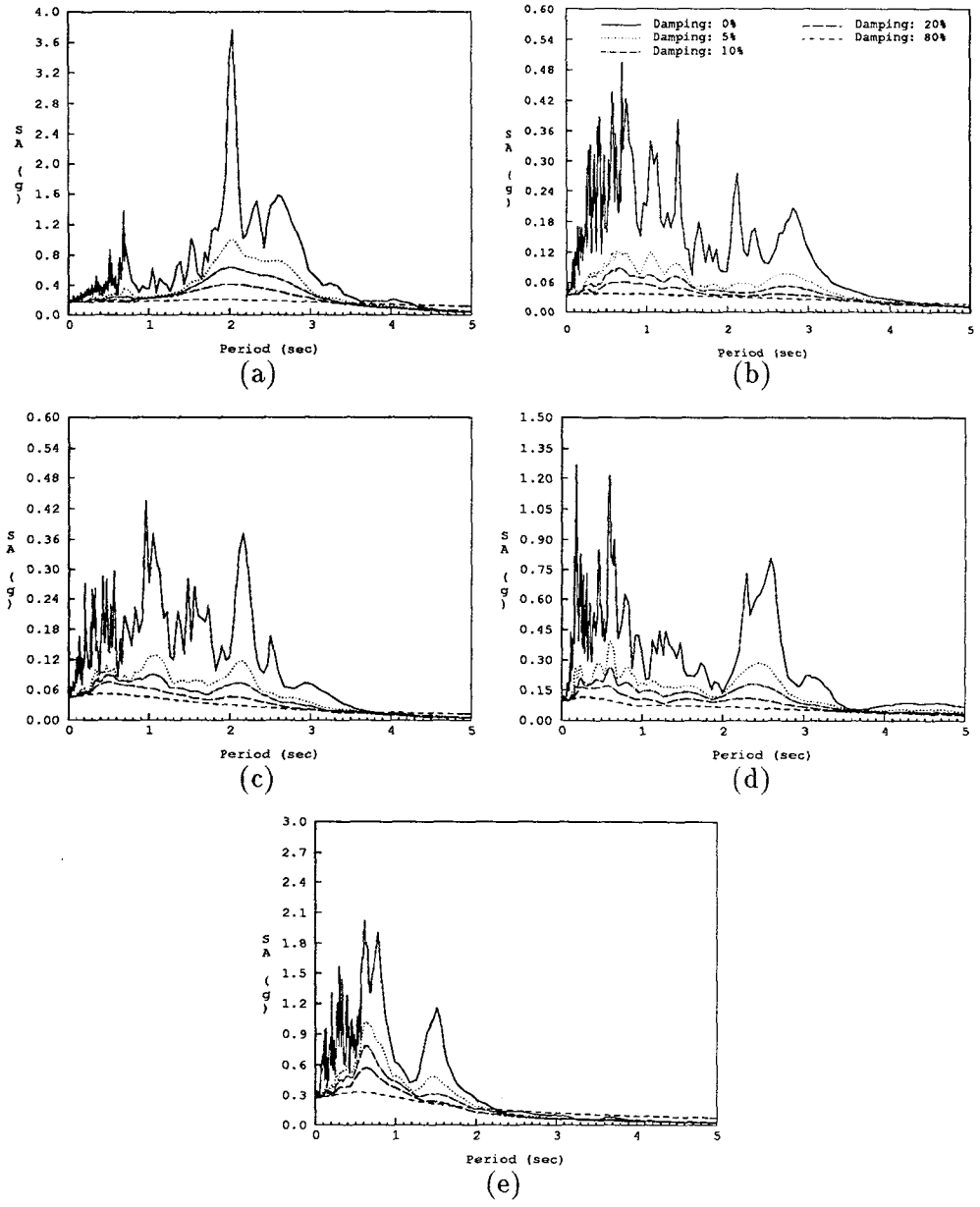

Figure C.2: Linear response spectra, soft soils. (a) SCT Transverse Mexico 1985. (b) CSMIP Station 57357, NS, Morgan Hill 1984. (c) CSMIP Station 57357, NS, Mt. Lewis 1986. (d) CSMIP Station 57357, NS, Santa Cruz Mountains, Loma Prieta 1989. (e) Oakland Wharf, 305 Deg, Santa Cruz Mountains, Loma Prieta 1989.

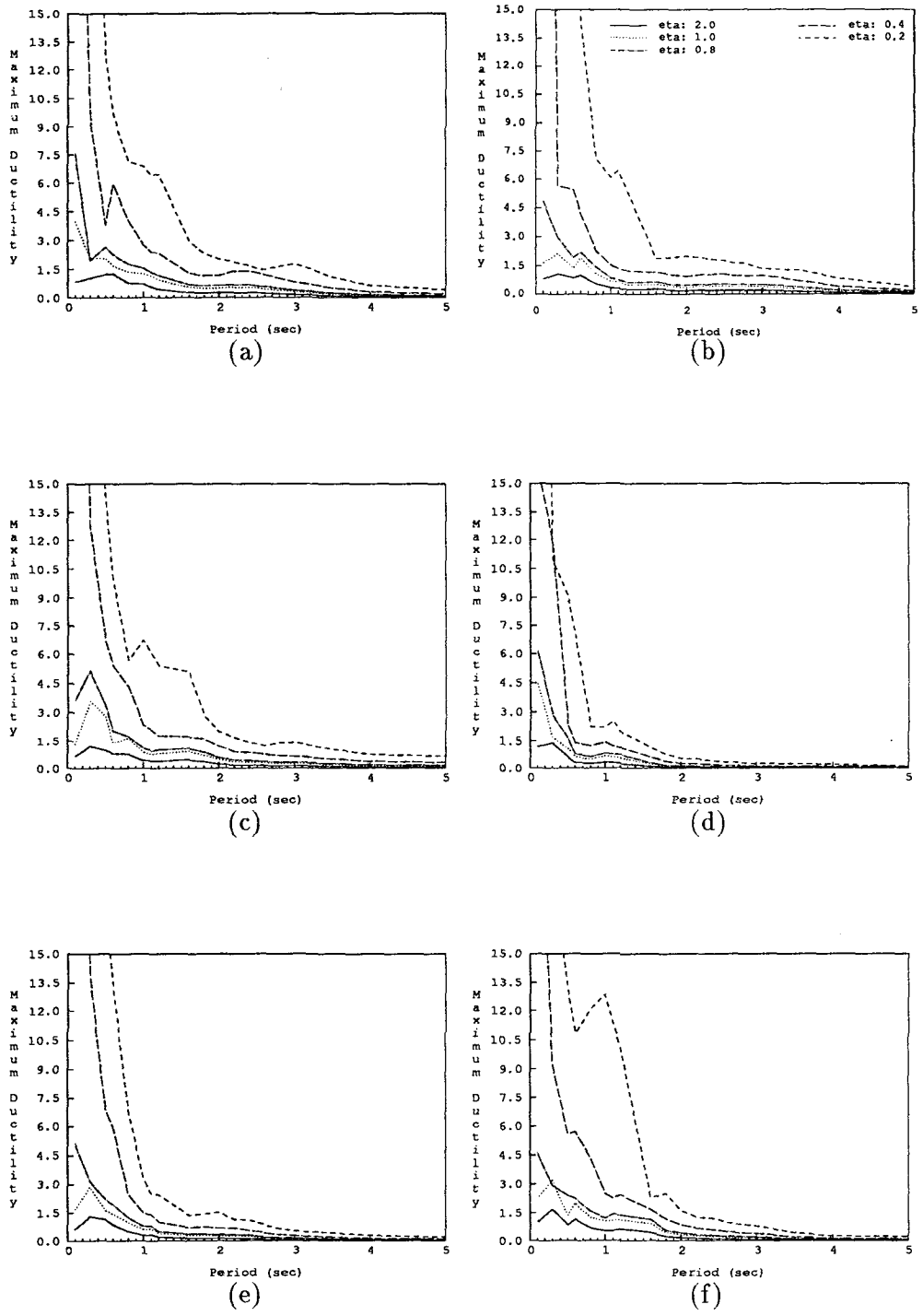

Figure C.3: Maximum ductility demand, firm soils, 5% damping. (a) El Centro NS 1940. (b) Olympia N86E 1949. (c) Taft S69E 1952. (d) Santa Cruz EW, Santa Cruz Mountains, Loma Prieta 1989. (e) Corralitos NS, Santa Cruz Mountains, Loma Prieta 1989. (f) Capitola EW, Santa Cruz Mountains, Loma Prieta 1989.

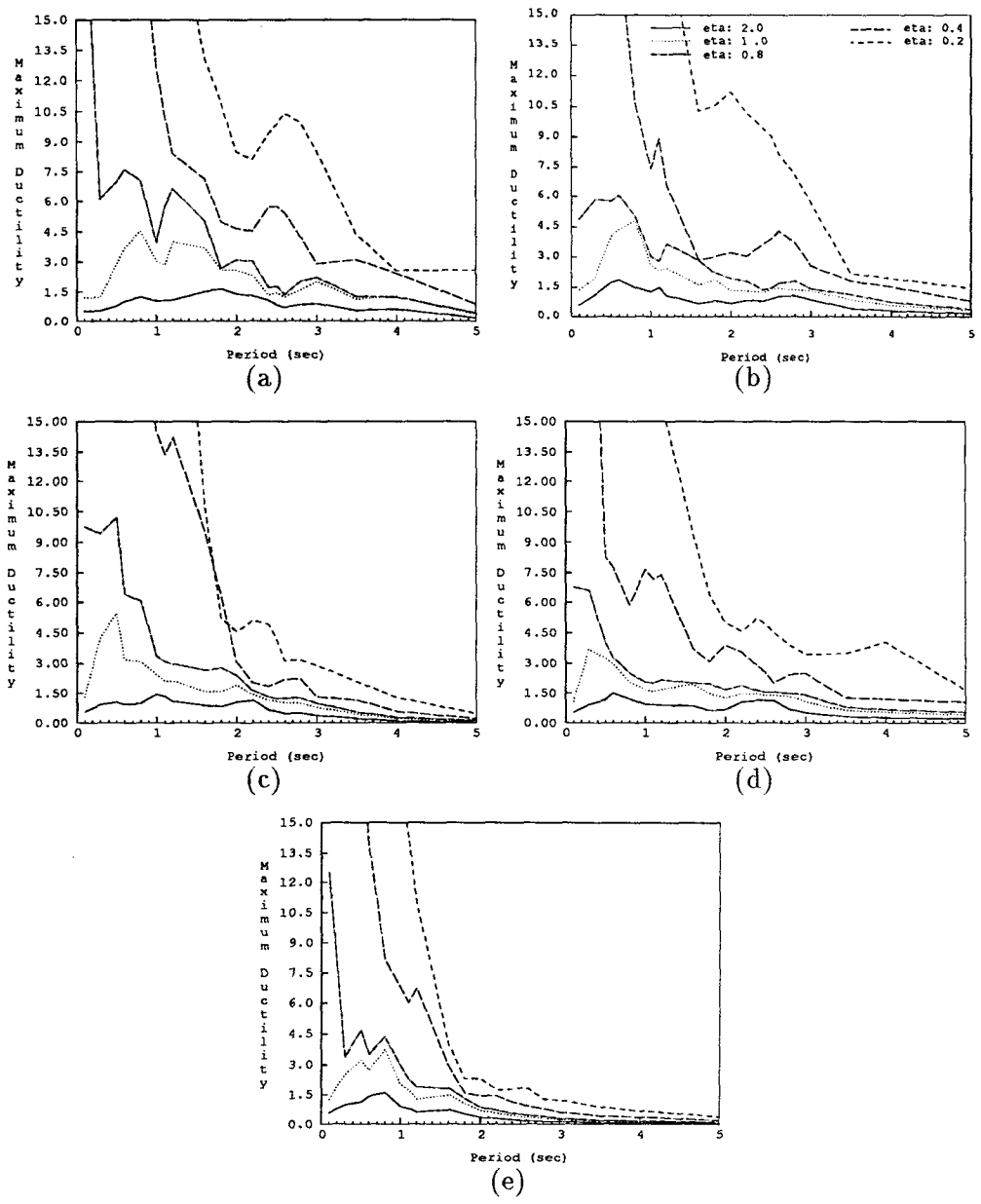

Figure C.4: Maximum ductility demand, soft soils, 5% damping. (a) SCT Transverse Mexico 1985. (b) CSMIP Station 57357, NS, Morgan Hill 1984. (c) CSMIP Station 57357, NS, Mt. Lewis 1986. (d) CSMIP Station 57357, NS, Santa Cruz Mountains, Loma Prieta 1989. (e) Oakland Wharf, 305 Deg, Santa Cruz Mountains, Loma Prieta 1989.

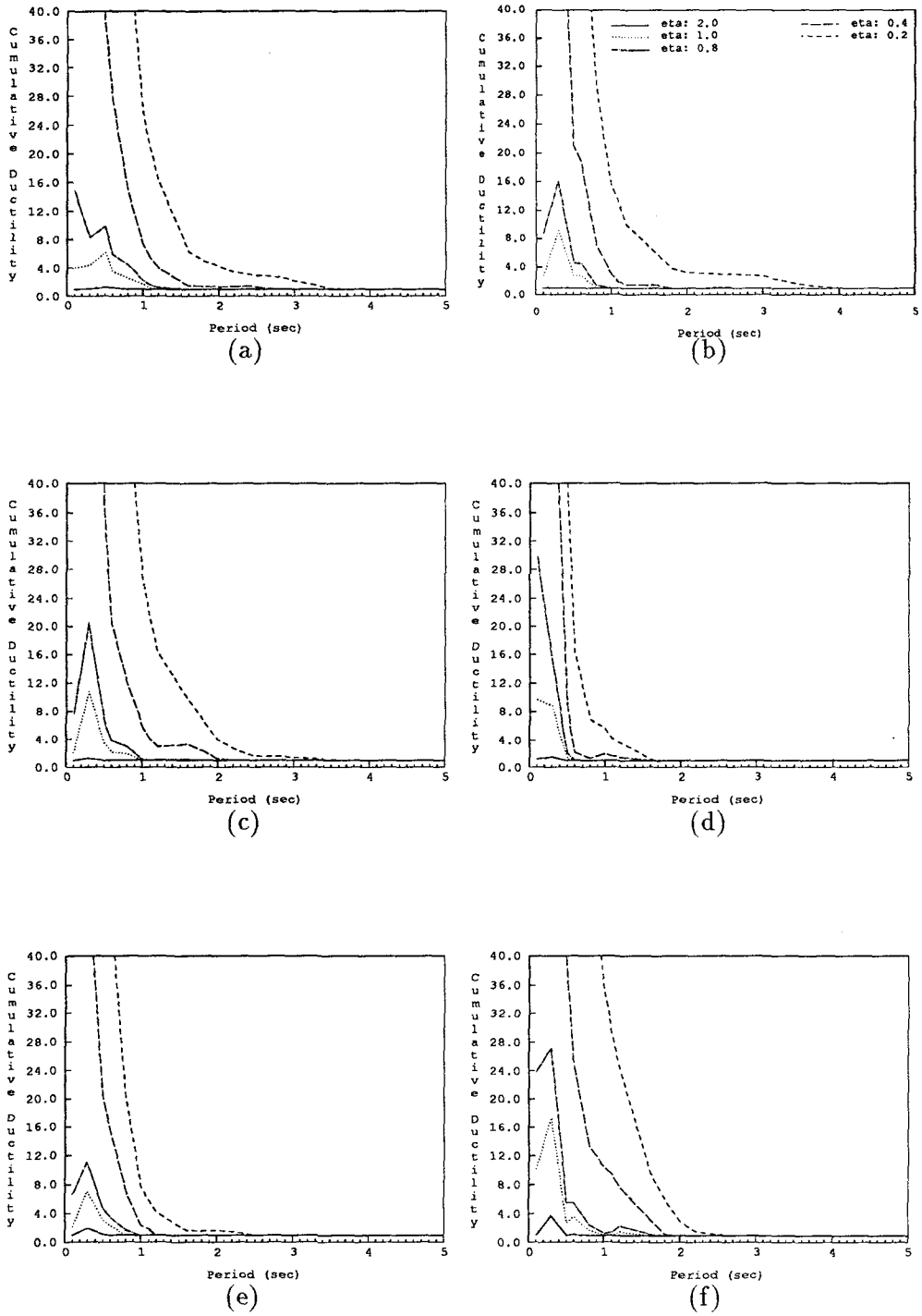

Figure C.5: Cumulative ductility demand, firm soils, 5% damping. (a) El Centro NS 1940. (b) Olympia N86E 1949. (c) Taft S69E 1952. (d) Santa Cruz EW, Santa Cruz Mountains, Loma Prieta 1989. (e) Corralitos NS, Santa Cruz Mountains, Loma Prieta 1989. (f) Capitola EW, Santa Cruz Mountains, Loma Prieta 1989.

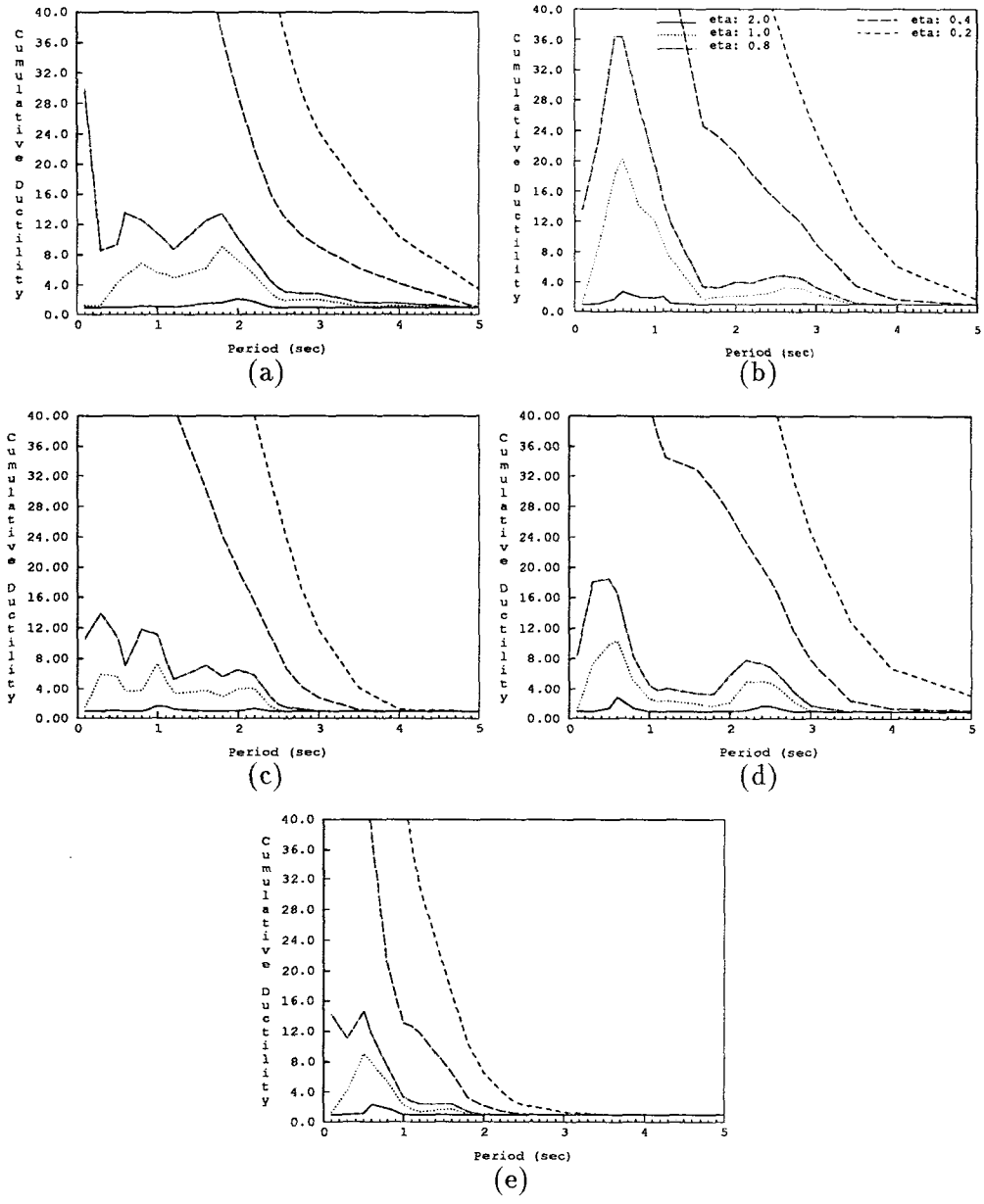

Figure C.6: Cumulative ductility demand, soft soils, 5% damping. (a) SCT Transverse Mexico 1985. (b) CSMIP Station 57357, NS, Morgan Hill 1984. (c) CSMIP Station 57357, NS, Mt. Lewis 1986. (d) CSMIP Station 57357, NS, Santa Cruz Mountains, Loma Prieta 1989. (e) Oakland Wharf, 305 Deg, Santa Cruz Mountains, Loma Prieta 1989.

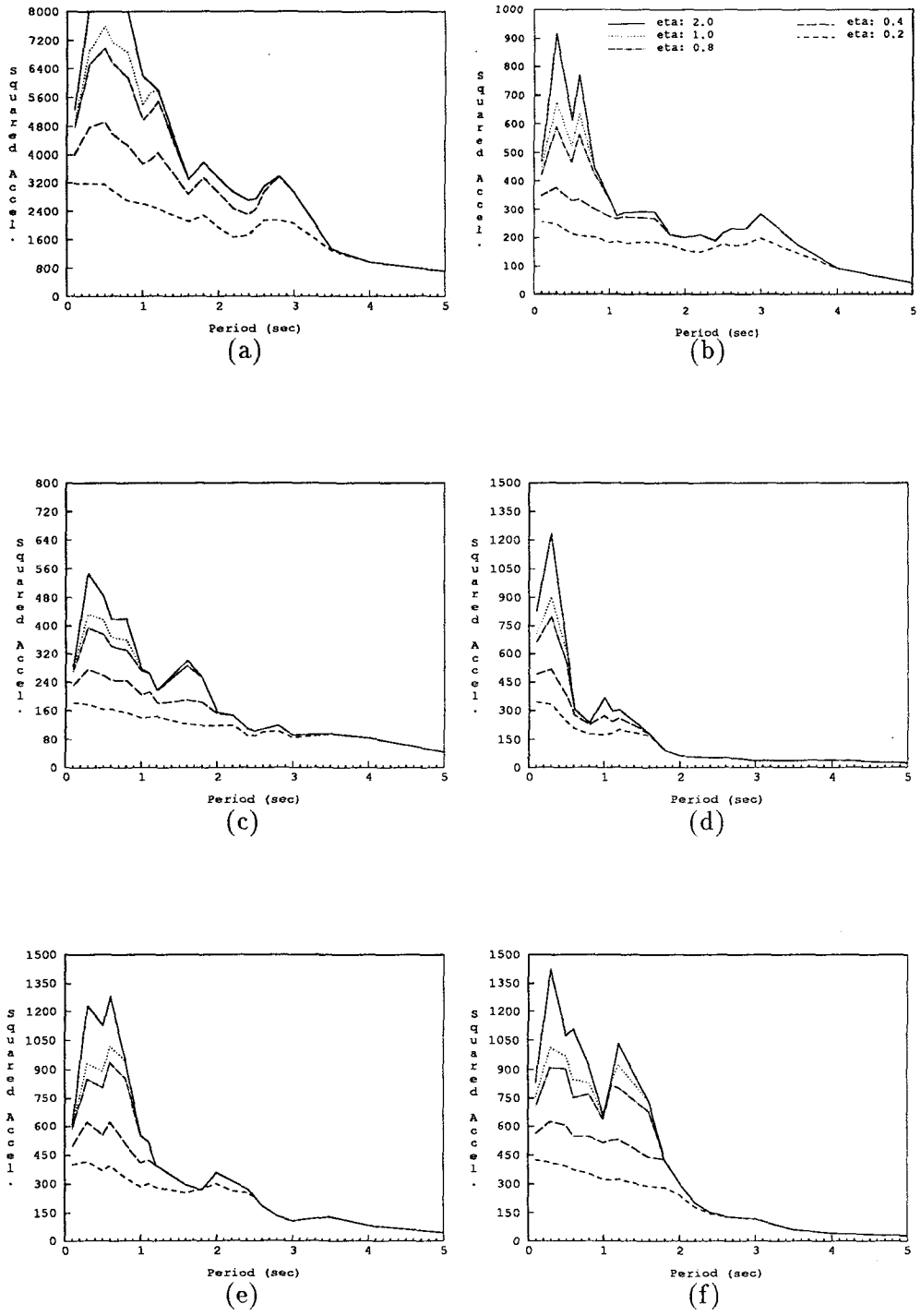

Figure C.7: Squared Acceleration, firm soils, 5% damping. (a) El Centro NS 1940. (b) Olympia N86E 1949. (c) Taft S69E 1952. (d) Santa Cruz EW, Santa Cruz Mountains, Loma Prieta 1989. (e) Corralitos NS, Santa Cruz Mountains, Loma Prieta 1989. (f) Capitola EW, Santa Cruz Mountains, Loma Prieta 1989.

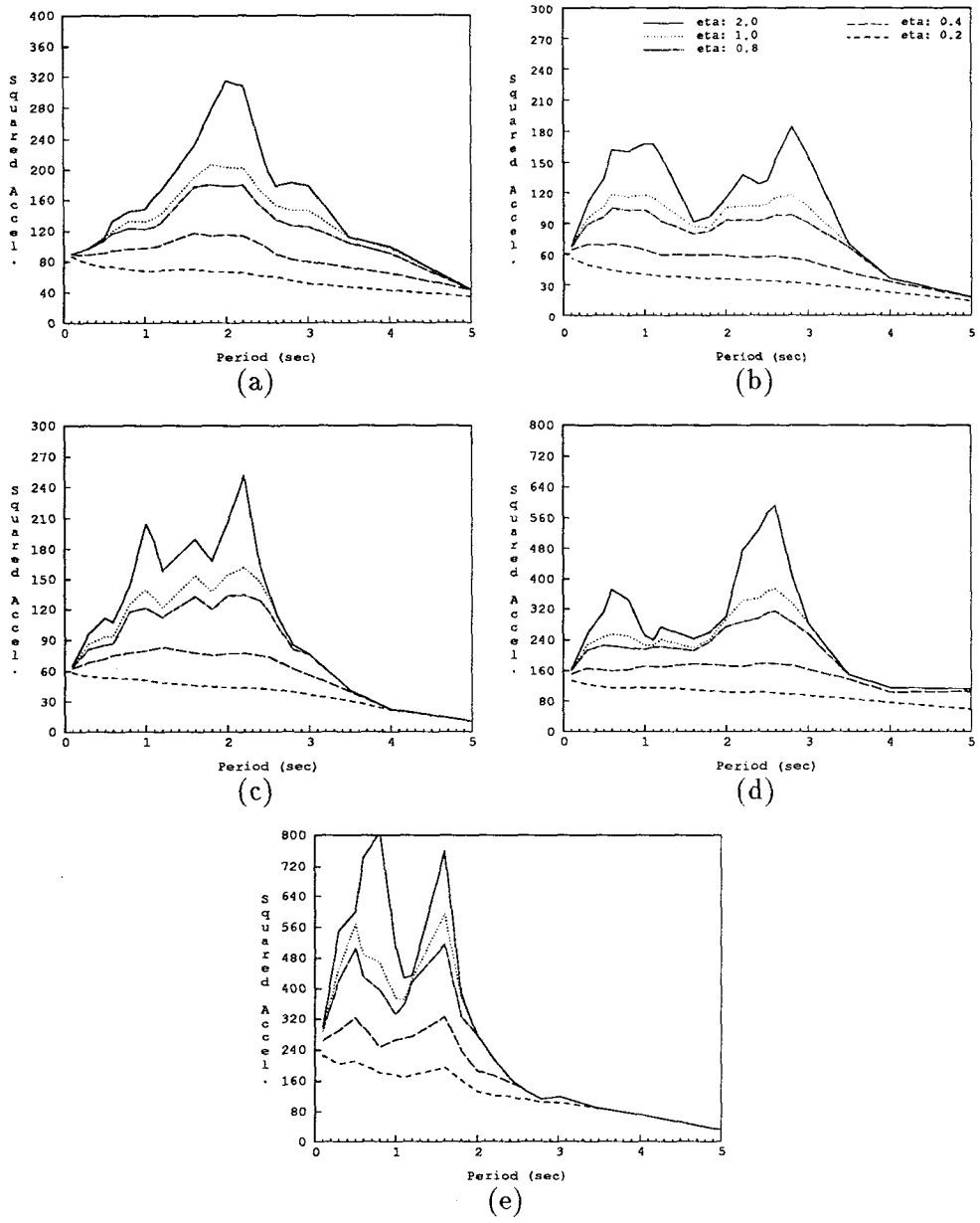

Figure C.8: Squared Acceleration, soft soils, 5% damping. (a) SCT Transverse Mexico 1985. (b) CSMIP Station 57357, NS, Morgan Hill 1984. (c) CSMIP Station 57357, NS, Mt. Lewis 1986. (d) CSMIP Station 57357, NS, Santa Cruz Mountains, Loma Prieta 1989. (e) Oakland Wharf, 305 Deg, Santa Cruz Mountains, Loma Prieta 1989.

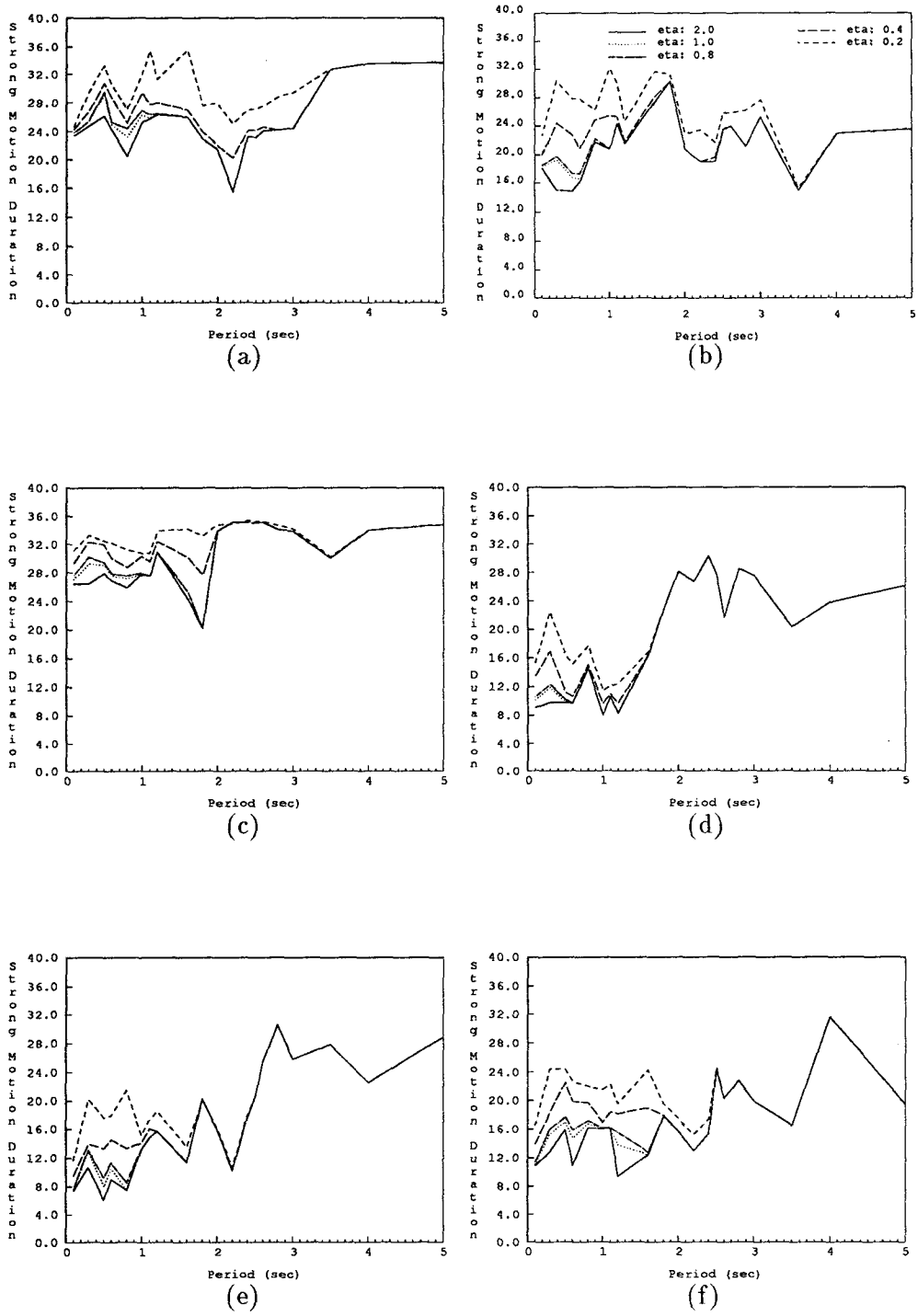

Figure C.9: Strong Motion Duration, firm soils, 5% damping. (a) El Centro NS 1940. (b) Olympia N86E 1949. (c) Taft S69E 1952. (d) Santa Cruz EW, Santa Cruz Mountains, Loma Prieta 1989. (e) Corralitos NS, Santa Cruz Mountains, Loma Prieta 1989. (f) Capitola EW, Santa Cruz Mountains, Loma Prieta 1989.

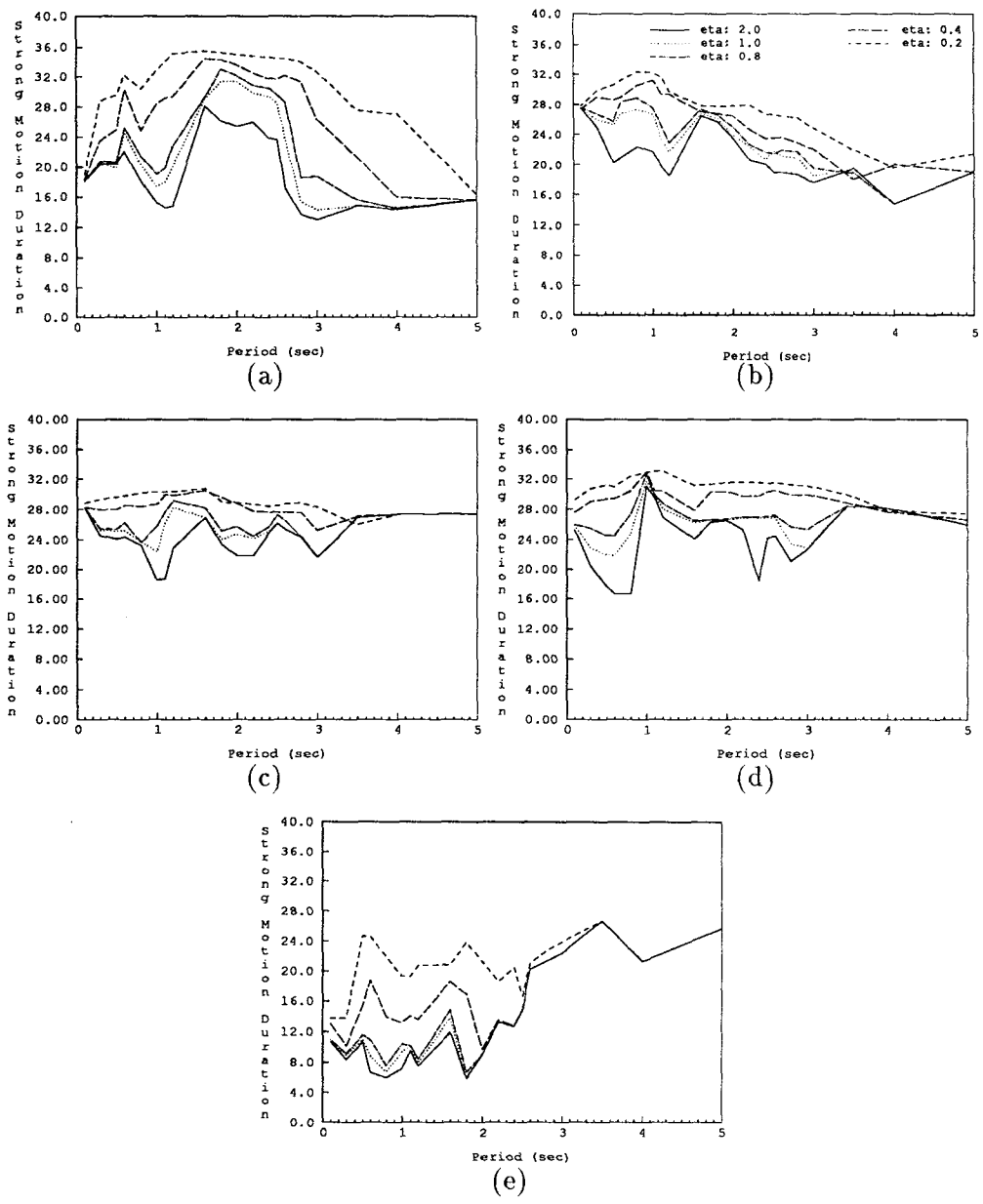

Figure C.10: Strong Motion Duration, soft soils, 5% damping. (a) SCT Transverse Mexico 1985. (b) CSMIP Station 57357, NS, Morgan Hill 1984. (c) CSMIP Station 57357, NS, Mt. Lewis 1986. (d) CSMIP Station 57357, NS, Santa Cruz Mountains, Loma Prieta 1989. (e) Oakland Wharf, 305 Deg, Santa Cruz Mountains, Loma Prieta 1989.

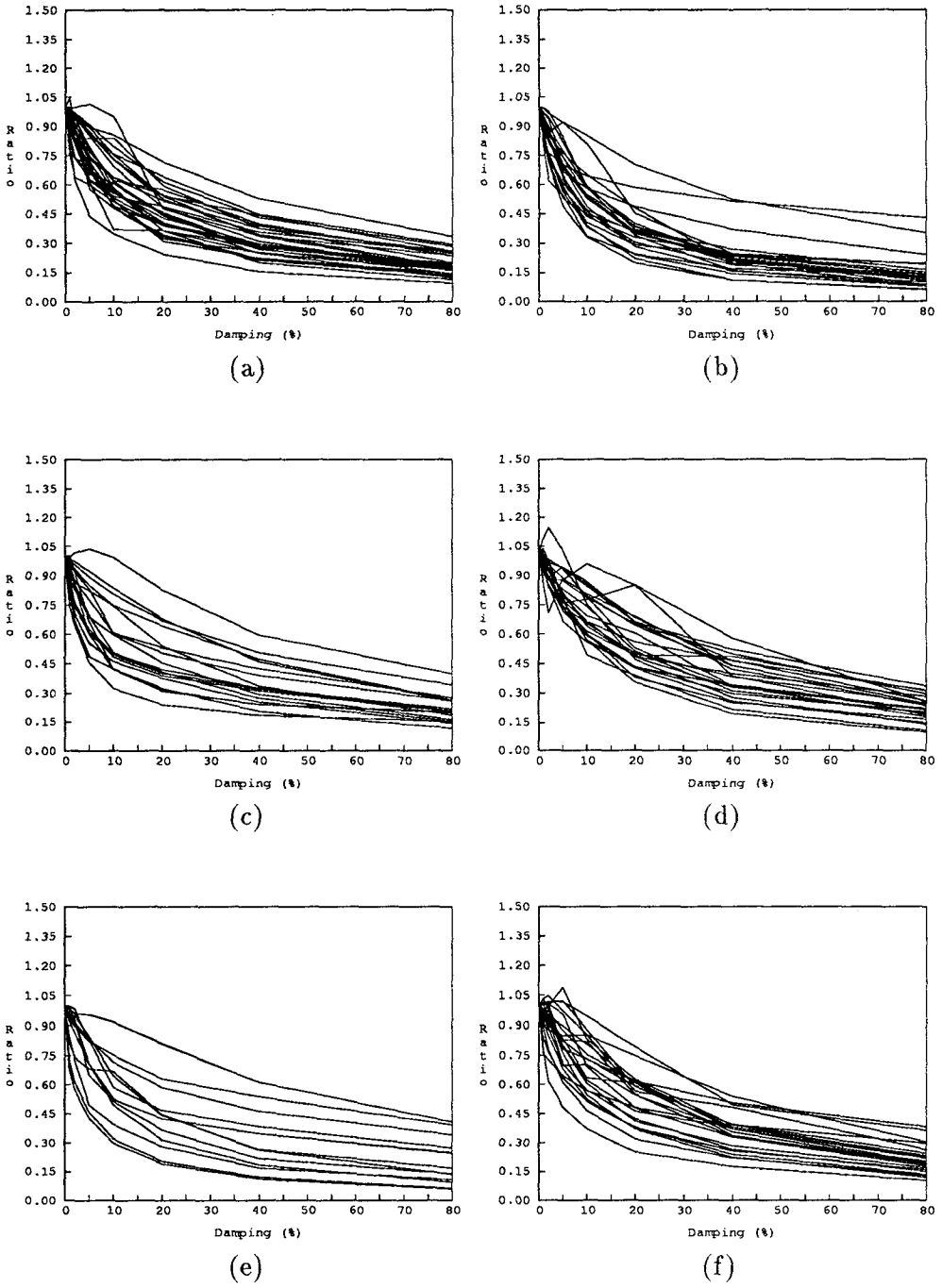

Figure C.11: Damping effect on maximum ductility demand. All yield capacities (η), all records. (a) Period 0.5 sec. Hard Soils. (b) Period 0.5 sec. Soft Soils. (c) Period 2.0 sec. Hard Soils. (d) Period 2.0 sec. Soft Soils. (e) Period 3.0 sec. Hard Soils. (f) Period 3.0 sec. Soft Soils.

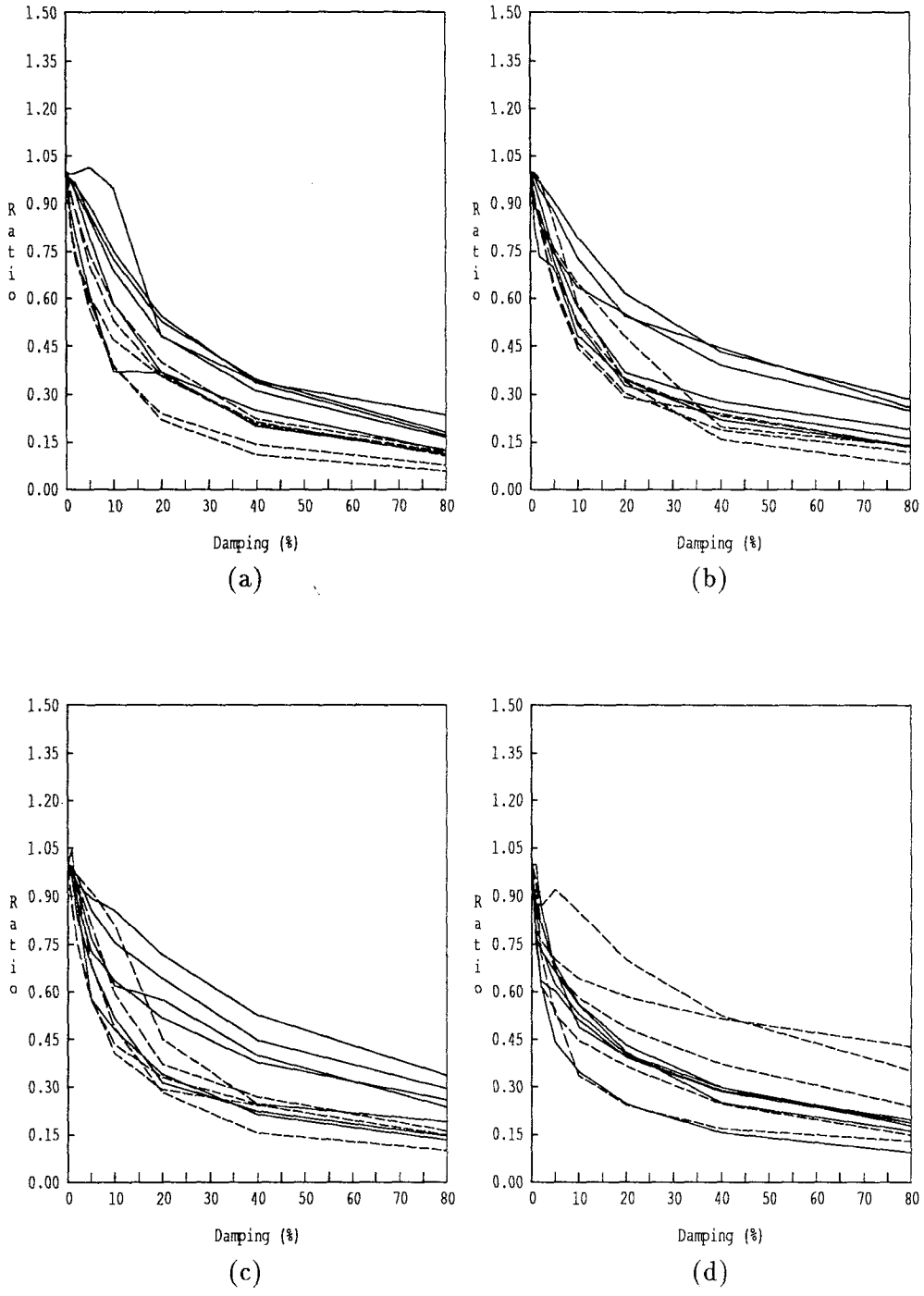

Figure C.12: Damping effect on maximum ductility demand. Period 0.5 sec. All records. Soft Soils - - - - -, Hard Soils——. (a) η=0.2. (b) η=0.8. (c) η=1.0. (d) η=2.0.

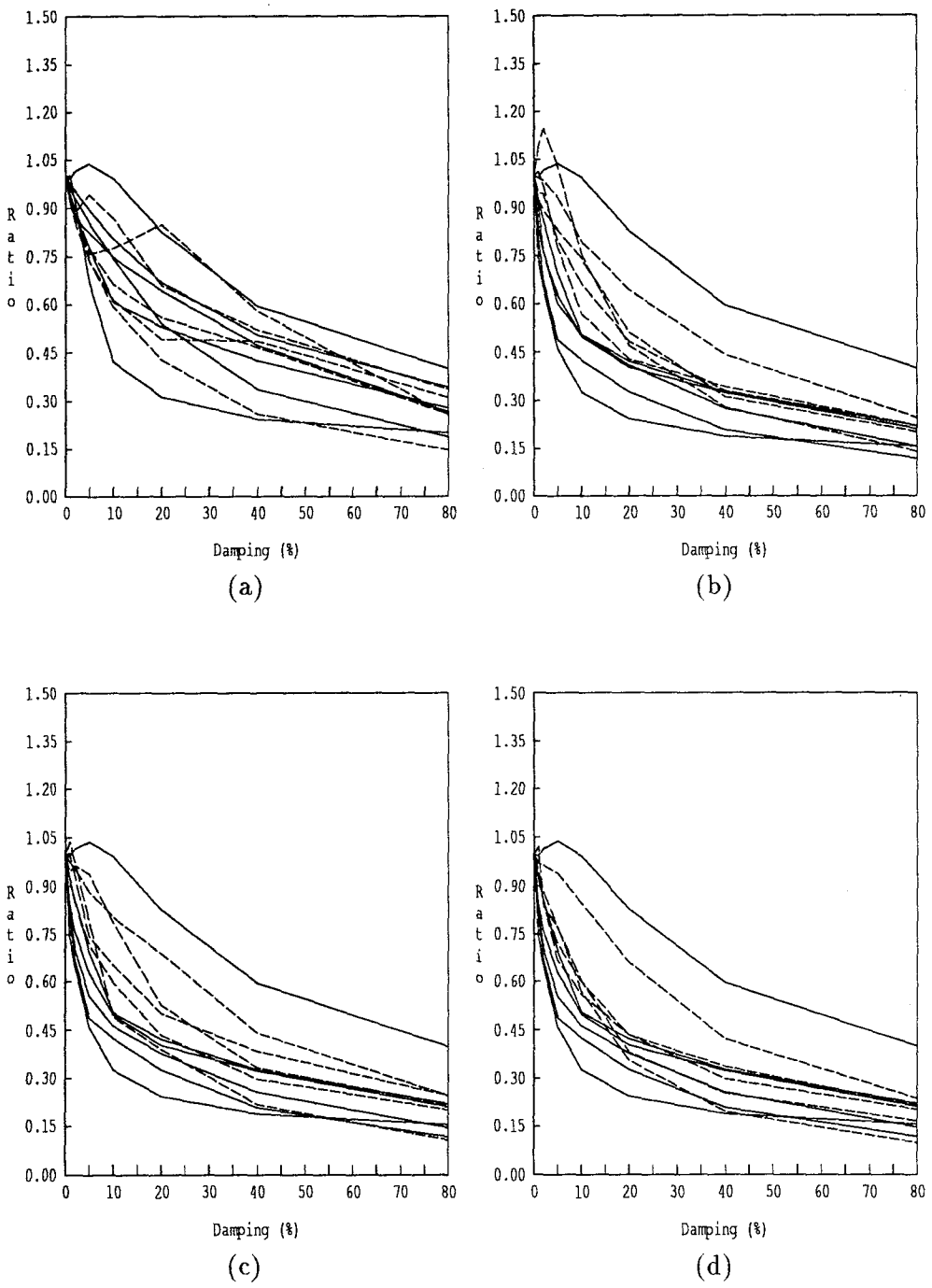

Figure C.13: Damping effect on maximum ductility demand. Period 2.0 sec. All records. Soft Soils - - - - -, Hard Soils ——. (a) η=0.2. (b) η=0.8. (c) η=1.0. (d) η=2.0.

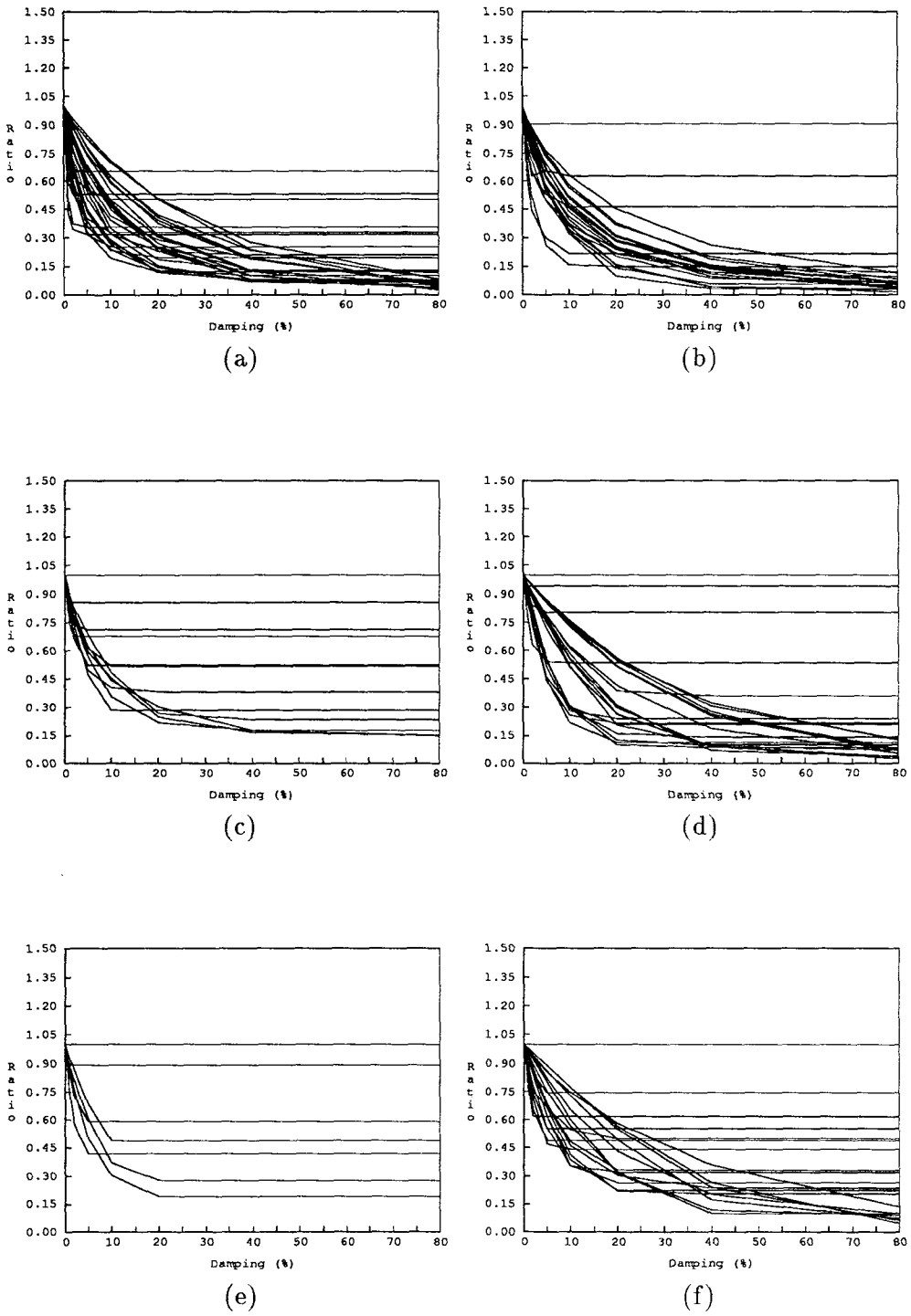

Figure C.14: Damping effect on cumulative ductility demand. All yield capacities (η), all records. (a) Period 0.5 sec. Hard Soils. (b) Period 0.5 sec. Soft Soils. (c) Period 2.0 sec. Hard Soils. (d) Period 2.0 sec. Soft Soils. (e) Period 3.0 sec. Hard Soils. (f) Period 3.0 sec. Soft Soils.

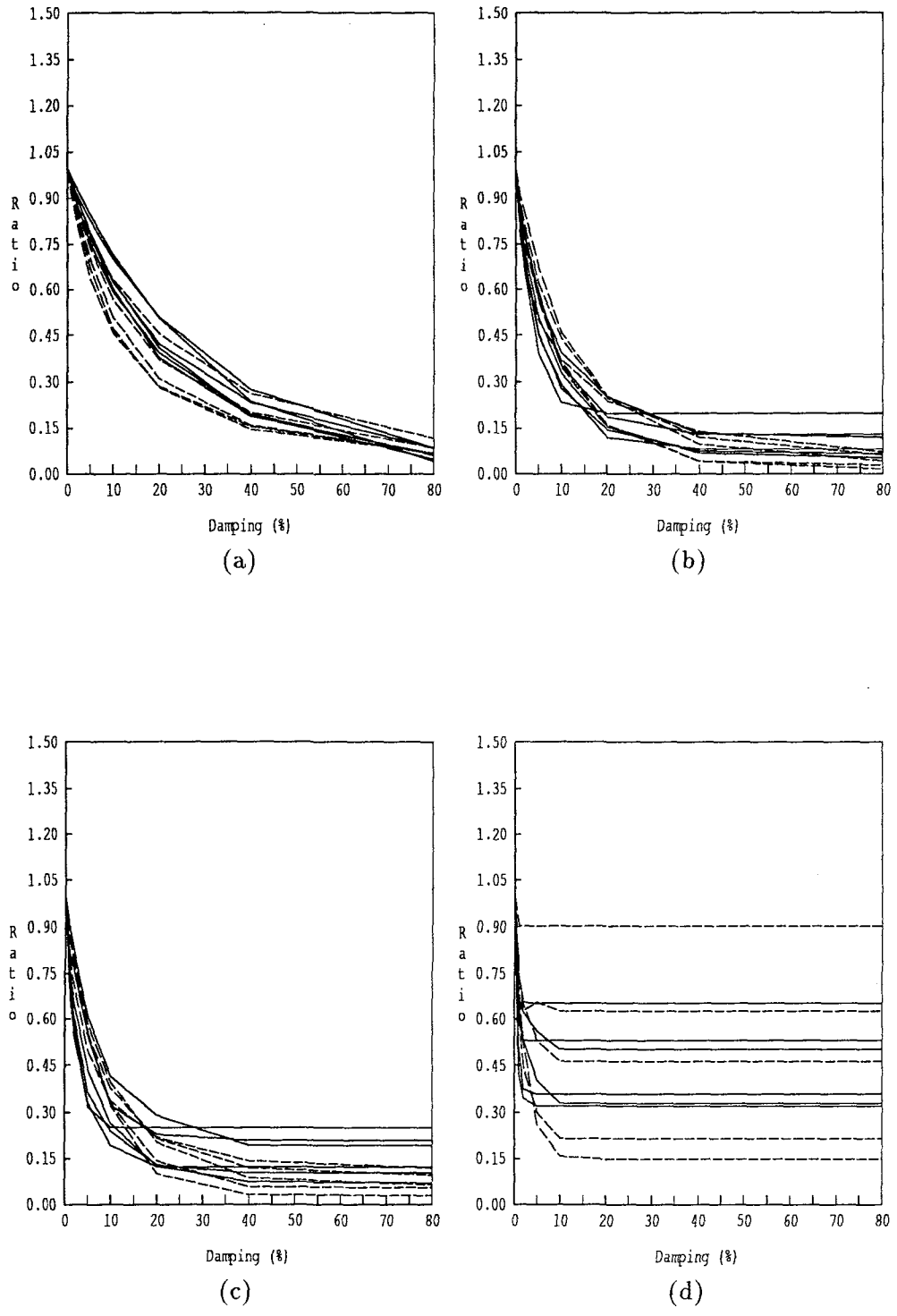

Figure C.15: Damping effect on cumulative ductility demand. Period 0.5 sec. All records. Soft Soils - - - - -, Hard Soils ——. (a) η=0.2. (b) η=0.8. (c) η=1.0. (d) η=2.0.

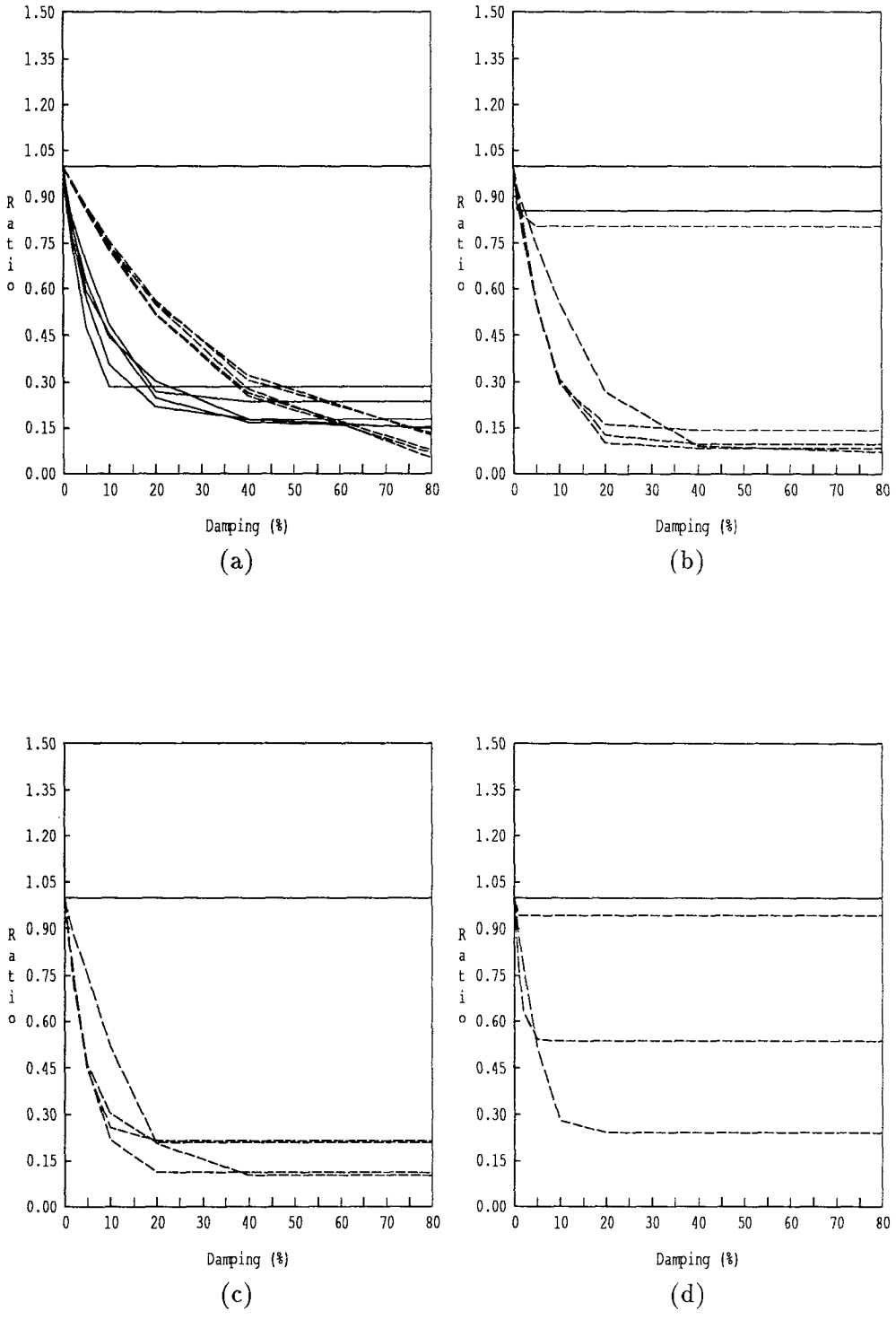

Figure C.16: Damping effect on cumulative ductility demand. Period 2.0 sec. All records. Soft Soils - - - - -, Hard Soils ——. (a) η=0.2. (b) η=0.8. (c) η=1.0. (d) η=2.0.

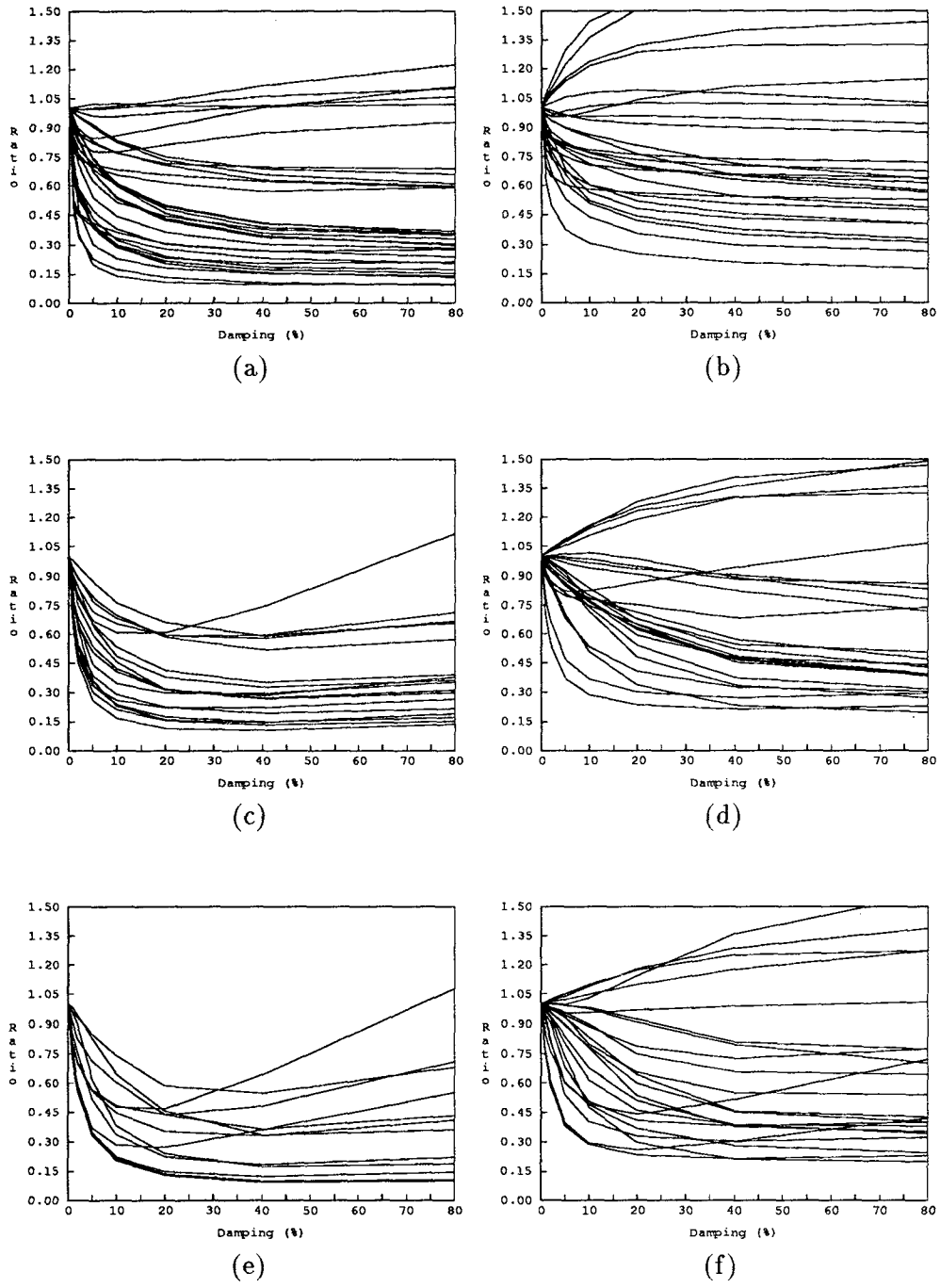

Figure C.17: Damping effect on sum of the squared acceleration. All yield capacities (η), all records. (a) Period 0.5 sec. Hard Soils. (b) Period 0.5 sec. Soft Soils. (c) Period 2.0 sec. Hard Soils. (d) Period 2.0 sec. Soft Soils. (e) Period 3.0 sec. Hard Soils. (f) Period 3.0 sec. Soft Soils.

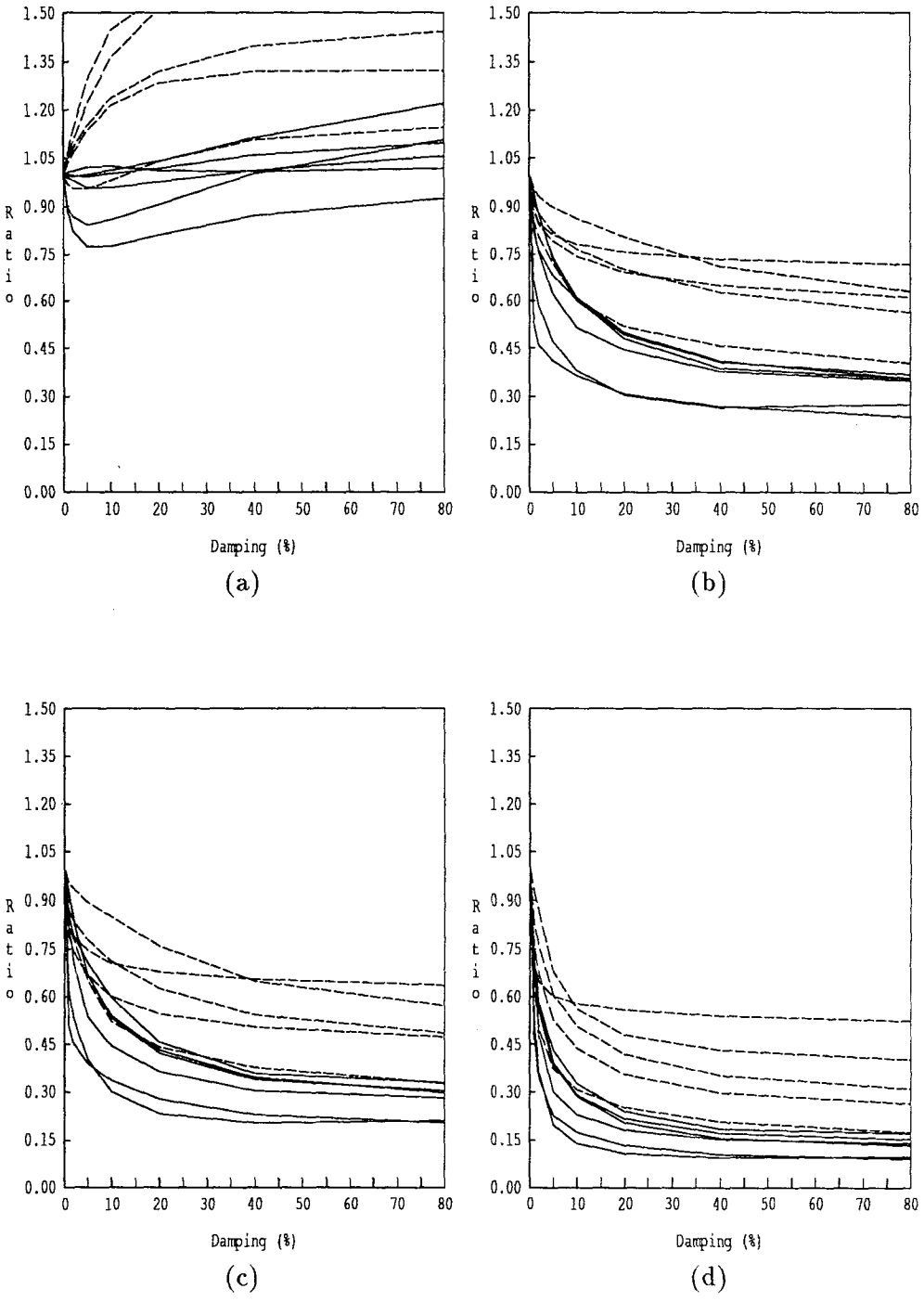

Figure C.18: Damping effect on sum of the squared acceleration. Period 0.5 sec. All records. Soft Soils - - - - -, Hard Soils ——. (a) η=0.2. (b) η=0.8. (c) η=1.0. (d) η=2.0.

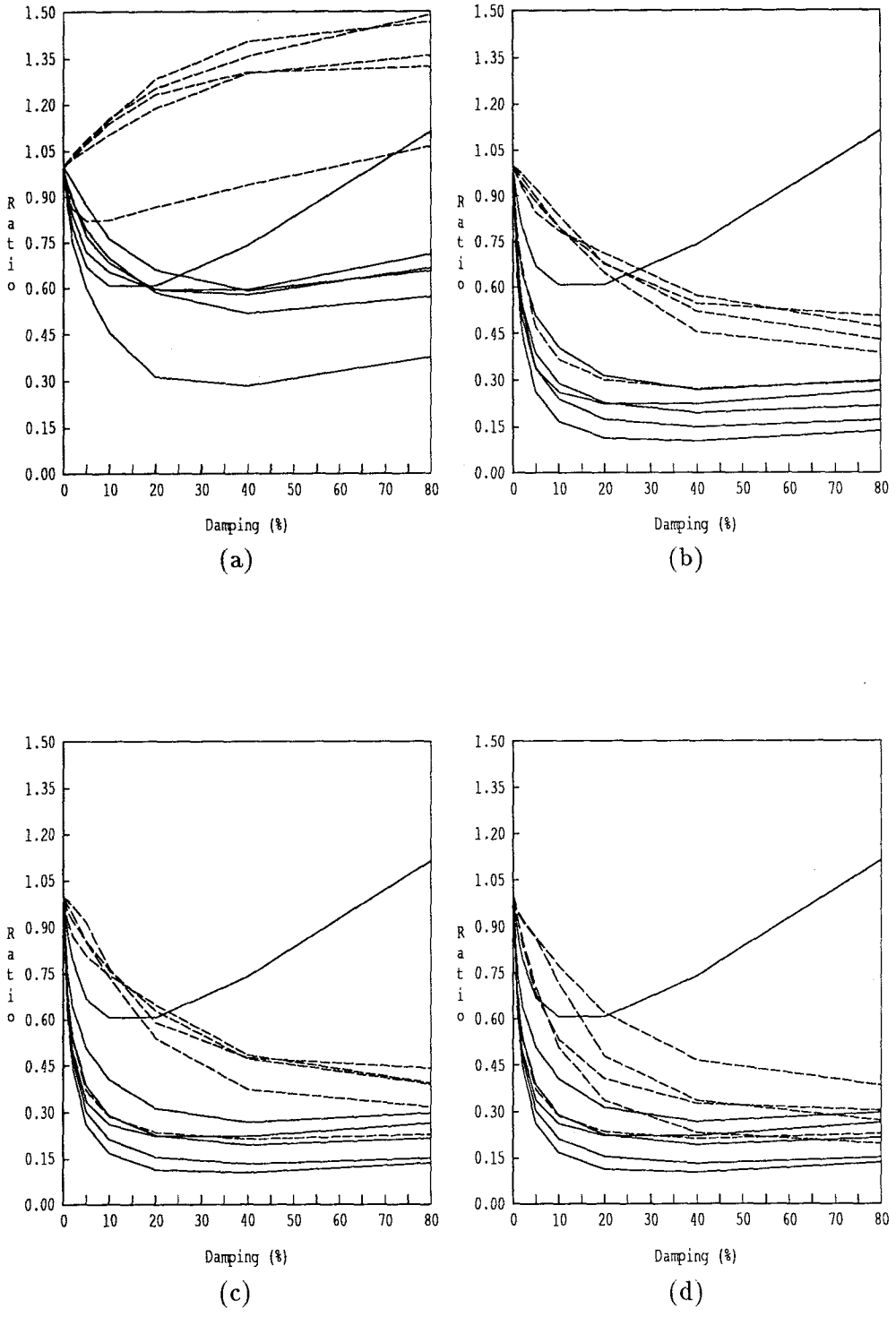

Figure C.19: Damping effect on sum of the squared acceleration. Period 2.0 sec. All records. Soft Soils - - - - -, Hard Soils ——. (a) η=0.2. (b) η=0.8. (c) η=1.0. (d) η=2.0.

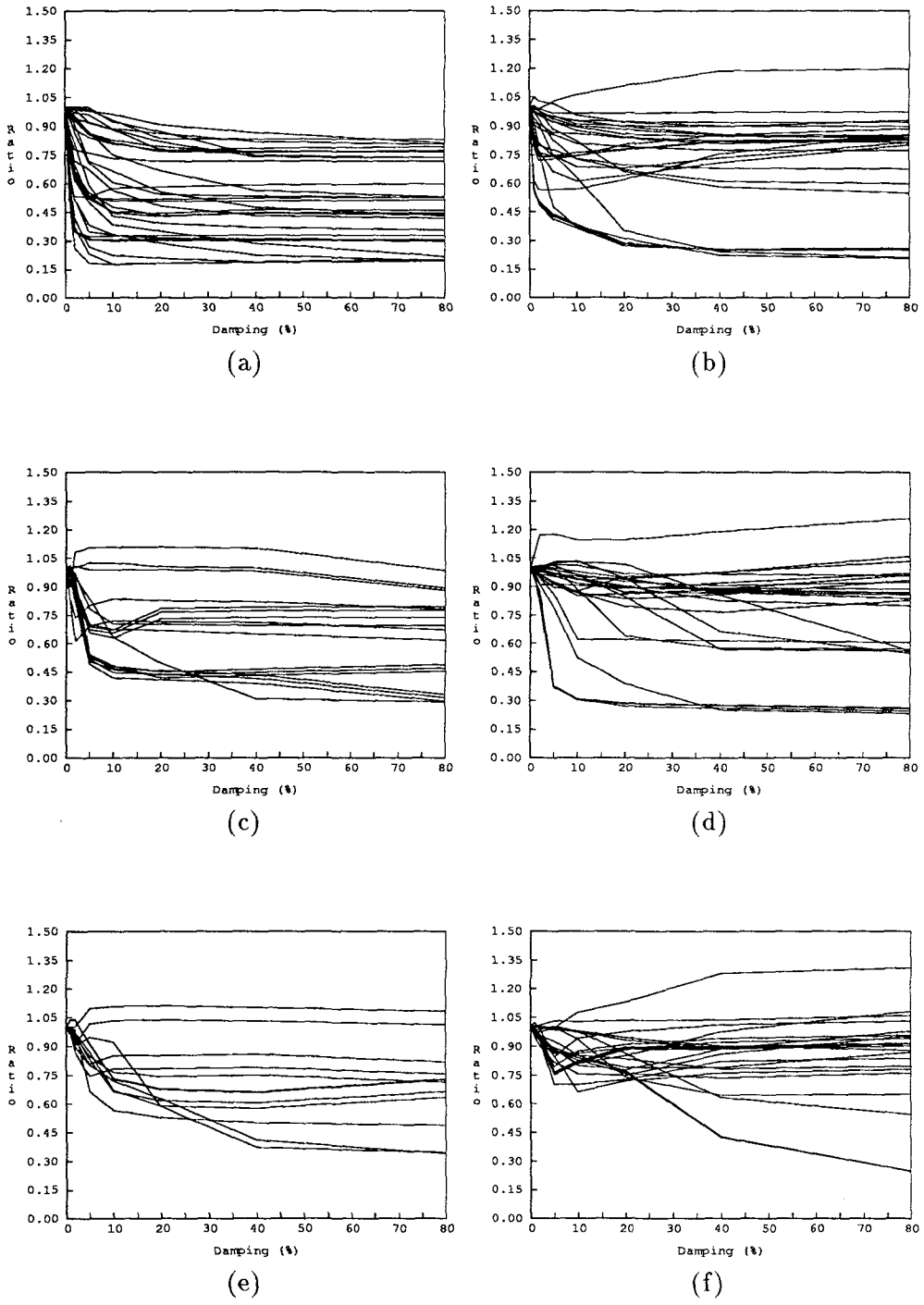

Figure C.20: Damping effect on strong motion duration. All yield capacities (η), all records. (a) Period 0.5 sec. Hard Soils. (b) Period 0.5 sec. Soft Soils. (c) Period 2.0 sec. Hard Soils. (d) Period 2.0 sec. Soft Soils. (e) Period 3.0 sec. Hard Soils. (f) Period 3.0 sec. Soft Soils.

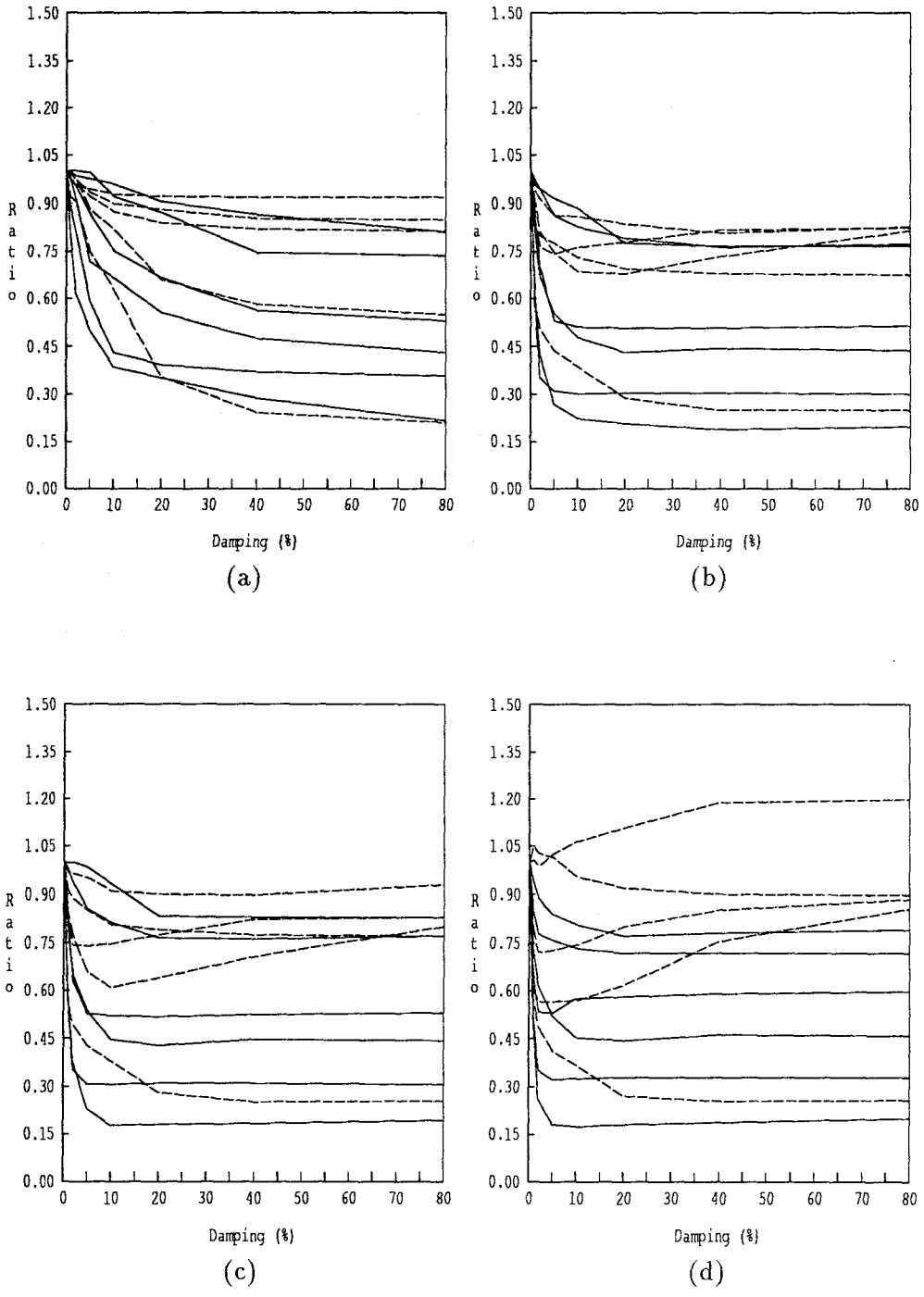

Figure C.21: Damping effect on strong motion duration. Period 0.5 sec. All records. Soft Soils - - - - -, Hard Soils ——. (a) η=0.2. (b) η=0.8. (c) η=1.0. (d) η=2.0.

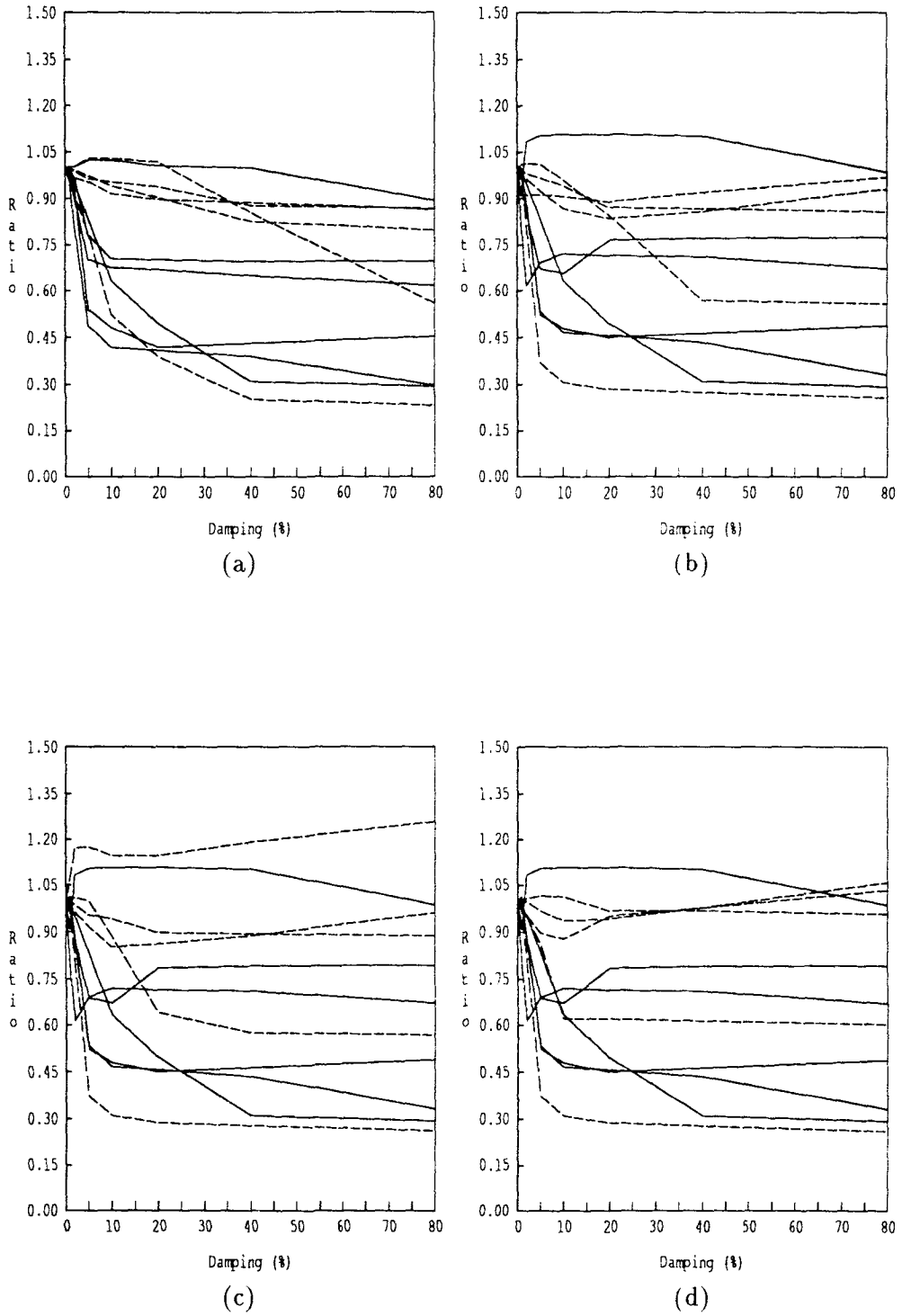

Figure C.22: Damping effect on strong motion duration. Period 2.0 sec. All records. Soft Soils - - - - -, Hard Soils ——. (a) η=0.2. (b) η=0.8. (c) η=1.0. (d) η=2.0.

EARTHQUAKE ENGINEERING RESEARCH CENTER REPORT SERIES

EERC reports are available from the National Information Service for Earthquake Engineering (NISEE) and from the National Technical Information Service (NTIS). Numbers in parentheses are Accession Numbers assigned by the National Technical Information Service; these are followed by a price code. Contact NTIS, 5285 Port Royal Road, Springfield Virginia, 22161 for more information. Reports without Accession Numbers were not available from NTIS at the time of printing. For a current complete list of EERC reports (from EERC 67-1) and availablity information, please contact University of California, EERC, NISEE, 1301 South 46th Street, Richmond, California 94804.

UCB/EERC-82/01 "Dynamic Behavior of Ground for Seismic Analysis of Lifeline Systems," by Sato, T. and Der Kiureghian, A., January 1982, (PB82 218 926)A05.

UCB/EERC-82/02 "Shaking Table Tests of a Tubular Steel Frame Model," by Ghanaat, Y. and Clough, R.W., January 1982, (PB82 220 161)A07.

UCB/EERC-82/03 "Behavior of a Piping System under Seismic Excitation: Experimental Investigations of a Spatial Piping System supported by Mechanical Shock Arrestors," by Schneider, S., Lee, H.-M. and Godden, W. G., May 1982, (PB83 172 544)A09.

UCB/EERC-82/04 "New Approaches for the Dynamic Analysis of Large Structural Systems," by Wilson, E.L., June 1982, (PB83 148 080)A05.

UCB/EERC-82/05 "Model Study of Effects of Damage on the Vibration Properties of Steel Offshore Platforms," by Shahrivar, F. and Bouwkamp, J.G., June 1982, (PB83 148 742)A10.

UCB/EERC-82/06 "States of the Art and Practice in the Optimum Seismic Design and Analytical Response Prediction of R/C Frame Wall Structures," by Aktan, A.E. and Bertero, V.V., July 1982, (PB83 147 736)A05.

UCB/EERC-82/07 "Further Study of the Earthquake Response of a Broad Cylindrical Liquid-Storage Tank Model," by Manos, G.C. and Clough, R.W., July 1982, (PB83 147 744)A11.

UCB/EERC-82/08 "An Evaluation of the Design and Analytical Seismic Response of a Seven Story Reinforced Concrete Frame," by Charney, F.A. and Bertero, V.V., July 1982, (PB83 157 628)A09.

UCB/EERC-82/09 "Fluid-Structure Interactions: Added Mass Computations for Incompressible Fluid," by Kuo, J.S.-H., August 1982, (PB83 156 281)A07.

UCB/EERC-82/10 "Joint-Opening Nonlinear Mechanism: Interface Smeared Crack Model," by Kuo, J.S.-H., August 1982, (PB83 149 195)A05.

UCB/EERC-82/11 "Dynamic Response Analysis of Techi Dam," by Clough, R.W., Stephen, R.M. and Kuo, J.S.-H., August 1982, (PB83 147 496)A06.

UCB/EERC-82/12 "Prediction of the Seismic Response of R/C Frame-Coupled Wall Structures," by Aktan, A.E., Bertero, V.V. and Piazzo, M., August 1982, (PB83 149 203)A09.

UCB/EERC-82/13 "Preliminary Report on the Smart 1 Strong Motion Array in Taiwan," by Bolt, B.A., Loh, C.H., Penzien, J. and Tsai, Y.B., August 1982, (PB83 159 400)A10.

UCB/EERC-82/14 "Seismic Behavior of an Eccentrically X-Braced Steel Structure," by Yang, M.S., September 1982, (PB83 260 778)A12.

UCB/EERC-82/15 "The Performance of Stairways in Earthquakes," by Roha, C., Axley, J.W. and Bertero, V.V., September 1982, (PB83 157 693)A07.

UCB/EERC-82/16 "The Behavior of Submerged Multiple Bodies in Earthquakes," by Liao, W.-G., September 1982, (PB83 158 709)A07.

UCB/EERC-82/17 "Effects of Concrete Types and Loading Conditions on Local Bond-Slip Relationships," by Cowell, A.D., Popov, E.P. and Bertero, V.V., September 1982, (PB83 153 577)A04.

UCB/EERC-82/18 "Mechanical Behavior of Shear Wall Vertical Boundary Members: An Experimental Investigation," by Wagner, M.T. and Bertero, V.V., October 1982, (PB83 159 764)A05.

UCB/EERC-82/19 "Experimental Studies of Multi-support Seismic Loading on Piping Systems," by Kelly, J.M. and Cowell, A.D., November 1982, (PB90 262 684)A07.

UCB/EERC-82/20 "Generalized Plastic Hinge Concepts for 3D Beam-Column Elements," by Chen, P. F.-S. and Powell, G.H., November 1982, (PB83 247 981)A13.

UCB/EERC-82/21 "ANSR-III: General Computer Program for Nonlinear Structural Analysis," by Oughourlian, C.V. and Powell, G.H., November 1982, (PB83 251 330)A12.

UCB/EERC-82/22 "Solution Strategies for Statically Loaded Nonlinear Structures," by Simons, J.W. and Powell, G.H., November 1982, (PB83 197 970)A06.

UCB/EERC-82/23 "Analytical Model of Deformed Bar Anchorages under Generalized Excitations," by Ciampi, V., Eligehausen, R., Bertero, V.V. and Popov, E.P., November 1982, (PB83 169 532)A06.

UCB/EERC-82/24 "A Mathematical Model for the Response of Masonry Walls to Dynamic Excitations," by Sucuoglu, H., Mengi, Y. and McNiven, H.D., November 1982, (PB83 169 011)A07.

UCB/EERC-82/25 "Earthquake Response Considerations of Broad Liquid Storage Tanks," by Cambra, F.J., November 1982, (PB83 251 215)A09.

UCB/EERC-82/26 "Computational Models for Cyclic Plasticity, Rate Dependence and Creep," by Mosaddad, B. and Powell, G.H., November 1982, (PB83 245 829)A08.

UCB/EERC-82/27 "Inelastic Analysis of Piping and Tubular Structures," by Mahasuverachai, M. and Powell, G.H., November 1982, (PB83 249 987)A07.

UCB/EERC-83/01 "The Economic Feasibility of Seismic Rehabilitation of Buildings by Base Isolation," by Kelly, J.M., January 1983, (PB83 197 988)A05.

UCB/EERC-83/02 "Seismic Moment Connections for Moment-Resisting Steel Frames.," by Popov, E.P., January 1983, (PB83 195 412)A04.

UCB/EERC-83/03 "Design of Links and Beam-to-Column Connections for Eccentrically Braced Steel Frames," by Popov, E.P. and Malley, J.O., January 1983, (PB83 194 811)A04.

UCB/EERC-83/04 "Numerical Techniques for the Evaluation of Soil-Structure Interaction Effects in the Time Domain," by Bayo, E. and Wilson, E.L., February 1983, (PB83 245 605)A09.

UCB/EERC-83/05 "A Transducer for Measuring the Internal Forces in the Columns of a Frame-Wall Reinforced Concrete Structure," by Sause, R. and Bertero, V.V., May 1983, (PB84 119 494)A06.

UCB/EERC-83/06 "Dynamic Interactions Between Floating Ice and Offshore Structures," by Croteau, P., May 1983, (PB84 119 486)A16.

UCB/EERC-83/07 "Dynamic Analysis of Multiply Tuned and Arbitrarily Supported Secondary Systems," by Igusa, T. and Der Kiureghian, A., July 1983, (PB84 118 272)A11.

UCB/EERC-83/08 "A Laboratory Study of Submerged Multi-body Systems in Earthquakes," by Ansari, G.R., June 1983, (PB83 261 842)A17.

UCB/EERC-83/09 "Effects of Transient Foundation Uplift on Earthquake Response of Structures," by Yim, C.-S. and Chopra, A.K., June 1983, (PB83 261 396)A07.

UCB/EERC-83/10 "Optimal Design of Friction-Braced Frames under Seismic Loading," by Austin, M.A. and Pister, K.S., June 1983, (PB84 119 288)A06.

UCB/EERC-83/11 "Shaking Table Study of Single-Story Masonry Houses: Dynamic Performance under Three Component Seismic Input and Recommendations," by Manos, G.C., Clough, R.W. and Mayes, R.L., July 1983, (UCB/EERC-83/11)A08.

UCB/EERC-83/12 "Experimental Error Propagation in Pseudodynamic Testing," by Shing, P.B. and Mahin, S.A., June 1983, (PB84 119 270)A09.

UCB/EERC-83/13 "Experimental and Analytical Predictions of the Mechanical Characteristics of a 1/5-scale Model of a 7-story R/C Frame-Wall Building Structure," by Aktan, A.E., Bertero, V.V., Chowdhury, A.A. and Nagashima, T., June 1983, (PB84 119 213)A07.

UCB/EERC-83/14 "Shaking Table Tests of Large-Panel Precast Concrete Building System Assemblages," by Oliva, M.G. and Clough, R.W., June 1983, (PB86 110 210/AS)A11.

UCB/EERC-83/15 "Seismic Behavior of Active Beam Links in Eccentrically Braced Frames," by Hjelmstad, K.D. and Popov, E.P., July 1983, (PB84 119 676)A09.

UCB/EERC-83/16 "System Identification of Structures with Joint Rotation," by Dimsdale, J.S., July 1983, (PB84 192 210)A06.

UCB/EERC-83/17 "Construction of Inelastic Response Spectra for Single-Degree-of-Freedom Systems," by Mahin, S. and Lin, J., June 1983, (PB84 208 834)A05.

UCB/EERC-83/18 "Interactive Computer Analysis Methods for Predicting the Inelastic Cyclic Behaviour of Structural Sections," by Kaba, S. and Mahin, S., July 1983, (PB84 192 012)A06.

UCB/EERC-83/19 "Effects of Bond Deterioration on Hysteretic Behavior of Reinforced Concrete Joints," by Filippou, F.C., Popov, E.P. and Bertero, V.V., August 1983, (PB84 192 020)A10.

UCB/EERC-83/20 "Correlation of Analytical and Experimental Responses of Large-Panel Precast Building Systems," by Oliva, M.G., Clough, R.W., Velkov, M. and Gavrilovic, P., May 1988, (PB90 262 692)A06.

UCB/EERC-83/21 "Mechanical Characteristics of Materials Used in a 1/5 Scale Model of a 7-Story Reinforced Concrete Test Structure," by Bertero, V.V., Aktan, A.E., Harris, H.G. and Chowdhury, A.A., October 1983, (PB84 193 697)A05.

UCB/EERC-83/22 "Hybrid Modelling of Soil-Structure Interaction in Layered Media," by Tzong, T.-J. and Penzien, J., October 1983, (PB84 192 178)A08.

UCB/EERC-83/23 "Local Bond Stress-Slip Relationships of Deformed Bars under Generalized Excitations," by Eligehausen, R., Popov, E.P. and Bertero, V.V., October 1983, (PB84 192 848)A09.

UCB/EERC-83/24 "Design Considerations for Shear Links in Eccentrically Braced Frames," by Malley, J.O. and Popov, E.P., November 1983, (PB84 192 186)A07.

UCB/EERC-84/01 "Pseudodynamic Test Method for Seismic Performance Evaluation: Theory and Implementation," by Shing, P.-S.B. and Mahin, S.A., January 1984, (PB84 190 644)A08.

UCB/EERC-84/02 "Dynamic Response Behavior of Kiang Hong Dian Dam," by Clough, R.W., Chang, K.-T., Chen, H.-Q. and Stephen, R.M., April 1984, (PB84 209 402)A08.

UCB/EERC-84/03 "Refined Modelling of Reinforced Concrete Columns for Seismic Analysis," by Kaba, S.A. and Mahin, S.A., April 1984, (PB84 234 384)A06.

UCB/EERC-84/04 "A New Floor Response Spectrum Method for Seismic Analysis of Multiply Supported Secondary Systems," by Asfura, A. and Der Kiureghian, A., June 1984, (PB84 239 417)A06.

UCB/EERC-84/05 "Earthquake Simulation Tests and Associated Studies of a 1/5th-scale Model of a 7-Story R/C Frame-Wall Test Structure," by Bertero, V.V., Aktan, A.E., Charney, F.A. and Sause, R., June 1984, (PB84 239 409)A09.

UCB/EERC-84/06 "Unassigned," by Unassigned, 1984.

UCB/EERC-84/07 "Behavior of Interior and Exterior Flat-Plate Connections Subjected to Inelastic Load Reversals," by Zee, H.L. and Moehle, J.P., August 1984, (PB86 117 629/AS)A07.

UCB/EERC-84/08 "Experimental Study of the Seismic Behavior of a Two-Story Flat-Plate Structure," by Moehle, J.P. and Diebold, J.W., August 1984, (PB86 122 553/AS)A12.

UCB/EERC-84/09 "Phenomenological Modeling of Steel Braces under Cyclic Loading," by Ikeda, K., Mahin, S.A. and Dermitzakis, S.N., May 1984, (PB86 132 198/AS)A08.

UCB/EERC-84/10 "Earthquake Analysis and Response of Concrete Gravity Dams," by Fenves, G.L. and Chopra, A.K., August 1984, (PB85 193 902/AS)A11.

UCB/EERC-84/11 "EAGD-84: A Computer Program for Earthquake Analysis of Concrete Gravity Dams," by Fenves, G.L. and Chopra, A.K., August 1984, (PB85 193 613/AS)A05.

UCB/EERC-84/12 "A Refined Physical Theory Model for Predicting the Seismic Behavior of Braced Steel Frames," by Ikeda, K. and Mahin, S.A., July 1984, (PB85 191 450/AS)A09.

UCB/EERC-84/13 "Earthquake Engineering Research at Berkeley - 1984," by EERC, August 1984, (PB85 197 341/AS)A10.

UCB/EERC-84/14 "Moduli and Damping Factors for Dynamic Analyses of Cohesionless Soils," by Seed, H.B., Wong, R.T., Idriss, I.M. and Tokimatsu, K., September 1984, (PB85 191 468/AS)A04.

UCB/EERC-84/15 "The Influence of SPT Procedures in Soil Liquefaction Resistance Evaluations," by Seed, H.B., Tokimatsu, K., Harder, L.F. and Chung, R.M., October 1984, (PB85 191 732/AS)A04.

UCB/EERC-84/16 "Simplified Procedures for the Evaluation of Settlements in Sands Due to Earthquake Shaking," by Tokimatsu, K. and Seed, H.B., October 1984, (PB85 197 887/AS)A03.

UCB/EERC-84/17 "Evaluation of Energy Absorption Characteristics of Highway Bridges Under Seismic Conditions - Volume I (PB90 262 627)A16 and Volume II (Appendices) (PB90 262 635)A13," by Imbsen, R.A. and Penzien, J., September 1986.

UCB/EERC-84/18 "Structure-Foundation Interactions under Dynamic Loads," by Liu, W.D. and Penzien, J., November 1984, (PB87 124 889/AS)A11.

UCB/EERC-84/19 "Seismic Modelling of Deep Foundations," by Chen, C.-H. and Penzien, J., November 1984, (PB87 124 798/AS)A07.

UCB/EERC-84/20 "Dynamic Response Behavior of Quan Shui Dam," by Clough, R.W., Chang, K.-T., Chen, H.-Q., Stephen, R.M., Ghanaat, Y. and Qi, J.-H., November 1984, (PB86 115177/AS)A07.

UCB/EERC-85/01 "Simplified Methods of Analysis for Earthquake Resistant Design of Buildings," by Cruz, E.F. and Chopra, A.K., February 1985, (PB86 112299/AS)A12.

UCB/EERC-85/02 "Estimation of Seismic Wave Coherency and Rupture Velocity using the SMART 1 Strong-Motion Array Recordings," by Abrahamson, N.A., March 1985, (PB86 214 343)A07.

UCB/EERC-85/03 "Dynamic Properties of a Thirty Story Condominium Tower Building," by Stephen, R.M., Wilson, E.L. and Stander, N., April 1985, (PB86 118965/AS)A06.

UCB/EERC-85/04 "Development of Substructuring Techniques for On-Line Computer Controlled Seismic Performance Testing," by Dermitzakis, S. and Mahin, S., February 1985, (PB86 132941/AS)A08.

UCB/EERC-85/05 "A Simple Model for Reinforcing Bar Anchorages under Cyclic Excitations," by Filippou, F.C., March 1985, (PB86 112 919/AS)A05.

UCB/EERC-85/06 "Racking Behavior of Wood-framed Gypsum Panels under Dynamic Load," by Oliva, M.G., June 1985, (PB90 262 643)A04.

UCB/EERC-85/07 "Earthquake Analysis and Response of Concrete Arch Dams," by Fok, K.-L. and Chopra, A.K., June 1985, (PB86 139672/AS)A10.

UCB/EERC-85/08 "Effect of Inelastic Behavior on the Analysis and Design of Earthquake Resistant Structures," by Lin, J.P. and Mahin, S.A., June 1985, (PB86 135340/AS)A08.

UCB/EERC-85/09 "Earthquake Simulator Testing of a Base-Isolated Bridge Deck," by Kelly, J.M., Buckle, I.G. and Tsai, H.-C., January 1986, (PB87 124 152/AS)A06.

UCB/EERC-85/10 "Simplified Analysis for Earthquake Resistant Design of Concrete Gravity Dams," by Fenves, G.L. and Chopra, A.K., June 1986, (PB87 124 160/AS)A08.

UCB/EERC-85/11 "Dynamic Interaction Effects in Arch Dams," by Clough, R.W., Chang, K.-T., Chen, H.-Q. and Ghanaat, Y., October 1985, (PB86 135027/AS)A05.

UCB/EERC-85/12 "Dynamic Response of Long Valley Dam in the Mammoth Lake Earthquake Series of May 25-27, 1980," by Lai, S. and Seed, H.B., November 1985, (PB86 142304/AS)A05.

UCB/EERC-85/13 "A Methodology for Computer-Aided Design of Earthquake-Resistant Steel Structures," by Austin, M.A., Pister, K.S. and Mahin, S.A., December 1985, (PB86 159480/AS)A10 .

UCB/EERC-85/14 "Response of Tension-Leg Platforms to Vertical Seismic Excitations," by Liou, G.-S., Penzien, J. and Yeung, R.W., December 1985, (PB87 124 871/AS)A08.

UCB/EERC-85/15 "Cyclic Loading Tests of Masonry Single Piers: Volume 4 - Additional Tests with Height to Width Ratio of 1," by Sveinsson, B., McNiven, H.D. and Sucuoglu, H., December 1985, (PB87 165031/AS)A08.

UCB/EERC-85/16 "An Experimental Program for Studying the Dynamic Response of a Steel Frame with a Variety of Infill Partitions," by Yanev, B. and McNiven, H.D., December 1985, (PB90 262 676)A05.

UCB/EERC-86/01 "A Study of Seismically Resistant Eccentrically Braced Steel Frame Systems," by Kasai, K. and Popov, E.P., January 1986, (PB87 124 178/AS)A14.

UCB/EERC-86/02 "Design Problems in Soil Liquefaction," by Seed, H.B., February 1986, (PB87 124 186/AS)A03.

UCB/EERC-86/03 "Implications of Recent Earthquakes and Research on Earthquake-Resistant Design and Construction of Buildings," by Bertero, V.V., March 1986, (PB87 124 194/AS)A05.

UCB/EERC-86/04 "The Use of Load Dependent Vectors for Dynamic and Earthquake Analyses," by Leger, P., Wilson, E.L. and Clough, R.W., March 1986, (PB87 124 202/AS)A12.

UCB/EERC-86/05 "Two Beam-To-Column Web Connections," by Tsai, K.-C. and Popov, E.P., April 1986, (PB87 124 301/AS)A04.

UCB/EERC-86/06 "Determination of Penetration Resistance for Coarse-Grained Soils using the Becker Hammer Drill," by Harder, L.F. and Seed, H.B., May 1986, (PB87 124 210/AS)A07.

UCB/EERC-86/07 "A Mathematical Model for Predicting the Nonlinear Response of Unreinforced Masonry Walls to In-Plane Earthquake Excitations," by Mengi, Y. and McNiven, H.D., May 1986, (PB87 124 780/AS)A06.

UCB/EERC-86/08 "The 19 September 1985 Mexico Earthquake: Building Behavior," by Bertero, V.V., July 1986.

UCB/EERC-86/09 "EACD-3D: A Computer Program for Three-Dimensional Earthquake Analysis of Concrete Dams," by Fok, K.-L., Hall, J.F. and Chopra, A.K., July 1986, (PB87 124 228/AS)A08.

UCB/EERC-86/10 "Earthquake Simulation Tests and Associated Studies of a 0.3-Scale Model of a Six-Story Concentrically Braced Steel Structure," by Uang, C.-M. and Bertero, V.V., December 1986, (PB87 163 564/AS)A17.

UCB/EERC-86/11 "Mechanical Characteristics of Base Isolation Bearings for a Bridge Deck Model Test," by Kelly, J.M., Buckle, I.G. and Koh, C.-G., November 1987, (PB90 262 668)A04.

UCB/EERC-86/12 "Effects of Axial Load on Elastomeric Isolation Bearings," by Koh, C.-G. and Kelly, J.M., November 1987.

UCB/EERC-87/01 "The FPS Earthquake Resisting System: Experimental Report," by Zayas, V.A., Low, S.S. and Mahin, S.A., June 1987, (PB88 170 287)A06.

UCB/EERC-87/02 "Earthquake Simulator Tests and Associated Studies of a 0.3-Scale Model of a Six-Story Eccentrically Braced Steel Structure," by Whittaker, A., Uang, C.-M. and Bertero, V.V., July 1987, (PB88 166 707/AS)A18.

UCB/EERC-87/03 "A Displacement Control and Uplift Restraint Device for Base-Isolated Structures," by Kelly, J.M., Griffith, M.C. and Aiken, I.D., April 1987, (PB88 169 933)A04.

UCB/EERC-87/04 "Earthquake Simulator Testing of a Combined Sliding Bearing and Rubber Bearing Isolation System," by Kelly, J.M. and Chalhoub, M.S., December 1990.

UCB/EERC-87/05 "Three-Dimensional Inelastic Analysis of Reinforced Concrete Frame-Wall Structures," by Moazzami, S. and Bertero, V.V., May 1987, (PB88 169 586/AS)A08.

UCB/EERC-87/06 "Experiments on Eccentrically Braced Frames with Composite Floors," by Ricles, J. and Popov, E., June 1987, (PB88 173 067/AS)A14.

UCB/EERC-87/07 "Dynamic Analysis of Seismically Resistant Eccentrically Braced Frames," by Ricles, J. and Popov, E., June 1987, (PB88 173 075/AS)A16.

UCB/EERC-87/08 "Undrained Cyclic Triaxial Testing of Gravels-The Effect of Membrane Compliance," by Evans, M.D. and Seed, H.B., July 1987, (PB88 173 257)A19.

UCB/EERC-87/09 "Hybrid Solution Techniques for Generalized Pseudo-Dynamic Testing," by Thewalt, C. and Mahin, S.A., July 1987, (PB 88 179 007)A07.

UCB/EERC-87/10 "Ultimate Behavior of Butt Welded Splices in Heavy Rolled Steel Sections," by Bruneau, M., Mahin, S.A. and Popov, E.P., September 1987, (PB90 254 285)A07.

UCB/EERC-87/11 "Residual Strength of Sand from Dam Failures in the Chilean Earthquake of March 3, 1985," by De Alba, P., Seed, H.B., Retamal, E. and Seed, R.B., September 1987, (PB88 174 321/AS)A03.

UCB/EERC-87/12 "Inelastic Seismic Response of Structures with Mass or Stiffness Eccentricities in Plan," by Bruneau, M. and Mahin, S.A., September 1987, (PB90 262 650/AS)A14.

UCB/EERC-87/13 "CSTRUCT: An Interactive Computer Environment for the Design and Analysis of Earthquake Resistant Steel Structures," by Austin, M.A., Mahin, S.A. and Pister, K.S., September 1987, (PB88 173 339/AS)A06.

UCB/EERC-87/14 "Experimental Study of Reinforced Concrete Columns Subjected to Multi-Axial Loading," by Low, S.S. and Moehle, J.P., September 1987, (PB88 174 347/AS)A07.

UCB/EERC-87/15 "Relationships between Soil Conditions and Earthquake Ground Motions in Mexico City in the Earthquake of Sept. 19, 1985," by Seed, H.B., Romo, M.P., Sun, J., Jaime, A. and Lysmer, J., October 1987, (PB88 178 991)A06.

UCB/EERC-87/16 "Experimental Study of Seismic Response of R. C. Setback Buildings," by Shahrooz, B.M. and Moehle, J.P., October 1987, (PB88 176 359)A16.

UCB/EERC-87/17 "The Effect of Slabs on the Flexural Behavior of Beams," by Pantazopoulou, S.J. and Moehle, J.P., October 1987, (PB90 262 700)A07.

UCB/EERC-87/18 "Design Procedure for R-FBI Bearings," by Mostaghel, N. and Kelly, J.M., November 1987, (PB90 262 718)A04.

UCB/EERC-87/19 "Analytical Models for Predicting the Lateral Response of R C Shear Walls: Evaluation of their Reliability," by Vulcano, A. and Bertero, V.V., November 1987, (PB88 178 983)A05.

UCB/EERC-87/20 "Earthquake Response of Torsionally-Coupled Buildings," by Hejal, R. and Chopra, A.K., December 1987.

UCB/EERC-87/21 "Dynamic Reservoir Interaction with Monticello Dam," by Clough, R.W., Ghanaat, Y. and Qiu, X-F., December 1987, (PB88 179 023)A07.

UCB/EERC-87/22 "Strength Evaluation of Coarse-Grained Soils," by Siddiqi, F.H., Seed, R.B., Chan, C.K., Seed, H.B. and Pyke, R.M., December 1987, (PB88 179 031)A04.

UCB/EERC-88/01 "Seismic Behavior of Concentrically Braced Steel Frames," by Khatib, I., Mahin, S.A. and Pister, K.S., January 1988, (PB91 210 898/AS)A11.

UCB/EERC-88/02 "Experimental Evaluation of Seismic Isolation of Medium-Rise Structures Subject to Uplift," by Griffith, M.C., Kelly, J.M., Coveney, V.A. and Koh, C.G., January 1988, (PB91 217 950/AS)A09.

UCB/EERC-88/03 "Cyclic Behavior of Steel Double Angle Connections," by Astaneh-Asl, A. and Nader, M.N., January 1988, (PB91 210 872)A05.

UCB/EERC-88/04 "Re-evaluation of the Slide in the Lower San Fernando Dam in the Earthquake of Feb. 9, 1971," by Seed, H.B., Seed, R.B., Harder, L.F. and Jong, H.-L., April 1988, (PB91 212 456/AS)A07.

UCB/EERC-88/05 "Experimental Evaluation of Seismic Isolation of a Nine-Story Braced Steel Frame Subject to Uplift," by Griffith, M.C., Kelly, J.M. and Aiken, I.D., May 1988, (PB91 217 968/AS)A07.

UCB/EERC-88/06 "DRAIN-2DX User Guide.," by Allahabadi, R. and Powell, G.H., March 1988, (PB91 212 530)A12.

UCB/EERC-88/07 "Theoretical and Experimental Studies of Cylindrical Water Tanks in Base-Isolated Structures," by Chalhoub, M.S. and Kelly, J.M., April 1988, (PB91 217 976/AS)A05.

UCB/EERC-88/08 "Analysis of Near-Source Waves: Separation of Wave Types Using Strong Motion Array Recording," by Darragh, R.B., June 1988, (PB91 212 621)A08.

UCB/EERC-88/09 "Alternatives to Standard Mode Superposition for Analysis of Non-Classically Damped Systems," by Kusainov, A.A. and Clough, R.W., June 1988, (PB91 217 992/AS)A04.

UCB/EERC-88/10 "The Landslide at the Port of Nice on October 16, 1979," by Seed, H.B., Seed, R.B., Schlosser, F., Blondeau, F. and Juran, I., June 1988, (PB91 210 914)A05.

UCB/EERC-88/11 "Liquefaction Potential of Sand Deposits Under Low Levels of Excitation," by Carter, D.P. and Seed, H.B., August 1988, (PB91 210 880)A15.

UCB/EERC-88/12 "Nonlinear Analysis of Reinforced Concrete Frames Under Cyclic Load Reversals," by Filippou, F.C. and Issa, A., September 1988, (PB91 212 589)A07.

UCB/EERC-88/13 "Implications of Recorded Earthquake Ground Motions on Seismic Design of Building Structures," by Uang, C.-M. and Bertero, V.V., November 1988, (PB91 212 548)A06.

UCB/EERC-88/14 "An Experimental Study of the Behavior of Dual Steel Systems," by Whittaker, A.S. , Uang, C.-M. and Bertero, V.V., September 1988, (PB91 212 712)A16.

UCB/EERC-88/15 "Dynamic Moduli and Damping Ratios for Cohesive Soils," by Sun, J.I., Golesorkhi, R. and Seed, H.B., August 1988, (PB91 210 922)A04.

UCB/EERC-88/16 "Reinforced Concrete Flat Plates Under Lateral Load: An Experimental Study Including Biaxial Effects," by Pan, A. and Moehle, J.P., October 1988, (PB91 210 856)A13.

UCB/EERC-88/17 "Earthquake Engineering Research at Berkeley - 1988," by EERC, November 1988, (PB91 210 864)A10.

UCB/EERC-88/18 "Use of Energy as a Design Criterion in Earthquake-Resistant Design," by Uang, C.-M. and Bertero, V.V., November 1988, (PB91 210 906/AS)A04.

UCB/EERC-88/19 "Steel Beam-Column Joints in Seismic Moment Resisting Frames," by Tsai, K.-C. and Popov, E.P., November 1988, (PB91 217 984/AS)A20.

UCB/EERC-88/20 "Base Isolation in Japan, 1988," by Kelly, J.M., December 1988, (PB91 212 449)A05.

UCB/EERC-89/01 "Behavior of Long Links in Eccentrically Braced Frames," by Engelhardt, M.D. and Popov, E.P., January 1989, (PB92 143 056)A18.

UCB/EERC-89/02 "Earthquake Simulator Testing of Steel Plate Added Damping and Stiffness Elements," by Whittaker, A., Bertero, V.V., Alonso, J. and Thompson, C., January 1989, (PB91 229 252/AS)A10.

UCB/EERC-89/03 "Implications of Site Effects in the Mexico City Earthquake of Sept. 19, 1985 for Earthquake-Resistant Design Criteria in the San Francisco Bay Area of California," by Seed, H.B. and Sun, J.I., March 1989, (PB91 229 369/AS)A07.

UCB/EERC-89/04 "Earthquake Analysis and Response of Intake-Outlet Towers," by Goyal, A. and Chopra, A.K., July 1989, (PB91 229 286/AS)A19.

UCB/EERC-89/05 "The 1985 Chile Earthquake: An Evaluation of Structural Requirements for Bearing Wall Buildings," by Wallace, J.W. and Moehle, J.P., July 1989, (PB91 218 008/AS)A13.

UCB/EERC-89/06 "Effects of Spatial Variation of Ground Motions on Large Multiply-Supported Structures," by Hao, H., July 1989, (PB91 229 161/AS)A08.

UCB/EERC-89/07 "EADAP - Enhanced Arch Dam Analysis Program: Users's Manual," by Ghanaat, Y. and Clough, R.W., August 1989, (PB91 212 522)A06.

UCB/EERC-89/08 "Seismic Performance of Steel Moment Frames Plastically Designed by Least Squares Stress Fields," by Ohi, K. and Mahin, S.A., August 1989, (PB91 212 597)A05.

UCB/EERC-89/09 "Feasibility and Performance Studies on Improving the Earthquake Resistance of New and Existing Buildings Using the Friction Pendulum System," by Zayas, V., Low, S., Mahin, S.A. and Bozzo, L., July 1989, (PB92 143 064)A14.

UCB/EERC-89/10 "Measurement and Elimination of Membrane Compliance Effects in Undrained Triaxial Testing," by Nicholson, P.G., Seed. R.B. and Anwar, H., September 1989, (PB92 139 641/AS)A13.

UCB/EERC-89/11 "Static Tilt Behavior of Unanchored Cylindrical Tanks," by Lau, D.T. and Clough, R.W., September 1989, (PB92 143 049)A10.

UCB/EERC-89/12 "ADAP-88: A Computer Program for Nonlinear Earthquake Analysis of Concrete Arch Dams," by Fenves, G.L., Mojtahedi, S. and Reimer, R.B., September 1989, (PB92 139 674/AS)A07.

UCB/EERC-89/13 "Mechanics of Low Shape Factor Elastomeric Seismic Isolation Bearings," by Aiken, I.D., Kelly, J.M. and Tajirian, F.F., November 1989, (PB92 139 732/AS)A09.

UCB/EERC-89/14 "Preliminary Report on the Seismological and Engineering Aspects of the October 17, 1989 Santa Cruz (Loma Prieta) Earthquake," by EERC, October 1989, (PB92 139 682/AS)A04.

UCB/EERC-89/15 "Experimental Studies of a Single Story Steel Structure Tested with Fixed, Semi-Rigid and Flexible Connections," by Nader, M.N. and Astaneh-Asl, A., August 1989, (PB91 229 211/AS)A10.

UCB/EERC-89/16 "Collapse of the Cypress Street Viaduct as a Result of the Loma Prieta Earthquake," by Nims, D.K., Miranda, E., Aiken, I.D., Whittaker, A.S. and Bertero, V.V., November 1989, (PB91 217 935/AS)A05.

UCB/EERC-90/01 "Mechanics of High-Shape Factor Elastomeric Seismic Isolation Bearings," by Kelly, J.M., Aiken, I.D. and Tajirian, F.F., March 1990.

UCB/EERC-90/02 "Javid's Paradox: The Influence of Preform on the Modes of Vibrating Beams," by Kelly, J.M., Sackman, J.L. and Javid, A., May 1990, (PB91 217 943/AS)A03.

UCB/EERC-90/03 "Earthquake Simulator Testing and Analytical Studies of Two Energy-Absorbing Systems for Multistory Structures," by Aiken, I.D. and Kelly, J.M., October 1990.

UCB/EERC-90/04 "Damage to the San Francisco-Oakland Bay Bridge During the October 17, 1989 Earthquake," by Astaneh-Asl, A., June 1990.

UCB/EERC-90/05 "Preliminary Report on the Principal Geotechnical Aspects of the October 17, 1989 Loma Prieta Earthquake," by Seed, R.B., Dickenson, S.E., Riemer, M.F., Bray, J.D., Sitar, N., Mitchell, J.K., Idriss, I.M., Kayen, R.E., Kropp, A., Harder, L.F., Jr. and Power, M.S., April 1990.

UCB/EERC-90/06 "Models of Critical Regions in Reinforced Concrete Frames Under Seismic Excitations," by Zulfiqar, N. and Filippou, F.C., May 1990.

UCB/EERC-90/07 "A Unified Earthquake-Resistant Design Method for Steel Frames Using ARMA Models," by Takewaki, I., Conte, J.P., Mahin, S.A. and Pister, K.S., June 1990.

UCB/EERC-90/08 "Soil Conditions and Earthquake Hazard Mitigation in the Marina District of San Francisco," by Mitchell, J.K., Masood, T., Kayen, R.E. and Seed, R.B., May 1990.

UCB/EERC-90/09 "Influence of the Earthquake Ground Motion Process and Structural Properties on Response Characteristics of Simple Structures," by Conte, J.P., Pister, K.S. and Mahin, S.A., July 1990.

UCB/EERC-90/10 "Experimental Testing of the Resilient-Friction Base Isolation System," by Clark, P.W. and Kelly, J.M., July 1990, (PB92 143 072)A08.

UCB/EERC-90/11 "Seismic Hazard Analysis: Improved Models, Uncertainties and Sensitivities," by Araya, R. and Der Kiureghian, A., March 1988.

UCB/EERC-90/12 "Effects of Torsion on the Linear and Nonlinear Seismic Response of Structures," by Sedarat, H. and Bertero, V.V., September 1989.

UCB/EERC-90/13 "The Effects of Tectonic Movements on Stresses and Deformations in Earth Embankments," by Bray, J. D., Seed, R. B. and Seed, H. B., September 1989.

UCB/EERC-90/14 "Inelastic Seismic Response of One-Story, Asymmetric-Plan Systems," by Goel, R.K. and Chopra, A.K., October 1990.

UCB/EERC-90/15 "Dynamic Crack Propagation: A Model for Near-Field Ground Motion.," by Seyyedian, H. and Kelly, J.M., 1990.

UCB/EERC-90/16 "Sensitivity of Long-Period Response Spectra to System Initial Conditions," by Blasquez, R., Ventura, C. and Kelly, J.M., 1990.

UCB/EERC-90/17 "Behavior of Peak Values and Spectral Ordinates of Near-Source Strong Ground-Motion over a Dense Array," by Niazi, M., June 1990.

UCB/EERC-90/18 "Material Characterization of Elastomers used in Earthquake Base Isolation," by Papoulia, K.D. and Kelly, J.M., 1990.

UCB/EERC-90/19 "Cyclic Behavior of Steel Top-and-Bottom Plate Moment Connections," by Harriott, J.D. and Astaneh-Asl, A., August 1990, (PB91 229 260/AS)A05.

UCB/EERC-90/20 "Seismic Response Evaluation of an Instrumented Six Story Steel Building," by Shen, J.-H. and Astaneh-Asl, A., December 1990, (PB91 229 294/AS)A04.

UCB/EERC-90/21 "Observations and Implications of Tests on the Cypress Street Viaduct Test Structure," by Bollo, M., Mahin, S.A., Moehle, J.P., Stephen, R.M. and Qi, X., December 1990.

UCB/EERC-91/01 "Experimental Evaluation of Nitinol for Energy Dissipation in Structures," by Nims, D.K., Sasaki, K.K. and Kelly, J.M., 1991.

UCB/EERC-91/02 "Displacement Design Approach for Reinforced Concrete Structures Subjected to Earthquakes," by Qi, X. and Moehle, J.P., January 1991.

UCB/EERC-91/03 "A Long-Period Isolation System Using Low-Modulus High-Damping Isolators for Nuclear Facilities at Soft-Soil Sites," by Kelly, J.M., March 1991.

UCB/EERC-91/04 "Dynamic and Failure Characteristics of Bridgestone Isolation Bearings," by Kelly, J.M., April 1991.

UCB/EERC-91/05 "Base Sliding Response of Concrete Gravity Dams to Earthquakes," by Chopra, A.K. and Zhang, L., May 1991.

UCB/EERC-91/06 "Computation of Spatially Varying Ground Motion and Foundation-Rock Impedance Matrices for Seismic Analysis of Arch Dams," by Zhang, L. and Chopra, A.K., May 1991.

UCB/EERC-91/07 "Estimation of Seismic Source Processes Using Strong Motion Array Data," by Chiou, S.-J., July 1991.

UCB/EERC-91/08 "A Response Spectrum Method for Multiple-Support Seismic Excitations," by Der Kiureghian, A. and Neuenhofer, A., August 1991.

UCB/EERC-91/09 "A Preliminary Study on Energy Dissipating Cladding-to-Frame Connection," by Cohen, J.M. and Powell, G.H., September 1991.

UCB/EERC-91/10 "Evaluation of Seismic Performance of a Ten-Story RC Building During the Whittier Narrows Earthquake," by Miranda, E. and Bertero, V.V., October 1991.

UCB/EERC-91/11 "Seismic Performance of an Instrumented Six Story Steel Building," by Anderson, J.C. and Bertero, V.V., November 1991.

UCB/EERC-91/12 "Performance of Improved Ground During the Loma Prieta Earthquake," by Mitchell, J.K. and Wentz, Jr., F.J., October 1991.

UCB/EERC-91/13 "Shaking Table - Structure Interaction," by Rinawi, A.M. and Clough, R.W., October 1991.

UCB/EERC-91/14 "Cyclic Response of RC Beam-Column Knee Joints: Test and Retrofit," by Mazzoni, S., Moehle, J.P. and Thewalt, C.R., October 1991.

UCB/EERC-91/15 "Design Guidelines for Ductility and Drift Limits: Review of State-of-the-Practice and State-of-the-Art in Ductility and Drift-Based Earthquake-Resistant Design of Buildings," by Bertero, V.V., Anderson, J.C., Krawinkler, H., Miranda, E. and The CUREe and The Kajima Research Teams,, July 1991.

UCB/EERC-91/16 "Evaluation of the Seismic Performance of a Thirty-Story RC Building," by Anderson, J.C., Miranda, E., Bertero, V.V. and The Kajima Project Research Team,, July 1991.

UCB/EERC-91/17 "A Fiber Beam-Column Element for Seismic Response Analysis of Reinforced Concrete Structures," by Taucer, F., Spacone, E. and Filippou, F.C., December 1991.

UCB/EERC-91/18 "Investigation of the Seismic Response of a Lightly-Damped Torsionally-Coupled Building," by Boroschek, R. and Mahin, S.A., December 1991.